



**Annual Report on Major Results and Progress of
Naka Fusion Research Establishment of JAERI
from April 1 to September 30, 2005 and
Fusion Research and Development Directorate of JAEA
from October 1, 2005 to March 31, 2006**

Fusion Research and Development Directorate

September 2006

Japan Atomic Energy Agency

日本原子力研究開発機構

本レポートは日本原子力研究開発機構が不定期に発行する成果報告書です。

本レポートの入手並びに著作権利用に関するお問い合わせは、下記あてにお問い合わせ下さい。

なお、本レポートの全文は日本原子力研究開発機構ホームページ (<http://www.jaea.go.jp/index.shtml>)
より発信されています。このほか財団法人原子力弘済会資料センター*では実費による複写頒布を行っ
ております。

〒319-1195 茨城県那珂郡東海村白方白根 2 番地 4

日本原子力研究開発機構 研究技術情報部 研究技術情報課

電話 029-282-6387, Fax 029-282-5920

*〒319-1195 茨城県那珂郡東海村白方白根 2 番地 4 日本原子力研究開発機構内

This report is issued irregularly by Japan Atomic Energy Agency

Inquiries about availability and/or copyright of this report should be addressed to

Intellectual Resources Section, Intellectual Resources Department,

Japan Atomic Energy Agency

2-4 Shirakata Shirane, Tokai-mura, Naka-gun, Ibaraki-ken 319-1195 Japan

Tel +81-29-282-6387, Fax +81-29-282-5901

© Japan Atomic Energy Agency, 2006

Annual Report on Major Results and Progress of
Naka Fusion Research Establishment of JAERI from April 1 to September 30, 2005 and
Fusion Research and Development Directorate of JAEA from October 1, 2005 to March 31, 2006

Fusion Research and Development Directorate

Japan Atomic Energy Agency
Naka-shi, Ibaraki-ken

(Received July 31, 2006)

This annual report provides an overview of major results and progress on research and development (R&D) activities at Naka Fusion Research Establishment of Japan Atomic Energy Research Institute (JAERI) during the period from April 1 to September 30, 2005 and at Fusion Research and Development Directorate of Japan Atomic Energy Agency (JAEA) from October 1, 2005 to March 31, 2006, including those performed in collaboration with other research establishments of JAERI, research institutes, and universities.

In JT-60, ferritic steel tiles (FSTs) were installed inside the vacuum vessel of JT-60U to reduce the toroidal field ripple. After the installation of FSTs, a high normalized beta plasma at $\beta_N \sim 2.3$ was sustained for 28.6s with ELMy H-mode confinement as required for an ITER hybrid operation scenario. National Centralized Tokamak was placed as the ITER satellite tokamak in collaboration with the EU fusion community, and the facility design was modified strongly in support of ITER.

In theoretical and analytical researches, studies on H-mode confinement, ITB in reversed shear plasmas, aspect ratio effects on external MHD modes and magnetic island evolution in a rotating plasma were progressed. Progress was also made in the NEXT project in which the behaviors of collisionless MHD modes and the dynamics of zonal flows were simulated.

In fusion reactor technologies, R&Ds for ITER and fusion DEMO plants have been carried out. For ITER, a steady state operation of the 170GHz gyrotoron up to 1000 s with 0.2MW was demonstrated. Also current density of the neutral beam injector has been extended to 134A/m² at 0.75MeV. In the ITER Test Blanket Module (TBM), designs of Water and Helium Cooled Solid Breeder TBMs and R&Ds of tritium breeder/multiplier materials were progressed. Tritium processing technology for breeding blankets was also progressed. For the DEMO reactors, high temperature superconductor such as Bi2212 has been examined. In plasma facing components, critical heat flux of a screw tube has been examined. Neutronics integral experiments with a blanket mockup were also progressed. For ITER TBMs and DEMO blankets, irradiation effects on F82H characteristics were progressed using HFIR, JMTR and so on. In the IFMIF program, transitional activities were also progressed. Vacuum technology and its application to industries have been examined.

In the ITER Program, under the framework of the ITER Transitional Arrangements, the Design and R&D Tasks have been carried out by the Participant Teams along the work plan approved on September 2005. In FY 2005, JAERI/JAEA has performed sixty-six Design Tasks and has completed thirty-four Tasks that make the implementation of preparing the procurement documents for facilities and equipments that are scheduled to be ordered at an early stage of ITER construction. The work plan for the "Broader Approach" Program has been continuously discussed through the bilateral negotiation meetings between Japan and the EU, and JAERI/JAEA provided the technical support for the meetings.

Finally, in fusion reactor design studies, a reactor concept of SlimCS was proposed to demonstrate an electric power generation of 1GW level, self-sufficiency of tritium fuel and year-long continuous operation.

Keywords; JAERI, JAEA, Fusion Research, Fusion Technology, JT-60, ITER, Broader Approach, IFMIF, Fusion Power, DEMO Plant, Fusion Reactor

Editors: Yoshida, H., Oasa, K., Hayashi, T., Nakamura, H., Ogawa, H.

那珂研究所／核融合研究開発部門 英文年報（平成 17 年度）

日本原子力研究開発機構
核融合研究開発部門

（2006 年 7 月 31 日 受理）

日本原子力研究所那珂研究所（2005 年 4 月 1 日～同年 9 月 30 日）及び日本原子力研究開発機構核融合研究開発部門（2005 年 10 月 1 日～2006 年 3 月 31 日）における平成 17 年度の研究開発（R&D）活動の主な成果と進捗について、所内の他研究所や機構内の研究開発部門および所外の研究機関並びに大学との協力により実施された研究開発を含めて報告する。

JT-60 では、トロイダル磁場リップル低減を目的に真空容器内部にフェライト鋼を設置した。その結果、ITER のハイブリッド運転で要求されるように、ELMy H モード閉じ込めで規格化ベータ値 2.3 の高ベータプラズマを 28.6 秒間維持することに成功した。また、JT-60 を超伝導化改造するトカマク国内重点化装置は、欧州核融合界との密接な協力の下に ITER のサテライト装置として位置付けられ、ITER を強力に支援すべく設計が見直された。

理論および解析研究では、H モード閉じ込め特性、負磁気シアプラズマの内部輸送障壁特性、MHD モードへのアスペクト比の効果、回転するプラズマ中での磁気島成長過程などの研究が進展した。また、トカマク数値実験プロジェクト(NEXT)においては、無衝突 MHD モードの挙動及び帯状流のダイナミックスのシミュレーションを行った。

核融合炉工学では、ITER および発電実証プラント（DEMO 炉）のために、R&D の研究開発が推進された。ITER に向けた R&D では、中性粒子入射器の電流密度が、エネルギー 0.75 MeV で 134 A/m^2 に拡張された。175 GHz ジャイラトロンでは、0.2 MW で 1000 秒の定常運転が実証された。テストブランケットモジュール(TBM) では、水冷固体増殖材およびヘリウム冷却固体増殖材方式の TBM 設計および増殖増媒材の R&D に進展が見られた。DEMO 炉に向けた R&D では、Bi2212 の高温超伝導材やスクリー管付きダイバータの評価試験が行われた。また、ブランケットモックアップによる中性子工学実験にも進展が見られた。更に、ITER TBM や DEMO 炉ブランケットのための構造材料 F82H の HFIR, JMTR 等における照射効果評価にも進展が見られた。IFMIF 計画では、移行期活動が進展した。この他、真空技術や産業界への技術移転が実施された。

ITER 計画では、ITER 移行措置の枠組みのもとで 2005 年 9 月に承認された作業計画に沿って、参加極チームによって設計および R&D タスク作業が進められた。2005 年度、原研/原子力機構は、建設の早い段階において発注が予定される設備と機器に関し、調達書類の準備を行う 66 件の設計タスク作業を進め、34 件のタスクを完了した。また、この間継続して“幅広いアプローチ”計画の具体化に関する協議が日欧間で進められ、原研/原子力機構は必要な支援作業を実施した。

最後に、核融合炉設計研究では、核融合炉で要求される 1GW 相当の電力発生、トリチウム燃料の自給、一年間の連続運転を実証する SlimSC 炉の概念設計が提案された。

Contents

I.	JT-60 Program	1
1.	Experimental Results and Analyses	1
1.1	Insertion of the Ferritic Steel Tile and Extended Plasma Regimes	1
1.2	Heat, Particle and Rotation Transport	2
1.3	MHD Instabilities and Control	6
1.4	H-Mode and Pedestal Research	10
1.5	Divertor/SOL Plasmas and Plasma-Wall Interaction	13
2.	Operation and Machine Improvements	17
2.1	Tokamak Machine	17
2.2	Control System	19
2.3	Power Supply System	20
2.4	Neutral Beam Injection System	22
2.5	Radio-Frequency Heating System	25
2.6	Diagnostics Systems	26
3.	Design Progress of the National Centralized Tokamak Facility	29
3.1	Physics Estimation	29
3.2	Engineering Design	30
4.	Domestic and International Collaborations	31
4.1	Domestic Collaboration	31
4.2	International Collaboration	32
II.	Theory and Analysis	33
1.	Confinement and Transport	33
1.1	Origin of the Various Beta Dependence of ELMy H-mode Confinement	33
1.2	Internal Transport Barriers in JT-60U Reversed-Shear Plasmas	33
2.	MHD Stability	34
2.1	Aspect Ratio Effect on the Stability of the External MHD Mode in Tokamaks	34
2.2	Role of Anomalous Transport in Neoclassical Tearing Modes	34
2.3	Magnetic Island Evolution in Rotating Plasma	35
2.4	Mechanism of Rotational Stabilization of High-n Ballooning Modes	35
3.	Integrated Simulation	36
3.1	Integrated Simulation Code for Burning Plasma Analysis	36
3.2	Development of Integrated SOL/Divertor Code and Simulation Study	36
3.3	Transient Behaviour of SOL-Divertor Plasmas after an ELM Crash	36
4.	Numerical Experiment of Tokamak (NEXT)	37
4.1	Nonlinear Behaviors of Collisionless Double Tearing and Kink Modes	37
4.2	Stability of Double Tearing Mode and its Effects on Current Hole Formation	37
4.3	ZF/GAM Dynamics and Ion Turbulent Transport in Reversed Shear Tokamaks	38
4.4	Development of Gyrokinetic Vlasov CIP Code	38
5.	Atomic and Molecular Data	39
III.	Technology Development	41
1.	Superconducting Magnet	41
2.	Neutral Beam Injection Heating	42
2.1	Acceleration of 1 MeV Class and High Current Density H ⁺ Ion Beam	42
2.2	Improvement of Beam Uniformity in a Large Negative Ion Source	43
2.3	Transport Process of Surface Produced H ⁺ Ions in a Negative Ion Source	44
3.	Radio Frequency Heating	45
3.1	Development of 170GHz Gyrotron	45
3.2	Development of Millimeter Wave Launcher	46
3.3	Application of High Power RF	47
4.	Blanket	48
4.1	Fabrication of Partial First Wall Mockup	48
4.2	Corrosion Performance of Cooling Channels in Supercritical Water	48
4.3	Thermo-Mechanical Performance of Breeder Pebble Bed	49
4.4	Design of Test Blanket Module	51
4.5	Development of Tritium Breeder and Neutron Multiplier Materials	53
4.6	Irradiation Technology Development for In-Pile Functional Tests	54

5.	Plasma Facing Components -----	55
5.1	Critical Heat Flux of a Copper Screw Tube under High Temperature Pressurized Coolant Condition -----	55
5.2	High Heat Flux Test of a Tungsten Armored Divertor -----	55
6.	Structural Material -----	56
6.1	Development of Structural Materials for Blanket -----	56
6.2	Transition Phase Activities in IFMIF -----	58
7.	Tritium Technology -----	60
7.1	Tritium Processing Technology Development for Breeding Blanket -----	60
7.2	Tritium Accounting Technology Development -----	61
7.3	Basic Study on Tritium Behavior -----	61
7.4	Successful Operation Results of Tritium Safety Systems in TPL -----	63
8.	Fusion Neutronics -----	63
8.1	Blanket Neutronics Experiments -----	63
8.2	Cross Section Measurements of Fusion Materials -----	65
8.3	Beam Analyses of the Armor Tiles -----	66
8.4	Gamma-Ray Measurement for Alpha Particle Diagnostics in Plasma -----	66
8.5	Operation of the FNS Facility -----	67
9.	Vacuum Technology -----	67
10.	Technology Transfer -----	68
IV.	International Thermonuclear Experimental Reactor (ITER) and Broader Approach (BA) -----	69
1.	Overview of the ITER Program and Activities -----	69
1.1	ITER Transitional Arrangements (ITA) -----	69
1.2	Progress of Negotiations and Prospective Schedules -----	69
2.	ITA Design Task -----	71
2.1	Superconducting Magnet -----	71
2.2	Vacuum Vessel -----	73
2.3	Blanket and Divertor -----	73
2.4	Remote Maintenance -----	74
2.5	EC and NBI Heating System -----	74
2.6	Operation Scenario -----	75
2.7	Tritium-Material Interaction -----	76
2.8	Neutronics -----	77
2.9	Plasma Diagnostics -----	77
3.	Domestic Activities -----	79
3.1	Site Preparation -----	79
3.2	Codes and Standards -----	79
4.	Contributions to International Tokamak Physics Activity (ITPA) -----	80
4.1	Transport Physics Topical Group -----	80
4.2	Confinement Database and Modeling Topical Group -----	80
4.3	Pedestal and Edge Physics Topical Group -----	80
4.4	Steady-State Operation Topical Group -----	80
4.5	MHD Topical Group -----	80
4.6	Scrape-Off-Layer and Divertor Physics Topical Group -----	80
4.7	Diagnostics Topical Group -----	80
5.	CODAC Design Activity -----	81
6.	Broader Approach Activities -----	82
V.	Fusion Reactor Design Study -----	83
1.	Conceptual Design of DEMO Reactor -----	83
2.	Non-Inductive Current Ramp Simulation -----	84
3.	Study of Advanced Shield Materials -----	84
Appendix -----		
A.1	Publication List (April 2005 - March 2006) -----	85
A.2	Organization-----	107
A.3	Personnel Data -----	109

目次

I.	JT-60 計画	1
1.	実験の結果と解析	1
1.1	フェライト鋼タイルの導入とプラズマ運転領域の拡大	1
1.2	熱、粒子、回転運動量の輸送	2
1.3	MHD 不安定性と制御	6
1.4	Hモードとペデスタル研究	10
1.5	ダイバータ/SOL プラズマとプラズマ-壁相互作用	13
2.	運転と装置改良	17
2.1	トカマク装置	17
2.2	制御設備	19
2.3	電源設備	20
2.4	中性粒子入射装置	22
2.5	高周波加熱装置	25
2.6	計測装置	26
3.	トカマク国内重点化装置設計の進展	29
3.1	物理設計	29
3.2	工学設計	30
4.	国内協力・国際協力	31
4.1	国内協力	31
4.2	国際協力	32
II.	理論と解析	33
1.	閉じ込めと輸送	33
1.1	ELMy Hモード閉じ込めの多様な β 依存性の起源	33
1.2	JT-60U 負磁気シアプラズマの強い内部輸送障壁	33
2.	MHD 安定性	34
2.1	トカマクにおける外部 MHD モードの安定性に対するアスペクト比の影響	34
2.2	新古典テアリングモードへの異常輸送の効果	34
2.3	回転プラズマ中の磁気島の発展	35
2.4	高- n バルーンモードの回転安定化の機構	35
3.	統合化シミュレーション	36
3.1	燃焼プラズマ解析のための統合化シミュレーションコード	36
3.2	SOL/ダーバータコードの開発とシミュレーション研究	36
3.3	ELM 崩壊後の SOL-ダイバータプラズマの過渡的挙動の粒子シミュレーション	36
4.	数値トカマク計画 (NEXT)	37
4.1	無衝突ダブルテアリング及びキンクモードの非線形発展	37
4.2	ダブルテアリングモードの安定性と電流ホール形成への影響	37
4.3	反転磁気シアプラズマ中の帯状流-GAM ダイナミクスとイオン乱流輸送	38
4.4	ジャイロ運動論的ブラソフ CIP コードの開発	38
5.	原子分子データ	39
III.	技術開発	41
1.	超伝導マグネット	41
2.	中性粒子入射加熱	42
2.1	1MeV 級、高電流密度の水素負イオンビーム加速	42
2.2	大型負イオン源での負イオン生成の一様性の改善	43
2.3	負イオン源内における表面生成水素負イオンの輸送課程	44
3.	高周波加熱	45
3.1	170GHz ジャイロトロンの開発	45
3.2	ミリ波入射のための RF ランチャーの開発	46
3.3	大電力高周波の応用	47
4.	ブランケット	48
4.1	部分第一壁モックアップの製作	48
4.2	超臨界圧水中における冷却管の腐食特性	48
4.3	増殖材充填層の熱・機械的特性	49

4.4	テストブランケット・モジュールの設計	51
4.5	トリチウム増殖材と中性子増倍材の開発	53
4.6	インパイル機能試験のための照射技術開発	54
5.	プラズマ対向機器	55
5.1	高温、高圧条件における銅スクリー冷却管の限界熱流束特性	55
5.2	タングステンアーマ付きダイバータ試験体の高熱負荷実験	55
6.	構造材料	56
6.1	ブランケットのための構造材料の開発	56
6.2	国際核融合材料照射施設(IFMIF)の移行活動	58
7.	トリチウム技術	60
7.1	増殖ブランケットのためのトリチウム・プロセス技術の開発	60
7.2	トリチウム計測技術の開発	61
7.3	トリチウム挙動特性に関する基礎的研究	61
7.4	TPL におけるトリチウム安全設備の運転成果	63
8.	核融合中性子工学	63
8.1	ブランケットに関する中性子工学実験	63
8.2	核融合炉用材料の核反応断面積の測定	65
8.3	アーマタイル材のビーム分析	66
8.4	プラズマ内アルファ粒子診断のためのガンマ線計測	66
8.5	FNS 施設の運転	67
9.	真空技術	67
10.	技術移転	68
IV.	国際熱核融合実験炉 (ITER) と幅広いアプローチ (BA)	69
1.	ITER 計画と活動の概要	69
1.1	ITER 移行措置 (ITA)	69
1.2	政府間協議の進捗と今後の見通し	69
2.	ITA 設計タスク	71
2.1	超電導磁石	71
2.2	真空容器	73
2.3	ブランケット及びダイバータ	73
2.4	遠隔保守	74
2.5	EC 及び NBI 加熱システム	74
2.6	運転シナリオ	75
2.7	トリチウム・壁相互作用	76
2.8	中性子工学	77
2.9	プラズマ診断	77
3.	国内活動	79
3.1	サイト準備	79
3.2	規格基準	79
4.	国際トカマク物理活動への貢献	80
4.1	輸送物理	80
4.2	閉じ込めデータベースとモデリング	80
4.3	周辺及びペデスタルの物理	80
4.4	定常運転	80
4.5	MHD	80
4.6	スクレイプ・オフ層及びダイバータの物理	80
4.7	計測	80
5.	CODAC 設計活動	81
6.	幅広いアプローチ	82
V.	核融合炉設計研究	83
1.	原型炉概念設計	83
2.	非誘導電流立ち上げシミュレーション	84
3.	先進遮蔽材料の研究	84
付録		
A.1	平成 17 年度 (2005 年 4 月～2006 年 3 月) 発表文献リスト	85
A.2	組織	107
A.3	人員に関するデータ	109

FOREWORD

In October 1, 2005, the Japan Atomic Energy Agency (JAEA) has made its first steps as an independent administrative institution, integrating the Japan Atomic Energy Research Institute (JAERI) and the Japan Nuclear Cycle Development Institute (JNC). Before the integration, in June 28, 2005, the decision to site ITER at Cadarache in France was reached by six-Party agreement with the joint declaration. At the same occasion, a bilateral agreement between EURATOM and Japan has been reached over the roles of the Host and the non-Host for the ITER project including ITER construction, Broader Approach and DEMO Reactor. This report presents the major results and progress on research and development activities for fusion energy at JAERI and continuously at JAEA in the progressive FY2005.

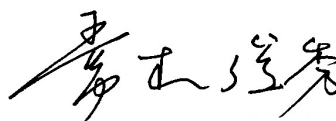
The research on JT-60 has made remarkable progress in expanding the plasma discharge regime into the ITER hybrid operation regime, where a reactor-relevant plasma with both high confinement and stability was sustained up to 28.6 s. Installation of ferritic steel tiles inside the vacuum vessel in 2005 to reduce the toroidal field ripple played a key role to accomplish the result. A lot of progress was made in plasma physics researches on confinement, transport and stability from the viewpoint of both experiment and theory. The design research of "JT-60 Super Advanced (JT-60SA)," which is the modification of JT-60 for a superconducting tokamak, has progressed to play a role as the ITER satellite tokamak closely in collaboration with EU fusion community. Steady progress was also made in the NEXT (Numerical Experiment of Tokamak) project.

The research and development on fusion reactor technologies have been carried out to further improve technologies necessary for ITER construction. For the ITER radio frequency heating system, a steady state operation of the 170 GHz gyrotron up to 1000 s with 0.2 MW was demonstrated. As the Japanese implementing institute of ITER Transitional Arrangements, JAERI/JAEA has performed sixty-six Design Tasks and completed thirty-four Tasks in FY 2005 that contribute to the preparation of the procurement documents for facilities and equipments, and has supported an activity of the International Team at the Naka site.

With the expectation of starting the Engineering Validation and Engineering Design Activities (EVEDA) under Broader Approach (BA), JAERI/JAEA has been participating in the transition activities of the International Fusion Materials Irradiation Facilities (IFMIF). Paralleling the bilateral negotiations on BA agreement between EURATOM and Japan, the technological studies have been made for BA projects including the facilities for the computer simulation, the remote access to ITER experiments and so on as well as JT-60SA and IFMIF-EVEDA.

The research and development on fusion reactor technologies have been implemented to accumulate technological database to assure the design of fusion DEMO plants. With respect to ITER Test Blanket Module (TBM), designs of Water and Helium Cooled Solid Breeder TBMs and R&Ds of tritium breeder/multiplier materials were progressed. Neutron irradiation on F82H, one of the most promising structural materials for the ITER TBM and DEMO blankets, has been continued using HFIR and JMTR. As to the design study for DEMO plant, a new concept with compact-sized reactor was proposed from an economical point of view.

FY2005 was the year for the start of new period in the fusion research in the world. In accordance with the world-wide strategy, the fusion development at JAEA has been in progress and will be continued.



Toshihide Tsunematsu

Director General

Fusion Research and Development Directorate, JAEA

I. JT-60 PROGRAM

1. Experimental Results and Analyses

1.1 Insertion of the Ferritic Steel Tile and Extended Plasma Regimes

Modification of the control systems for the operation, heating and diagnostics has brought a new regime in the advanced tokamak plasma research with longer time scales than the current relaxation time (τ_R) on JT-60U. However, further pursuit of long sustainment of high performance plasmas has been prevented by the loss of fast ions due to the toroidal field ripple, since the loss decreases the net heating power, increases heat load to the wall and lower hybrid (LH) wave launcher located at a horizontal port, and limits controllability of the toroidal rotation (V_T) profile due to formation of an inward electric field. In order to reduce the toroidal field ripple, ferritic steel tiles (FSTs), which cover $\sim 10\%$ of the vacuum vessel surface, have been installed inside the JT-60U vacuum vessel on the low field side [1.1-1]. After the installation of FSTs, high normalized beta (β_N) of 2.3 is successfully maintained for 28.6 s with good confinement close to ITER hybrid operation scenario [1.1-2].

1.1.1 Ferritic Tile Insertion

Specifications of the FST is described in the section 2.1.2. Installation of the FSTs was optimized based on a typical large bore discharge ($I_p=1.1\text{MA}$, $B_t=1.86\text{T}$) in which the fast ion loss is larger using fully three Dimensional magnetic field orbit-following Monte-Carlo code (F3D OFMC) [1.1-1]. The final

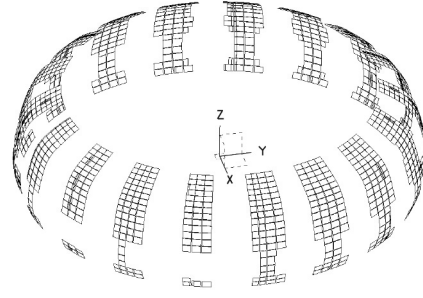


Fig. I.1.1-1 Bird's eye view of ferritic insertion. Thickness of the FST is 23mm

design is shown in Fig. I.1.1-1. With this design, the evaluation results show that total absorbed NB power can be increased by about 13%, and the increase in the absorbed power of the perpendicular beams can be 15%. Moreover, the heat load to the LH launcher can be reduced by a factor of ~ 3 .

After the installation, the heat load to the outer wall was evaluated by the infrared camera, and found to be consistent with the calculation.

1.1.2 Sustainment of High β_N with High Confinement

The reduction of toroidal field ripple increases absorbed heating power at the same injection power. The increase in absorbed power can reduce the required NB units to sustain a given β_N and then increase flexibility of combination of tangential NB units to vary torque input. The reduction of fast ion losses can also reduce formation of an inward electric field, which may induce a counter toroidal rotation. All these factors can be expected to contribute in extending the sustainable

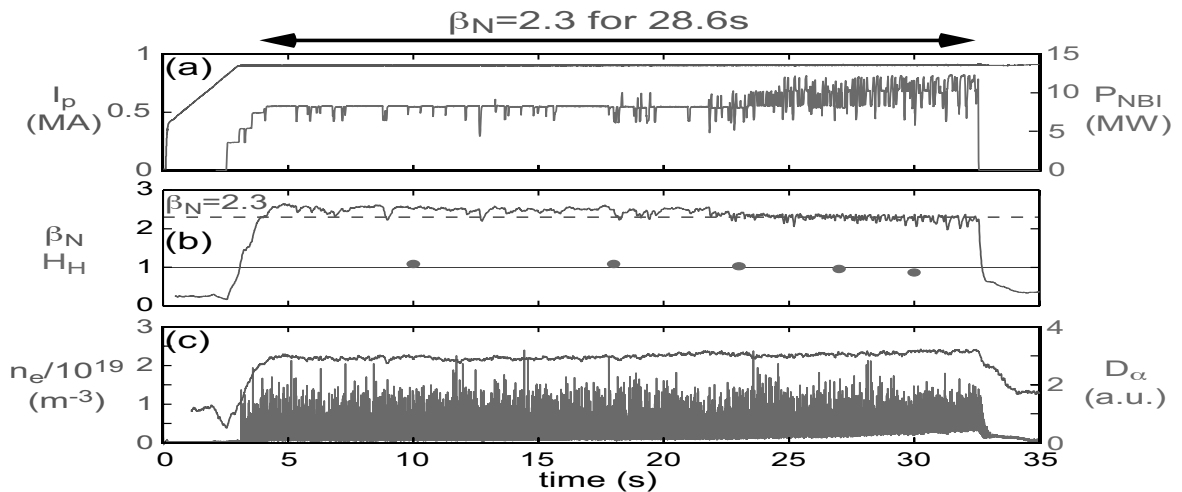


Fig. I.1.1-2 Waveforms of a typical high β_N long-pulse plasma (E45436), (a) plasma current and heating power, (b) normalized beta, β_N , and confinement factor, H_{98} , and (c) line-averaged density and divertor D_α intensity.

duration of high β_N plasma. Therefore, optimization had been carried out, and high β_N of 2.3 was successfully sustained for 28.6s. The typical waveforms of the discharge ($I_p=0.9\text{MA}$, $B_T=1.58\text{T}$, $q_{95}\sim 3.3$) are shown in Fig. I.1.1-2. Increase in the absorbed power and plasma confinement has enabled to sustain high β_N with smaller injection power. As the result, enough power to keep β_N is maintained until the end of the pulse. Smaller injection power also prevented increase in the temperature of the divertor tiles, which causes increase in the particle recycling. The increase in the particle recycling would degrade plasma confinement. In this discharge, the particle recycling is increasing (Fig. I-1.1-2 (c)), but limited low. It should be noted that in this discharge, a high bulk energy confinement ($H_{98(y,2)}$) of about 1.1 is maintained up to $t\sim 22\text{s}$ with $\beta_N \geq 2.4$ as shown in Fig. I-1.1-2. Also in this discharge high value of the product $\beta_N H_{98(y,2)}$, which is a measure of the fusion performance, is maintained above 2.2 for 23.1s ($>12\tau_R$). It is noted that this value of $\beta_N H_{98(y,2)}$ can satisfy the ITER Hybrid scenario.

References

- 1.1-1 Shinohara, K., and the JT-60 Team, "Review of Recent Steady-State Advanced Tokamak Research, and Its Further Pursuit by Reduction of TF Ripple on JT-60U," to be published in *J. Korean Phys. Soc.*.
- 1.1-2 Oyama, N., *et al.*, "Enhanced ELMy H-mode Performance with Reduced Toroidal Field Ripple in JT-60U," *Proc. 33rd EPS Conf. on Plasma Phys.*.

1.2 Heat, particle and rotation transport

1.2.1 Temporal Variation of Density Fluctuation and Transport in Reversed Shear Plasmas [1.2-1]

In reversed shear (RS) plasmas, an internal transport barrier (ITB) is formed due to suppression of anomalous turbulent transport. Many types of fluctuation with various spatial scales exist in plasmas. The anomalous turbulent heat transport for ion and electron channels and also the anomalous turbulent particle transport could be dominated by different types of fluctuation with different spatial scale such as ion temperature gradient (ITG) mode, trapped electron mode (TEM) and electron temperature gradient (ETG) mode. In a JT-60U RS plasma, further reduction of the transport was induced by a pellet injection after the ITB formation. The temporal variation of the density fluctuation and its relation to the electron and ion heat transport and the

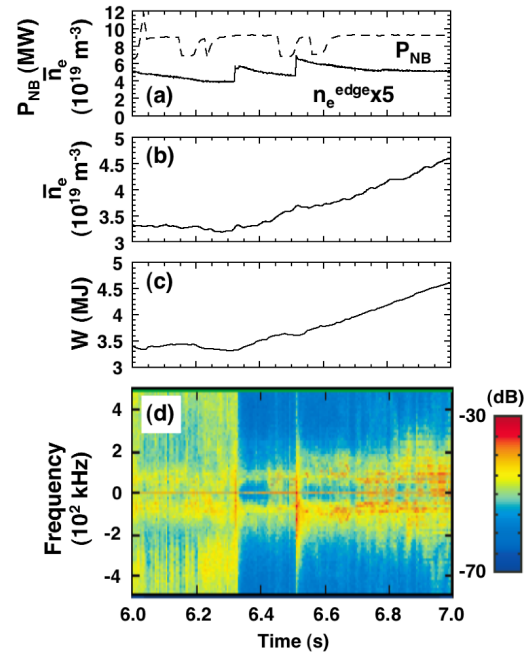


Fig. I.1.2-1 Wave-forms in a RS plasma with pellet injections. (a) The solid line shows edge line-averaged electron density. The dashed line shows NB heating power. (b) Center line-averaged electron density, (c) stored energy and (d) spectrogram of the O-mode reflectometer signal.

particle transport were investigated for the further reduction of the transport.

Figure I.1.2-1 shows wave-forms in a RS plasma with further reduction of the transport after the pellet injection. Pellets were injected into the RS plasma from the high-field-side at the top after the ITB formation. The plasma current (I_p) was 2.2MA, the toroidal magnetic field (B_T) was 4.3T, and the safety factor at 95% flux surface (q_{95}) was 3.8. The first pellet was injected at $t=6.32\text{s}$, as shown by the edge density jump, during the I_p flat-top phase with constant heating power of neutral beam (NB). After the first pellet injection, the central density and the stored energy started to increase. A high frequency component ($|f|>200\text{kHz}$) of the O-mode reflectometer signal was drastically reduced, as well as a low frequency component ($50\text{kHz}<|f|<20\text{kHz}$), $\sim 5\text{ms}$ after the pellet injection. In this case, the cut-off layer was located in the ITB region ($r/a=0.45-0.5$). The central density and the stored energy seemed to start to increase simultaneously with the reduction of the high and low frequency components. The reduction of the high and low frequency components of the O-mode reflectometer signal indicated change of density fluctuation level. The density fluctuation level was estimated to be 1-2% before and 0.4-0.5% after the first

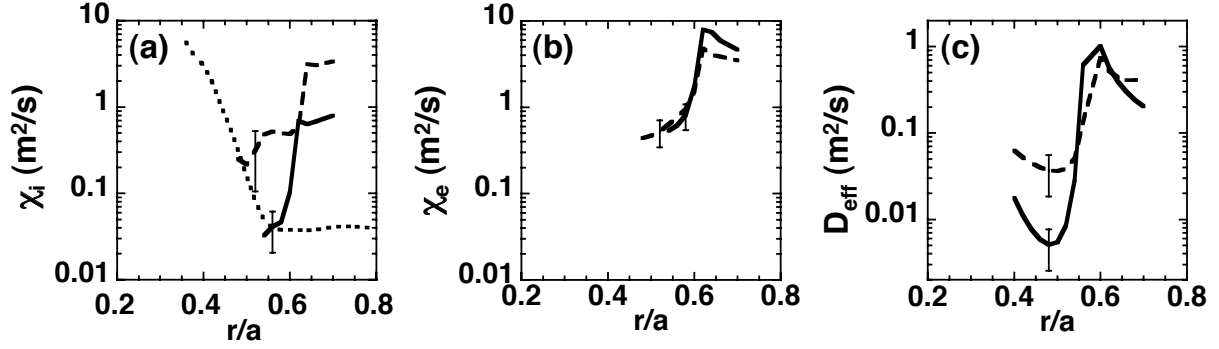


Fig. I.1.2-2 (a) Ion thermal diffusivity, (b) electron thermal diffusivity and (c) effective particle diffusivity. The dashed lines show the data before the first pellet injection at $t=6.3$ s and the solid lines show the data after the pellet injection at $t=7.0$ s. The dotted line in (a) shows the neoclassical ion thermal diffusivity.

pellet injection, respectively, [1.2-2] based on the analytical solution of time-dependent 2D full-wave equation [1.2-3]. The wave number of the measured density fluctuation was estimated to be of the order of 1cm^{-1} , which was consistent with the spatial scale of ITG and/or TEM. After another pellet injection at $t=6.51$ s, the spectrum of the O-mode reflectometer signal was unchanged, and the central density and the stored energy continued to increase. The energy confinement time (τ_E) and the confinement enhanced factor over ITER-89P L-mode scaling ($H_{89\text{PL}}$) increased from $\tau_E=0.5$ s and $H_{89\text{PL}}=1.6$ at $t=6.3$ s to $\tau_E=1.0$ s and $H_{89\text{PL}}=2.6$ at $t=7$ s.

The density substantially increased inside the ITB foot, while the edge density slightly increased. The ion and electron temperature profiles did not change significantly. The profiles of the ion and electron thermal diffusivities (χ_i and χ_e) and the effective particle diffusivity (D_{eff}) estimated by the particle and power balance analysis without consideration of the pinch term (considering only the diffusion term) are shown in Fig. I.1.2-2. The values of χ_i and D_{eff} decreased by one order of magnitude after the pellet injection. However, no reduction of χ_e was observed. The equi-partition heat transfer from ions to electrons increased due to the substantial increase in the central density, but no change of difference between ion and electron temperature was observed. The ion temperature gradient in the ITB region was maintained with the decreased ion heat flux after the pellet injections due to χ_i reduced to a neoclassical level. The increase in the electron stored energy (density increase with a constant electron temperature) was attributed to the increase in the equi-partition heat transfer from ions. The particle and power balance analysis indicated that the particle and

ion heat transport are coupled with the measured density fluctuation with spatial scale of the order of 1cm^{-1} , while the electron heat transport was decoupled.

1.2.2 Degradation of Internal Transport Barrier by ELM Crashes [1.2-4]

In order to sustain burning plasmas in ITER and the steady-state tokamak power plants, we need to achieve high values of the energy confinement improvement factor (HH_{y2}), normalized beta (β_N), bootstrap and non-inductively driven current fractions, plasma density, fuel purity and radiation power simultaneously. It is widely recognized that the high H-mode pedestal pressure and the ITB formation are important for achieving the above highly integrated plasma performance. However, high pedestal pressure may induce large ELMs. The compatibility of large ELMs with the ITB is an important issue to develop the highly integrated plasma. In JT-60U, the compatibility of type I ELMs and the ITB has been good enough to sustain a HH_{y2} factor value of 1–2 in long pulse discharges of the high β_p H-mode (weak positive magnetic shear) and the RS H-mode [1.2-5]. Up to $I_p=1.5$ MA, the sustainable maximum plasma stored energy and β_N have been limited by the appearance of neoclassical tearing modes (NTM) for the positive shear cases ($q_{95}=3.2\text{--}9$ at $I_p=1$ MA, $q_{95}=4\text{--}5$ at $I_p=1.5$ MA) [1.2-5]. However, at higher $I_p=1.8$ MA ($q_{95}=4.1$), we found some cases where the plasma stored energy was degraded by type I ELMs.

Figure I.1.2-3 shows the time evolution of the high β_p ELMy H-mode discharge E39713 ($I_p=1.8$ MA, $B_T=4.05$ T, $q_{95}=4.1$), where a full non-inductive current drive was achieved [1.2-6]. The total plasma stored energy (W_{dia}) reached 7.6MJ, which was the highest value achieved so far at $I_p=1.8$ MA in JT-60U. In the flat

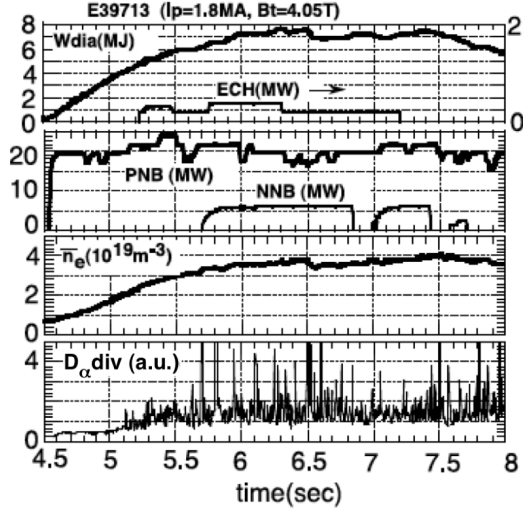


Fig. I.1.2-3 Time evolutions of total stored energy, heating powers for EC wave injection and for positive and negative ion based NBs, line averaged electron density and $D\alpha$ emission intensity from the divertor area in the high β_p ELMy H-mode discharge at $I_p=1.8$ MA.

top phase of W_{dia} , the ITB-foot location was around 65% of the minor radius and the location of the top of the pedestal was around 90% of the minor radius. The central safety factor (measured by MSE) was 1.4 and thus there was no sawtooth activity. In Fig. I.1.2-3, a drop of W_{dia} was seen at $t\sim 6.5$ s to coincide with a drop in the line averaged density and an increase in the $D\alpha$ emission from the divertor area. In this phase, no signature of an NTM was observed.

In order to evaluate the penetration of an ELM crash, we performed ECE measurement using the heterodyne radiometer system with a radial resolution of 2cm. The minor radius of this discharge was 79cm. Figure I.1.2-4 shows the measured profiles of the

electron temperature (T_e) and the relative change in T_e at the ELM crashes ($=\Delta T_e/T_e$) at $t=5.35$ s and $t=6.49$ s in the discharge shown in Fig. I.1.2-3. In order to evaluate the ELM crash itself (the eigenfunction of the instability), $\Delta T_e/T_e$ was calculated within 600 μ s. We defined the ELM penetration radius by the deepest radial location with $\Delta T_e/T_e > 1\%$. At $t=5.35$ s, the ELM crash depth was away from the ITB-foot, while at $t=6.49$ s, it reached the ITB-foot.

In the early phase ($t < 5.8$ s) the ITB-foot radius expanded and the ELM penetration radius deepened gradually. This deepening of the ELM penetration seemed to coincide with an increase in pedestal stored energy (while the pedestal electron collisionality was almost constant). Then the ELM penetration radius and the ITB-foot met each other at $t\sim 5.8$ s. After that, the ‘balanced phase’ lasted for ~ 0.7 s. Interestingly, the ITB-foot seemed to behave as a barrier against ELM crash penetration, and after around ten ELM attacks the ITB-foot shrank. Then the ELM penetration followed the shrinking ITB-foot. This behavior was shown in greater detail in T_e at various radial locations. Before $t=6.492$ s, a sudden drop in T_e was seen up to $r/a=0.615$ (\sim ITB-foot), while no change in T_e at each ELM occurs inside the ITB. At $t=6.492$ s, the ITB was broken at the original ITB-foot radius. Then degradation of T_e penetrated gradually into the inner region and, at the same time, T_e in the outer region increased and the ELM period shortened due to a release of the stored energy. As the result of this degradation of the ITB from $t=6.492$ s to $t=6.56$ s, the stored energy decreased by about 10% (0.8MJ). ELM control for small amplitude such as type

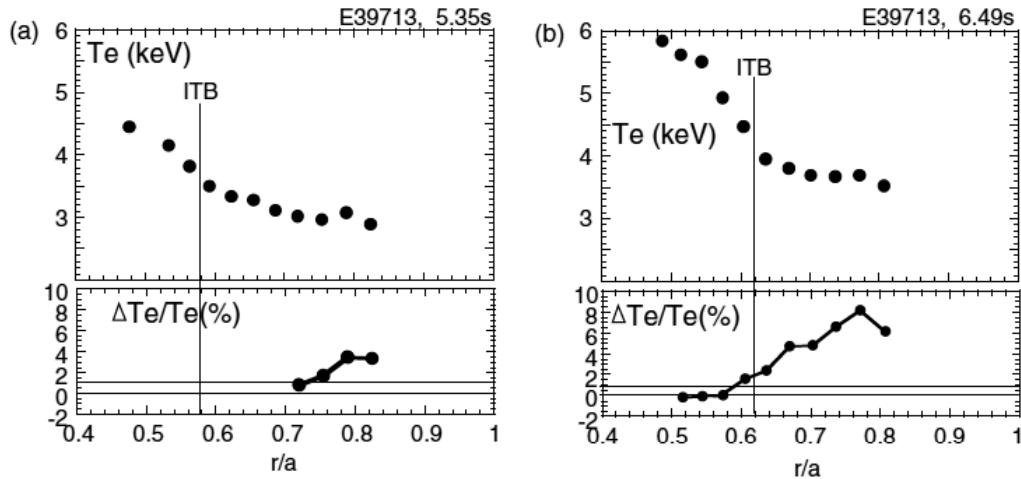


Fig. I.1.2-4 Profiles of electron temperature (T_e) and relative change of T_e within 600 μ s at an ELM crash ($=\Delta T_e/T_e$) appeared at (a) $t=5.35$ s and (b) $t=6.59$ s in the high β_p ELMy H-mode discharge shown in Fig. I.1.2-3.

II ELM is important not only to reduce transient heat load to the divertor plates but also to achieve highly integrated plasma performance.

1.2.3 Response of Toroidal Rotation Velocity to Electron Cyclotron Wave Injection [1.2-7]

In tokamak plasmas, toroidal rotation velocity and its shear (or radial electric field (E_r) shear) play an important role in stability and transport. In present tokamak devices, the toroidal rotation velocity profile can be easily controlled by toroidal momentum input from NBs. In contrast, the control of toroidal rotation velocity profile by NBs will be difficult in a burning plasma. Therefore, the development of other actuators to control the toroidal rotation velocity profile is important for the control of a burning plasma. Recently, the change in toroidal rotation velocity profile induced by ICRF heating has been reported [1.2-8]. In JT-60U, the spontaneous toroidal rotation velocity under the no/low direct toroidal momentum input was investigated using electron cyclotron (EC) wave injection.

In order to investigate the response of the toroidal rotation velocity to on-axis EC wave injection, EC power of 2.7MW was injected into L-mode plasma ($I_p=1\text{MA}$, $B_T=1.9\text{T}$ for the second harmonic EC central injection, $q_{95}=3.4$ and $n_e \sim 1.0 \times 10^{19} \text{m}^{-3}$ at the centre). In this plasma, low power NBs were applied, which consisted of counter-NB (0.9MW) for the motional Stark effect (MSE) diagnostic and perpendicular-NB (2.3MW) for the CXRS diagnostic. Since the fundamental O-mode (or the second harmonic X-mode) with an oblique toroidal injection angle was launched from the low-field-side for the current drive in JT-60U, EC injection was not for the electron heating only but also for the current drive. Figure I.1.2-5 shows the profiles of the toroidal rotation velocity and electron temperature just before and during the EC wave injection. As EC wave was injected, the central electron temperature increased from 2 to 6keV. The ion temperature just outside the EC wave deposition ($r/a \sim 0.25$) and the electron density at $r/a \sim 0.13$ were kept almost constant during EC wave injection. The toroidal rotation velocity at $r/a \sim 0.25$ was changed from ~ 100 to $\sim 60 \text{km/s}$ in the counter-direction during the EC wave injection as shown in Fig. I.1.2-5. The region of change in toroidal rotation velocity was up to $r/a \sim 0.6$ from the centre, which was wider than the EC wave power

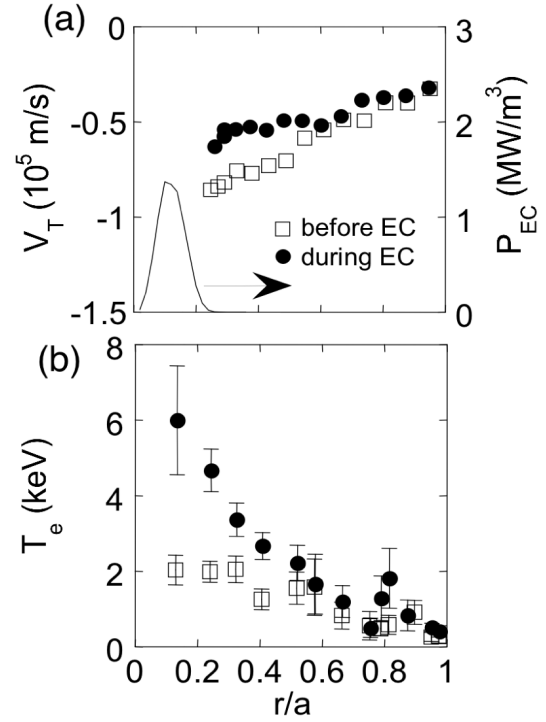


Fig. I.1.2-5 Profiles of (a) toroidal rotation velocity and (b) electron temperature just before (squares) and during (circles) EC wave injection. The solid line in (a) shows profile of the EC wave power deposition.

deposition profile. Although the change in toroidal rotation velocity at the core region coincided with the increase in electron temperature, the timescale of change in the toroidal rotation velocity was slower than that in the electron temperature. It should be mentioned that the change in toroidal rotation velocity at $r/a \sim 0.37$ was delayed from that at $r/a \sim 0.25$. This indicated that the change in the toroidal rotation velocity propagated from the centre to the peripheral.

In order to investigate the propagating response of the toroidal rotation velocity to EC wave injection (2MW), the short pulse (0.1s) off-axis EC wave injection into the L-mode plasma heated by diagnostics NBs (counter-NB: 0.76MW, perpendicular-NB: 2MW) was performed, as shown in Fig. I.1.2-6. Here, I_p , B_T and q_{95} were 0.8MA, 2.1T and 5.1 for the second harmonic EC injection, the line averaged electron density was $\sim 0.8 \times 10^{19} \text{m}^{-3}$. Figure I.1.2-6 shows response of the toroidal rotation velocity in the core region to the short pulse of the off-axis EC wave injection. The peak of the absorbed EC wave power deposition was located at $r/a \sim 0.7$, and there was no EC wave power source in the region of $r/a < 0.5$. The perturbation of the toroidal rotation velocity towards co-direction (or reduced counter-rotation) was observed

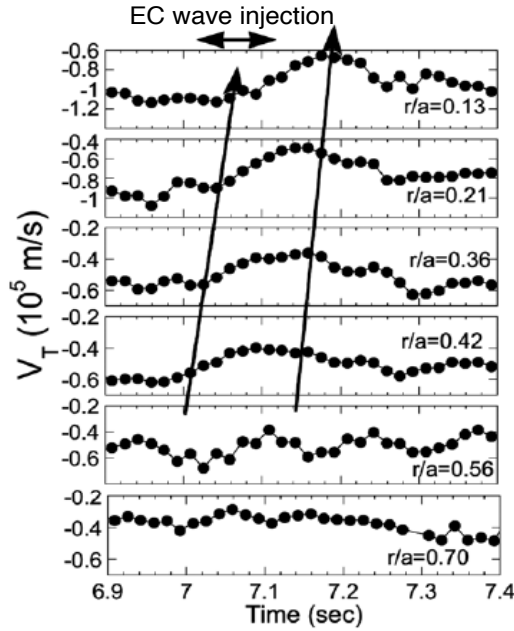


Fig. I.1.2-6 Propagating perturbations in toroidal rotation velocity at several radii, induced by the short pulse off-axis EC wave injection ($t=7.02-7.12$ s).

clearly in the region of $r/a < 0.5$ and it propagated from the half of the minor radius to the centre, as shown in Fig. I.1.2-6. On the other hand, the propagation of the perturbation of the toroidal rotation velocity in the opposite direction was not obvious in this discharge. The propagation of the heat pulse was also observed in the electron temperature. The propagation speed for the perturbation of the toroidal rotation velocity was much slower than that of electron temperature. This suggests that the toroidal rotation velocity was not simply determined by the local electron pressure gradient. The perturbation amplitude of the toroidal rotation velocity increased when the perturbation propagated, suggesting existence of an inward pinch in momentum transport. The turbulence driven theory predicted that the density and/or temperature gradient, as well as the velocity gradient, generate the momentum flux [1.2-9]. The investigation of the response of the toroidal rotation velocity to the EC wave injection is necessary with various plasma parameters to clarify the mechanisms determining the momentum transport.

References

- 1.2-1 Takenaga, H., *et al.*, *Plasma Phys. Control. Fusion*, **48**, A401 (2006).
 - 1.2-2 Oyama, N., *et al.*, *Plasma Phys. Control. Fusion*, **46**, A355 (2004).
 - 1.2-3 Bruskin, L.G., *et al.*, *Plasma Phys. Control. Fusion*, **44**, 2305 (2002).
 - 1.2-4 Kamada, Y., *et al.*, *Plasma Phys. Control. Fusion*, **48**, A419 (2006).
 - 1.2-5 Kamada, Y., *et al.*, *Nucl. Fusion*, **41**, 1311 (2001).
 - 1.2-6 Isayama, A., *et al.*, *Nucl. Fusion*, **43**, 1272 (2003).
 - 1.2-7 Sakamoto, Y., *et al.*, *Plasma Phys. Control. Fusion*, **48**, A63 (2006).
 - 1.2-8 Noterdaeme, J.-M., *et al.*, *Nucl. Fusion*, **43**, 274 (2003).
 - 1.2-9 Itoh, S.-I., *Phys. Fluids*, **B4**, 796 (1992).
- ### 1.3 MHD Instabilities and Control
- #### 1.3.1 Stabilization of the Neoclassical Tearing Mode
- In a fusion reactor such as ITER, stationary sustainment of a high-beta and high confinement plasma is essential. From the viewpoint of MHD stability, suppression of neoclassical tearing modes (NTMs) is the most critical issue in optimizing the discharge scenario of the high-performance plasmas. In JT-60U, in addition to the experimental demonstration of NTM suppression, progress has been made in simulation of NTM evolution by extending the transport code TOPICS [1.3-1, 1.3-2].
- #### (1) Simulation of Evolution of Magnetic Island
- Evolution of magnetic island associated with an NTM is described by the modified Rutherford equation. The equation is composed of the effects of the equilibrium current profile, the bootstrap current, the toroidal geometry (Glasser-Greene-Johnson effect), the ion polarization current, and the EC-driven current. Since each term contains a coefficient which cannot be determined with high accuracy by theory alone, in JT-60U, the coefficients have been determined by comparing between TOPICS simulation and NTM experiments.
- Temporal evolution of magnetic island width of an $m/n=3/2$ NTM evaluated with the TOPICS code is shown in Fig. I.1.3-1 (a). Here, m and n are the poloidal and toroidal mode numbers, respectively. In this simulation, equilibrium and pressure profile in an NTM experiment are used, and EC wave power P_{EC} of 2.6MW, which corresponds to 4-unit injection in JT-60U, is injected from $t=7.6$ s. Other typical parameters are as follows: plasma current $I_p=1.5$ MA, toroidal field $B_t=3.6$ T, safety factor at 95% flux surface $q_{95}=3.9$, island width before EC wave injection $W(7.5s)=0.125$, full-width at half-maximum (FWHM) of ECCD profile $\delta_{EC}=0.12$, mode rational surface $\rho_s=0.4$ in the volume-averaged normalized minor radius ρ . If EC wave is deposited at the island center, the 3/2 NTM

is completely stabilized in 1.3s at $t=8.8$ s (case A in Fig. I.1.3-1(a)). If the deposition location is misaligned by 0.01 in ρ , time for stabilization is prolonged (case B in Fig. I.1.3-1(a)). Figure I.1.3-1 (b) shows the island width at $t=10$ s, $W(10s)$, for different deposition locations. As shown in this figure, stabilization effect by ECCD is significantly decreased with increasing the distance between ρ_s and ECCD location ρ_{EC} . Complete stabilization can be achieved within the misalignment of $|\rho_{EC} - \rho_s|/W(7.5s) \leq 0.5$, that is, about a half of the island width. This suggests that precise adjustment of ECCD location is essential, as recognized in experiments in JT-60U. It is notable that island width increases when the deposition location is misaligned by about W . The simulation also shows that it is mainly attributed to a destabilization effect of the ECCD term due to the misaligned injection.

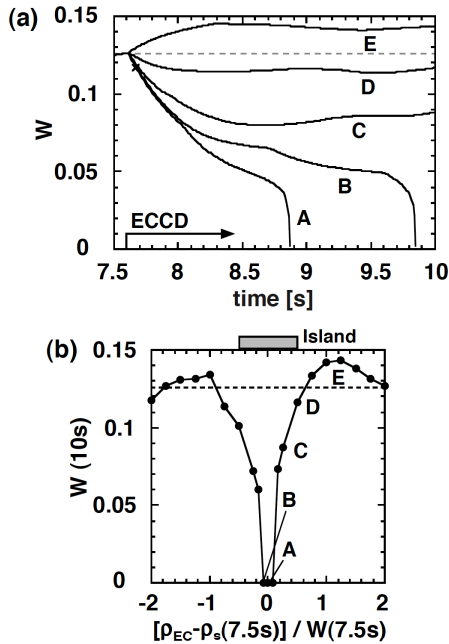


Fig. I.1.3-1 (a) Temporal evolution of magnetic island width for different ECCD locations and (b) island width at $t = 10$ s. ECCD location is fixed at $\rho=0.40$ (A), 0.39 (B), 0.43 (C), 0.46 (D) and 0.55 (E).

(2) Effect of ECCD Profile on Stabilization

In NTM stabilization, ECCD profile is important as well as injection power. The effect has been numerically evaluated by TOPICS simulation. Figure I.1.3-2 (a) shows the dependence of magnetic island width during ECCD on P_{EC} for different ECCD width. Here, W^* and δ_{EC}^* are the island width and FWHM of ECCD profile normalized by the island width before ECCD, respectively. It can be seen that the stabilization effect strongly depends on the width of ECCD profile. Since

the maximum value of the ECCD profile decreases with increasing δ_{EC}^* at fixed EC power, both δ_{EC}^* and P_{EC} must be considered in evaluating the stabilization effect. In Fig. I.1.3-2 (b), W^* is plotted as a function of δ_{EC}^* and P_{EC} . In general, magnetic island associated with an NTM is spontaneously decays due to the polarization current effect when its width is decreased to a certain value. In JT-60U, complete stabilization can be achieved for $W^* \leq 0.3$. The TOPICS code simulation shows that the threshold for complete stabilization increases with $P_{EC}^{0.6}$, which indicates that EC wave power required for complete stabilization can be significantly reduced by narrowing the ECCD width. In NTM experiments in JT-60U, EC-driven current density J_{EC} is comparable to the bootstrap current density J_{BS} at the mode rational surface. Since the ECCD profile is close to the Gaussian distribution function, the maximum current density linearly increases with decreasing the FWHM under a fixed injection power. This suggests that complete stabilization can be achieved even with $J_{EC}/J_{BS} < 1$ if narrow ECCD profile is obtained.

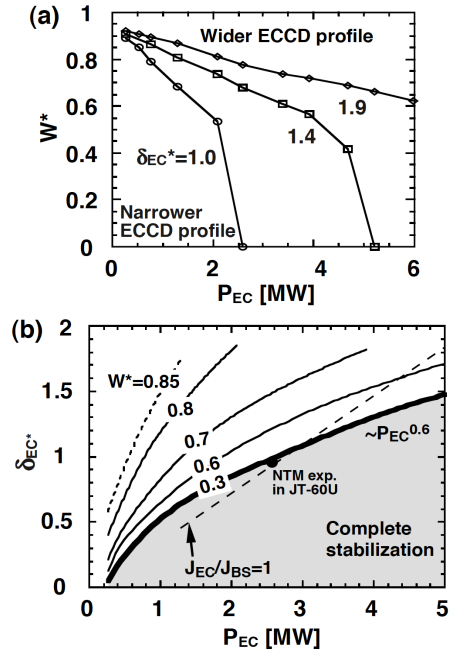


Fig. I.1.3-2 (a) Dependence of magnetic island width on EC wave power, and (b) contour plot of island width during ECCD as a function of ECCD width and EC wave power.

1.3.2 Stability of Resistive Wall Mode

Steady-state high- β plasma is required for future fusion reactors. In ideal MHD stability, achievable β is mostly limited by pressure-driven instabilities such as the kink-ballooning modes. Although these instabilities can be stabilized by placing a perfectly conducting wall (ideal wall), the actual wall has a finite resistivity and

then generates an other branch as a resistive wall mode (RWM). Therefore, the stabilization of the RWM is required for a high performance plasma. To stabilize the RWM, mainly two methods are proposed; active feedback control and plasma rotation effect. As for the RWM experiment, an advantage of JT-60U is various tangential NBs; therefore, the plasma rotation can be controlled. We have performed the RWM experiments focused on the stabilization effects due to the wall and the plasma rotation.

(1) Current-Driven RWM Experiment

1) Wall Stabilization Effect

To investigate the basic features of the RWM, we have performed current-driven RWM experiments. When q_{eff} was below 3, a instability grew with about 10 ms without oscillation and a plasma collapse was observed. Note that this mode has $m/n = 3/1$ mode structure. Since the wall skin time of JT-60U is about 10ms, this mode can be identified as the RWM. To confirm the wall stabilization effect on RWM, plasma is systematically shifted away from the outer wall. Figure I.1.3-3 shows experimental growth rates γ versus the normalized wall radius. In Fig. I.1.3-3, solid line shows the dispersion relation without plasma rotation and dissipation in cylindrical geometry. When the plasma is moved away from the wall, the growth rates of RWM become larger, as is consistent with the dispersion relation.

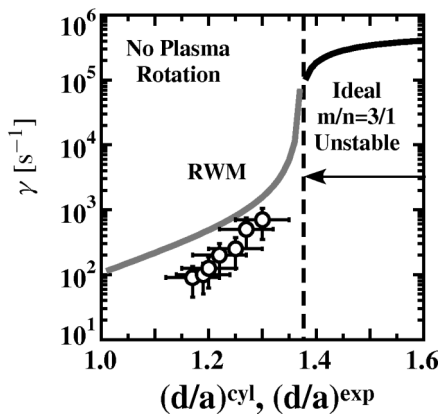


Fig. I.1.3-3 Experimental growth rates versus normalized wall radii. Solid lines show a dispersion relation without plasma rotation and dissipation.

2) Plasma Rotation Effect

To investigate the stabilization effect of the plasma rotation, we performed experiments with different plasma rotation which was controlled by tangential NBs. Figure I.1.3-4 (a) shows two profiles of the toroidal

plasma rotation V_{tor} at $\delta L = 10\text{cm}$, where δL denotes the clearance between the plasma surface and the first wall at low field side. The experimental growth rates at $\delta L = 10, 20, 30$ and 40cm with different plasma rotation are shown in Fig. I.1.3-4 (b). Note that the experimental data at zero rotation are in ohmic discharges. For the $\delta L = 10$ and 20cm case, the growth rates with a slow plasma rotation become twice smaller than that with a fast plasma rotation. However, for $\delta L = 30\text{cm}$ case, the growth rates become larger. In the case $\delta L \leq 30$, the instabilities were occurred with $q_{\text{eff}} \leq 3$, while in the $\delta L = 40\text{cm}$ case, the instabilities were observed with $q_{\text{eff}} \leq 4$. Although the resistive wall can stabilize $m/n = 4/1$ mode with wall positions $\delta L \leq 30$, the wall can no longer stabilize this mode in the $\delta L = 40\text{cm}$ case. These data shows that the plasma rotation tends to stabilize RWM. However, in this experiment, NBs, which were injected to control plasma rotation, increased a plasma pressure. Therefore, not only a current but also pressure must be considered as driving force of instabilities. Further analysis taking into account both driving force is required.

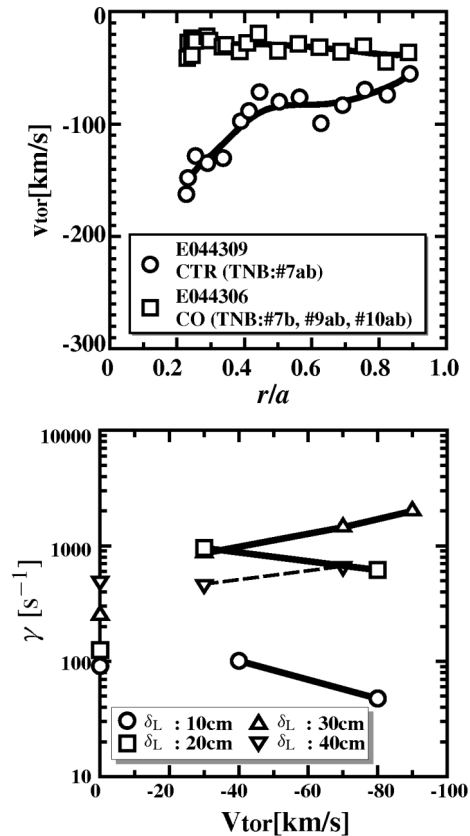


Fig. I.1.3-4 (a) Profiles of toroidal plasma rotation for current-driven RWM experiment. (b) Growth rates versus toroidal plasma rotation at the edge ($r/a = 0.9$).

(2) Pressure-Driven RWM Experiment

To induce RWM near the wall, a lot of NBs were injected to a negative shear plasma ($l_i \sim 0.7$), which has a lower critical β_N . At β_N reached 2.4, plasma disrupted with an instability (Fig. I.1.3-5). According to ideal MHD stability calculation, $\beta_{no-wall N}$ is about 2.2. The decomposed magnetic fluctuations show that $n = 1$ was dominant and the growth rate is 10ms which is similar to the wall penetration time. Consequently, we have identified that this mode is the $n = 1$ pressure-driven RWM.

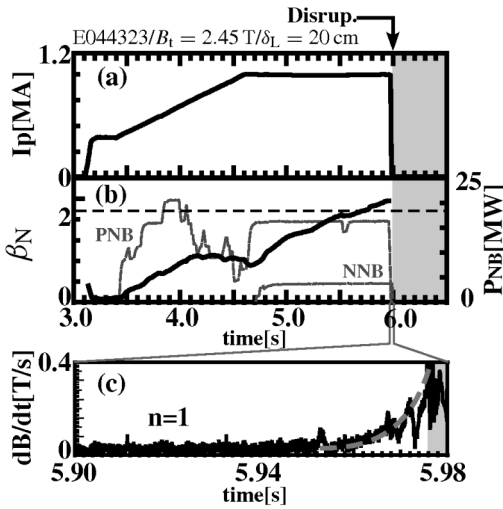


Fig. I.1.3-5 Waveforms of the pressure-driven RWM experiment. (a) Plasma current, (b) β_N and NB heating powers. (c) Normal magnetic fields fluctuation decomposed as $n = 1$.

1.3.3 Confinement Degradation of Energetic Ions due to Alfvén Eigenmodes

MHD instabilities driven by energetic ions, such as TAE, has been widely studied, because these instabilities can enhance the transport of α -particles from core region of the plasma, and then degrade the performance of burning plasmas. Recently, AEs, whose frequency rapidly sweeps and then saturate as the minimum value of the safety factor, q_{min} , decreases, which are mainly observed in reversed-shear plasmas, have been extensively studied. These frequency behavior can be explained by reversed-shear induced AEs (RSAEs) [1.3-3] or Alfvén Cascades (ACs) [1.3-4] and its transition to TAEs. In the previous studies in JT-60U, it has been reported that the transition phase was most unstable. However, the effect of these AEs on confinement of energetic ions has not been understood yet. In this work, the effect due to these AEs has been

investigated. Figure I.1.3-6 shows time trace of (a) q_{min} and (b) frequency spectrum of $n = 1$ instabilities measured by Mirnov coils in the NNB injected weak reversed shear plasma (E43978, $B_T = 1.7T$, $I_p = 1.0MA$, $P_{NNB} = 4.0MW$, $E_{NNB} = 370keV$). Frequency of these instabilities swept up rapidly and saturated as q_{min} decreased from 4.6 to 5.5s. After that, these instabilities were almost stabilized. Thick broken lines in Fig. I.1.3-6 (b) denote estimated frequency of $n = 1$ AEs with RSAE model described in Ref. 1.3-3. As shown in Fig. I.1.3-6 (b), observed frequency behavior can be explained by RSAEs and its transition to TAEs. Solid line in Fig. I.1.3-6 (c) shows time trace of total neutron emission rate (Sn). Increase of Sn was suppressed with RSAEs and TAEs. After these AEs were stabilized at $t \sim 5.5s$, the increasing rate of Sn was enhanced rapidly. This suggests confinement degradation of energetic ions due to these AEs. Then, in order to evaluate how confinement of energetic ions was degraded, Sn was calculated with OFMC code, taking into account the changes in the bulk plasma. The calculation was performed assuming that the confinement was classical and beam-thermal neutron was dominant. Actually, beam-thermal neutron emission rate accounted for $\sim 90\%$ of total neutron emission rate according to the

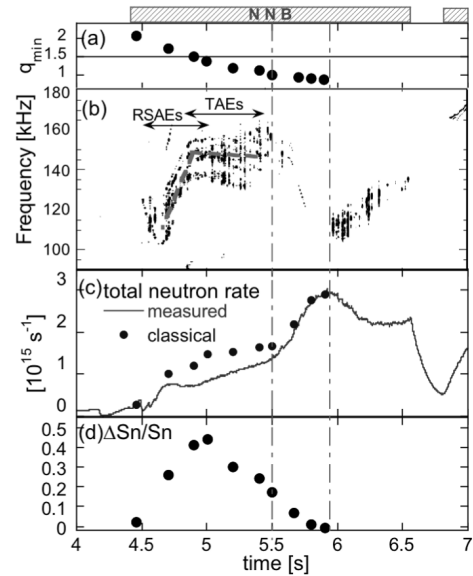


Fig. I.1.3-6 Time trace of (a) q_{min} , (b) frequency spectrum of magnetic fluctuation. Thick broken lines denote estimated frequency from the RSAE model. Frequency behavior can be explained by RSAEs and its transition to TAEs. Time trace of (c) measured total neutron emission rate (solid line) and calculated one by classical theory (classical) (circle) (d) reduction rate of Sn.

calculation with a transport code TOPICS. Shown in circles of Fig. I.1.3-6 (c) is calculated S_n by classical theory. It is found that measured S_n is smaller than calculated one in the presence of these AEs. Whereas, after AEs were stabilized, measured one became close to calculated one, then was consistent with that at $t \sim 5.9$ s. This evaluation indicates confinement degradation of energetic ions due to AEs was confirmed. Fig. I.1.3-6 (d) shows time trace of reduction rate of S_n , which was estimated from the ratio of measured S_n to calculated one. One can see that the rate is largest in the transition phase from RSAEs to TAEs. The previous studies that the transition phase from RSAEs to TAEs was most unstable [1.3-3] support this result. Here, the maximum reduction rate is estimated as $(\Delta S_n/S_n)_{\max} \sim 45\%$ at $t \sim 5.0$ s. Confinement degradation of energetic ions in the presence of RSAEs and TAEs is quantitatively evaluated for the first time [1.3-5].

References

- 1.3-1 Isayama, A., *et al.*, *Plasma Sci. Technol.*, **8**, 36 (2006).
- 1.3-2 Nagasaki, K., *et al.*, *Nucl. Fusion*, **45**, 160 (2005).
- 1.3-3 Akechi, M., *et al.*, *Phys. of Plasmas*, **12**, 82509 (2005).
- 1.3-4 Berk, H.L., *et al.*, *Phys. Rev. Lett.*, **87**, 185002 (2001).
- 1.3-5 Ishikawa, M., *et al.*, "Observation of Confinement Degradation of Energetic Ions due to Alfvén Eigenmodes in Weak Shear Plasmas on JT-60U," submitted to *Nucl. Fusion*.

1.4 H-mode and Pedestal Research

1.4.1 Roles of Plasma Rotation and Toroidal Field Ripple on H-mode Confinement in JT-60U [1.4-1]

The edge pedestal structure characterized by the formation of the H-mode edge transport barrier (ETB) is known to determine the boundary condition of the heat transport in the plasma core. It has prevalently been believed that the $\mathbf{E} \times \mathbf{B}$ flow shear in the peripheral region plays an important role in suppressing the level of turbulence and in reducing correlation length of the turbulence that helps the formation of the ETB structure. In ITER, the toroidal field ripple is estimated as 0.5-1%. However, the influence of the toroidal field ripple on the pedestal structure and plasma confinement quality is not known. It is presumed that the toroidal field ripple induces the toroidal rotation towards the counter direction. It is likely that in the peripheral region the ripple loss of fast ions produces an inward electric field, which drives the counter-directed toroidal rotation. In this study, conducting the power scans for a variation of the toroidal momentum sources, the characteristics of the H-mode confinement have been investigated. Although it is hard to modify the arrangement of the toroidal field coils from the viewpoint of the technological constraint, the effect of the toroidal field ripple can be examined by changing the plasma configuration.

The experiments were carried out at three cases of geometrical configurations. With increasing the plasma volume V_p from 'small' ($V_p \sim 52\text{m}^3$), 'medium' ($V_p \sim 65\text{m}^3$)

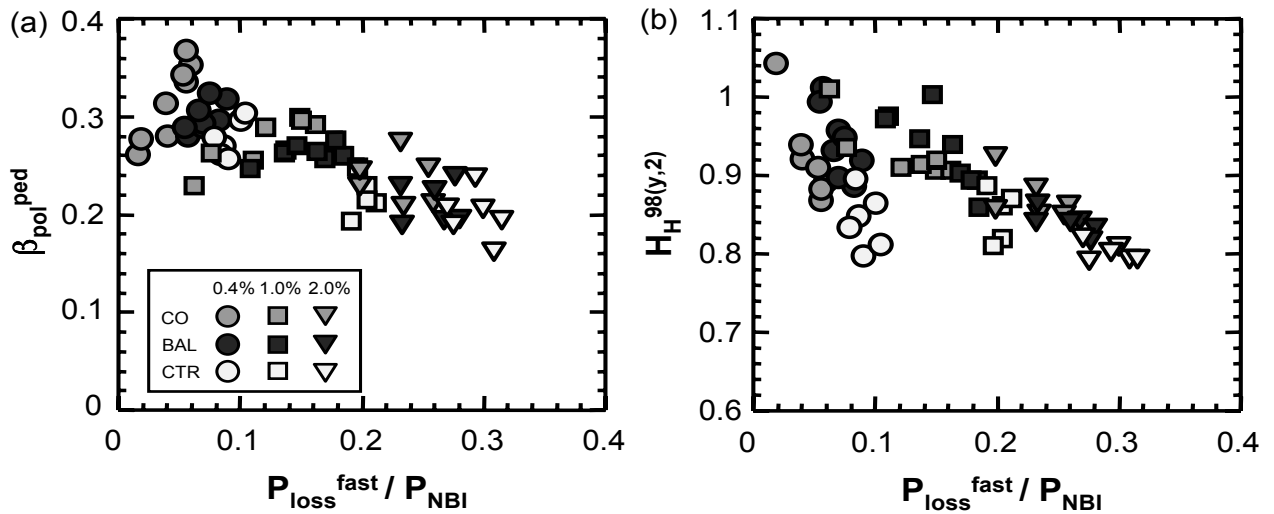


Fig. I.1.4-1 (a) Dependence of the β_{pol}^{ped} on P_L^{fast} / P_{in} . (b) Dependence of the H_H -factor based on the IPB98(y,2) scaling on P_L^{fast} / P_{in} .

and 'large' size ($V_p \sim 75\text{m}^3$) in turn, the toroidal field ripple increases from 0.4, 1.0 and 2.0%, respectively. Figure I.1.4-1(a) shows the dependence of the $\beta_{\text{pol}}^{\text{ped}}$ on the ratio of the loss power of the fast ions to the NB injection power or $P_L^{\text{fast}}/P_{\text{in}}$. It is found that the $\beta_{\text{pol}}^{\text{ped}}$ tends to increase when the fast ions' loss power fraction decreases. The observed increase of $\beta_{\text{pol}}^{\text{ped}}$ at fixed toroidal field ripple and momentum source comes from the increased absorbed power. When β_{pol} in the plasma core is raised by high power heating, it has been known that the MHD stability boundary at the plasma edge is improved. Figure I.1.4-1(b) shows the dependence of the H_H -factor on $P_L^{\text{fast}}/P_{\text{in}}$. It is shown that operating at smaller loss power fraction of fast ions does not always produce high energy confinement while the achievable confinement performance tends to decrease with increasing $P_L^{\text{fast}}/P_{\text{in}}$. The H-mode plasmas with the toroidal momentum source heading for the co-direction are sensitive to the ripple loss of fast ions.

The H-mode plasmas with small ripple loss at the momentum source for co-direction clearly show the highest performance. However, the energy confinement with the toroidal momentum source heading for the ctr-direction does not vary when the ripple loss of fast ions is changed.

One can find that the toroidal plasma rotation for co-direction displays its potential on the improvement of the energy confinement through the enhanced pedestal pressure. The temperature profiles in the H-mode plasmas are in many cases characterized by the minimum critical scale length of the temperature gradient L_T . Thus, it will be investigated whether the high confinement with the momentum source in the co-direction is due to the change of the critical L_T or the increase of the pedestal temperature.

1.4.2 Characterization of Type-I ELMs in Tangential Co-, Balanced-, and Counter- Plus Perpendicular NBI Heated Plasmas on JT-60U [I.4-2]

Effects of plasma rotation on the Type-I ELM characteristics have been systematically studied in the JT-60U tokamak, scanning combinations of NBI (tangential co-, balanced-, and counter-NBI plus perpendicular NBI) in the three different plasma volume to change the toroidal field ripple at the plasma edge, corresponding ripple amplitude for small, medium and large volume plasma were $\delta_r \sim 0.4, 1.0$ and

2.0%, respectively. We performed the following experiment under the condition of the plasma current, $I_p = 1.2\text{MA}$ and toroidal magnetic field, $B_1 = 2.6\text{T}$ at the $n_e/n_{\text{GW}} \sim 0.4-0.5$ with $q_{95} \sim 4.1$.

Figure I.1.4-2 shows the ELM characteristics in the small volume plasma case. As can be seen in Fig. I.1.4-2(a), ELM frequency, f_{ELM} , increased with the heating power crossing the separatrix, P_{SEP} , as $df_{\text{ELM}}/dP_{\text{SEP}} \geq 0$. This power dependence in the f_{ELM} was

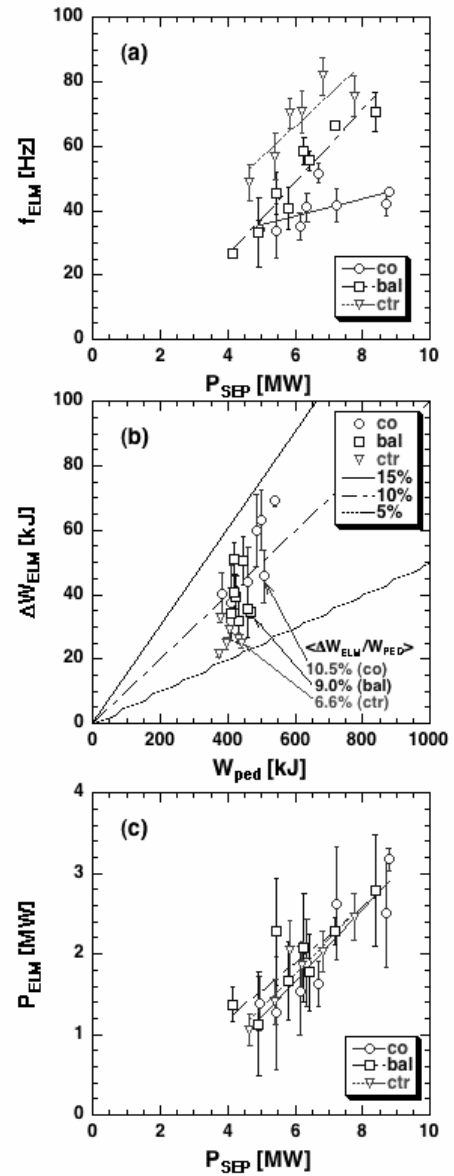


Fig. I.1.4-2 Plots of (a) ELM frequency versus heating power crossing the separatrix, (b) ELM energy loss versus pedestal stored energy, and (c) power loss due to ELM, $P_{\text{ELM}} (= \Delta W_{\text{ELM}} \times f_{\text{ELM}})$, normalized by P_{SEP} . These data are taken in the small volume configuration. Circles, squares and inverse-triangles indicate the tangential co-, balanced-, and counter-, plus perpendicular-NBI heated plasmas, respectively.

confirmed in all plasma configurations and so that observed ELM in these scan could be classified into type-I ELM.

The ELM energy loss normalized by pedestal stored energy, $\Delta W_{\text{ELM}}/W_{\text{ped}}$, appears to be smaller when the external momentum input is in the counter direction, especially in small volume configuration case as shown in Fig.I.1.4-2(b). Although each data point has somewhat large statistic error, the averaged value, $\langle \Delta W_{\text{ELM}}/W_{\text{ped}} \rangle$, in the co-NBI discharge is significantly higher than that in the counter-NBI. In this analysis, it is noted that each ΔW_{ELM} is the averaged value during ELM cycles over an interval of $\Delta T \sim 100\text{ms}$, and the corresponding error bar is its statistical error of this averaging process.

The most interesting point is the dependences of the power loss due to ELM, $P_{\text{ELM}} (= \Delta W_{\text{ELM}} \times f_{\text{ELM}})$, normalized by P_{SEP} , which is constant among co-, balanced, and counter-NBI, suggesting that the power loss due to inter-ELM transport, $P_{\text{inter-ELM}}$, is almost unchanged among co-, balanced, and ctr-NBI plasmas (i.e. $P_{\text{inter-ELM}}/P_{\text{SEP}} \sim 1 - P_{\text{ELM}}/P_{\text{SEP}}$). As a result, we have demonstrated that ELM energy loss can be controlled by means of counter-NBI in a clear Type-I ELM regime, while keeping confinement quality fixed. On the other hand, when the plasma configuration changed from small to middle and large, the $P_{\text{ELM}}/P_{\text{SEP}}$ decreases with increasing the plasma volume, suggesting an increase in the inter-ELM transport.

1.4.3 Pedestal Conditions for Small ELM Regimes in Tokamaks [1.4-3]

Several small/no ELM regimes such as EDA, grassy ELM, HRS, QH-mode, type II and V ELMs with good confinement properties have been obtained in Alcator C-Mod, ASDEX-Upgrade (AUG), DIII-D, JET, JFT-2M, JT-60U and NSTX. All these regimes show considerable reduction of instantaneous ELM heat load onto divertor target plates in contrast to conventional type I ELM, and ELM energy losses are evaluated as less than 5% of the pedestal stored energy. In order to compare the pedestal conditions in these many regimes, they have been categorized into four main groups (grassy ELM regime, type II ELM regime, QH-mode regime and enhanced recycling with high v_e^* regime) in terms of ELM energy loss and pedestal electron collisionality v_e^* , which plays a significant role in

pedestal stability through modification of the edge bootstrap current. Moreover, ITER will have a low collisionality pedestal.

Achieved pedestal pressure in the type II ELM regime is comparable to the usual type I ELM regime in spite of the existence of edge fluctuations. Moreover, higher pedestal pressure can be obtained in JET. Because of a requirement of high density, the edge collisionality remained at moderate values ($v_e^* > 0.8$). It should be noted that a narrow operational window in density ($0.85 < \bar{n}_e^{\text{ped}} / n_{\text{GW}} < 0.95$) is observed in AUG.

On the other hand, the grassy ELM regime was found in JT-60U as another small ELM regime at lower v_e^* in high β_p plasmas with simultaneously high q_{95} and high δ . In recent experiments on JET and AUG, grassy-like ELMs were also observed following the grassy ELM prescription with high β_p plasmas ($\beta_p > 1.7$) at high q_{95} ($q_{95} \sim 7$) and high triangularity ($\delta > 0.4$).

Figure I.1.4-3 shows the comparison of the non-dimensional operational regime in β_p - δ space between high n_e type II ELM and grassy ELM regimes.

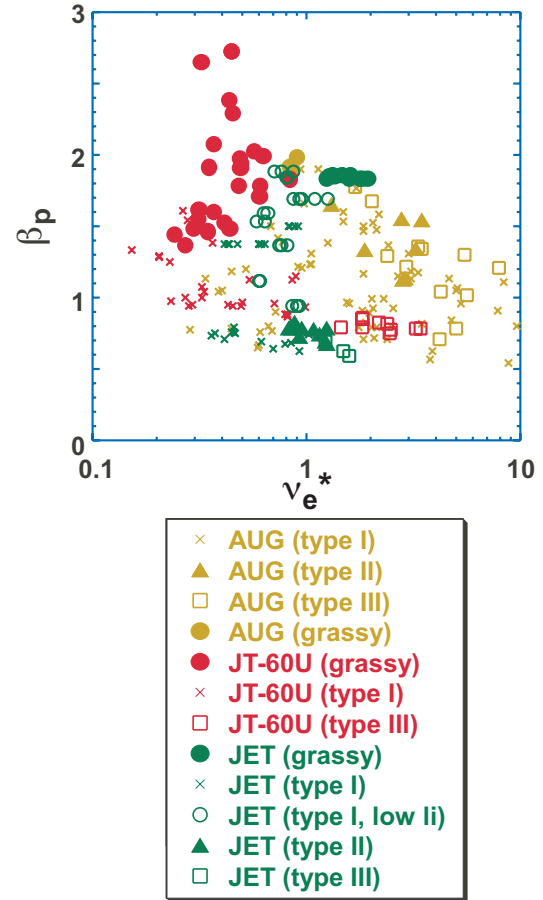


Fig. I.1.4-3 Operational space in v_e^* versus β_p for small/no ELM regimes and type I/III ELM regime.

It suggests that there is not a large requirement of poloidal beta β_p for type II ELM in contrast to the grassy ELM regime. On the other hand, a quasi-double null (QDN) configuration is required in AUG, where the typical operational value is $\delta > 0.4$.

As can be seen in Fig. I.1.4-3, grassy ELMs can be obtained at low collisionality of ~ 0.3 in JT-60U. Nevertheless, achieved v_e^* in grassy ELM plasmas was comparable to type II ELM plasmas in JET. It is noted that no significant edge fluctuations related to enhanced losses were observed in any devices with grassy ELMs.

The required condition to enter the small/no ELM regimes in terms of the plasma shape is also important to investigate further, because ITER cannot operate using a double null configuration and Δ_{sep} (the distance between the separatrix and the flux surface through the upper X-point at the outer midplane) should be kept larger than 4cm. So far, a QDN configuration is required both for type II ELMs and for grassy ELMs in AUG. In JET, type II ELM does not require QDN configuration, while grassy ELM has been observed in QDN configuration so far. Grassy ELMs in JT-60U have often been observed for lower single null (LSN) operation without a second separatrix and type V ELM in NSTX also requires LSN configuration. On the other hand, higher δ is an important condition for small ELM regimes. Since it is difficult to separate between effects of δ and Δ_{sep} in some devices due to the hardware limitations, we should consider these issues in further experiments.

References

- 1.4-1 Urano, H., *et al.*, *Plasma Phys. Control. Fusion*, **48**, A193 (2006).
- 1.4-2 Kamiya, K., *et al.*, *Plasma Phys. Control. Fusion*, **48**, A131 (2006).
- 1.4-3 Oyama, N., *et al.*, *Plasma Phys. Control. Fusion*, **48**, A171 (2006).

1.5 Divertor/SOL Plasmas and Plasma-Wall Interaction

1.5.1 Fluctuations in High- and Low-Field-Side SOL

Study of the ELM radial propagation to the first wall was presented in the 32nd EPS [1.5-1] with improving sampling rate of 500kHz for the Mach probes (at outer midplane and X-point) and magnetic pick-up coils. In 2005, measurement of the plasma fluctuations both at HFS and LFS SOLs has been, for the first time, performed in JT-60U since electrodes of the HFS reciprocating Mach probe was repaired. Statistical analysis such as a probability distribution function (p.d.f.) described intermittent (non-diffusion) transport in SOL plasma fluctuations as shown in Fig.I.1.5-1 [1.5-2]. Fluctuation level of the ion saturation current ($\delta j_s / \langle j_s \rangle$) at HFS was 1/3-1/10 smaller than that at LFS. It was found that the positive bursty events appeared most frequently at LFS midplane distance from separatrix (Δr) ~ 5 cm, and flat far SOL was formed in outer flux surfaces ($\Delta r > 5$ cm). Positive bursty events were seen in wide SOL radii ($\Delta r < 7$ cm) only at LFS midplane, where the “flow reversal” of the SOL plasma was observed. Influences of the radial transport of the convective blobby plasma on the SOL formation and the flow reversal were investigated.

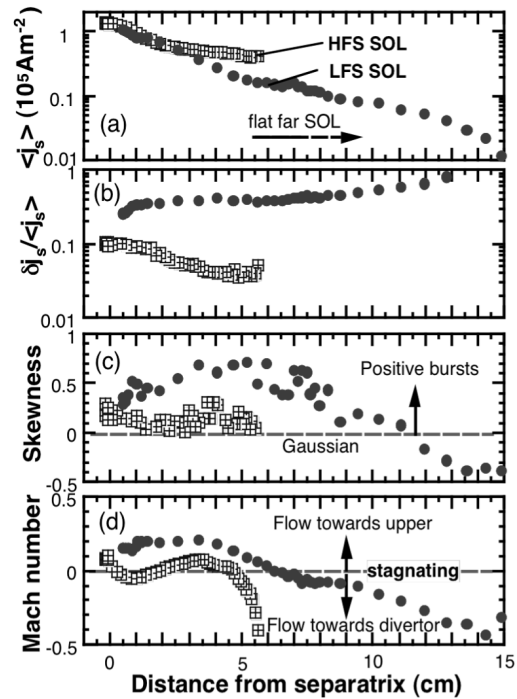


Fig. I.1.5-1 (a) j_s profiles measured with LFS midplane (circles) and HFS (squares) Mach probes in L-mode. (b) fluctuation level of j_s , (c) Skewness, (d) Mach number. HFS baffle is located at the flux surface of 6cm LFS midplane distance.

1.5.2 Modeling of Divertor Pumping Using SOLDOR/NEUT2D Code

To characterize the divertor pumping for particle and heat control in the SOL/divertor, simulations using the SOLDOR/ NEUT2D code developed originally [1.5-3] were performed to the JT-60U long pulse discharge [1.5-4]. The simulation reproduces the neutral pressure and pumping flux in the exhaust chamber at the experiment by treating the desorbed flux from the wall similar as the gas puff flux (Fig. I.1.5-2). Heat loads on the divertor targets satisfy the heat balance consistently. Parametric survey shows the pumping efficiency (ratio of pumping flux to generated flux around the divertor targets) [1.5-5] increasing with the pumping speed. It is found that the pumping speed higher than the present capability ($26\text{m}^3/\text{s}$) is necessary for the active particle control under the wall saturation condition. On the other hand, shortening the strike-point distance (distance from extension point of the private dome wing on the divertor target to the strike point) from 10cm to 2cm, the pumping efficiency is enlarged by a factor of 1.5 with increase of the viewing angle from strike point to pumping slot and the incident flux into exhaust chamber.

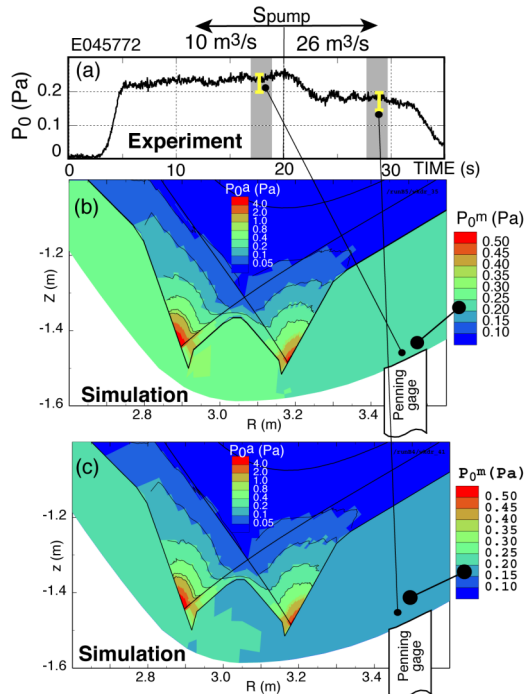


Fig. I.1.5-2 (a); Time evolutions of neutral pressure in front of penning gage, when the pumping speed S_{pump} is increased from $10\text{m}^3/\text{s}$ to $26\text{m}^3/\text{s}$ at $t = 20\text{s}$ in JT-60U long pulse discharge under the wall saturation condition. (b) and (c); Simulated contour plots of neutral pressure (molecular pressure in the exhaust chamber and atom pressure in the divertor region) for (b) $S_{\text{pump}}=10\text{m}^3/\text{s}$ and (c) $S_{\text{pump}}=26\text{m}^3/\text{s}$.

A virtual tilt of the divertor targets to 15° vertically enhances the pumping efficiency by a factor of 1.2 with a low target heat load.

1.5.3 Two-Dimensional Structure of Volume Recombination of Hydrogen and Impurity Ions

In order to investigate two-dimensional structure of divertor plasmas, a spectrometer with 92 viewing chords (vertically 60ch and horizontally 32ch) has been prepared, and a computer tomography technique using a maximum entropy method has been developed. Figure I.1.5-3 shows reconstructed emission profiles of D I ($n=2-5$) and C IV ($n=6-7$) during an X-point MARFE. The emission peaks of D I ($n=2-5$) are found above the outer and the inner strike point. In contrast, the emission peak of C IV ($n=6-7$) is found in the main plasma just above the X-point. Because these two lines are emitted predominantly, resulting from volume recombination of D^+ and C^{4+} , respectively, these emission profiles are interpreted as the two-dimensional structures of volume recombination.

Because the ratio of D I ($n=2-6$) to D I ($n=2-5$) gives electron temperature of recombining plasma, the two-dimensional structure of electron temperature can

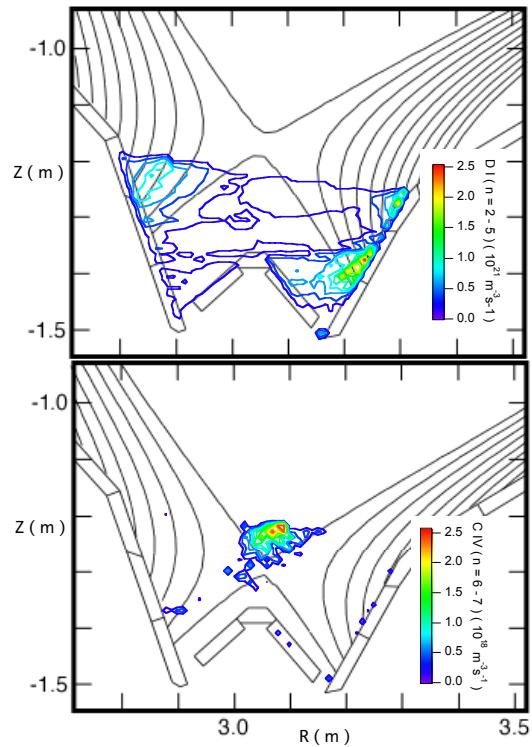


Fig. I.1.5-3 Emissivity of (a) D I ($n = 2-5$) and (b) C IV ($n = 6-7$) during an X-point MARFE, reconstructed by a computer tomography technique (tentative version for demonstration).

be obtained from the ratio of the reconstructed emission profiles of these lines. This method is in progress.

1.5.4 Emission Rates of CH/CD and C₂ Spectral Bands for Loss-Events of CD₄ and C₂H₆

To evaluate hydrocarbon sputtering flux from emission intensities of CH/CD and C₂ spectral bands, the numbers of CH/CD and C₂ photons until one hydrocarbon molecule is ionized in plasma, are required. The reciprocals of these numbers, hereafter called loss-events / photon, have been measured.

To measure the CD₄-loss-events / CD photon, CD₄ was injected at a known rate into the outer divertor plasma. The CD emission was measured along two similar viewing chords: one views the plasma in front of the gas-puff nozzle and the other does not. The difference of the CD emission measured with the two viewing chords is originated from the injected CD₄. Hence, the CD₄-loss-events/CD photon was determined as the ratio of injected CD₄ flux to the difference of the CD emission. Similar measurements for C₂H₆ to determine the C₂H₆-loss-events/CH photon and the C₂H₆-loss-events/C₂ photon were done [1.5.6].

Figure I.1.5-4 shows the measured loss-events/photon. The loss-events/photon is positive dependence on the electron temperature, which is similar to those measured in PISCES [1.5.7]. It was found that that dependence of C₂H₆-loss-events/C₂ photon is stronger than that of C₂H₆-loss-events/CH photon. In addition, at 20eV, the absolute values agree within a factor of 2. The data obtained in the present work will be used to measure the CH₄/CD₄ and C₂H_x/C₂D_x sputtering yields.

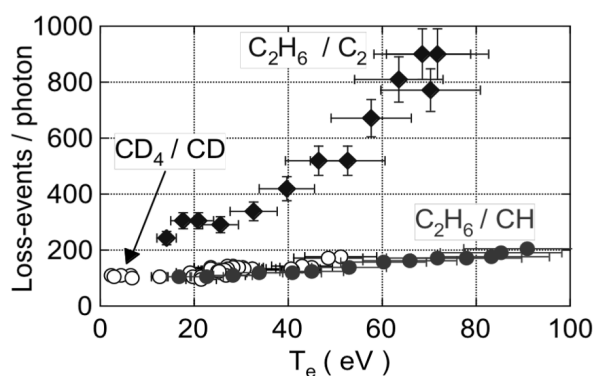


Fig. I.1.5-4 Loss-events as a function of electron temperature. Open circles indicate the ratio of CD₄-loss-events to a CD-spectral-band photon, closed circles and diamonds the ratios of C₂H₆-loss-events to a CD- and to a C₂-spectral-band photon, respectively.

1.5.5 Carbon Deposition and Hydrogen Isotope Retention in the JT-60U Plasma Facing Wall

Erosion/deposition analyses for the plasma facing wall showed that deposition was dominant at the inner divertor (A) and the outer dome wing (C), whereas erosion dominant at the outer divertor (D) and the inner dome wing (B) (Fig. I.1.5-5). The upper area of the first wall was mainly eroded, while the bottom area of the inboard wall was deposition dominated [1.5-8]. In deposition analyses for the plasma shadowed area, thick deposition (~several 10μm) was observed on the bottom side of the outer dome wing tile, and no deposition was found on the bottom edge of the inner divertor tile. These results indicated that local transport of eroded carbon to inboard direction plays an important role on the carbon redeposition process.

Distribution of deuterium and hydrogen retained in graphite tiles placed in the divertor region of JT-60U with the both side pumping geometry was investigated by thermal desorption spectroscopy. The retention of hydrogen isotopes is nearly proportional to the thickness of carbon redeposited layers, though their concentration changes with the location of the tiles. The least concentration of ~ 0.02 in (H+D)/C is found in the redeposited layers on the inner divertor tile. This value agrees well with H/C of ~0.030 observed for the redeposited layers on the divertor tiles exposed to HH discharges in the JT-60 open divertor, and H+D/C of ~0.032 in the inner divertor tiles exposed to the DD discharges in the JT-60U with the inner side pumping system. Rather high hydrogen concentration is found in the redeposited layers on plasma-shadowed area.

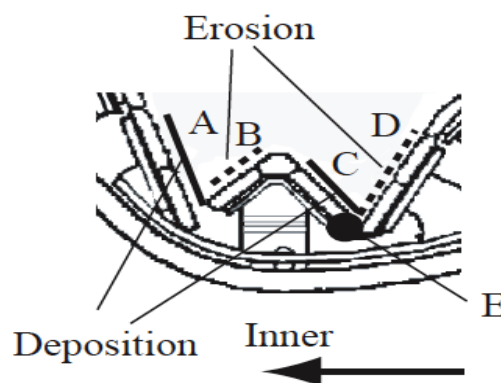


Fig. I.1.5-5 Location of the erosion and deposition dominated area in the JT-60U W-shaped divertor. The results showed the eroded carbon was transported to the inboard direction. The highest hydrogen isotope retention was found at the bottom side of the outer dome wing tile (E).

In particular, the redeposited layers on the bottom side of the outer wing tile (see Fig. I.1.5-5,E) shadowed from plasma and facing to the pumping slot shows the highest concentration of ^{13}C in (H+D)/C [1.5-9]. In JT-60U, however, the deposition at the shadowed area is very small, which is a candidate to explain the smallest total retention in the divertor area compared with other large tokamaks.

1.5.6 ^{13}C Tracing and Deposition

To clarify the transport and deposition places of carbon impurities, the $^{13}\text{CH}_4$ gas puffing experiment was carried out in JT-60U [1.5-10]. Figure I.1.5-6 shows the location of the gas puffing port and a plasma configuration for the experiment. The total of $\sim 2 \times 10^{23}$ $^{13}\text{CH}_4$ molecules was puffed into 13 L-mode plasma discharges. Deposition layers of thicker than $200\mu\text{m}$ were observed on the outer divertor tile adjacent to the gas puffing port. The poloidal distribution of the ^{13}C deposition adjacent to the $^{13}\text{CH}_4$ gas puffing port agrees well with that of the positioning frequency on the outer divertor tiles. Therefore it is considered that a large amount of carbon impurity generated at the outer divertor re-deposited near eroded place and was transported by repetition of erosion and redeposition.

Although the first wall located in the inner side was thought to be exposed to SOL plasma during the discharges, deposited ^{13}C on the first wall was the lowest among the analyzed tiles. This suggests that carbon impurities transport from the inner to the outer divertor region through SOL takes a long term. The ^{13}C

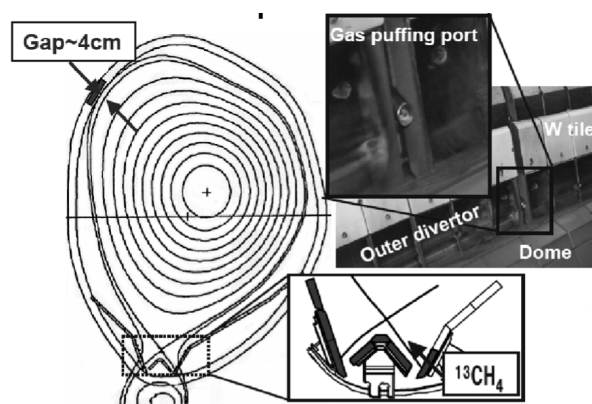


Fig. I.1.5-6 Location of the gas puffing port and a plasma configuration for the experiment. Thirteen L-mode discharges were performed at almost same plasma configuration. Totally, 2.0×10^{23} ^{13}C were puffed during the discharges.

surface density peaked at the lower side of the inner striking point on the inner divertor tile as shown in Fig. I.1.5-7. It is suggested that a large part of ^{13}C puffed from the outer divertor is transported through the drift flux toward the inner divertor. This result indicates the existence of another transport path of carbon impurities generated in the outer divertor region in addition to the SOL flow.

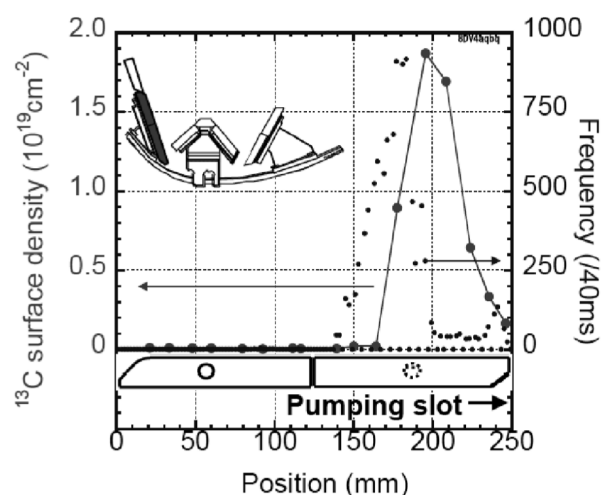


Fig. I.1.5-7 ^{13}C surface density of the inner divertor tile and frequency distribution of inner divertor leg. The peak position of the ^{13}C surface density was found at the lower side (i.e. near pumping slot) of the strike point.

References

- 1.5-1 Asakura, N., *et al.*, Proc. 32nd EPS Plasma Phys. Conf., P5.006 (2005).
- 1.5-2 Miyoshi, H., *et al.*, Proc. 32nd EPS Plasma Phys. Conf., P1.045 (2005).
- 1.5-3 Kawashima, H., *et al.*, Plasma and Fusion Res., **1**, 031 (2006).
- 1.5-4 Kawashima, H., *et al.*, Proc. 17th PSI conf., Hefei P1-78 (2006).
- 1.5-5 Kawashima, H., *et al.*, Fusion Eng. Design, **81**, 1613 (2006).
- 1.5-6 Nakano, T., *et al.*, Proc. 32nd EPS Plasma Physics Conf., P-5.007 (2005).
- 1.5-7 Pospieszczyk, Y.R., *et al.*, UCLA-PPG-1251 (1989).
- 1.5-8 Oya, Y., *et al.*, "Hydrogen Isotope Behavior in the First Wall of JT-60U after DD Discharge," Proc. 12th ICFRM (2005) to be published in J. Nucl. Mater..
- 1.5-9 Hirohata, Y., *et al.*, "Distribution of Hydrogen Isotopes Retained in the Divertor Tiles Used in JT-60U," Proc. 12th ICFRM (2005) to be published in J. Nucl. Mater..
- 1.5-10 Ishimoto, Y., *et al.*, "Transport of Carbon Impurity Using $^{13}\text{CH}_4$ Gas Puffing in JT-60U," Proc. 12th ICFRM (2005) to be published in J. Nucl. Mater..

2. Operation and Machine Improvements

Two cycles of the JT-60 operation were implemented in FY 2005, which included 945 shots of plasma pulse discharge, 104 shots of commissioning pulse sequence, 30 hours of Taylor-type discharge cleaning and 323 hours of glow discharge cleaning.

In order to reduce a large ripple of toroidal field, which had been considered to limit operational performance of large-volume plasmas in JT-60U, ferritic steel tiles were newly installed as a part of the first wall in place of carbon tiles during the maintenance period in 2005. To compensate the magnetic influence of the ferritic tile insertion on plasma equilibrium, a new real-time program was developed to correct the magnetic sensor signals including poloidal magnetic field and flux from the ferritic steel magnetized by the toroidal magnetic field. The plasma magnetic surface calculated in consideration of the ferritic tiles agrees to the separatrix line reproduced by CXRS measurement results near the upper port within a few centimeters in the largest magnetization case at $B_t=2T$. After careful confirmation of position and shape reconstruction accuracy, JT-60 experiments were successfully performed on schedule.

2.1 Tokamak Machine

2.1.1 Improvement of Pellet Injector for Long Pulse Operation

In order to extend the JT-60 operation to high density regime and to investigate the impact of particle fuelling on confinement and pedestal parameters, the pellet injector has been under modification to have long injection duration (~ 60 s) and high repetitive injection frequency (≤ 20 Hz). The pellet extruder was changed from the piston type to the screw type (Fig. I.2.1-1). This screw type pellet extruder can produce a 2.1 mm x 2.1 mm ice rod with an extrusion speed of 46 mm/s for 60 s or with a extrusion speed of 38 mm/s for 360 s. The new screw type pellet extruder was assembled into the present centrifugal pellet injector used for JT-60U. The production of a transparent ice rod has been confirmed in some operation conditions. The liquefier and nozzle temperatures are being optimized.

2.1.2 Installation of Supersonic Molecular Beam

Supersonic molecular beam injectors (SMBI) were installed both at the high-field-side and low-field-side of the JT-60U Vacuum Vessel in collaboration with CEA Cadarache. The injector head is the same as that installed in Tore Supra (Fig. I.2.1-2). The SMBI can be operated with a frequency of 8-10 Hz and 2 ms duration per pulse. Theoretical gas flow was evaluated to be $510 \text{ Pam}^3/\text{s}$ with a Mach number of 4.1 (speed of 2.2 km/s) at operation temperature of 150°C and fueling pressure of 0.5 MPa. The particle fueling to a plasma with the SMBI is expected to be deeper than gas puffing, but shallower than pellet injection. The gas injection test into the JT-60U vacuum vessel was carried out using helium gas at operation temperature of 150°C and fueling pressure of 0.2 MPa. The amount of injected gas from the low-field-side injector was estimated to be 0.14 Pam^3 per pulse.

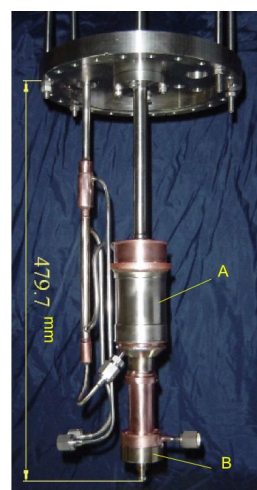


Fig. I.2.1-1 The screw type pellet extruder installed into the centrifugal pellet injector of JT-60 (A: Liquefier, B: Nozzle).

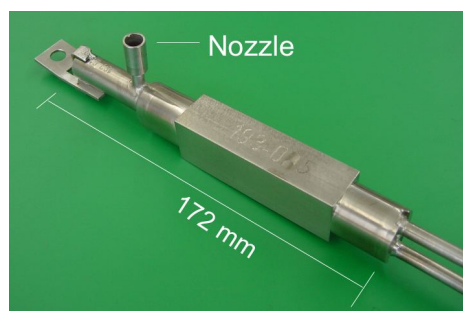


Fig. I.2.1-2 An injector head of the Supersonic molecular beam injector (SMBI) installed both on the inboard and outboard side in the vacuum vessel.

2.1.3 Installation of Ferritic Steel Tiles as the Outboard First Wall [2.1-1]

In order to reduce the toroidal magnetic field (TF) ripple, 8Cr-2W-0.2V ferritic steel tiles were installed at the out board wall inside the vacuum vessel (Fig. I.2.1-3). 8Cr-2W-0.2V ferritic steel was selected among candidate ones such as F82H developed as a low activation ferritic steel, because the saturated magnetization of 8Cr-2W-0.2V ferritic steel was high enough for the experiments planned with the toroidal magnetic field, and the low activation was not critical at the present level of neutron production in JT-60. By August 2005, 1122 carbon tiles near the inside of the TF coils were replaced to ferritic steel tiles with reinforcement of stud nuts. The dimensions of the most tiles are 130 mm(length) x 185 mm(width) x 23 mm(thickness), which is 2 mm thinner than the carbon tiles. The surfaces position of the ferritic tiles were arranged at more than 1.5mm below those of the carbon tiles. Slits were made in each tile to reduce the electromagnetic force due to eddy current.

Fifty-five plates of 8Cr-2W-0.2V ferritic steel were manufactured from the 2.6 ton ingots made by 20 ton vacuum induction melting in January 2006. Magnetic properties of the ferritic steel plates fabricated in large scale melting were investigated. It was shown that the average saturated magnetization was 1.838 Tesla, and the confidence interval of 95% was between 1.833 and 1.843 Tesla at ambient temperature. The variation among the plates fabricated was confirmed to be

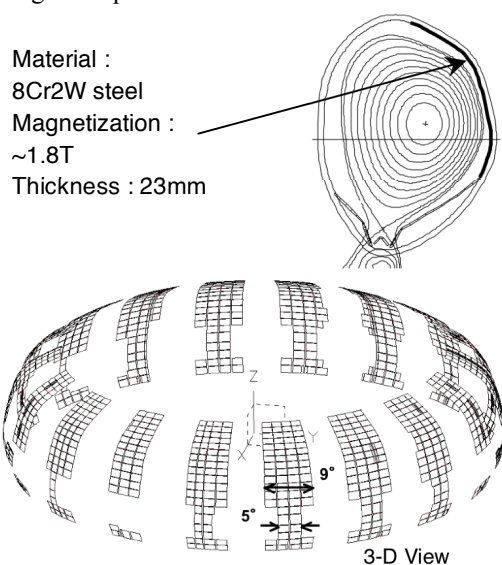


Fig. I.2.1-3 Ferritic steel tiles installed at the out board wall inside the JT-60U vacuum vessel.

sufficiently small. The saturated magnetization was 1.66 Tesla at 573 K, the maximum baking temperature of the relaxation of the activation-element. Although it was lower than the expected value, it was confirmed by a numerical calculation that the saturated magnetization of 1.7 Tesla was still sufficient for the JT-60 experiment.

2.1.4 Study of the Plasma-Surface Interaction

The cooperative research program between JAEA and universities using the JT-60 first wall tile was initiated in 2001. Under the program, various studies on the plasma facing materials have progressed. Major research activities conducted in FY 2005 except for the results mentioned in Section I.1.5 [1.5-8, 1.5-9, 1.5-10] are as follows:

(1) Measurement of Tritium Distribution at the Tile Gap [2.1-2]

Tritium retention on the side surfaces which locate at gaps between the W-shaped divertor tiles was analyzed by the imaging plate technique and a combustion method. The samples measured were exposed in the plasma discharges from June 1997 to March 2003. Total amount of tritium generated was $\sim 5.7 \times 10^{19}$ (~ 102 GBq) during this period.

Tritium retention was essentially correlated with the carbon deposition profile at the gap. On the both toroidal sides (i.e. toroidal gaps), the tritium concentration exponentially decreased with the distance from the front end to the bottom end with the e-folding length of around 3 mm.

Tritium retention profiles on the poloidal sides (i.e. poloidal gaps) varied with their location. Relatively high tritium retention was found at (i) the gaps between the inner target tiles and (ii) the bottom side of the outer divertor tile facing to the outer pumping slot. According to SEM observation, those side surfaces were covered by the redeposited layers with the maximum thickness of $\sim 80 \mu\text{m}$ (i) and $\sim 90 \mu\text{m}$ (ii), indicating that tritium was incorporated in the redeposited layers.

The amount of the tritium retention in the divertor tile gaps determined by the combustion method was approximately 67 MBq (assuming full toroidal symmetry in the tritium retention profiles), which corresponds to $\sim 0.07 \%$ of the total generated tritium.

(2) Exhaust Gas Analysis during Experimental Operation [2.1-3, 2.1-4]

The exhaust gas from JT-60U during the experimental operation has been investigated to understand behavior of hydrogen as fuel and to obtain basic data of impurity. Exhaust gas was measured with Mass Spectrometer, Micro Gas Chromatography and Ion Chamber. Because we didn't individually measure hydrogen isotopes (H, D, T) in the experiment, all three hydrogen isotopes are described as H. On the other hand, some impurity species could be individually measured during plasma discharges. The ratio of CH₄, CO₂, C₂H₂+C₂H₄ and C₂H₆ were 44%, 42%, 12% and 2%, respectively. These ratios of impurity species were independent on the wall temperature, even though the amounts of exhausted H and impurities increased with the wall temperature due to high recycling. Concentration of carbon compounds varied in each shot and the maximum amount of exhausted carbon was several mg in a shot. There was a tendency between the exhaust gas and the plasma parameter, indicating that the amounts of exhausted H and impurities increased with the maximum electron density of the plasma.

References

- 2.1-1 Kudo, Y., *et al.*, "Fabrication of 8Cr-2W Ferritic Steel Tile for Reduction in Toroidal Magnetic Field Ripple on JT-60U," *Proc. 5th Asia Plasma & Fusion Association (2005)*, to be published in *J. Korean Physical Society*.
- 2.1-2 Sugiyama, K., "Tritium Distribution Measurement of the Tile Gap of JT-60U," *Proc. 12th ICFRM (2005)*, to be published in *J. Nucl. Mater.*.
- 2.1-3 Isobe, K., *et al.*, *Fusion Eng. Des.*, **81**, 827 (2006).
- 2.1-4 Kobayashi, Y., *et al.*, *Proc. 21th SOFE*, (CD-ROM) (2005).

2.2 Control System

2.2.1 Innovative Integrator Resistant to Plasma Instabilities

In the development of a precise integrator for magnetic measurements aiming at long pulse operation, saturation of an amplifier caused by exposure of excessive voltage input from the sensor is the only remaining issue [2.2-1, 2.2-2].

Figure I.2.2-1 (a) shows a good, accurate integration result for the output of a magnetic probe in a discharge with a disruption; no baseline change was

observed before and after plasma discharge. Unexpectedly, soon after a few disruption shots, clear baseline gap was again observed, as shown in Fig. I.2.2-1 (b). This was caused by the damage of the FET-Zener diode elements in the signal input circuit.

To find out a proper method to provide the required durability under the repeated disruptive instabilities, we made and tested three trial signal input circuits; board #I with high voltage (± 2 kV) resistant diode, board #II with power Mos FET ($+1$ kV/ -0.6 kV) and board #III with a precise attenuator insertion with an FB compensator. The linearity errors of the board #I and #II exceeded the specification of the employed operational amplifier ($\pm 0.001\%$) for three ranges 10V, 100V, and 1000V. The cause was considered to be a large leakage current of the signal input protection elements. The linearity error of the board #III was smaller than 0.001%. Therefore, the board #III has been applied to the input circuit. Furthermore, to correctly integrate fast varying input signals during disruptions, the time resolution has been improved by increasing the integration cycle from 1.0kHz to 10kHz. Figure I.2.2-2 shows an example of good result. The integration error caused by over-range input had been successfully corrected. This development has been carried out as ITA (ITER Transitional Arrangements) task for ITER.

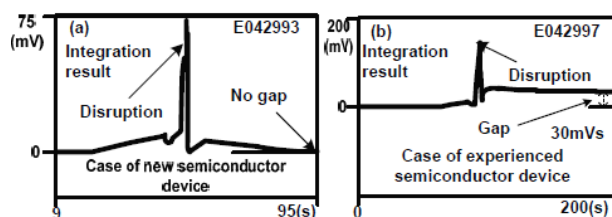


Fig. I.2.2-1 A gap of integral results occurred after several exposures to high voltage at a disruption.

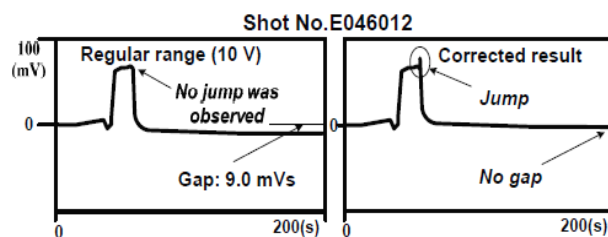


Fig. I.2.2-2 Corrected integration result.

2.2.2 Plasma Movie Database System

A plasma movie is generally expected as one of the most efficient methods to know how plasma discharge has been conducted in the experiment. On this motivation, a real-time plasma shape visualization system has been developed and operated over ten years. The current plasma movie is composed of (1) video camera picture of cross-sectional view of a plasma, (2) computer graphic (CG) picture, and (3) magnetic probe signal as a sound channel.

In order to use this movie efficiently, a new system having the following functions has been developed; (a) to store a plasma movie in the movie database system automatically after a discharge sequence, and (b) to make a plasma movie be available (downloadable) for experiment data analyses at the Web-site, as shown in Fig.I.2.2-3.

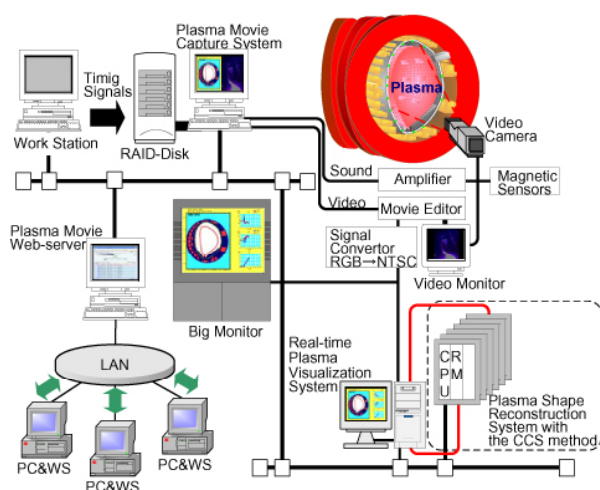


Fig.I.2.2-3 Configuration of the Plasma Movie Database System.

The plasma movie capture system stores the movie file in a format of MPEG2 first. Secondly, it transfers a movie file in a MPEG4 format to the plasma movie web-server. In response to the user's request, the plasma movie web-server transfers a stored movie data. The movie data amount for the MPEG2 format is about 50Mbyte/shot (65s discharge), and that for the MPEG4 format is about 7 Mbyte/shot. It has been confirmed that the transfer of plasma movie takes a few seconds through a local area network. After one plasma discharge sequence is finished, the plasma movie file for the 15s to 65s pulse discharge comes to be available for the web-users in about 6 to 16 minutes.

References

- 2.2-1 Kurihara, K., *et al.*, *Proc. 17th Symp. on Fusion Eng.*, 799 (1997).
 2.2-2 Kawamata, Y., *et al.*, *Proc. 19th Symp. on Fusion Eng.*, 172 (2002).

2.3 Power Supply System

Annual inspections and regular maintenances for the power supply systems have been conducted to maintain availability of high power operations as shown in Table I.2.3-1. These activities contributed to achieve safe operation of the power supplies.

Table I.2.3-1 Inspections and overhaul of the power supply systems.

Item	Term
Overhaul of the Oil-cooled Transformer	April
Detail Inspection of the Motor Generator and the Poloidal Field Coil Power Supply	August~October
Regular Inspection of the Grounding and Lightning systems	September
Regular Inspection of the Toroidal Field Coil Power Supply	September~October
Regular Inspection of the Power Supply for Additional Heating Facilities	September~October
Regular Inspection of the Power Distribution Systems	October

2.3.1 Overhaul of the Oil-Cooled Transformer

The regular gas chromatograph analysis of insulating oil in the oil-cooled transformers for TFC power supply detected abnormal quantities of flammable gas, C_2H_4 , C_2H_2 , etc., in January, 2005. This transformer for the thyristor drive device of the motor generator has a zero-voltage tap changer. The specifications and outer appearance are shown in Table I.2.3-2 and Fig.I.2.3-1. The pattern of the gas contents showed flammable gas was produced by overheats of the oil. A spring-forced metal contact could produce "creep" on a contact surface. This would result in a temperature rise at the contact surface, and generate carbide layers for a certain period. This scenario seems to be supported by observation of the tap contact as shown in Fig.I.2.3-2. To avoid this phenomenon, the changeable tap contact was replaced by the fixed one.

Table I.2.3-2 Specifications of the oil-cooled transformer.

Capacitor (kVA)	28,000
Primary voltage (V)	10,500~11,500
Secondary voltage (V)	17,000
Oil quantity (L)	10,700
Weight (kg)	40,200

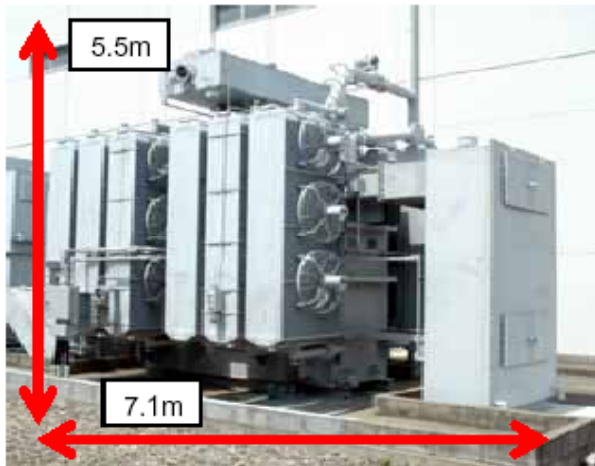


Fig.I.2.3-1 The oil-cooled transformer for the thyristor drive device of the TF-PS motor generator.

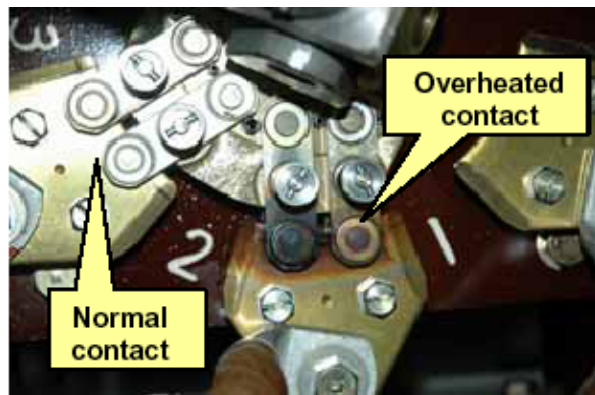


Fig.I.2.3-2 The overheated tap contact.

2.3.2 New AC Power System for Satellite Tokamak

The satellite tokamak, the modification of JT-60 to a super-conducting tokamak, is planned to have a 41MW-100s heating operation through the Japan-Europe negotiation in 2005. The planned powers for the heating facilities are summarized in Table I.2.3-3. AC power of 130MW-100s (13GJ) is necessary for the operation with all the heating facilities, but cannot be supplied by the present motor generator for additional heating facilities (H-MG: 400MVA, 2.65GJ). The reuse of the present power supply is a basic policy of the satellite tokamak project to save the cost. Therefore, we have studied possible AC power systems that are

reconstructed with the present JT-60 power supply system.

(1) Configuration of a New AC Power System

The new AC power system would be constituted of the 275kV commercial line (Tr-1) and the motor generator for the current TFC-PS (T-MG). The configuration of the new AC system is shown in Fig. I.2.3-3. The AC powers of 88MW for P-NBI and ECRF and 40MW for NNBI are supplied from the Tr-1 line and from T-MG, respectively.

Table I.2.3-3 Nominal power for Additional Heating Facilities.

Unit	Heating Power (MW)	Active Power (MW)	Reactive Power (MVar)
P-NBI	24.0	60.3	80.1
N-NBI	10.0	40.5	54.0
ECRF	7.0	28.0	21.0

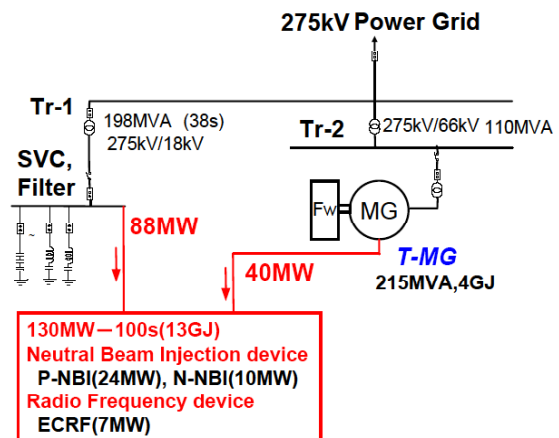


Fig. I.2.3-3 A possible configuration of the new AC power system for additional heating facilities.

(2) Design Study of a New Reactive Power Compensator

Power consumption of 88 MW through Tr-1 would induce voltage variation and higher harmonic currents at 275 kV power grid exceeding the values restricted by the contract with the commercial power company, TEPCO. To reduce such influence on the commercial line, a reactive power compensator consisting of a harmonic filter set and a power-factor improvement capacitor set to be installed in the circuit were designed. In the design, the existing harmonic filters and power-factor improvement capacitors were assumed to be reused as a part of the reactive power compensator.

We made the model of additional heating facilities for the simulation codes PSCAD/EMTDC. First, the response of the circuit without the reactive power compensator was simulated. The results are shown in Table I.2.3-4, and the harmonic current is shown in Fig. I.2.3-4. The equivalent disturbing current calculated with the harmonic current is 4.94A. This value does not satisfy the contract condition with TEPCO, allowable equivalent disturbing current of 1.9A.

Table I.2.3-4 Simulation result from the case without a reactive power compensator.

Active Power (MW)	84.4
Reactive Power (MVar)	105.0
Power Factor	0.63
275kV line Voltage regulation (%)	0.8
18kV line Voltage regulation (%)	10.0

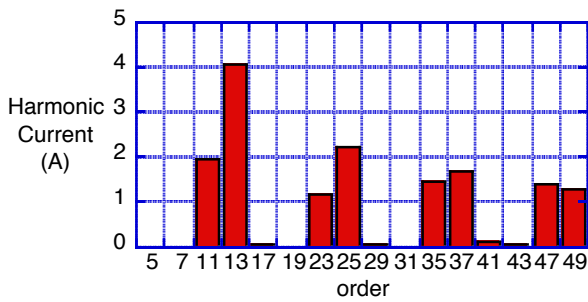


Fig. I.2.3-4 Harmonic current of 275kV power grid without reactive power compensator.

Table I.2.3-5 Simulation result from the case with a reactive power compensator.

Active Power (MW)	87.4
Reactive Power (MVar)	59.2
Power Factor	0.82
275kV line Voltage regulation (%)	0.4
18kV line Voltage regulation (%)	5.5

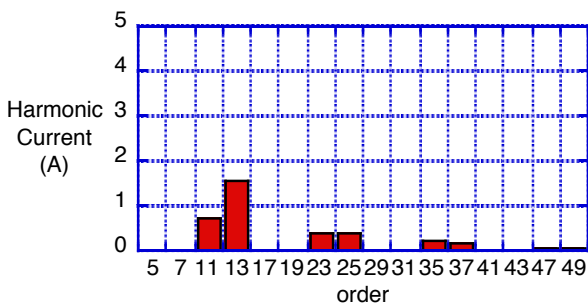


Fig. I.2.3-5 Harmonic current of 275kV power grid with reactive power compensator.

To explore the resolution, the simulation for the case with the reactive power compensator was conducted, and the results are shown in Table I.2.3-5. The harmonic current is shown in Fig. I.2.3-5. In the simulation, it was assumed that 11, 13 order harmonic filters were substituted by the new ones, while 18 and higher order harmonic filters and the power-factor improvement capacitors of 40MVar were reused. The equivalent disturbing current improved to 1.54A, and satisfied the contract condition. It was, therefore, concluded that a new AC power system for the satellite tokamak additional heating facilities was feasible.

2.4 Neutral Beam Injection System

The main objectives of the NBI system is to extend its pulse duration up to 30s so as to study long pulse plasmas whose duration is much longer than the current diffusion time. Four tangential positive ion-based NBI (P-NBI) units have been routinely operated up to 30s with 2MW/unit at 85keV. Also, seven perpendicular P-NBI units have been operated in series for the total pulse duration of 30s. As for the negative ion-based NBI (N-NBI) system, the long pulse operation of 10 s with two ion sources has been achieved. The high performance of NBI system at the injection power of ~ 10 MW for 30s has been contributed to achieve high $\beta_n \sim 2.3$ for 28s. Moreover, the critical issues for long pulse operation are specified, such as stable source plasma control, high voltage holding and reduction of heat load of the accelerator and beamline components. Design of the upgrade of the NBI system has been started, where the total injection power of 34 MW for 100 s is planned for the satellite tokamak.

2.4.1 Renewal of Control System for Cryogenic Facility

The NBI system needs deuterium gas fueling of 3-5Pam³/s for source plasma production and neutralization. A large cryopumping system with pumping speed of 20000m³/s is used to quickly exhaust the residual gas so as to avoid re-ionization of the neutral beam. The cryopumping system is cooled down by a liquid He cryogenic facility with a cooling capacity of 2.4kW. The control system of the cryogenic facility was constructed with Distributed Control System (DCS) computer about 20 years ago. Recently, the frequency of troubles in the control system has

increased due to its ageing. Therefore, the control system has been renewed using functional and inexpensive commercial Programmable Logic Controllers (PLC). Figure I.2.4-1 shows the block diagram of the new control system. The new control system is composed of four PC computers and PLCs, each of which is connected with Ethernet. The PLCs are connected with double control loops to keep a high reliability. The control program in the original DCS, consisting of about 400 feedback control loop with ~400 digital and ~800 analog data, was transferred to the program in the PLC. A distributed processing method was used to control the cryopumps independently. About 200 control views were created to obtain a high man-machine interface. The new control system was completed in September 2005 and has shown its high reliability without troubles to date. This is a new approach of the commercial PLC to the dynamic control system in the large plant [2.4-1].

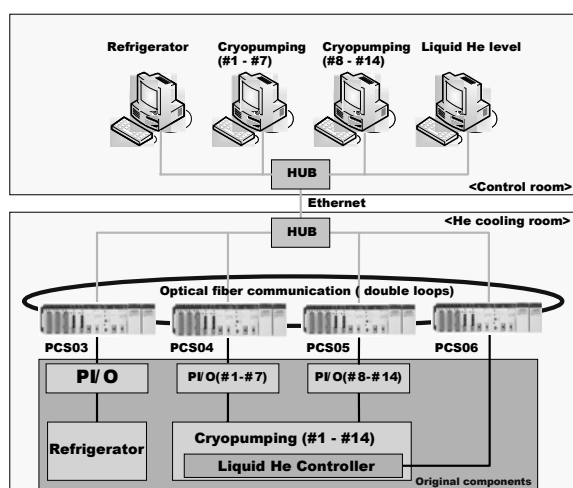


Fig. I.2.4-1 Block diagram of the new control system for a cryogenic facility.

2.4.2 Progress in N-NBI System

The long pulse more than 10 sec was carried out with one ion source only in 2004. In 2005, the optimization of 10 sec operation with two ion sources has been intended. Figure I.2.4-2 shows the progress of the injection power with two ion sources. A long pulse injection at ~3.3MW for 10sec, where the acceleration beam energy and current are 340keV, ~33A, has been achieved.

Some critical issues for long pulse operation have been specified through the optimization study [2.4-2].

The first issue is to keep the negative ion production constant for long pulse operation. Once the arc discharge starts, the discharge current flows into the filament, changing its temperature distribution. Feedback control of the arc current is effective in keeping the source plasma parameters. It is also confirmed that the cesium effect depends on the temperature of the plasma grid in the large ion source. This result indicates that active temperature control of the plasma grid is essential for long pulse operation.

The second issue is to improve the high voltage holding capability of the accelerator. It was found that outgassing increased in the range of 10^{-4} Pa during voltage holding even when there was no-breakdown in the ion source (base pressure: $1-2 \times 10^{-4}$ Pa). When the outgassing was well suppressed after sufficient conditioning, breakdowns were well suppressed. The main component of the outgassing was $m/e=28$. There was no component of $m/e=14$. Therefore, the outgassing was supposed to be hydro-carbon species. This result indicates that the improvement of FRP (fiberglass-reinforced plastic) insulator, which is composed of hydro-carbons, may be a key to achieve high voltage holding in the accelerator.

The third issue is to reduce the heat load of the acceleration grids and beam line components. The investigation of the negative ion beam deflection, which was measured by the infrared camera on the target plate set 3.5m away from the grid, indicates that the spread of beamlet-bundle is in proportion to the current density. Field-shaping plates attached on the extraction grid were effective in modifying the local electric field and reducing the heat load of the acceleration grid [2.4-3]. It was also found that some

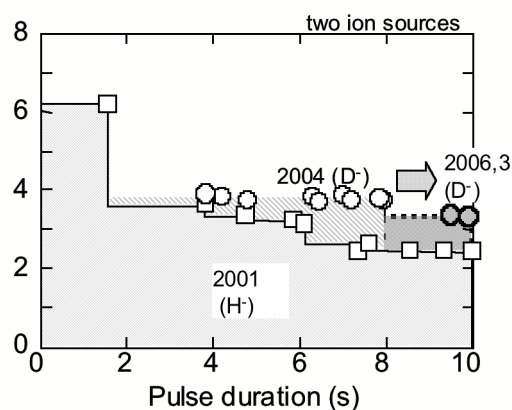


Fig. I.2.4-2 Progress of the injection power and pulse duration with two ion sources.

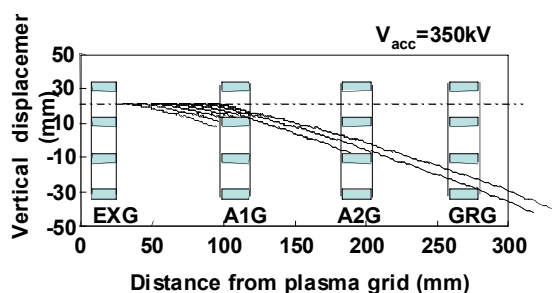


Fig. I.2.4-3 Electron beam trajectory in the three stage accelerator. Some electron produced at the first stage is deflected by the PG magnetic field and is accelerated, passing through the next accelerator grids (A2G, GRG).

part of the stripped electrons produced at the first stage accelerator were accelerated and passed through the down pitch of the multi-apertures in the next acceleration grid and then collided the beam line as shown in Fig.I.2.4-3. It is important to investigate in detail the negative ion-beam and electron-beam trajectory not only inside of the ion source, but also downstream from the ion source for further long pulse operation [2.4-4].

2.4.3 Design Study of NBI System for the Satellite Tokamak

Modification of JT-60U to the satellite tokamak has been planned to contribute to ITER and DEMO. The NBI system is required to inject 34MW for 100s. The upgraded NBI system consists of P-NBI units and one N-NBI unit. The injection power of each P-NBI unit is 2MW at 85keV, and that of one N-NBI unit will be 10MW at 500keV. There are three types of P-NBI units (perpendicular: 8 units, co-tangential: 2 units, counter-tangential: 2 units) to control deposition profile and plasma rotation. The beam line of the co-tangential N-NBI unit will be shifted downward from the equatorial plane by $\sim 0.6\text{m}$ to drive off-axis plasma current that is necessary for producing reversed shear with a high bootstrap current fraction. Figure I.2.4-4 shows the side view of the NBI system for the satellite tokamak.

The critical issue of the modified NBI system is to extend the pulse duration up to 100s. In long pulse operation of P-NBI unit at 2MW for 30s, the temperature rise of the cooling water in the ion source has been found to get almost saturated at less than 10°C at $\sim 15\text{ s}$ after the start of injection, indicating that the present ion source of P-NBI may operate for 100 s without modification. Under the KBSI-JAERI

collaborative program, a long pulse operation of P-NBI ion source has been demonstrated up to 200s at KSTAR NBI test facility though the beam current is $\sim 20\text{A}$ at 60kV due to the power supply capability. In the preliminary study, the present high voltage DC power supply for P-NBI unit can drive the ion source for 100s by modifying some resistances and employing active cooling of the inner conductor in the high voltage feeder duct. The available beam voltage of the present N-NBI is less than 400keV. Thus, the main issue of N-NBI unit is to improve the voltage holding of the ion source up to 500kV. A modification of the accelerator such as the insulator structure is under consideration. The present acceleration power supply of 500kV, 64A with an inverter switching system will also be modified to extend its pulse duration from 10s to 100s by adding more converter-inverter components. The last item is shielding of the leakage magnetic field of the satellite tokamak. The leakage field will be about five times larger from the JT-60U, so attachment of high permeability metal on the ion tank is required, in addition to strengthening the canceling coils. The detailed design study is under development [2.4-5].

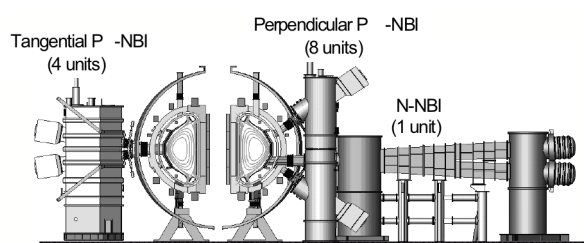


Fig. I.2.4-4 Side view of NBI systems for satellite tokamak.

Reference

- 2.4-1 Okano, F., *et al.*, *Keiso*, **49**, 22 (2006) (in Japanese).
- 2.4-2 Ebisawa, N., *et al.*, "Recent Activities of Negative Ion Based NBI System on JT-60U," *Proc. 21st Symp. on Fusion Eng.*, (CD-ROM) (2005).
- 2.4-3 Ikeda, Y., *et al.*, "Present Status of Negative Ion Based NBI System for Long Pulse Operation on JT-60U," *Proc. 4th IAEA TM on Negative Ion Based Neutral Beam Injectors*, (CD-ROM) (2005).
- 2.4-4 Umeda, N., *et al.*, *Rev. Sci. Instrum.*, **77**, 03A529 (2006).
- 2.4-5 Ikeda, Y., *et al.*, "Progress of Neutral Beam Injection System on JT-60U for Long Pulse Operation," *Proc. 5th General Scientific Assembly of Asia Plasma & Fusion Association*, (CD-ROM) (2005).

2.5 Radio-Frequency Heating System

2.5.1 Long-Pulse Operation of the ECH System

Trail of Pulse extension of the ECH system is being carried out to enhance the plasma performance in the recent experiment campaign in JT-60U focusing on long sustainment of high performance plasmas. Improvements of the gyrotron and development of advanced operation techniques are keys to extend the ECH pulse. A difficulty in the pulse extension was to keep the oscillation condition against decreasing collector current because of cathode cooling due to continuous electron emission. The techniques of controlling heater current and anode voltage during the pulse developed by FY2004 [2.5-1] were refined and pulse duration of 17 s at 0.4 MW (at gyrotron) has been achieved.

The mechanism of this control is regarded as follows; the increase in heater current is a direct method to compensate the cathode temperature drop, and the change in anode voltage changes the oscillation condition by modifying the electron pitch angle. As an advanced feature of the real time heater current and anode voltage control, automatic recovery from the oscillation termination was also achieved. The termination was detected from the voltage signal from the directional coupler and the diode detector, then the anode voltage was increased by 2.2 kV and the

oscillation successfully recovered as shown in Fig. I.2.5-1.

It is important to estimate the power of injected millimeter waves for the ECH system. However, power measurement by a dummy load, used as a basic and common power measurement method, assumes reproducibility and stability of the gyrotron oscillation. A model calculation showed that the disk edge temperature of the diamond vacuum window (diameter: 60 mm, thickness: 1.72 mm) in the waveguide (inner diameter: 31.75 mm) gap was sufficient to estimate the transmission power at 1 MW and 110 GHz with a response time of ~ 0.2 s, because of the high thermal conductivity of diamond. This suggests that quasi-real-time power measurement can be achieved using a high response thermometer such as a very thin thermocouple or an infrared radiation thermometer. The initial high power test with a thermocouple ($\phi = 0.5$ mm) demonstrated successful power measurement for ~ 1 MW, 4 s pulses with response time of < 1 s as shown in Fig. I.2.5-2.

2.5.2 Operation and R&D of the LH System

The performance of the modified launcher with the developed carbon grills showed sufficient abilities as a high power LH launcher, for instance, moderate current drive efficiency [2.5-2]. For the modified LH launcher,

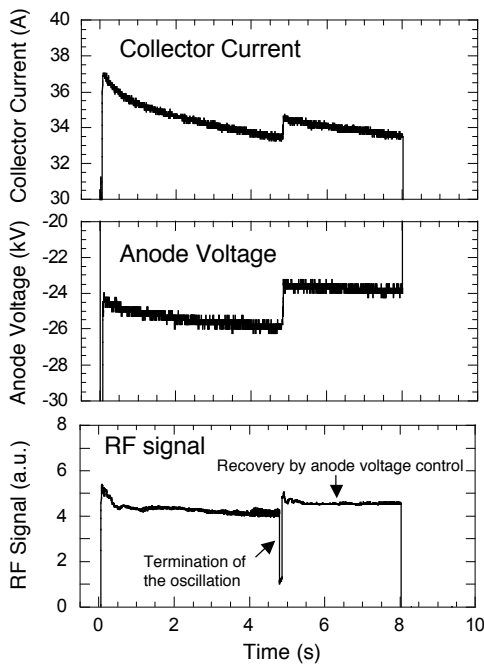


Fig. I.2.5-1 Oscillation recovery by anode voltage control.

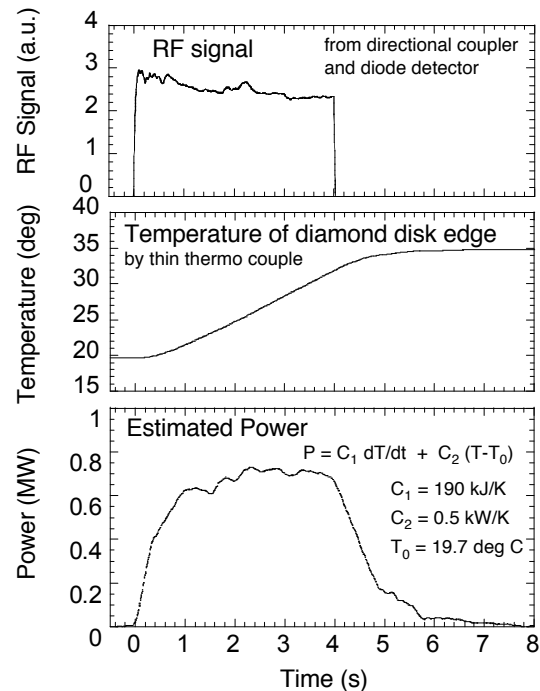


Fig. I.2.5-2 Power measurement by the diamond disk set in the waveguide gap.

the technical key issue was to obtain sufficient electrical contact along the carbon grills, even though for this purpose a thin RF contactor made of copper was inserted between the base frame and the carbon grill mouth. After large energy injection such as ~ 16 MJ, the carbon grills seemed to be of integrity, however, severe damages were observed around a few base frames by RF breakdown due to insufficient electrical contact and low responses of the arc monitor system to protect them against RF breakdown in the LH launcher. Therefore, at first the arc monitor system was improved such as re-installation of the checking lamps that clearly check whether the protection system works well or not. Next, the eight carbon grills were removed from the base frames welded with the LH launcher, and these base frames were repaired smoothly. Unfortunately, two base frames were so injured that high RF power could not be injected. Conditioning of the LH launcher through the six base frames was performed with plasma by using the power-modulated injection method like as discontinued injection of 50ms-on/10ms-off. The conditioning has progressed up to ~ 1.5 MW and/or ~ 9.3 MJ, as shown in Fig. I.2.5-3. Moreover, the real time current profile control by LH injection was successfully demonstrated via real-time adjustment of input power and phase difference with monitoring current profile estimated with MSE measurement.

In order to improve insufficient electrical contact along the carbon grill, a new carbon grill has been

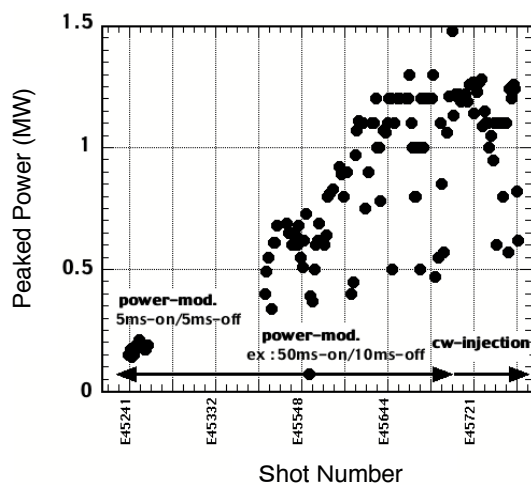


Fig. I.2.5-3 Progress of conditioning using the LH launcher with 6 base frames. A power modulation method is used for efficient conditioning. In the latter phase, power is injected continuously.

developed as shown in Fig. I.2.5-4. The four-divided (4-div.) grill made of graphite is joined with the 4-div. pedestal by a “diffusion bonding method”. In this new carbon grill, the position of electrical contact is between the 4-div. pedestal made of stainless steel and the base frame. Enough electrical contact is expected because pressing is stronger than the former type. This new carbon grill shows enough power capability of ~ 500 kW even in short time. Up to now, high power of 300 kW - 10 s can be transmitted without heavy RF breakdown.

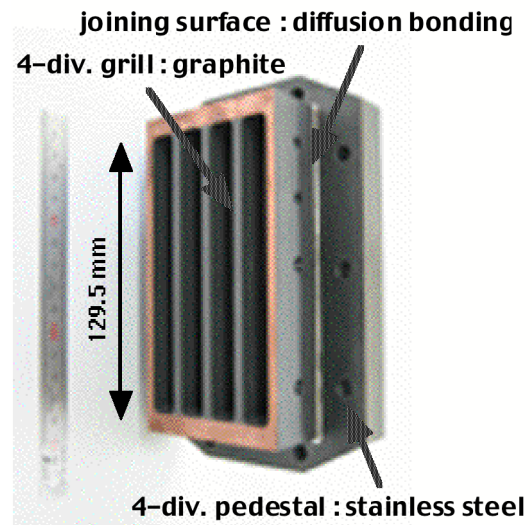


Fig. I.2.5-4 Overview of the new carbon grill.

References

- 2.5-1 Moriヤマ, S., *et al.*, *Fusion Eng. Des.*, **74**, 343 (2005).
- 2.5-2 Seki, M., *et al.*, *Fusion Eng. Des.*, **74**, 273 (2005).

2.6 Diagnostics Systems

2.6.1 High-Repetition CO₂ Laser for Collective Thomson Scattering Diagnostic [2.6-1]

A diagnostic of fusion-generated alpha particles is important for understanding of their contribution to plasma heating and plasma instabilities. However, the effective and reliable measurement method has not yet been established.

To establish a diagnostic method of confined α -particles in burning plasmas, a high-repetition and high-energy Transversely Excited Atmospheric (TEA) carbon dioxide (CO₂) laser (Fig. I.2.6-1) for a collective Thomson scattering (CTS) diagnostic has been developed. To excite a single-transverse and

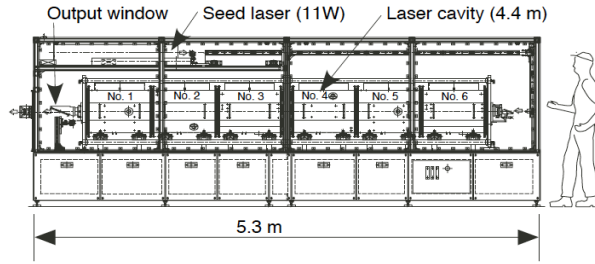


Fig. I.2.6-1 Schematic view of newly developed TEA CO₂ laser. The dimensions of the laser casing are 5.3m long, 1.9m high, 1.1m wide.

single longitudinal mode, the laser has an unstable resonator with a cavity length of ~ 4.4 m and continuous wave seed laser is injected. Pulse energy of 10J with a repetition rate of 10Hz has been achieved in the single-mode operation. The beam size is 40mm in diameter. Pulse energy of 18J with a repetition rate of 10 Hz and 36J with single shot operation has also been achieved in the multimode operation. These results give an outlook for the CTS diagnostic on ITER, which requires single-mode energy of 20J with a repetition rate of 40Hz. A proof-of-principle test will be performed with the improved laser system on JT-60U.

2.6.2 Density Fluctuation Measurement Using Motional Stark Effect Optics [2.6-2]

The motional Stark effect (MSE) diagnostic system has been modified to work as a beam emission spectroscopic (BES) diagnostic. By fast sampling (0.5-1MHz) of the photo-multiplier signals, the system can simultaneously measure density fluctuation in addition to the pitch angle of the magnetic field. In the core

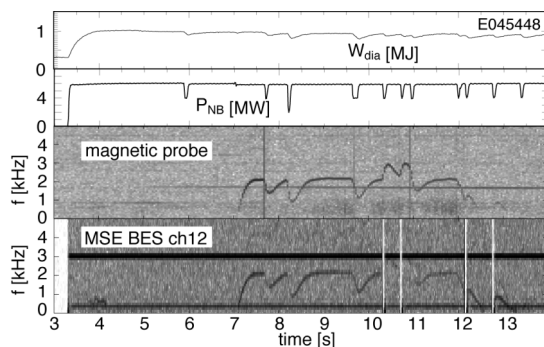


Fig. I.2.6-2 Time evolution of a discharge in which density fluctuation induced by rotating tearing mode islands was observed. Diamagnetic stored energy (W_{dia}), NB heating power (P_{NB}), spectrogram of magnetic fluctuation measured with a magnetic probe, and spectrogram of fluctuation in a photo-multiplier signal of the MSE diagnostic system.

plasmas, density fluctuation induced by rotating tearing mode islands has been observed. In the scrape-off layer of an ELMy H-mode plasma, outward propagation of strong intermittent emission coinciding with ELM crashes has been observed.

Figure I.2.6-2 shows time evolution of a discharge in which density fluctuation induced by rotating tearing mode islands was observed. An MHD fluctuation is observed from $t=7$ s at a frequency of ~ 2.2 kHz, using magnetic probes. The poloidal and toroidal mode numbers are 2 and 1, respectively. Several channels of the MSE BES diagnostic near $q=2$ surface detected the MHD fluctuation having the same temporal evolution of frequency. The phase of the fluctuations measured by the MSE BES diagnostic is inverted at the $q=2$ surface measured by the MSE diagnostic, where the phase of the electron temperature fluctuations measured by an electron cyclotron emission diagnostic is also inverted. The phase inversion of the temperature and density fluctuations indicates a rotating island structure of the magnetic field.

2.6.3 Neutron Detector with Fast Digital Signal Processor [2.6-3]

Neutron emission profiles are routinely measured and used for transport studies of energetic ions. In order to measure neutrons effectively in the mixed neutron and gamma-ray field, Stilbene neutron detectors (SNDs) have been used. The SND combines a Stilbene crystal scintillation detector (SD) with an analog neutron-gamma pulse shape discrimination (PSD) circuit to select only neutron events. Although the SND has many advantages as a neutron detector, the maximum count rate is limited up to $\sim 1 \times 10^5$ counts/s due to pile up effect in the analog PSD circuit. Under this situation, it is difficult to investigate transport of energetic ions due to MHD instabilities such as Alfvén Eigenmodes with frequency of \sim MHz range.

To overcome this issue, a digital signal processing system (DSPS) using a Flash ADC (Acqiris DC252, 8 GHz, 10bit) has been developed at Cyclotron and Radioisotope Center in Tohoku University. In this system anode signals from the photomultiplier of the SD are directly stored and digitized sequentially. Then, neutron-gamma PSD is performed using software. This system allows neutron measurements with a high counting rate of $> 1 \times 10^6$ counts/s. Good neutron-gamma

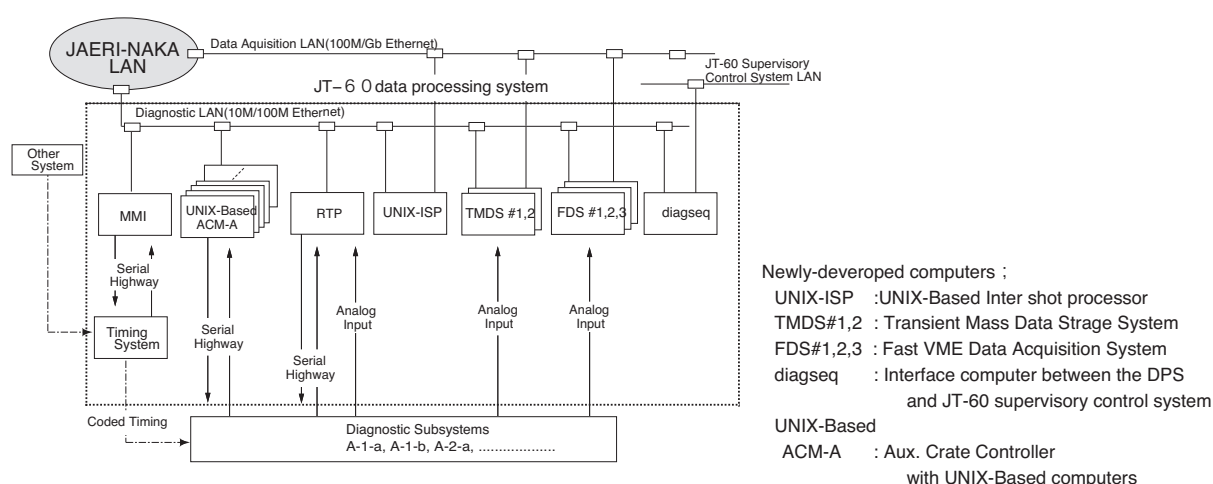


Fig.I. 2.6-3 The configuration of the new data processing system.

discrimination of this system was verified by performance tests using neutron-gamma sources. Then, it has been installed in the center channel of the vertical neutron collimator system in JT-60U and applied to deuterium experiments. As a result, it is confirmed that the PSD is sufficiently performed and collimated neutron flux are successfully measured with a count rate up to $\sim 5 \times 10^5$ counts/s without pile up of detected pulses. Thus, the performance of the DSPS as a neutron detector, which supersedes the SND, is demonstrated.

2.6.4 Data Processing System [2.6-4]

In order to meet demands for the advanced diagnostics, the JT-60 data processing system (DPS) has been modified from a three-level hierarchy system to a two-level hierarchy system. The old DPS had a mainframe computer at the top level of the hierarchy. The mainframe computer communicated with the JT-60 supervisory control system and supervised internal communication inside the DPS. The middle level of the hierarchy had minicomputers, and the bottom level had individual diagnostic subsystems. The mainframe computer at the top level limited the total performance of the DPS. The new DPS is a decentralized data processing system using UNIX-based workstations and network technology. The configuration of the new DPS is shown in Fig. I.2.6-3. The mainframe computer was replaced with a UNIX-based workstation. All the computers in the middle level of the hierarchy are now UNIX-based workstations. The new DPS started operation in October 2005.

References

- 2.6-1 Kondoh, T., *et al.*, "High-Repetition CO2 Laser for Collective Thomson Scattering Diagnostic of α -Particles in Burning Plasmas," submitted to *Rev. Sci. Instrum.*.
- 2.6-2 Suzuki, T., *et al.*, "Density Fluctuation Measurement Using Motional Stark Effect Optics in JT-60U," to be published in *Rev. Sci. Instrum.*.
- 2.6-3 Ishikawa, M., *et al.*, "Fast Collimated Neutron Flux Measurement using Stilbene Scintillator and Flash-ADC in JT-60U," submitted to *Rev. Sci. Instrum.*.
- 2.6-4 Sakata, S., *et al.*, "Progress of Data Processing System in JT-60 -Development of Remote Experiment System-," to be published in *Fusion Eng. Des.*.

3. Design Progress of the National Centralized Tokamak Facility

The project has been positioned as an ITER satellite tokamak based on the close collaboration with EU fusion community. The facility design and the research strategy have been discussed in the JA-EU Satellite Tokamak Working Group. According to the discussion, the facility design is modified to strongly support the ITER.

Corresponding to the joint Japan-EU framework, the nickname of the facility is changed to 'JT-60 Super Advanced (JT-60SA)', with the emphasis on the succeeding of achievement in present JT-60U research.

3.1 Physics Estimation

The nominal power of heating and current drive systems is increased as shown in Table I.3.1-1. With the optimized combination of those systems, capability to conduct the ITER and DEMO oriented research is evaluated on the view points of operation scenario, MHD stability and control, power and particle control [3.1-1, 3.1-2, 3.1-3].

Table. I.3.1-1 Heating and current drive systems.

	injection	source	power
P-NB (85keV)	co	2MW 2units	4MW
	ctr.	2MW 2units	4MW
	perp.	2MW 8units	16MW
N-NB (500keV)	co	10MW 1unit	10MW
EC	110GHz	0.75MW 4units	3MW
	140GHz	0.8MW 5units	4MW
total			41MW

3.1.1 Operation Scenario

Capability for exploration of ELMy H-mode and hybrid scenarios is analyzed. The operation with $I_p=3.5\text{MA}$, $B_T=2.42\text{T}$ and with ITER similar plasma shape is available for 100s by the heating power of 41MW, which contributes to physics assessment and databases for ITER operation scenario. High performance H-mode in higher plasma current and higher density region also becomes in the scope by the increased heating power.

Full non-inductive steady-state operation scenario is also analyzed. The operations at $I_p=3\text{MA}$, $B_T=2.44\text{T}$,

$q_{95}=5.3$, $f_{bs}=0.56$, $f_{GW}=0.55$, $HH_{98y2}=1.3$, $\beta_N=3.6$, and at $I_p=2.4\text{MA}$, $B_T=1.79\text{T}$, $q_{95}=5.5$, $f_{bs}=0.7$, $f_{GW}=0.88$, $HH_{98y2}=1.32$, $\beta_N=4.4$ are available with the proper control of MHD stability. Current diffusion time in those scenarios is estimated less than 20s, so that the steady state condition in the current profile is expected. As shown in Fig. I.3.1-1, the parameter window of full non-inductive current drive operation is extended into higher plasma current, higher bootstrap current fraction, and higher density region by the increased heating power of 41MW.

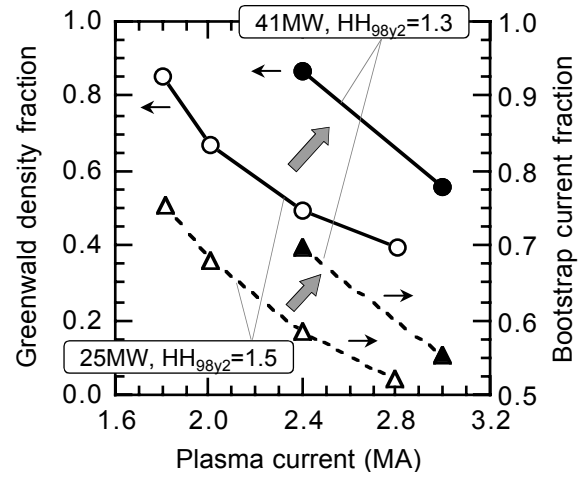


Fig. I.3.1-1 Parameter window for full non-inductive current drive operation.

3.1.2 MHD Control

In order to cover the wide range in stabilization of neoclassical tearing mode (NTM), two frequency EC systems with 110GHz, and 140GHz are designed. With such two EC systems, the simultaneous stabilization of $m/n=3/2$ and $2/1$ mode on the different magnetic surfaces can be expected. Moreover, the amplitude modulation with 5kHz for 140GHz system enhances the controllability.

Valen code analysis of resistive wall mode (RWM) stabilization shows that the critical normalized beta value will rise to $\beta_N \sim 5.6$ if the sector coil is located between plasma and stabilization plate [3.1-4]. Remarkable improvement in critical β_N compared to that in the location of sector coil behind the stabilization plate suggests that the stabilization wall disturbs the effective radial magnetic flux made by sector coils coupled with the plasma. Therefore, actual sector coils are designed to be located around the port hole in the vacuum vessel.

3.1.3 Heat and Particle Control

The maximum heat flux in the steady state is 15MW/m^2 and 10MW/m^2 at outside, and inside divertor target, respectively, while that for short pulse length of about 10s is 20MW/m^2 and 15MW/m^2 , respectively. Carbon-composite material is expected as the plasma facing component at the first experimental stage, however, the replace to the metal (mainly tungsten), which is the dominant candidate in DEMO, should be in the scope at the later phase.

In order to control the divertor plasma detachment, pumping speed of about $100\text{m}^3/\text{s}$ is required [3.1-5]. On the other hand, the private dome top should be lower to ensure the flexible plasma shape, which in turn reduces the effective space for cryopanel beneath the private dome. Therefore, the location of cryopanel is changed beneath the outer baffle plate for inside as well as outside divertor pumping keeping with the in/out separation. The pellet injection with high throughput and repetition rate ($\sim 50\text{Pam}^3/\text{s}$) will play a significant role for core particle fuelling and ELM control.

References

- 3.1-1 Tamai, H., *et al.*, *Nucl. Fusion*, **45**, 1676 (2005).
- 3.1-2 Kikuchi, M., *et al.*, *Nucl. Fusion*, **46**, S29 (2006).
- 3.1-3 Tsuchiya, K., *et al.*, "Engineering Design and Control Scenario for Steady-State High-Beta Operation in National Centralized Tokamak (NCT)," *7th ISFNT* (2005).
- 3.1-4 Kurita, G., *et al.*, *Nucl. Fusion*, **46**, 383 (2006).
- 3.1-5 Kawashima, H., *et al.*, "Divertor Modeling for the Design of the National Centralized Tokamak with High Beta Steady-State Plasmas," *7th ISFNT* (2005).

3.2 Engineering Design

Facility designs are modified to be tolerable for the increased heating power and neutron yields. Design concept is also changed on the viewpoint of the cost and the manufacturing [3.2-1, 3.2-2].

3.2.1 TF and PF Coils

NbTi can be used in the TF coils because of the low operating field of 6.4T. The substantial saving in cost and minimizing of manufacture risk will be expected [3.2-3].

Operational region of the NbTi strand adopted for the TF coil conductor is shown in Fig.I.3.2-1. The turn number in the coil is determined to 86 turns in order to supply a sufficient flux of $B_T R = 8.2\text{Tm}$. On the other

hand, the radial build of the TF coils becomes larger which leads the decrease in the CS diameter. Therefore, the magnetic field of the CS coils is increased to 10 T in order to provide a sufficient CS flux.

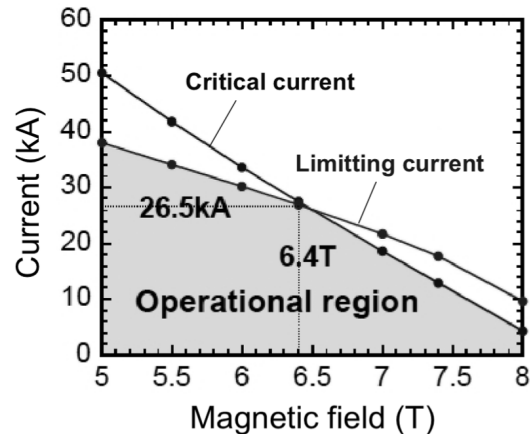


Fig. I.3.2-1 Specification of the strand of NbTi for TF coil conductor.

3.2.2 Power Supplies

In order to realize the maximum plasma heating power of 41MW for 100s, AC supplied power for the heating facility of about 130MW at 18kV is required. Two power source systems are considered for this power request; one is by present flywheel generator (T-MG) of about 40MW, and the other is the commercial AC line of about 90MW. Delicate adjustment between two power sources with different frequency is required.

3.2.3 Vacuum Vessel (VV)

In order to reinforce the shielding characteristics for increased neutron yield, boronised water with 95% B^{10} is filled between the double wall VV each of which consists of low-cobalt containing stainless steel ($\text{Co} < 0.05\text{wt}\%$) with 24mm in thickness. The boronized water is heated 200°C at 2MPa for the baking of VV. 80K thermal shield consists of silver coating at the VV side for the suppression of thermal radiation and of super insulation at the superconducting coil side. Support leg of VV is located every 40° (every 2 sectors) in the toroidal direction, which is connected to the support ring at the bottom of cryostat. At another sectors, vertical ports for diagnostic equipments are installed.

3.2.4 In-Vessel Components

In order to ensure the heat removal characteristic, the divertor target plate is changed to monoblock-type in

which the CFC armor-block is directly welded on the cooling pipe of copper alloy, the same as that in ITER (allowable heat flux: 15-20MW/m²). Both of lower and upper divertor target plates have the same heat allowance to correspond the flexible plasma shape from ITER like single null to double null with high triangularity. The structures of divertor tile and first wall tile are available to handle with the remote handling system for the maintenance.

For the requirement of flow velocity in coolant water of 10-12m/s, supplement of buffer tank and water pump is considered.

3.2.5 Cryostat

Basic concept is spherical double wall with inner diameter of 13.4m which is divided into top, bottom and seven middle parts. Spherical part has inner skin of 34mm in thickness with low-cobalt containing stainless steel. In the gap between outer skin of 6mm in thickness, boron-doped reduced activation concrete is filled (≥ 160 mm in thickness) [3.2-4]. Support structure consists of the support ring, nine support legs, and the base plate.

3.2.6 Remote Handling System

Considering the expected high activation level with extended heating power, a remote handling (RH) system will be required. Considering the shape and weight of in-vessel components handled by RH system, vehicle type tested in ITER R&D of blanket maintenance is hopeful. Four large horizontal ports are to be used for the rail extension, hold and transport of components and mechanical tools. Compatible design of vacuum vessel, cryostat and in-vessel components with RH should be considered.

References

- 3.2-1 Matsukawa, M., *et al.*, "Optimization Study of Poloidal Field Coil Configuration for Improving Plasma Shaping Capability and the Flexibility in NCT," 19th MT (2005).
- 3.2-2 Kizu, K., *et al.*, "Effects of Tensile and Compressive Strain on Critical Currents of Nb₃Al Strand and Cable-in-Conduit Conductor," *ibid.*
- 3.2-3 Takahashi, H., *et al.*, "Fracture Mechanics Analysis Including the Butt Joint Geometry for the Superconducting Conductor Conduit of National Centralized Tokamak," 7th ISFNT (2005).
- 3.2-4 Morioka, A., *et al.*, "Development of 300°C Heat Resistant Boron-Loaded Resin for Neutron Shielding," 12th ICFRM (2005).

4. Domestic and International Collaborations

4.1 Domestic Collaboration

JT-60U was assigned as a core national device for joint research by the Nuclear Fusion Working Group of the Special Committee on Basic Issues of the Subdivision on Science in the Science Council of MEXT in January 2003. Using the JT-60 tokamak and other facilities, JAEA has been striving for research collaboration with the universities and NIFS. Accordingly, the joint experiments on JT-60 between JAEA and the universities by assigning university professionals as leaders of some research task forces has been successfully performed. The number of collaborators increased significantly from FY 2003, and then gradually increased year by year, reaching 176 persons in FY 2005, as shown in Fig. I.4-1. They came from 24 research organs in Japan. The number of leaders from universities and NIFS also increased significantly from FY 2003, and reached 6 persons in FY 2005.

The number of research subjects of the joint research was in total 31 in FY 2005, categories of which are shown in Table I.4-1. 18 journal papers were published as a result of the joint research in FY 2005.

Table I.4-1 Number of research subjects of the JT-60 joint research according to category in FY 2005.

Category	No. of research subjects
Core plasma	11
SOL/Divertor, heat & particles	4
Plasma-surface interaction	4
Modeling/simulation	4
Diagnostics/heating system	8
Total	31

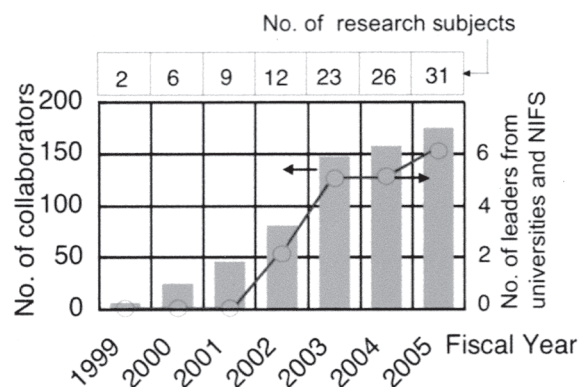


Fig. I.4-1 Evolution of the JT-60 joint research.

4.2 International Collaboration

Status of collaborative research based on the IEA Implementing Agreement on co-operation on the Large Tokamak Facilities is described, following the annual progress report 2005 of the executive committee, which was presented at the 35th Meeting of the Fusion Power Coordinating Committee on Feb 28 – March 1, 2006. This report covers from June 2004 to June 2005. In this period, there were personnel exchanges among the three Parties. The number of personnel exchanges, to which JAEA relates, is 15 in total. 3 personnel exchanges are from JAEA to EU, 7 from US to JAEA, 5 from EU to JAEA.

The exchanges from EU relate to the pedestal study titled “Participation in ITPA Coordinated Experiments and Analysis on Pedestal Characteristics on JT-60U and JET”. The aim of the experiments was to understand the mechanism for the improvement of pedestal performance and change of ELM characteristics, when perpendicular NBI was replaced by tangential Negative-NBI, in particular regarding the role of rotation and ripple loss on the pedestal and ELMs. During the stay, approximately 15 discharges with the JET similarity shape were run over several days on JT-60U. The overall results of the previous experiments were confirmed, but the aim of producing data to distinguish the effect of rotation and ripple losses on pedestal parameters was not achieved. The analysis and the discussion are continuing.

Three exchanges from US relates to the NNB study titled “Long Pulse Neutral Beam Physics”, one relates to the Alfvén eigenmodes study titled “TAE Experiments involving N-NBI”, and one relates to the Resistive Wall Mode (RWM) study titled “Resistive Wall Mode studies”. For the Alfvén eigenmodes study, the discussion about the reverse shear Alfvén eigenmode was carried out for a publication of experimental studies in JT-60U. For RWM study, a visitor from US participated in the experiment for RWM and discussed the results.

II. THEORY AND ANALYSIS

Much progress was made in confinement, transport and MHD researches, such as beta dependence of ELMy H-mode confinement, ITB in reversed shear plasma, aspect ratio effect on external MHD modes and magnetic island evolution in rotating plasma. Integrated simulation code for burning plasma analysis is being developed and validated by fundamental researches of JT-60U experiments. Progress has been made in the NEXT project to investigate complex physical processes in MHD and transport phenomena. The behaviors of the collisionless MHD modes in high temperature plasmas, and the effect of MHD modes on current hole formation were shown. The dynamics of the zonal flows and geodesic acoustic modes (GAMs) were understood in reversed shear configuration and a new gyrokinetic Vlasov code was developed. Cross section data for atomic and molecular collisions and spectral data relevant to fusion research have been compiled and produced.

1. Confinement and Transport

1.1 Origin of the Various Beta Dependence of ELMy H-mode Confinement

Dependence of the energy confinement in ELMy H-mode tokamak on the beta has been investigated for a long time, but a common conclusion has not been obtained so far. Recent non-dimensional transport experiments in JT-60U demonstrated clearly the beta degradation. A database for JT-60U ELMy H-mode confinement was assembled. Analysis of this database is carried out, and the strong beta degradation consistent with above experiments is confirmed. Two subsets of ASDEX Upgrade and JET data in the ITPA H-mode confinement database are analyzed to find the origin of the various beta dependences. The shaping of the plasma cross section, as well as the fuelling condition, affects the confinement performance. The beta dependence is not identical for different devices and conditions. The shaping effect, as well as the fuelling effect, is a possible candidate to cause the variation of beta dependence. [1.1-1]

Reference

1.1-1 Takizuka, T., *et al.*, *Plasma Phys. Control. Fusion*, **48**, 799 (2006).

1.2 Internal Transport Barriers in JT-60U Reversed-Shear Plasmas

Physics of strong internal transport barriers (ITBs) in JT-60U reversed-shear (RS) plasmas has been studied through the modeling on the 1.5 dimensional transport simulation. Key physics to produce two scalings on the basis of the JT-60U box-type ITB database are identified. Figure II.1.2-1 shows the ITB width, Δ_{ITB} , as a function of the ion poloidal gyroradius at the ITB centre, $\rho_{\text{pi,ITB}}$. The standard model reproduces the JT-60U scaling ($\Delta_{\text{ITB}} \sim 1.5\rho_{\text{pi,ITB}}$), while other models does not. As a result, as for the scaling for the narrow ITB width proportional to the ion poloidal gyroradius, the following three physics are important: (1) the sharp reduction of the anomalous transport below the neoclassical level in the RS region, (2) the autonomous formation of pressure and current profiles through the neoclassical transport and the bootstrap current, and (3) the large difference between the neoclassical transport and the anomalous transport in the normal-shear region. As for the scaling for the energy confinement inside ITB ($\epsilon_f \beta_{\text{p,core}} \sim 0.25$ where ϵ_f is the inverse aspect ratio at the ITB foot and $\beta_{\text{p,core}}$ is the core poloidal beta value), the value of 0.25 is found to be a saturation value due to the MHD equilibrium. The value of $\epsilon_f \beta_{\text{p,core}}$ reaches the saturation value, when the box-type ITB is formed in the strong RS plasma with the large asymmetry of the poloidal magnetic field, regardless of details of the transport and the non-inductively driven current [1.2-1].

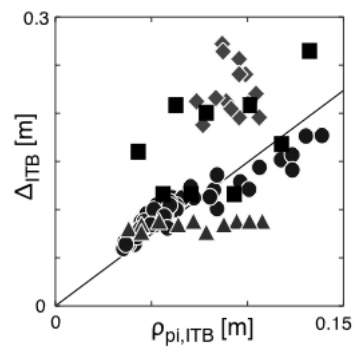


Fig. II.1.2-1 shows Δ_{ITB} versus $\rho_{\text{pi,ITB}}$ for several types of models. Standard model (●) is modified so that neoclassical transport is replaced by gyro-Bohm type (▲), anomalous transport is reduced even in normal-shear region (■), and current profile with weakly-reversed-shear is fixed (◆). Solid line denotes JT-60 scaling.

Reference

1.2-1 Hayashi, H., *et al.*, *Plasma Phys. Control. Fusion*, **48**, A55 (2006).

2. MHD Stability

2.1 Aspect Ratio Effect on the Stability of the External MHD Mode in Tokamaks

The formulation for solving numerically the two-dimensional Newcomb equation is extended to calculate the vacuum energy integral. This extension realizes the stability analysis of ideal external MHD modes from low to high toroidal mode numbers. According to this extension, an effect of the aspect ratio on the achievable normalized plasma pressure (β_N), restricted by ideal external MHD modes whose toroidal mode number is from 1 to 10, is studied. Figure II.2.1-1 shows the decrease of the aspect ratio improves the achievable β_N value, and increases the toroidal mode

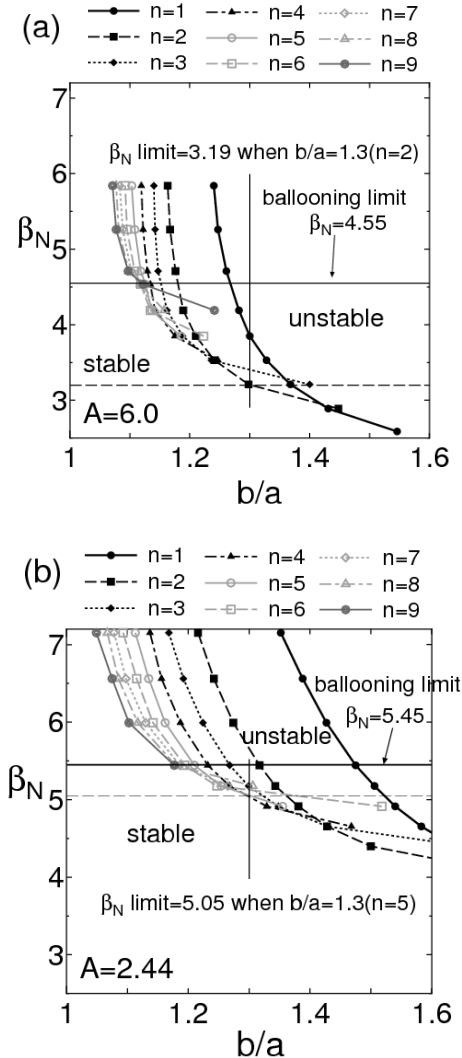


Fig. II.2.1-1 Dependence of the normalized pressure (β_N) limit on the wall position b/a when (a) $A=6.00$ and (b) $A=2.44$, where A is the aspect ratio. The edge safety factor is fixed as 4.44. The β_N limit improves and the toroidal mode number of the mode restricting the β_N limit increases as A decreases when the conducting wall is close to the plasma surface.

number of the external mode restricting the achievable β_N when the conducting wall is placed close to the plasma surface. This aspect ratio effect is confirmed when the safety factor at the plasma surface is between 4 and 5. These represent the importance of the stability of external MHD modes whose toroidal mode number is larger than 3 to determine the achievable β_N .

Reference

- 2.1-1 Aiba, N., *et al.*, "Analysis of an Aspect Ratio Effect on the Stability of External MHD Modes in Tokamaks with Newcomb Equation," to be published in *J. Plasma Phys.*

2.2 Role of Anomalous Transport in Neoclassical Tearing Modes

Role of anomalous transport in onset and evolution of neoclassical tearing modes (NTMs) is investigated. A key role in the evolution NTMs belongs to the radial profiles of the perturbed plasma flow, temperature and density which are determined by the conjunction of the longitudinal and cross-field transport. The influence of anomalous perpendicular heat transport and anomalous ion perpendicular viscosity on early stages of NTM evolution are studied.

Several parallel transport mechanisms competitive with anomalous cross-island heat transport in the formation of the perturbed electron and ion temperature profiles within the island are considered. The partial contributions from the plasma electron and ion temperature perturbations in the bootstrap drive of the mode and magnetic curvature effect were taken into account in construction of a generalized transport threshold model of NTMs. This model gives more favourable predictions for NTM stability and qualitatively modifies the scaling law for β_{onset} . The anomalous perpendicular ion viscosity is shown to modify the collisionality dependence of the polarization current effect, reducing it to the low collisionality limit. In its turn a viscous contribution to the bootstrap drive of NTMs is found to be of the same order as a conventional bootstrap drive for the islands of width close to the characteristic one of the transport threshold model. A viscous contribution to the perturbed bootstrap current is destabilizing for the island rotating in the ion diamagnetic drift direction [2.2-1].

Reference

- 2.2-1 Konovalov, S.V., *et al.*, *Plasma Phys. Control. Fusion*, **47**, B223 (2005).

2.3 Magnetic Island Evolution in Rotating Plasma

It has been well understood that, in tokamak plasmas, magnetic islands resonant with the low q rational surface deteriorate the plasma confinement. Hence, the suppression and control of the magnetic islands is an urgent subject in a tokamak fusion research. Thus, the time evolution of the magnetic island formed at the tearing stable rational surface by the external magnetic flux perturbation in the plasma with poloidal flow is investigated numerically by using the resistive MHD model. It was found that the magnetic island growth phase is divided into four phases, 1) flow-suppressed phase, 2) rapid growth phase, 3) transient phase, and 4) Rutherford type phase. It was also found that the onset condition of this rapid growth depends on the resistivity, but does not much depend on the viscosity. On the other hand, the time constant of the rapid growth phase is almost independent on both the plasma resistivity and the viscosity. After the rapid growth phase, the island enters a transient phase, which becomes clear in the low resistivity regime. Then, the magnetic island grows slowly. This phase seems to be the Rutherford type phase [2.3-1].

Reference

2.3-1 Ishii, Y., *et al.*, "Magnetic Island Evolution in Rotating Plasmas," to be published in *J. Plasma Phys.*.

plasmas.

References

- 2.4-1 Furukawa, M., *et al.*, *Phys. Rev. Lett.*, **94**, 175001 (2005).
- 2.4-2 Furukawa, M., *et al.*, *Phys. Plasmas*, **12**, 072517 (2005).

2.4 Mechanism of Rotational Stabilization of High- n Ballooning Modes

It has been clarified that ballooning modes in a shear toroidal rotating tokamak are stabilized by a countably infinite number of crossings among eigenvalues associated with ballooning modes in a static plasma. It was also found that the crossings cause energy transfer from an unstable mode to the infinite number of stable modes; such transfer works as the stabilization mechanism of the ballooning mode [2.4-1]. The method used in this research has been further explored from the view point of regularization of singular eigenfunctions of operators encountered often in plasma physics [2.4-2]. It has been confirmed that the set of regularized eigenfunctions does capture the transient behavior of the original equations of motion with singular operator for a finite time. Thus, this method will resolve the practical difficulties in analyzing various MHD phenomena with continuous spectra in tokamak

3. Integrated Simulation

3.1 Integrated Simulation Code for Burning Plasma Analysis

Strategy of integrated modeling for burning plasmas in Japan Atomic Energy Agency is as follows: In order to simulate the burning plasma which has a complex feature with wide time and spatial scales, a simulation code cluster based on the transport code TOPICS is being developed by the integration with heating and current drive, the impurity transport, edge pedestal model, divertor model, MHD and high energy behavior model. Developed integration models are validated by fundamental researches of JT-60U experiments and the simulation based on the first principle in our strategy.

The integration of MHD stability and the transport is progressed for three phenomena with different time scale of NTMs ($\sim \tau_{NTM} \sim 10^{-2} \tau_R$), beta limits ($\sim \tau_{Alfven}$) and ELMs (intermittent of τ_E and τ_{Alfven}). Here, τ_R , τ_{Alfven} and τ_E are the resistive skin time, the Alfven transit time and the energy confinement time, respectively. Integrated model of the NTM is produced by coupling the modified Rutherford equation with the transport equation. Integrated model of beta limits is developed by the low- n stability analysis of down streaming data from the TOPICS code. Integrated model of ELM is developed by the iterative calculation of the ideal MHD stability code MARG2D and the TOPICS code. These models are being validated by the data of JT-60 experiments and estimate the plasma performance for burning plasmas.

3.2 Development of Integrated SOL/Divertor code and Simulation Study

An integrated SOL/divertor code is being developed by the JAEA for interpretation and prediction studies of the behavior of plasmas, neutrals, and impurities in the SOL/divertor region [3.2-1]. A code system consists of the 2D fluid code for plasma (SOLDOR), the neutral Monte-Carlo code (NEUT2D), the impurity Monte-Carlo code (IMPMC), and the particle simulation code (PARASOL) as shown in Fig. II.3.2-1. The physical processes of neutrals and impurities are studied using the Monte Carlo (MC) code to accomplish highly accurate simulations. The so-called divertor code, SOLDOR/NEUT2D, has the following features: 1) a high-resolution oscillation-free scheme for solving fluid equations, 2) neutral transport calculation under the

condition of fine meshes, 3) successful reduction of MC noise, and 4) optimization of the massive parallel computer. As a result, our code can obtain a steady state solution within 3 ~ 4 hours even in the first run of a series of simulations, allowing the performance of an effective parameter survey. The simulation reproduces the X-point MARFE in the JT-60U. It is found that the chemically sputtered carbon at the dome causes radiation peaking near the X-point. The performance of divertor pumping in the JT-60U is evaluated based on particle balances. In regard to the design of NCT (National Centralized Tokamak, renaming to the JT-60SA Satellite Tokamak at present) divertor [3.2-1, 3.2-2], the simulation indicates that pumping efficiency is determined by the balance between the incident and back-flow fluxes into and from the exhaust chamber, which depends on the divertor geometry and operational conditions.

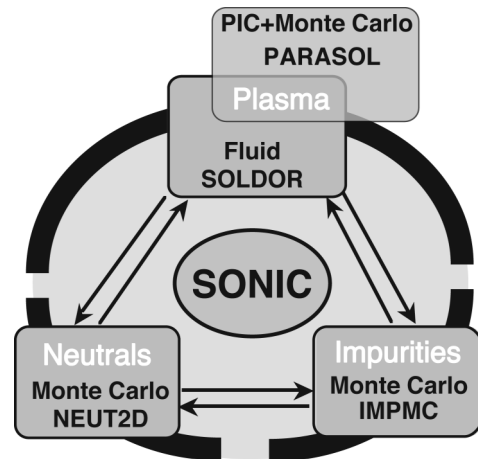


Fig. II.3.2-1 Development of SOL/divertor codes and integration in the JAEA [3.2-1].

References

- 3.2-1 Kawashima, H., *et al.*, *Plasma and Fusion Res.*, **1**, 031 (2006).
- 3.2-2 Kawashima, H., *et al.*, *Fusion Eng. Des.*, **81**, 1613 (2006).

3.3 Transient Behaviour of SOL-Divertor Plasmas after an ELM Crash

Enhanced heat flux to the divertor plates after an ELM crash in H-mode plasmas is a crucial issue for the tokamak reactor. Characteristic time of this heat flux is one of key factors of the influence on the plate. We investigate the transient behavior of SOL-divertor plasmas after an ELM crash with the use of a one-dimensional particle simulation code, PARASOL.

Influence of the collisionality and the recycling rate on characteristic times of the fast-time-scale response and of the slow-time-scale response are examined. The fast time scale is further classified into the supra-thermal-electron transit time scale and the thermal-electron-transit time scale. Supra-thermal electrons supplied by an ELM crash induce the large electron heat flux Q_e and the high sheath potential ϕ at the plate soon after the crash, while the time scale of electron temperature T_e is governed by the thermal electrons. Extremely large heat transmission factor and higher ϕ are observed in the low collisionality regime. In the higher collisionality regime, supra-thermal electrons are thermalized and the value of ϕ becomes proportional to T_e as usual. On the other hand, the slow-time-scale characteristic time is governed by the sound speed in the central SOL region, and is insensitive to the collisionality compared with the fast-time-scale one. The slow-time-scale phenomena are affected by the recycling condition in contrast to fast-time-scale behaviors being independent of the recycling. Peaks of particle and heat fluxes, Γ and Q , are delayed by the increase of recycling rate, though the arrival times of Γ and Q are not changed. Large recycling after the arrival of the enhanced Γ makes the flow speed small in the central SOL region, and the peaks are forced to be delayed. [3.3-1]

Reference

- 3.3-1 Takizuka, T., *et al.*, "Origin of the Various Beta Dependence of ELMy H-mode Confinement Properties," to be published in *Contrib. Plasma Phys.*.

4. Numerical Experiment of Tokamak (NEXT)

4.1 Nonlinear Behaviors of Collisionless Double Tearing and Kink Modes

In high temperature plasmas, the collisionless effects such as the electron inertia and the electron parallel compressibility become important for the magnetic reconnection in MHD modes. Thus, the behaviors of collisionless MHD modes were investigated by gyrokinetic particle simulations. The collisionless double tearing mode (DTM) grows at the Alfvén time scale due to the electron inertia, and nonlinearly induces the internal collapse when the helical flux at the magnetic axis is less than that at the outer resonant surface. It was found that, after the internal collapse, the secondary reconnection is induced by the current concentration due to the convective flow, and a new reversed shear configuration with resonant surfaces can be generated [4.1-1]. The collisionless internal kink mode was also studied in the parameter region where the effects of electron inertia and electron parallel compressibility are competitive for magnetic reconnection. Although the linear growth of the mode is dominated by the electron inertia, it was found that the growth rate can be nonlinearly accelerated due to the electron parallel compressibility proportional to the ion sound Larmor radius. The acceleration of growth is also observed in the nonlinear phase of the DTM [4.1-2].

References

- 4.1-1 Matsumoto, T., *et al.*, *Nucl. Fusion*, **45**, 1264 (2005).
 4.1-2 Matsumoto, T., *et al.*, *Phys. Plasmas*, **12**, 092505-1-7 (2005).

4.2 Stability of Double Tearing Mode and its Effects on Current Hole Formation

In tokamak plasmas with negative central current density, so called the current hole formation can be explained by the destabilization of $m=1/n=0$ resistive kink MHD mode. Here, a strong reversed magnetic shear configuration has two resonant surfaces for low mode numbers, thus DTM could become unstable before the hole formation. However, it was found that the stability of the resistive kink mode, so that the current density gradient to drive the mode, does not change much after a crash by DTM, although the current profile is flattened near the minimum safety factor region [4.2-1].

After a formation of the hole, no MHD activity identified to DTM was observed in experiments, and a resultant profile with two resonant surfaces could have a good stability for DTM. It was also found that the current profile with a strong peak around an inner resonant surface, as shown in Fig.II.4.2-1, is stable for DTM [4.2-2].

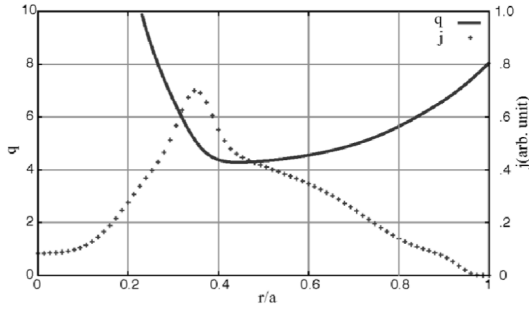


Fig. II.4.2-1 An example of stabilized current density j and safety factor q profiles. When a position of a current peak is shifted to an inner resonant surface for $m/n=5/1$ DTM, DTM becomes to be stable, where m and n are a poloidal and toroidal mode number, respectively.

References

- 4.2-1 Tuda, T., *et al.*, "Roles of Double Tearing Mode on the Formation of Current Hole," to be published in *J. Plasma Phys.*
 4.2-2 Tuda, T., *et al.*, "Stability of Double Tearing Mode in Current Hole Configuration," to be published in *J. Korean Phys. Soc.*

4.3 ZF/GAM Dynamics and Ion Turbulent Transport in Reversed Shear Tokamaks

Zonal flow behavior and its effect on turbulent transport in reversed magnetic shear tokamaks were investigated by global simulations of electrostatic ion temperature gradient driven turbulence. In a high safety factor case ($q_0=2.2$), Fig.II.4.3-1 shows that turbulent heat transport is high in a broad radial region because oscillatory zonal flows or GAMs are dominant. When q_0 is reduced from 2.2 to 1.8 with keeping the other parameters unchanged, zonal flows change from the GAMs to stationary flows in the region around the minimum q surface. As a result of the change in zonal flow behavior, the ion thermal diffusivity is reduced, as shown in Fig.II.4.3-1. This result indicates that the change of zonal flow behavior may trigger the formation of ion transport barriers in the minimum q region.

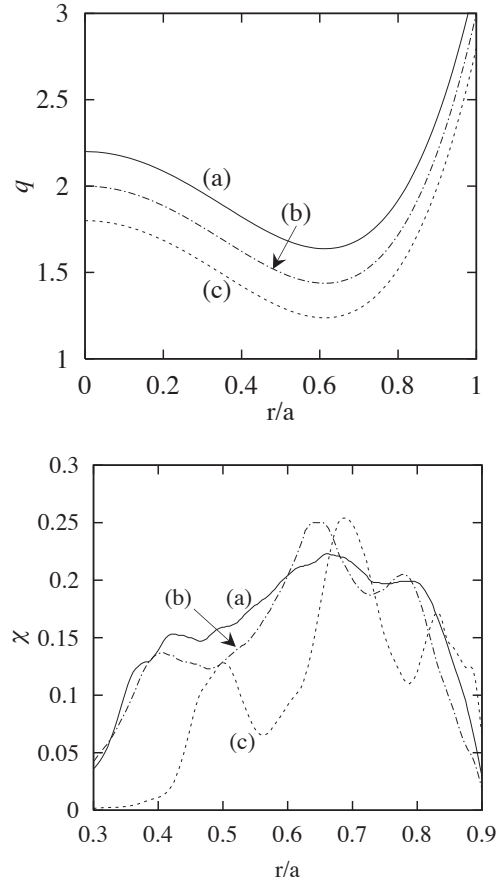


Fig. II.4.3-1 Radial profiles of the safety factor $q=q_0-3(r/a)^2+4(r/a)^4$ for (a) $q_0=2.2$, (b) $q_0=2.0$, and (c) $q_0=1.8$ (top), and the normalized ion thermal diffusivity χ (bottom).

Reference

- 4.3-1 Miyato, N., *et al.*, "Zonal Flow and GAM Dynamics and Associated Transport Characteristics in Reversed Shear Tokamaks," to be published in *J. Plasma Phys.*

4.4 Development of Gyrokinetic Vlasov CIP Code

A gyrokinetic simulation is an essential tool to study anomalous turbulent transport in tokamak plasmas. Although the δf Particle-In-Cell (PIC) method enabled an accurate gyrokinetic simulation of small amplitude turbulent fluctuations with $\sim 1\%$, the method has a difficulty in implementing non-conservative effects such as heat and particle sources and collisions are important, which are essential in realistic long time turbulence simulations. To overcome the difficulty, a new gyrokinetic Vlasov code has been developed using the Constrained-Interpolation-Profile (CIP) method. The code is numerically stable and numerical oscillations, which have been a critical issue in the previous Vlasov simulations, are quite small. In the benchmark tests of ion temperature gradient driven

(ITG) turbulence simulations, the linear growth rates, the nonlinear saturation levels, the zonal flow structures, and the conservation properties are almost the same between the PIC and CIP codes. In addition, computational costs are almost comparable between two codes. A possibility of a long time turbulence simulation was demonstrated from the viewpoints of numerical properties and a computational cost.

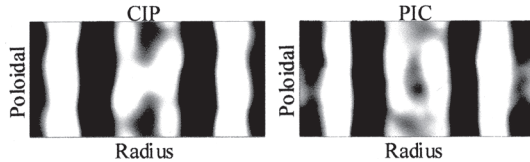


Fig. II.4.4-1 The radial-poloidal contour plots of f observed in the nonlinear quasi-steady phase of the ITG turbulence simulations with CIP (left) and PIC (right) codes. Both results show similar zonal flow patterns.

Reference

- 4.4-1 Idomura, Y., *et al.*, "Comparisons of Gyrokinetic PIC and CIP Codes," *Proc. 32nd EPS Plasma Physics Conf.*, p1.044 (2005), to be published in *J. Plasma Phys.*

5. Atomic and Molecular Data

We have been compiling and producing cross section data for atomic and molecular collisions and spectral data relevant to fusion research [5-1].

Cross sections for 74 processes in collisions of electrons with N_2 and N_2^+ have been compiled [5-2]. In tokamak fusion research, N_2 gas has been injected for heat control. The cross sections are plotted as a function of the electron collision energy, and recommended cross sections are expressed by analytic expressions to facilitate practical use of the data. Figure II.5-1 shows an example of the compiled cross section data. The data have been included in Japanese Evaluated Atomic and Molecular Data Library (JEAMDL), which is available through the Web at the URL <http://www-jt60.naka.jaea.go.jp/english/JEAMDL/index.html>. As to the data production, cross sections for various carbon containing molecules, which are produced from carbon-based plasma-facing materials, have been measured [5-3,4]. Charge transfer cross sections of impurity ions produced from the plasma-facing materials: Be, B, C, Cr, Fe and Ni ions, with gaseous atoms and molecules have also been measured [5-5]. Cross sections of state-selective electron capture in collisions of C^{+4} ions with H^* ($n=2$) atoms have been calculated using a molecular-bases close-coupling method [5-6].

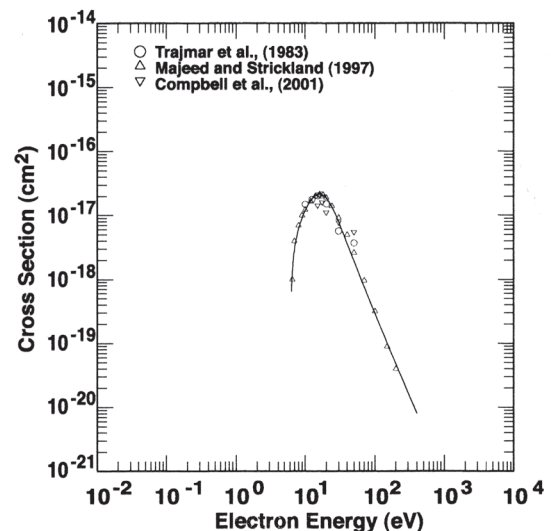


Fig. II.5-1 Cross sections of excitation to $A^3\Sigma_u^+$ for N_2 molecule. The data points indicate the measured cross sections, and the curve indicates an analytical fitting.

Regarding spectral data, wavelengths, energy levels, oscillator strengths, transition probabilities and ionization energies have been critically compiled for tungsten [5-7, 5-8] and gallium [5-9]. Tungsten is one of the candidate plasma-facing materials for future fusion devices, and gallium is a candidate material for liquid divertors.

References

- 5-1 Kubo, H., *et al.*, "Atomic and Molecular Data Activities for Fusion Research at JAERI," to be published in *J. Plasma Fusion Res.*
- 5-2 Tabata, T., *et al.*, *Atomic Data and Nuclear Data Tables*, **92**, 375 (2006).
- 5-3 Makochekanwa, C., *et al.*, *J. Phys. Chem.*, **124**, 024323 (2006).
- 5-4 Kusakabe, T., *et al.*, "Cross Sections of Charge Transfer by Slow Doubly-Charged Carbon Ions from Various Carbon Containing Molecules," to be published in *J. Plasma Fusion Res.*
- 5-5 Imai, M., *et al.*, "Production and Compilation of Charge Changing Cross Sections of Ion-Atom and Ion-Molecule Collisions," to be published in *J. Plasma Fusion Res.*
- 5-6 Shimakura, N., *et al.*, "Electron Capture Processes in Low-Energy Collisions of C^{4+} Ions with Excited H Atoms Using Molecular-Bases Close-Coupling Method," to be published in *J. Plasma Fusion Res.*
- 5-7 Kramida, A.E., *et al.*, "Compilation of Wavelengths, Energy Levels, and Transition Probabilities for W I and W II," to be published in *J. Phys. Chem. Ref. Data*.
- 5-8 Kramida, A.E., *et al.*, "Compilation of Wavelengths and Energy Levels of Tungsten, W III through W LXXIV," to be published in *J. Plasma Fusion Res.*
- 5-9 Shirai, T., *et al.*, "Spectral Data for Gallium: Ga I through Ga XXXI," to be published in *J. Phys. Chem. Ref. Data*.

III. TECHNOLOGY DEVELOPMENT

R&Ds of fusion reactor technologies have been carried out both to further improve technologies necessary for ITER construction, and to accumulate technological database to assure the design of fusion DEMO plants. In the International Fusion Materials Irradiation Facility (IFMIF) program, transitional activities have been continued.

This part is divided into the ten chapters; Super Conducting Magnet, Neutral Beam Injection Heating, Radio Frequency Heating, Blanket, Plasma Facing Components, Structural Material, Tritium Technology, Fusion Neutronics, Vacuum Technology and Technology Transfer. Progresses in FY2005 are described in the following chapters.

1. Superconducting Magnet

Superconducting magnet that can generate a high magnetic field of 16 to 20 T is required to a fusion DEMO plant, following ITER. JAEA is therefore developing high temperature superconductor (HTS) such as $\text{Bi}_2\text{Sr}_2\text{CaCu}_2\text{O}_x$ (Bi-2212) strand to realize a magnetic field of around 20 T.

To produce Bi-2212 superconductor, oxygen has to be supplied to the strand from its surface during heat treatment at around 900°C. Silver is the only material that can avoid melting and oxidation and allow oxygen penetration during heat treatment, and silver is commonly used in Bi-2212. However, for fusion application, the amount of silver in a strand has to be reduced because it is easily activated to produce a long half-life element and is expensive. A Bi-2212 strand having low silver-to-superconductor ratio of 1.3 has therefore been developed [1-1]. The cross-sectional

view of the strand is shown in Fig. III.1-1. Critical current density (J_c) was measured to be 3,000 A/mm^2 , at 4.2 K in a self-field condition. J_c dependence on magnetic field and temperature was also investigated using a high magnetic field facility in National Institute for Materials Science (NIMS).

Fig. III.1-2 shows measured J_c at a temperature of 4.2 K and at fields up to 16 T, and at temperatures of 8 K to 20 K and at fields from 12 T to 30 T. Although the measured J_c values correspond to around 70% of those of a conventional Bi-2212 strand (silver ratio is 2.8), the strand still shows high J_c values and there is no major problem for a practical use.

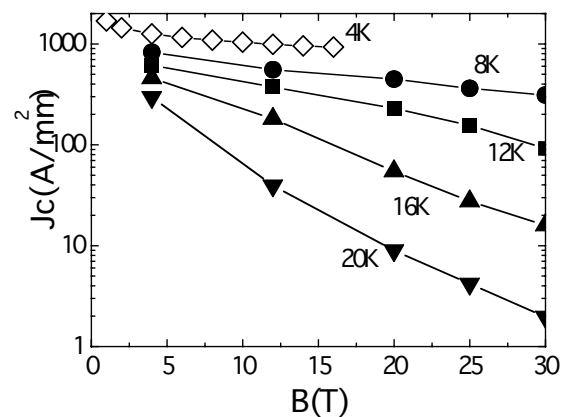


Fig. III.1-2 Critical current density (J_c) of Bi-2212 strand having low silver ratio.

Reference

- 1-1 Isono, T., *et al.*, *Fus. Eng. Des.*, **81**, 1257 (2006).

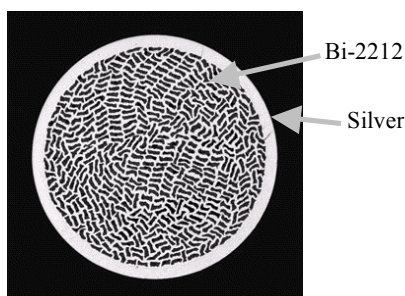


Fig. III.1-1 Cross-sectional view of Bi-2212 strand having low silver ratio. Diameter of the strand is 0.81 mm.

2. Neutral Beam Injection Heating

2.1 Acceleration of 1 MeV Class and High Current Density H⁻ Ion Beam

The ITER NB system requires a high energy and high current beam source, which can produce 40 A (current density: 200 A/m²) D⁻ ion beams at the energy of 1 MeV. To demonstrate the high power negative ion beam acceleration at the energy up to 1 MeV with ampere class, a five stage electrostatic accelerator (the MeV accelerator) has been developed at the MeV test facility of JAEA. After years of R&D, the voltage holding capability was drastically improved. One of the objectives of the present R&D is to accelerate the high current density beam up to the MeV class energy.

Figure III.2.1-1 shows a cross-sectional illustration of the MeV accelerator [2.1-1, 2.1-2]. The insulation gas such as SF₆ cannot be utilized for the beam source under the ITER radiation environment. And hence, whole the beam source structure is to be mounted in vacuum. To test this concept, the main structure of the MeV accelerator is installed in the vacuum inside an FRP (fiber reinforced plastic) insulator stack. The negative ions are generated in the KAMABOKO ion source mounted on the top of the accelerator and are extracted from 9 apertures of the plasma grid by potential difference of several kilo volts applied between the plasma grid and the extraction grid. The extracted negative ions are accelerated by the MeV accelerator, which is composed of 4 intermediate grids and a grounded grid. Between each grid, 200 kV dc voltages are applied to accelerate the H⁻ ions up to 1 MeV.

After installation of the accelerator and pumping down to vacuum, dc voltage is applied continuously to the accelerator. After 30 hours of conditionings without beam acceleration to sustain 1 MV, beam acceleration tests were started. To enhance the H⁻ production, Cs was

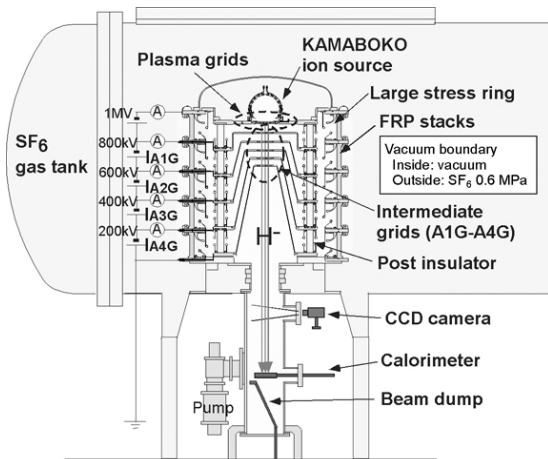


Fig. III.2.1-1 Illustration of JAEA MeV accelerator.

seeded in the KAMABOKO ion source. Figure III.2.1-2 summarizes the highest H⁻ ion current (I_{H⁻}) measured by the calorimeter at various acceleration voltages [2.1-3]. The highest H⁻ current at each acceleration voltages were obtained at the optimum extraction/acceleration voltage ratio of V_{ext}/V_{acc}=1/140. The current density increased according to the Child - Langmuir's law. The perveance ($P = I_{H^-}/V_{acc}^{3/2}$) almost corresponds to those of the ITER design value (200 A/m² at 1 MeV). Up to now, the H⁻ ion beam of 146 A/m² was successfully accelerated up to 836 keV, as the world record of the current density at the MeV level energy beams. The accelerated H⁻ ion current does not show clear saturation even in high voltage regime, which suggests production of enough amounts of H⁻ ions in the KAMABOKO source. In fact, the KAMABOKO source has already achieved 300 A/m² H⁻ ion production at low acceleration voltage (30 kV). Therefore, further increase of current density is expected towards the ITER requirement.

As for the beam quality, Fig. III.2.1-3 shows a profile of the H⁻ ion beam of 134 A/m² at 750 keV. The beam profile was estimated by light emission of residual H₂ gas molecule excited by the H⁻ ion beam at 2 m downstream of the MeV accelerator exit (grounded grid). The rows of 3 beamlets extracted from the 3 x 3 apertures can be clearly distinguished. By assuming a Gaussian profile for each beamlet, the beam divergence angle (e-folding half width) was estimated to be 5 mrad. Thus it was confirmed that the beams has the good quality even carrying the ITER relevant high power. Since the perveance of the H⁻ ion beam (750 keV, 134 A/m²) is almost the same as that of ITER requirement (1 MeV, 200 A/m²), this optics result supports the ITER design (< 7 mrad).

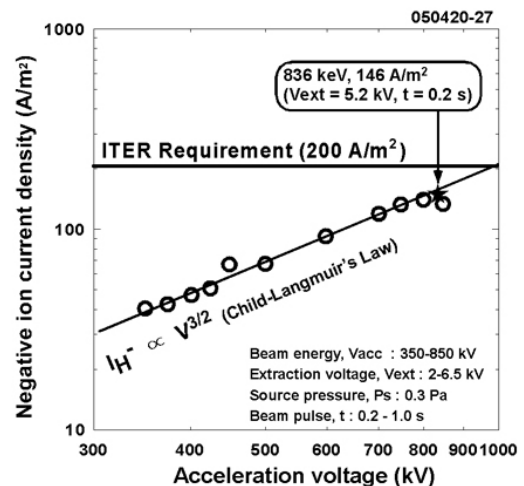


Fig. III.2.1-2 The H⁻ current density at various acceleration voltages.

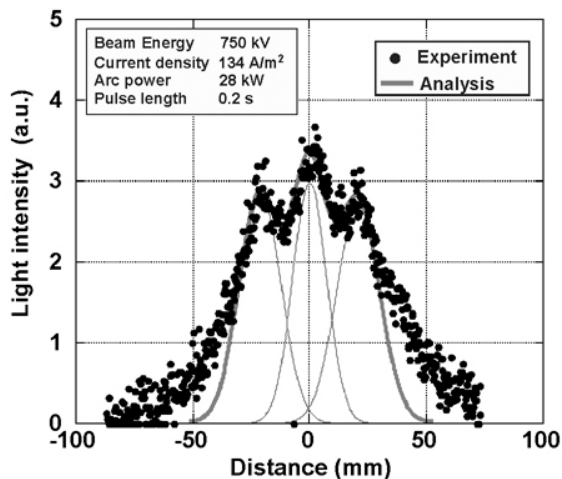


Fig. III.2.1-3 Beam profile of the 700 keV, 134 A/m² H⁻ ion beam measured by the CCD camera.

References

- 2.1-1 Inoue, T., *et al.*, *Nucl. Fusion*, **45**, 790 (2005).
 2.1-2 Inoue, T., *et al.*, *Nucl. Fusion*, **46**, S379 (2006).
 2.1-3 Taniguchi, M., *et al.*, "Acceleration of MeV-Class Energy, High-Current-Density H⁻ Ion Beams for ITER Neutral Beam System," *Rev. Sci. Instr.*, in press.

2.2 Improvement of Beam Uniformity in a Large Negative Ion Source

In the negative ion source for JT-60U, high current negative ion beam is produced from the large extraction area of 45 x 110 cm². However, the current density of extracted negative ions over the wide area is not uniform, which causes poor optics of the beams. Due to this poor beam optics, beam pulse length of JT-60 N-NBI has been limited to avoid high heat loadings on the acceleration grids and the beam line components.

To overcome this problem, experimental studies have been performed using the JAEA 10 A negative ion source whose magnetic configuration is similar to that of the large negative ion source for JT-60 N-NBI. As the results, following new findings were obtained [2.1-1, 2.1-2].

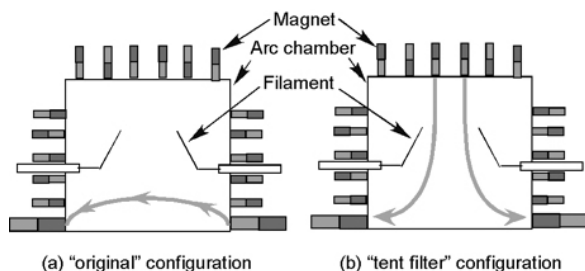


Fig. III.2.2-1 Magnetic configuration of the 10 A negative ion source. (a) "External filter" configuration, (b) "Tent filter" configuration.

- The residual magnetic filter field around the filaments causes a drift of fast electrons emitted from the filaments. Due to this electron drift, the source plasma is localized followed by the non-uniformity of the ion beam.
- The plasma uniformity was improved by reducing the magnetic filter strength. Under the Cs seeded operation, the H⁻ ion beam current was not degraded by the reduction of filter strength although electron temperature was increased to about 4 eV.

According to these results, the magnetic configuration of the JAEA 10 A negative ion source was modified in order to improve the beam uniformity (Fig. III.2.2-1). The transverse magnetic filter field over the plasma grid (external filter), which was used in the original configuration, was removed. Instead of the external filter field, a tent-shaped filter field was formed between the cusp magnet on the source back plate and the large magnets placed outside of the aperture area of the plasma grid. This "tent filter" is effective to suppress co-extracted electrons. In order to enhance the uniform production of atoms or protons, which are considered as primary species of negative ions, the cusp magnets on the source wall were also modified to form a large volume of field free region in the center of the ion source. Figure III.2.2-2 shows the longitudinal beam profile before and after the above modifications [2.2-3]. The beam profile with the external filter configuration showed the non-uniform profile with the deviation of 16%. In the tent filter configuration, the uniformity of the extracted beam was drastically improved, and the deviation of the beam profile was reduced to 8%. The co-extracted electron current was suppressed to a level equivalent to that of the H⁻ ion current. These results indicate that the tent filter configuration is effective to

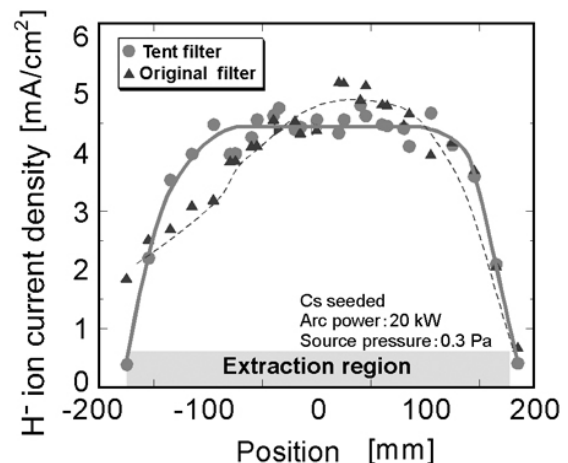


Fig. III.2.2-2 Beam profile for the tent filter configuration compared with the original.

improve the beam uniformity in the Cs seeded negative ion source.

References

- 2.2-1 Hanada, M., *et al.*, *Nucl. Fusion*, **46**, S318 (2005).
 2.2-2 Inoue, T., *et al.*, *Nucl. Fusion*, **45**, 790 (2005).
 2.2-3 Hanada, M., *et al.*, "Improvement of Beam Uniformity by Magnetic Filter Optimization in a Cs-Seeded Large Negative-Ion Source," *Rev. Sci. Instr.*, in press.

2.3 Transport Process of Surface Produced H^- ions in a Negative Ion Source

In order to obtain high current density negative ion beam, it is essential to realize H^- ion extraction at high efficiency. In a Cesium seeded operation as designed in ITER NBI, negative ions are considered to be produced on a surface of the plasma grid (PG) which has low work function by the Cs deposition. However, production mechanism and transport and extraction process have not been clarified enough. The objective of the present study is to clarify transport process of surface produced H^- ions near the PG using a conventional Langmuir probe.

The Langmuir probe is a simple diagnostic tool and gives local information with a spatial resolution, but its results must be applied with some assumptions due to a lack of the theory of sheath formation in plasmas containing negative ions. When the plasma contains negative ions, a decrease of the negative saturation current at the positive bias appears, because a mobility of negative ion is much smaller than that of electron. This fact means flux of negative particles (H^- and electron) into the probe decreases with an increase of negative ions. Thus, negative probe current is sensitive to the existence of negative ions. In the present experiment, distribution of negative ions near the PG, where the production of H^- occurs, was estimated by using a cylindrical probe.

Experiments were carried out using the JAEA 10 A negative ion source. In the present experiment, the tent filter configuration was employed [2.3-1]. The H^- ions were extracted from the extraction area of 140 mm \times 340 mm. In the Cs-seeded operation, negative ion production depends on the work function of PG that can be controlled by the grid temperature. When the temperature of PG increased from 60 degree to 300 degree at a constant arc power, the negative ion beam current I_{H^-} increased by a factor of four and current ratio $R (= J^- / J^+)$ near the PG is strongly correlated with the beam current, while the electron temperature and the ion saturation current remained almost constant. This result

indicates negative ion fraction can be estimated and the contribution of the surface produced H^- ions can be also evaluated through a comparison between the current ratio R obtained with and without Cs seeding operation.

Figure III.2.3-1(a) shows the current ratio R with and without Cs seeding obtained by sweeping the Langmuir probe in a direction perpendicular to the PG surface (Z-direction). It was observed that R decreases steeply near the PG in Cs seeded operation. It is estimated that the negative ion fraction near the PG is up to 40% on a typical operation condition as shown in Fig. III.2.3-1(b).

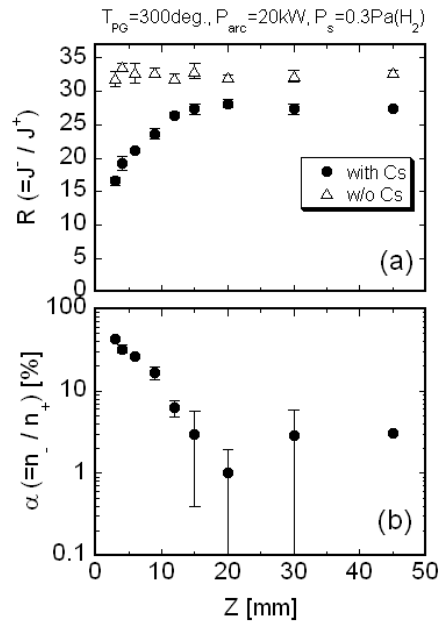


Fig. III.2.3-1 Comparison of current ratio distribution between with and without Cs-seeding.

A survival length of the surface produced H^- ions is also estimated from the Langmuir probe data. A decrement of R from without to with Cs seeding, defined as ΔJ , can be regarded as the effect of surface produced H^- ions. From these data, ΔJ is observed to decrease exponentially in Z-direction and its distribution is expressed approximately as $\exp(-Z / \lambda)$. A coefficient λ represents a survival length of the surface produced H^- ions and it has a value of 12 mm. This indicates that the surface produced H^- ions exist in a region of about 10mm from the PG surface effectively where an electric field configuration for efficient H^- ions acceleration must be optimized.

Reference

- 2.3-1 Hanada, M., *et al.*, *Fusion Eng. Des.*, **77**, 03A515 (2005).

3. Radio Frequency Heating

3.1 Development of 170GHz Gyrotron

Intensive development of a 170 GHz gyrotron (1 MW, continuous wave (CW) operation and 50% efficiency) has been proceeded for the ITER. Up to 2004, the quasi-steady state operation (0.5MW-100s) was demonstrated. To improve the gyrotron performance such as higher power and longer pulse by pre-programming control of beam current were significantly studied in 2005. In addition, we initiated to study the oscillation of higher order volume mode $TE_{31,12}$ for the advanced high power gyrotron, which can reduce the heat load to 1/3 at the cavity wall compared with conventional $TE_{31,8}$ mode.

3.1.1 Demonstration of Steady State Operation of the 170 GHz Gyrotron [3.1-1].

During the 0.5MW/100s operation, the beam current of the gyrotron decreased from 35A to 25A as the pulse duration and consequently, the output power decreased from ~0.6 MW to ~0.46 MW (average power during 100 s). It also causes the oscillation instability due to change of the oscillation mode from $TE_{31,8}$ to $TE_{30,8}$, so called mode jump. The current decrease is mainly caused by cathode cooling due to electron emission. In order to prevent the decrease of the beam current just after turning on, it is necessary to increase the emitter temperature rapidly. By the control of the cathode heater voltage during the shot, temperature of the electron emitter could be stabilized and the beam current drop-off was suppressed. As the countermeasure of the drop-off, pre-programming control of the cathode heater power was applied. Since the cathode heater has a large heat capacity and the temperature response on the electron emitter is slow for the feedback control of the heater voltage, the pre-programming is appropriate for the control. As a result, the stable and steady state operation of 1000 s with 0.2 MW and 600 s with 0.3 MW were demonstrated. The progress of the 170GHz gyrotron development is shown in Fig. III.3.1-1. During the oscillation, no arcing in the gyrotron observed, the vacuum pressure was at a low level of 10^{-5} Pa and the average output power measured by the dummy load was very stable. Temperatures of the inner components of the gyrotron and cooling water were constant for 1000 sec, which gives a prospect for CW operation at the higher power.

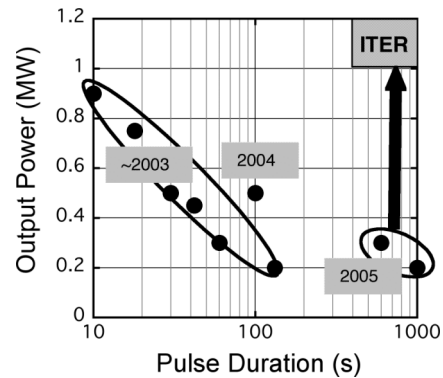


Fig. III.3.1-1 Progress of the 170GHz gyrotron development.

3.1.2 Higher Order Volume Mode Oscillation of $TE_{31,12}$ for an Advanced High Power Gyrotron [3.1-2].

The performance of the high-power operation with oscillation mode of $TE_{31,8}$ for CW, which is the present design for ITER gyrotron, is limited up to 1 MW by a peak heat load at the cavity wall due to ohmic loss. A direct method for heat load reduction is expansion of the cavity radius by applying a higher mode as an oscillation mode. For a 170 GHz advanced gyrotron with 1.5 – 2.0 MW output, higher order volume mode such as $TE_{31,12}$ must be used to keep the ohmic loss on the cavity wall at an acceptable level. On the other hand, as the mode number increases, the problem of mode competition becomes important. In 2005, a short pulse 170 GHz gyrotron with a conventional cylindrical cavity was fabricated and oscillation test without depressed collector was carried out. As an initial result, the stable single mode oscillation was demonstrated at higher order volume mode $TE_{31,12}$. The maximum output power of 1.56 MW with the beam parameter of 84 kV, 70 A and maximum efficiency of 30% at 1 MW output were performed as shown in Fig. III.3.1-2.

No tendency of power saturation was observed up to $I_b=70$ A. It was also obtained that the accurate adjustment of the axis between the gyrotron and the magnetic field was necessary for the stable and single mode oscillation of $TE_{31,12}$. In addition, it was confirmed that the control of the pitch factor of the electron beam just after turn-on was very important for the strong excitation of the target mode, $TE_{31,12}$. The results give the prospect of the advanced high power gyrotron with the stable oscillation of 1.5 MW level at 170 GHz using the standard cylindrical cavity. The

total efficiency of the gyrotron more than 50% would also be possible by applying the depressed collector.

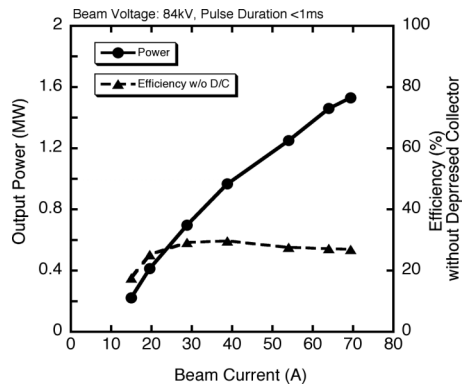


Fig. III.3.1-2 Dependence of output power and efficiency without depressed collector on beam current.

References

- 3.1-1 Kasugai, A., *et al.*, "Long Pulse Operation of 170GHz ITER Gyrotron by Beam Current Control," to be published in *Fusion Eng. Des.*.
- 3.1-2 Kasugai, A., *et al.*, "Digest of Int. Conf. of Infrared and Millimeter Waves," TB4-1 (2005).

3.2 Development of Millimeter Wave Launcher

Advantage of a millimeter (mm) wave launcher is the steering capability of mm-wave beams in order to control plasma heating and non-inductive current drive and suppress magneto-hydro-dynamic instabilities such as neoclassical tearing modes (NTMs) and sawteeth. It is simply achievable by a steering mirror, which is usually placed at the outlet of the waveguide. In a fusion reactor like International Thermonuclear Experimental Reactor (ITER) or DEMO, however, the robust structure against high heat and electromagnetic load are required.

3.2.1 Development of a Steering Mirror

The drawing of the steering mirror design for the ITER equatorial mm-wave launcher is shown in Fig. III.3.2-1[3.2-1]. It consists of a reflecting mirror made of Cu alloy and stainless steel tubes, a rotational shaft, bearings and spiral tubes to feed cooling water to the mirror. A HIP technique is assumed for the fabrication of the mirror. In the thermal and electromagnetic analysis, 1MW/CW per a beam line and the major disruption where plasma current linearly decreased within 40ms were assumed, respectively. It was verified

that temperature and induced stress on the mirror did not exceed the allowable level.

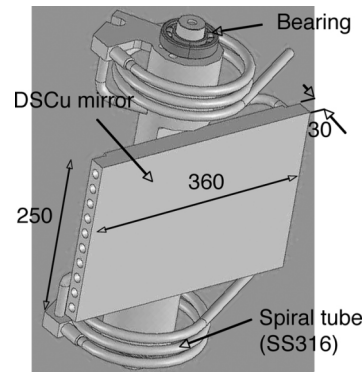


Fig. III.3.2-1 Drawing of the steering mirror for ITER millimeter wave launcher.

High heat load experiment of the mirror mock-up was carried out to investigate the heat resistance and the structure reliability and to demonstrate the cooling capability[3.2-2]. The mock-up is a quarter size of the mirror design shown in Fig. III.3.2-1. The experiment was carried out in JAEA Electron Beam Irradiation Stand (JEBIS) facility. Maximum heat load on the mock-up was 3.2-3.5MW/m² with Gaussian distribution where the waist radius was 25mm. This is the expected condition in the ITER. The pulse length was 30s comparable to steady state condition. Time variation of temperature in the mirror is shown in Fig. III.3.2-2.

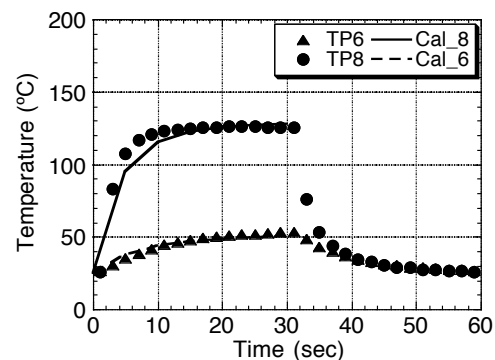


Fig. III.3.2-2 Time variation of temperature in the mirror. Circles and triangles are the experiment and the solid lines are the calculation.

Temperature was measured by thermocouples installed in 4mm-depth from the mirror surface. Circles and triangles are the measurement and the curves are the calculation. The number 6 and 8 indicate the different locations of thermocouples.

Their locations correspond to the X-Y coordinate of (0,45) and (0,15), respectively. “(0,0)” is the mirror center. It was obtained that the measurement agreed with the calculation. In addition, temperature increase rate was unchanged during the experiment. The total shot number was 3000. This result suggests the structure reliability of the bonding layer between Cu alloy and stainless steel tubes. It was concluded that the structure of the steering mirror was reliable and applicable for the ITER.

3.2.2 Development of an Actuator for Steering Mirrors

The development of an actuator for the steering mirror has been proceeded. The design concept of the actuator is a push-pull mechanism applying an ultrasonic (US) motor, a linear motion (LM) actuator that converts the rotation to the linear motion and a straight drive shaft. The advantage of this concept is “simple” and “non-magnetic”. Moreover, it can drive electronically in a magnetic field and therefore, the precise and quick control of the steering angle can be achieved. The drawing and the photograph of the mock-up are shown in Fig. III.3.2-3. The actuator can hold the torque of 3N-m, which would be induced by electromagnetic force at the ITER plasma disruption

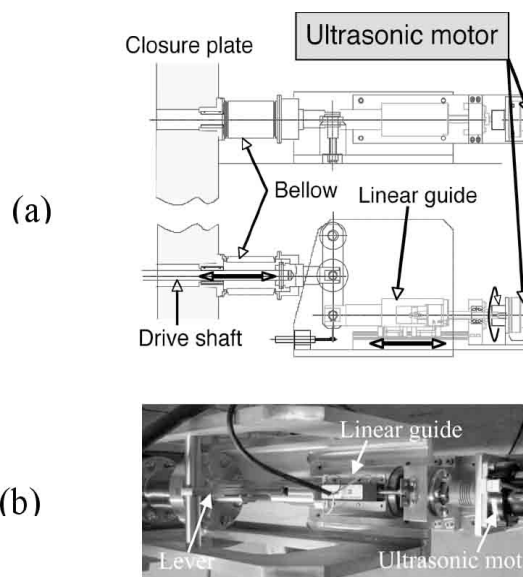


Fig. III.3.2-3 Drawing and the photograph of the actuator mock-up for the steering mirror. (a) Drawing and (b) photograph.

References

- 3.2-1 Takahashi, K., *et al.*, *J. Phys. Conf. Series*, **25**, 75 (2005).
- 3.2-2 Takahashi, K., *et al.*, “Recent Progress on Design and

Development of the ITER Equatorial EC Launcher,” to be published in *Proc. 14th Joint Workshop on ECE & ECRH*.

3.3 Application of High Power RF

Studies of a microwave beaming propulsion were proceeded as the application of high power RF generated by a 170GHz gyrotron under the collaboration between JAEA and University of Tokyo. When high power electromagnetic waves are injected into a thruster, an instantaneous breakdown occurs and atmospheric plasma is formed in the thruster. The plasma absorbs the following beam energy and propagates toward a beam source generating shock waves. The shock waves forms high pressure in the thruster. High pressure is exhausted and impulsive force is produced. Since the input energy to the vehicle is supposed to provide from the ground and atmospheric air is utilized as a propellant, no fuel needs to be loaded onto a vehicle, in principle. Consequently, a remarkably low launching cost is expected.

In 2005, the pressure change inside of the thruster composed only of a cylindrical tube was measured. The thrust generation model of a pulse detonation engine (PDE) was applied and the thrust was estimated from the measured pressure change. Millimeter wave pulses were injected repetitively at the frequency from 40Hz to 15Hz. Dependence of impulse on the repetition frequency was shown in Fig. III.3.3-1.

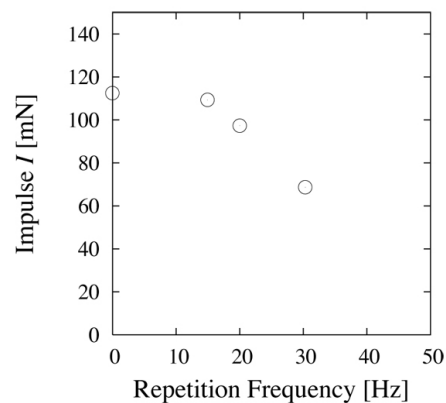


Fig. III.3.3-1 Dependence of impulse on repetition frequency.

Although impulsive thrust was decreased with pulse repetition frequency, the decrease in the thrust at the frequency lower than 20Hz was acceptably small. This result indicates that the maximum repetition frequency, which is necessary for the exhaust and an air-refill process in the thruster, is lower than 20Hz.

4. Blanket

4.1 Fabrication of Partial First Wall Mockup

The structural material for the Test Blanket Module (TBM), Reduced Activation Ferritic/Martensitic steel (RAF/Ms) is a kind of 8%-Cr heat resisting steel. This kind of steel is used for high temperature solution as well-established commercial material. This kind of steel is generally used as thick plate or thick tubes and the joint is performed by welding process. On the other hands, the breeding blanket components involve thin square cooling tubes in the thin first wall components to remove the high heat flux from the plasma. Hot Isostatic Pressing (HIP) is considered to be the most promising joining method for such a complex structure. Therefore, the development of thin components and HIP joining are peculiar to the fusion application. The recent status of these technologies is presented in this section.

4.1.1 Fabrication of Square Tubes by Cold Milling

Recent TBM design requires cylinder and square tubes with 1.5mm wall thickness. A RAF/Ms, F82H is cold-rolled to 15.9 mm in diameter x 1.5 mm thick cylindrical tube (Fig. III.4.1-1). And the cylindrical tube is cold-rolled to 11 mm in square x 1.5 mm thick square tubes (Fig. III.4.1-2). Cold rolling followed by stress relief heat treatment enables to fabricate this thin wall tubes without any break or twisting. The final length of the square tube is longer than 3500mm and it is long enough to fabricate the first wall without any joint in the cooling channels. The surface roughness (Rz) is less than 1 μ m and it is smooth enough to HIP joint.

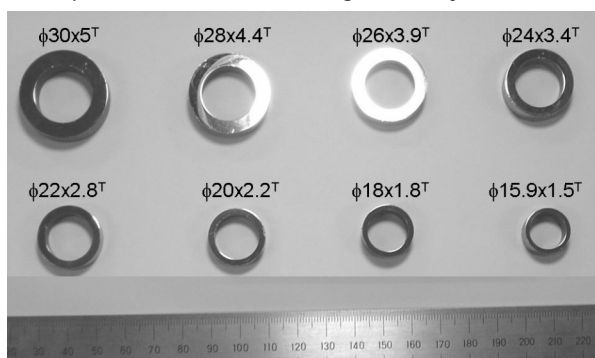


Fig. III.4.1-1 Cross section of F82H cylindrical tubes.

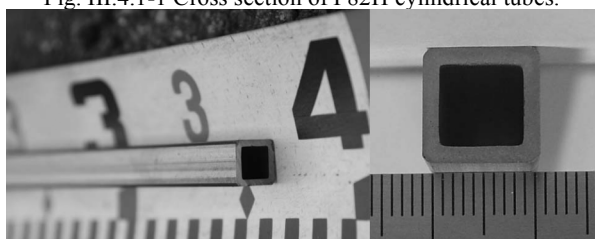


Fig. III.4.1-2 F82H square tube.

4.1.2 Manufacturing of First Wall Mock-Up

To validate the HIP processing for the first wall manufacture, the partial mockup has been fabricated by HIP process. The sixteen square tubes and thin outer/inner plates were bent to simulate a corner region. The radius of curvature was 50mm at the center of square tube. And the peripheral of assemble components were TIG welded to be HIPed. The HIP condition applied to this component was 1373K, 150MPa and 2h holding time. Normalizing at 1233K for 0.5h and tempering at 1023K were performed as post-HIP heat treatment [4.1-1, 4.1-2]. The HIPed first wall mockup is shown in Fig. III.4.1-3. This mockup is planned to be used for non destructive inspection of inner defects and for mechanical tests.

References

- 4.1-1 Hirose, T., *et al.*, *J. Nucl. Mater.*, **329-333**, 324 (2004).
- 4.1-2 Hirose, T., *et al.*, *Fus. Eng. Des.*, **81**, 645 (2006).

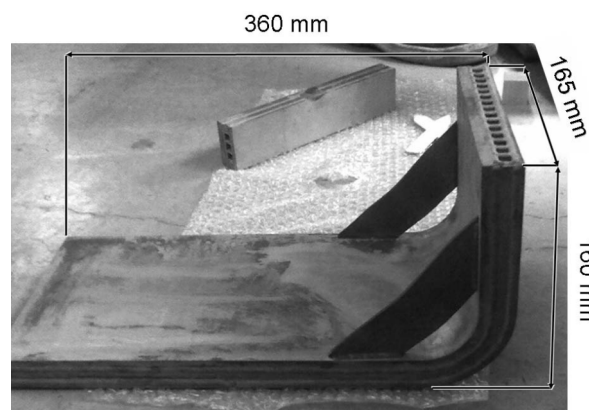


Fig. III.4.1-3 Partial first wall mockup.

4.2 Corrosion Performance of Cooling Channels in Supercritical Water

Japanese primary blanket option is the water cooled solid breeder (WCSB) blanket with the structural material, reduced activation ferritic/martensitic steel, F82H [4.2-1]. In the recent fusion DEMO concepts, supercritical water is attractive coolant options due to its higher thermal efficiency. In the WCSB concept, the corrosion property is one of the most important requirements for fusion structural material. Previous research has shown that F82H does not demonstrate stress corrosion susceptibility in SCW environment [4.2-2]. In this work, corrosion property of F82H was evaluated by weight measurement after ~1000 hour exposure to SCW environment. The exposure test was

conducted at 563-823 K in the high purity water at 23.5 MPa using SCW autoclave.

4.2.1 Weight Change of F82H in SCW Environment

The weight change as a function of test duration for F82H in SCPW is presented in Fig. III.4.2-1. The time dependence of weight change has been described through the plot of some parabolic curves. The weight gain of F82H was 5-6 times larger than that of SUS316 and was almost same as commercial 9%-Cr steel such as T91 and NF616 [4.2-3, 4.2-4].

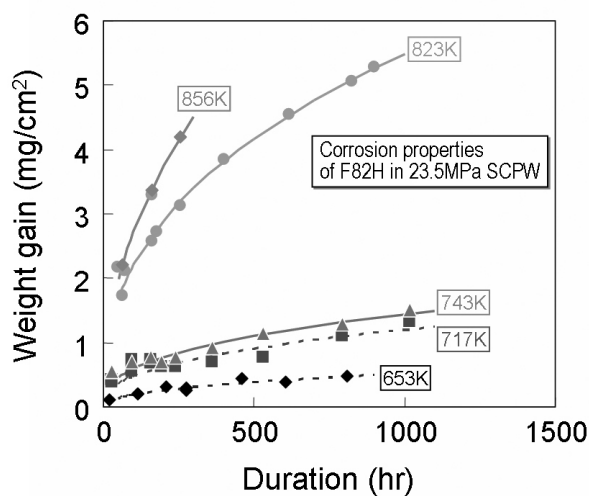


Fig. III.4.2-1 Weight change as a function of test duration for F82H in SCW.

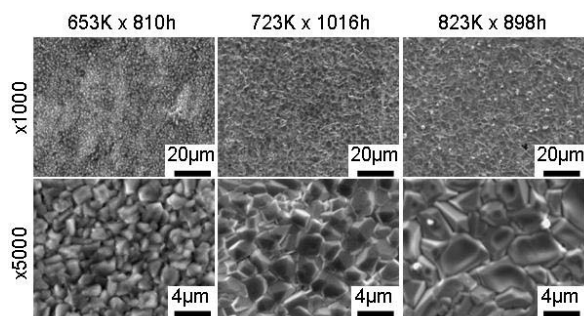


Fig. III.4.2-2 Surface morphologies of F82H after exposure to SCPW.

4.2.2 Morphology of Corrosion Products

The surface morphology of corrosion products is presented in Fig. III.4.2-2. The grain size of corrosion product is increased with test temperature and it is consistent with the weight change behavior. The corroded surface demonstrated neither cracking nor exfoliation, therefore the weight gain is considered to be simply caused by oxidation. The cross sectional

observation and elemental analysis revealed that the corrosion product is a typical duplex oxide structure, in which the scale consists of an outer blocky iron-rich oxide and an inner dense chromium-rich oxide (Fig. III.4.2-3). In the chromium image of elemental mapping, bright contrast which represents the precipitates along with grain boundaries was observed. It means the original F82H surface was the boundary between iron-rich layer and chromium-rich layer. And this means the chromium layer was formed by iron transfer to SCW/F82H boundary. According to the relationship between the thickness of chromium-rich oxide layer and the weight gain behavior, the thickness reduction rate of F82H in 823K SCPW could be roughly estimated to be 0.04 mm/year. This means F82H has good compatibility with SCW under appropriate water chemistry control.

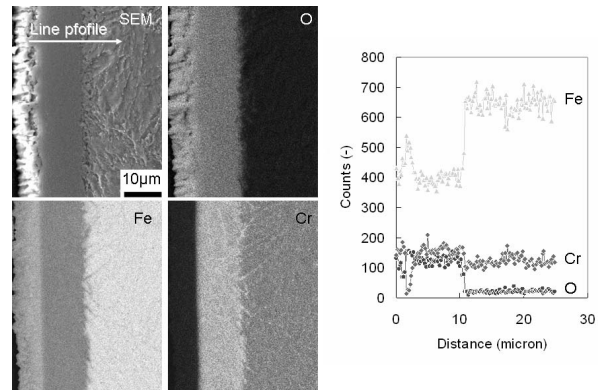


Fig. III.4.2-3 Cross sectional morphology and elemental analysis on F82H tested at 823K SCW.

References

- 4.2-1 Shiba, K., *et al.*, *J. Nucl. Mater.*, **329-333**, 243 (2004).
- 4.2-2 Hirose, T., *et al.*, *Proc. 12th Int. Conf. Fusion Reactor Materials*, ICFRM-12 (2005), submitted to *J. Nucl. Mater.*
- 4.2-3 Harada, M., *et al.*, *Kobe Steel Eng. Rep.*, **53**, 392 (2003).
- 4.2-4 Chen, Y., *et al.*, *Proc. of NACE-Corrosion Annual Conference* (2005).

4.3 Thermo-mechanical Performance of Breeder Pebble Bed

In the current design of the blanket with ceramic breeders, small pebbles of breeding materials are packed into a container and used as a pebble bed. In order to establish a reliable design of the blanket system, it is necessary to analyze heat transfer in the pebble bed. The pebble bed cannot exist without external conditions. Thermal and mechanical conditions on the bed affect

thermal and mechanical properties of the bed. Therefore, it is important to study combined phenomena of thermal and mechanical properties of the bed. However, these properties were investigated independently in the previous works. During the past several years, the group of authors has developed the apparatus that can measure thermal and mechanical properties of the bed simultaneously. In this year, thermal expansion of a Li_2TiO_3 pebble bed was analyzed.

Figure III.4.3-1 shows schematic diagram of the apparatus. It consists of a tensile test-apparatus, INSTRON, and a measurement chamber. Pebbles of Li_2TiO_3 with 2mm diameter were used. They were packed into a container made of alumina. The container was located in the measurement chamber. At first, thermal expansion of the apparatus was calibrated because the measured deformation included thermal expansions of the load rods and the container. Instead of the pebble bed, a column made of pure copper was installed and thermal expansion of the system was measured at different temperatures. Taking into account the estimated thermal expansion of the column of copper, thermal expansion of the rods and the container could be analyzed. Based on the correction, thermal expansion of the pebble bed was measured under compression of 0.1MPa. Temperature of the bed was regulated from room temperature to 973K. From the measured expansion of the bed, average thermal expansion coefficient was estimated. The atmosphere was kept at 0.1MPa of He gas.

Figure III.4.3-2 shows estimated average thermal expansion coefficient of the beds. For the beds with different packing factors ranging from 65.5 to 68.5%, thermal expansion coefficients were from 1.2 to $1.6 \times 10^{-5} \text{K}^{-1}$. In the present conditions, there was not correlation of the thermal expansion coefficient with the packing factor. In the first measurement of the beds without pre-loading, expansion coefficients were larger for the cooling process than heating. When the beds were successively heated and cooled, the difference decreased. This means that relocation of the pebbles arises in the first heat treatment and progress of compaction is larger in the cooling process than heating. After a few heat treatments, packing states of the beds reach stable and expansion coefficients for both heat and cooling processes are close. In the case of the beds that were loaded before the measurements, expansion

coefficients were largest in the first heating process. Fig. III.4.3-3 shows thermal expansion behavior of the pre-loaded bed. When the pre-loaded beds were heated, deformation caused by the pre-loading was relaxed and degree of compaction decreased. Hence, apparent expansion coefficient increased. The result suggests that residual stress in the bed caused by a compressive load can be annealed when the bed is heated without load.

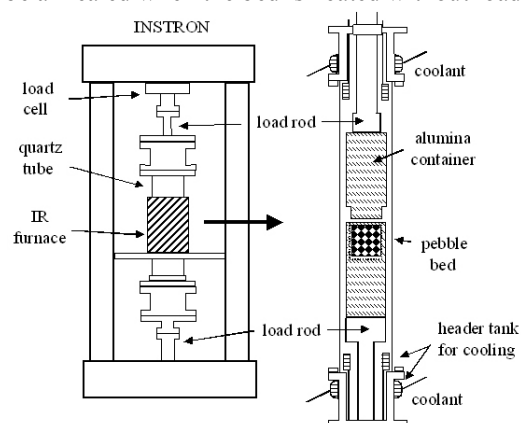


Fig. III.4.3-1 Developed apparatus for simultaneous measurement of thermal and mechanical properties of pebble bed.

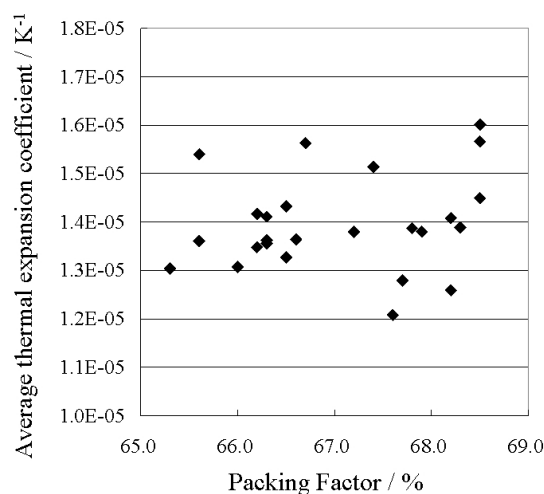


Fig. III.4.3-2 Average thermal expansion coefficient of Li_2TiO_3 pebble bed.

Using the developed apparatus, effective thermo-mechanical properties of the bed, expansion coefficient, stress-strain curves and thermal conductivity, have been obtained in a series of the works. It will be possible to analyze combined phenomena of thermal and mechanical properties for the pebble bed with the assumption that the bed was treated as a continuum model. In the next stage, it is important to confirm and refine the current design by the new calculation based on the present study.

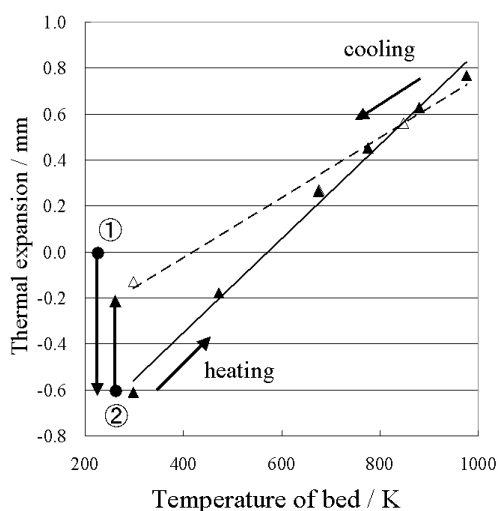


Fig. III.4.3-3 Thermal expansion and relaxation of residual deformation of pre-loaded Li_2TiO_3 pebble bed. (1. pre-loading up to 10MPa, 2. relaxation due to thermal treatment)

Reference

4.3-1 Enoeda, M., *et al.*, *Fusion Eng. Des.*, **81**, 415 (2006).

4.4 Design of Test Blanket Module

Test Blanket Module (TBM) test in ITER is one of the most important milestone in the development of the breeding blanket in Japan. This year, detailed structure designs of Water Cooled Solid Breeder (WCSB) TBM and Helium Cooled Solid Breeder (HCSB) TBM were performed, based on the estimation of coolant hydraulic performance [4.4-1].

Structure design of WCSB TBM has been performed, based on the design of the blanket design for the DEMO plant. The design of the WCSB TBM has the following features [4.4-2].

- (a) First wall and side walls are fabricated by Hot Isostatic Pressing (HIP) using RAFM to form built-in cooling channel structure.
- (b) Vertical slits were adopted to split the blanket module into smaller sub-modules, in less than 50 cm intervals, for the purpose of reducing the electro-magnetic force in plasma disruption events and increasing the endurance to internal over-pressure in the case of coolant ingress in the module. Sub-modules are integrated at rear wall by welding.
- (c) Breeder and multiplier are packed in layered pebble beds whose partition walls are integrated with cooling pipes. The internal structure is designed according to the same concept as the breeding blanket for the DEMO plant.

In the structure design, the coolant flow passage and hydraulic performance were considered as one of the key design issues, as well as the fabricability. TBM design conditions are listed in Table III.4.4-1 [4.4-1]. Figure III.4.4-1 shows the schematic 3 dimensional structure of WCSB TBM [4.4-2]. The structure design showed sound progress to establish detailed drawings with consideration of coolant route, fabrication and assembly procedures of modules including pebble packing. Thermo-mechanical integrity was evaluated by FEM analysis.

Table III.4.4-1 Major Specification of the WCSB and HCSB TBMs [4.4-1].

	WCSB	HCSB
Structural Material	F82H	
Coolant	Water	He gas
Neutron Multiplier	Be, or Be_{12}Ti	
Tritium Breeder	Li_2TiO_3 , or other Li ceramics	
Surface Heat Flux	0.3(aver.), 0.5(max.) MW/m^2	
Neutron Wall Loading	0.78(aver.) MW/m^2	
First Wall Area	$0.68 \times 1.94 \text{ m}^2$	$1.49 \times 0.91 \text{ m}^2$
Coolant Pressure	15.5 MPa	8 MPa
Inlet/Outlet	280/325 °C	300/500 °C
Heat Deposition	1.55 MW	1.61 MW
Tritium Production Rate	0.156g/FPD	0.18g/FPD
Coolant Flow Rate	5.18kg/s	1.8kg/s

Helium Cooled Solid Breeder TBM is designed with the same concept as the WCSB TBM, since the helium cooling is the backup cooling system option to the water cooled solid breeder blanket for the DEMO plant. Figure III.4.4-2 shows the typical drawing of horizontal cross sections of HCSB TBM [4.4-1]. Detailed dimensions of cooling tube sizes and pitch sizes, the first wall configuration and thickness of internal breeder and multiplier layers were decided taking into account the thermal-hydraulic characteristics and nuclear characteristics of He gas coolant. In the case of HCSB TBM, three sub-modules are integrated at the rear wall of the TBM. Internal structure of the sub-module has almost same box structure and multi-layer internal structure as that of the WCSB TBM. It is noted that there is a space of 96mm thickness in front of the back plate where neutron multiplier pebbles are not packed to lay coolant connecting pipes, helium

purge gas connecting pipes and cable conduits for instrumentations. The similar important analyses on neutronics, thermo-mechanical and tritium generation of the HCSB TBM have been also performed to show the integrity and functional performance.

With respect to the coolant flow route and hydraulic design of the WCSB TBM, the coolant is fed to the lower manifold of the back plate from the TBM cooling system which is common for two sub-modules. Coolant inlet condition is 15.5MPa, 280°C and 5.18 kg/s. The coolant flows in parallel for two sub-modules. First, the coolant flows upwards through the first wall rectangular channels (8mm by 8mm) with a pitch of 11mm and then down through the side wall rectangular channels (10mm by 10mm) with a pitch of 46mm. The superficial velocity of water coolant is set to 2.24 and 2.17 m/s for the first wall and side wall coolant channels [4.4-1]. The coolant from side walls is collected in a circular manifold below the breeding region per each sub-module. At the breeding region, the coolant flows upwards through the cooling panel nearest the first wall and then down through other cooling panels via the immediate manifold above the cooling region. Cooling channels of cooling panels consist of same tubes of 9mm ID with different pitches per each cooling panel according to the removal heat. Finally, the coolant flows upwards through circular

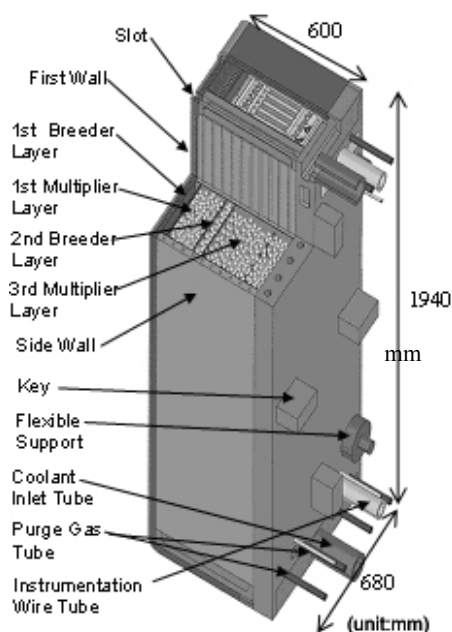


Fig. III.4.4-1 Three dimensional view of the structure of the WCSB TBM. [4.4-2]

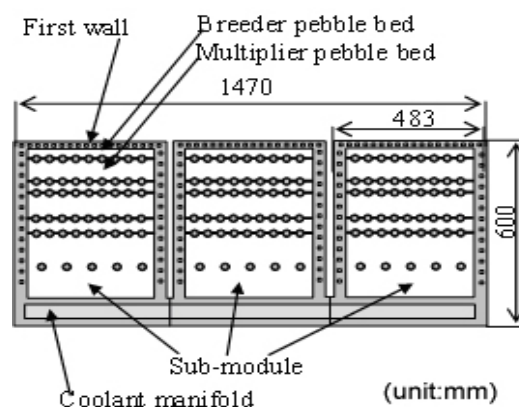


Fig. III.4.4-2 Structure of Typical Cross Sections of the HCSB TBM. [4.4-2]

channels of 28mm ID in the back plate and two cooling lines are integrated in the upper manifold of the back plate. The coolant heated up to 325°C returns to the TBM water cooling system.

With respect to the coolant flow route and hydraulic design of the HCSB TBM, coolant is fed to three sub-modules in parallel. Inlet flow rate is 1.8 kg/s. The coolant inlet temperature of 300°C is the maximum allowable temperature condition to keep the maximum temperature of F82H lower than the allowable temperature of 550°C at the first wall surface. As for the HCSB TBM sub-module proposed by Japan, coolant flow route is as follows. The coolant fed to the lower manifold of the back plate first flows upwards through the first wall rectangular channels (8mm by 8mm) with a pitch of 11mm and then down through the side wall rectangular channels (10mm by 10mm) with a pitch of 22.5mm same as the water-cooled TBM sub-modules. The superficial velocity of helium coolant is set to 35.1 and 25.9 m/s for the first wall and side wall coolant channels [4.4-1]. After cooling side walls, the coolant is split into two lines, the main cooling line and the bypass line, at the manifold below the breeding region to achieve the breeder and neutron multiplier material temperature as high as possible. At the main cooling line of which the flow rate is 0.43kg/s, the coolant flows upwards through all cooling panels in parallel and then flows out from the sub-module via to the upper manifold of the back plate. The coolant outlet temperature is up to 500°C. The bypass flow with 401 °C is extracted and mixed with the breeding zone outlet and finally the coolant conditions is made to 472.2°C

and 1.8 kg/s [4.4-1].

By the detailed structure designs of TBMs, detailed R&D issues for prototype TBM were clarified and incorporated in the R&D plan. Also, by using the detailed structure design, safety evaluation including the Failure Mode and Effect Analysis and preliminary safety analysis are foreseen as the preparation of the design description documents of the TBMs.

References

- 4.4-1 Nomoto, Y., *et al.*, *Fusion Eng. Des.*, **81**, 719 (2006).
 4.4-2 Enoda, M., *et al.*, *Fusion Eng. Des.*, **81**, 415 (2006).

4.5 Development of Tritium Breeder and Neutron Multiplier Materials

4.5.1 Development of Tritium Breeder

Lithium titanate (Li_2TiO_3) pebbles of 0.3-2 mm in diameter have been fabricated by a wet process, and evaluation of their mechanical and chemical properties has been performed for design of fusion blanket packing using small Li_2TiO_3 pebbles.

Collapse loads of Li_2TiO_3 pebbles with different diameters were measured by an unconfined compression tester, and contact strengths of these pebbles were evaluated by Hertzian contact theory. Figure III.4.5-1 [4.5-1] shows the relationship between the radius of the Li_2TiO_3 pebbles and the maximum contact strength of these pebbles. The maximum contact strength evaluated from the measured collapse loads of Li_2TiO_3 pebbles decreased with increasing the radius. The evaluated contact strength was in the range of about $\pm 30\%$ of the average value (about $7.08 \times 10^3 \text{ MPa}$) of the contact strength in this test. The average radial strength of Li_2TiO_3 pebbles was about 1.7 times large as the evaluated compression strength. The deviation of the strength was large because of the low density of 81-85%T.D. and poor sphericity of the Li_2TiO_3 pebbles. It is also noted in Fig. III.4.5-1 that the contact strength of Li_2TiO_3 pebbles was independent of ^6Li enrichment. Volatile species released from Li_2TiO_3 were evaluated under individual conditions of vacuum, D_2 , D_2O and O_2 atmospheres by means of an atmosphere-controlled high-temperature mass spectrometry [4.5-2].

Vapor species of Li(g) , LiOD(g) , $\text{D}_2\text{(g)}$ and $\text{D}_2\text{O(g)}$ were observed in the mass spectra when adding D_2 and D_2O gas, while in vacuum and O_2 atmosphere observed species were Li(g) , $\text{Li}_2\text{O(g)}$, LiO(g) and $\text{O}_2\text{(g)}$. The sum

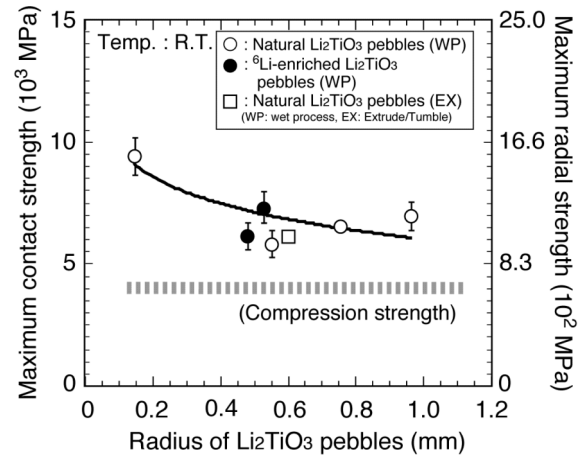


Fig. III.4.5-1 Relationship between radius of Li_2TiO_3 pebbles and maximum contact strength. Reprinted from Tsuchiya, K., *et al.*, *Fusion Eng. Des.*, **81**, 1065 (2006), with permission from Elsevier Ltd.

of the partial pressures of Li-containing species was calculated (see Fig. III.4.5-2).

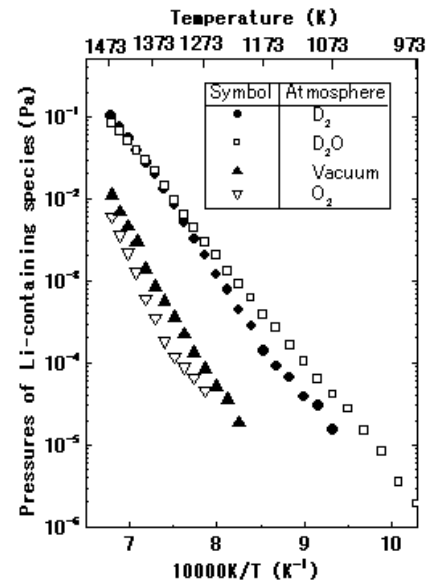


Fig. III.4.5-2 Pressures of Li-containing species ($P_{\text{Li}}^{\text{total}}$) over Li_2TiO_3 under the conditions of vacuum, D_2 , D_2O and O_2 atmospheres. Reprinted from Hoshino, T. *et al.*, *Fusion Eng. Des.*, **81**, 555 (2006), with permission from Elsevier Ltd.

Its order in these atmospheres was as follows:

$$P_{\text{Li}}^{\text{total}}(\text{D}_2\text{O}) = P_{\text{Li}}^{\text{total}}(\text{D}_2) > P_{\text{Li}}^{\text{total}}(\text{Vacuum}) > P_{\text{Li}}^{\text{total}}(\text{O}_2)$$

After the vapor pressure measurement in the D_2 atmosphere, the color of the sample was found to be changed from white to dark blue. This behavior implies the formation of oxygen deficient defects in the

reduction atmosphere. In the blanket design of fusion reactors, the calculation of the pressures of Li-containing species (P_{Li}^{total}) is important in order to estimate the amount of Li loss from Li_2TiO_3 .

In a related work, irradiation behavior of Li_2TiO_3 under a fusion reactor environment was simulated by simultaneous irradiation of Li_2TiO_3 with i) single ion beams and ii) triple ion beams simultaneously or sequentially of O^{2+} , He^+ and H^+ [4.5-3]. Results of Fourier transform-infrared photoacoustic spectroscopy (FT-IR PAS) suggest that the amount of TiO_2 formed is proportional to the displacements per atom (dpa) and that the method of irradiation, that is, the single, the simultaneous triple or the sequential triple irradiation, does not affect the formation of TiO_2 . On the other hand, dependence of the $3450cm^{-1}$ peak area, which is due to the O-H bond, on dpa suggests that the amount of lattice defects generated by irradiation, which is considered to trap hydrogen near the surface, is affected by the method of irradiation, as shown in Fig.III.4.5-3.

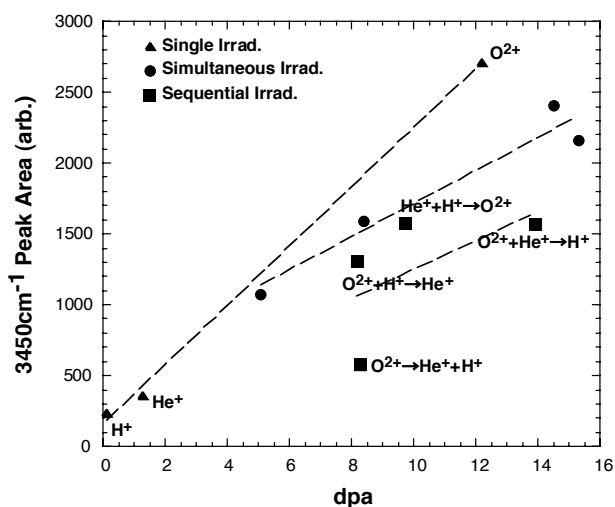


Fig. III.4.5-3 Dependence of the 3450 cm^{-1} peak area on dpa. Notation for the sequential irradiation as "A→B" means that irradiation of beam B was performed after closing of irradiation of beam A [4.5-3].

These results may suggest that H^+ implantation degrades the generation of hydroxyl (-OH) group near the surface by trapping hydrogen in the irradiation defects. This effect of the H^+ implantation is larger in the case where the implantation is performed after introducing the defects than that performed simultaneously.

4.5.2 Development of Neutron Multiplier

Beryllium alloys such as Be-Ti alloys have been

expected as promising candidates for advanced neutron multipliers. Recently, characteristics of $Be_{12}Ti$ and Be-Ti alloys with αBe phase have been evaluated for the pebble fabrication development [4.5-4].

As a part of the research, compatibility was evaluated between Be-Ti alloys (Be-3at%Ti, Be-5at%Ti and Be-7at%Ti) and F82H steel [4.5-5].

Reaction products such as Be_2Fe and Fe-Cr, as well as Be, were detected by X-ray diffraction analyses on the surface of F82H after annealing of the specimens.

The thickness of the reaction layer between Be-Ti alloys and F82H after annealing at $600^\circ C$ for 1000 h was less than 3mm, whereas the reaction layer on beryllium metal was about 15 mm thick. At $800^\circ C$ for 1000 h, the thickness of the reaction layer of Be-5at%Ti and Be-7at%Ti was less than 50 mm, whereas that of beryllium metal was about 200 mm. It is obvious that the compatibility between Be-Ti alloy and F82H was much better than that between Be and F82H.

References

- 4.5-1 Tsuchiya, K., *et al.*, "Evaluation of Contact Strength of Li_2TiO_3 Pebbles with Different Diameters," *Fusion Eng. Des.*, **81**, 1065 (2006).
- 4.5-2 Hoshino, T., *et al.*, "Vapor Species Evolved from Li_2TiO_3 Heated at High Temperature Under Various Conditions," *Fusion Eng. Des.*, **81**, 555 (2006).
- 4.5-3 Yamaki, D., *et al.*, "Observation of Microstructural Changes in Li_2TiO_3 Caused by Multi-ion Beam Irradiation," *JAEA-Review*, 2005-001, 212 (2006).
- 4.5-4 Mishima, Y., (Tsuchiya, K.), *et al.*, "Recent Results on Beryllium and Beryllides in Japan," *Proc. 12th Int. Conf. Fusion Reactor Materials*, ICFRM-12 (2006), to be published in *J. Nucl. Mater.*.
- 4.5-5 Tsuchiya, K., *et al.*, "Compatibility Between Be-Ti Alloys and F82H Steel," *Proc. 12th Int. Conf. Fusion Reactor Materials*, ICFRM-12 (2006), to be published in *J. Nucl. Mater.*.

4.6 Irradiation Technology Development for In-pile Functional Tests

Envisaging the irradiation tests of the Test Blanket Module (TBM) using ITER, development of irradiation technology has been progressed with the aim of performing reactor irradiation tests simulating the structure and environment of the TBM. For these purposes, research activities were made in 1) tests of ceramic coating for reduction of tritium permeation, and 2) analyses of irradiation data of a Li_2TiO_3 pebble bed.

4.6.1 Ceramic Coating for Reduction of Tritium Permeation

An irradiation test of ferritic steel (F82H) with a coating of $\text{Cr}_2\text{O}_3\text{-SiO}_2$ including CrPO_4 has been started in the Japan Materials Testing Reactor (JMTR). The specimen will be irradiated up to a fast neutron fluence ($E>1\text{MeV}$) of $2\times 10^{25} \text{ n/m}^2$ at a temperature range from 300°C to 400°C . Post-irradiation examinations (PIEs) will be carried out on observation of the coating by optical microscopy and scanning electron microscopy (SEM), and on other items.

In-pile experiments on tritium permeation were conducted for F82H steel with and without the coating of $\text{Cr}_2\text{O}_3\text{-SiO}_2$ including CrPO_4 , using a research reactor, IGV.1M, in Kazakhstan through an international cooperation of the International Science and Technology Center (ISTC). The tritium source used was liquid lithium-lead eutectics, Pb_{17}Li , which was poured into a space around a tubular diffusion cell as a specimen of F82H with or without the coating on the inner surface of the cell. The irradiation time at a full reactor power of 6MW was about 4 h, which corresponds to a fast neutron fluence of about $2\times 10^{21} \text{ n/m}^2$ ($E>1.1\text{MeV}$). Data on tritium fluxes and kinetics of tritium flux increase from the start point of the reactor irradiation have been obtained. Evaluation of these in-pile results has been started in detail.

4.6.2 Analyses of Irradiation Data of Li_2TiO_3 Pebble Bed

An irradiation test of a Li_2TiO_3 pebble bed was continued using JMTR [4.6-1]. The irradiation period was 15,250 hrs, and the fast ($E>1\text{MeV}$) and thermal ($<0.683\text{eV}$) neutron fluences were about 2×10^{23} and $2\times 10^{24} \text{ n/m}^2$, respectively. It was clarified that the tritium release properties were hardly changed by the irradiation so far. Besides, it was found that the thermal diffusivity of the Li_2TiO_3 pebble bed was also hardly changed by the irradiation up to the neutron fluence.

Reference

- 4.6-1 Tsuchiya, K., *et al.*, "Breeding Blanket Development –Tritium Release from Breeder–," *JAEA-Technology*, 2005-003 (2005).

5. Plasma Facing Components

5.1 Critical Heat Flux of a Copper Screw Tube under High Temperature Pressurized Coolant Condition

In the R&Ds on Plasma Facing Components (PFCs), JAERI/JAEA has developed a screw tube that has as high heat removal performance as a swirl tube. In FY05, its Incident Critical Heat Flux (ICHF) testing using a hydrogen ion beam facility was carried out to investigate the effect of subcooling of ICHF at the cooling conditions relevant to DEMO divertor. The test sample was the screw tube made of pure copper with the thread of M10 and its pitch of 1.5 mm. Figure III.5.1-1 shows experimental values of ICHF of the screw tube at the cooling tube wall with respect to the subcooling, T_{sub} , ranging from 60K to 200K at 4MPa, in which the saturated temperature of water is 250°C . ICHF depends strongly on T_{sub} and flow velocity of cooling water, and its dependency on T_{sub} is expressed by linear function within the present experimental condition. At the mass velocity of 0.56 kg/s, which corresponds to the axial flow velocity of 10 m/s at room temperature, the ICHF values of 48 MW/m^2 at T_{sub} of 200K (bulk temperature, T_{bulk} , is 50°C) was reduced to ICHF of 26 MW/m^2 at T_{sub} of 60 K ($T_{\text{bulk}}=190^\circ\text{C}$). Although the increasing of temperature of cooling water of 140 K causes 50% reduction of ICHF, ICHF of 26 MW/m^2 in the screw tube remains twice higher than that in smooth tube at the same cooling condition. This result encourages us to examine the applicability of screw tube to DEMO divertor.

5.2 High Heat Flux Test of a Tungsten Armored Divertor

As one of the R&D activities on the DEMO divertor, a tungsten armored divertor mockup has successfully been developed in JAERI/JAEA. In our present DEMO divertor design, the primary candidate structural material is a RAFM steel, F82H, and the primary candidate armor material is tungsten. From the view point of heavy neutron irradiation in the DEMO environment, direct bonding trial of these materials was made by using HIP bonding method. The bonding temperature was 970°C for 2 hours at 150 MPa, which combined with normalizing for F82H, followed by tempering at 750°C for 1.5 hours. These conditions are based on our previous test result [5.2-1]. A high

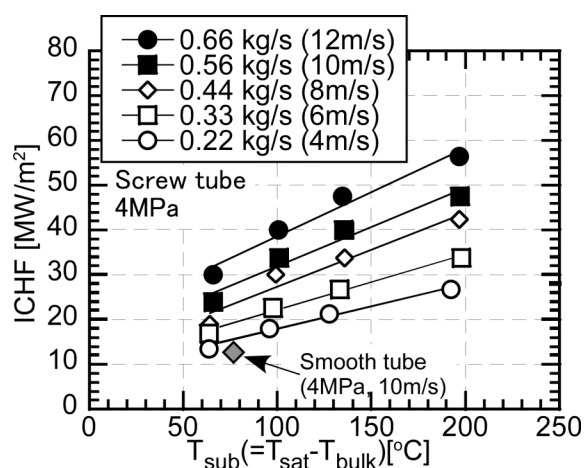


Fig. III.5.1-1 Dependency of ICHF of screw tube on subcooling, T_{sub} . Velocities in parentheses in the figure are axial flow velocity of cooling water in the screw reduced at the room temperature.

heat flux test of the divertor mockup with a screw cooling tube was performed at an electron beam test facility, JEBIS. Heat flux deposited on the tungsten armor was 10 MW/m^2 to simulate the DEMO divertor condition. The heat flux was cyclically loaded to the mockup. After 270 thermal cycles, the central armor tile showed debonding from the cooling tube, as shown in Fig. III.5.2-1. It was found that modification of the direct bonding method using HIP technique is necessary; insertion of a compliant material, such as copper alloys, will be one solution for F82H/tungsten joint.

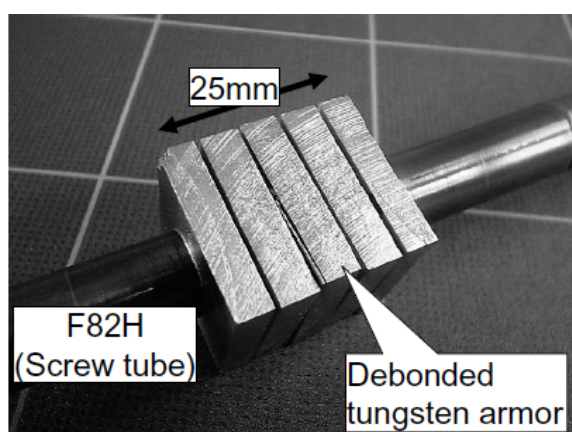


Fig. III.5.2-1 Tungsten divertor mockup after 270 thermal cycles at 10 MW/m^2 . The debonded tungsten armor also showed surface cracking.

Reference

5.2-1 Hirose, T., *et al.*, *J. Nucl. Mater.*, **329–333**, 324 (2004).

6. Structural Material

6.1 Development of Structural Materials for Blanket

The neutron irradiation effects of F82H, Reduced Activation Ferritic/Martensitic (RAFM) steel developed in JAEA, have been investigated as one of the most promising structural materials for the ITER breeding blanket modules and DEMO blankets. In 2005, neutron and ion irradiation experiments using HFIR, JMTR, and so on have been continued.

6.1.1 Irradiation Effects on Fracture Toughness Properties

Under the Japan-US collaboration of fusion materials research, neutron irradiation experiments using High Flux Isotope Reactor (HFIR) in ORNL are in progress. In 2005, the disassembly of a target capsule of JP26 and four rabbit capsules were completed. The JP26 mainly includes samples for the research of fracture toughness of F82H. Neutron irradiation was continued for the target capsules of JP27, JP28 and JP29, aiming at neutron irradiation damage level of 20, 50 and 50dpa, respectively.

It is well known that the mechanical properties of the steels like F82H shows strong dependence on the heat treatment conditions. The dependence of ductile-brittle transition temperature (DBTT) on tempering time and temperature was examined for F82H irradiated at 523K to a neutron dose of 1.9 dpa in the JMTR[6.1-1]. The heat treatment was performed at 1023K and 1053K for 0.5 h to 10 h after the normalizing at 1313K for 0.5 h. 1/3CVN specimens were used in this study, and the absorbed energies in the impact tests were measured as a function of temperature. As shown in Fig. III.6.1-1 DBTT of F82H steels irradiated at 523K to 1.9 dpa was ranged from 250K to

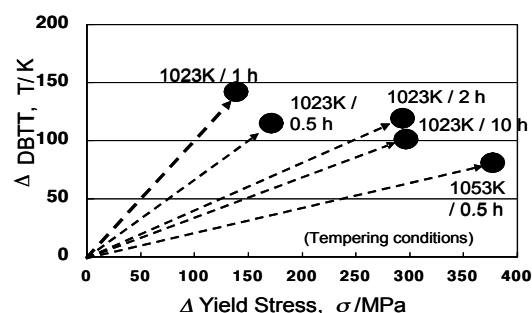


Fig. III.6.1-1 Relation of ΔDBTT and ΔYS due to irradiation at 523K to 1.9 dpa in F82H steels tempered with different conditions.

298K, and shows strong dependence on temperature and time of tempering, and it tended to decrease with increasing yield stress. The increment of DBTT (Δ DBTT) due to irradiation in the F82H steels irradiated at 523K tended to decrease with increasing time and temperature of tempering.

6.1.2 Irradiation Effects on Creep Properties

Irradiation creep has been recognized as one of the most important properties for engineering blanket structural design. Several researchers have reported irradiation creep and void swelling behavior of austenitic stainless steels (316SS, PCA) and ferritic steels (HT9, 9Cr-1Mo) irradiated above 673 K in FFTF, HFIR, etc. However, irradiation creep behavior of RAFs irradiated below 673 K has not yet been reported.

In this study, irradiation creep behavior of the F82H and several JLF-1 steels at 573 K has been measured up to 5 dpa, using pressurized creep tubes irradiated in HFIR.[6.1-2] These tubes were pressurized with high-purity helium to hoop stress levels of 0 to 400 MPa at the irradiation temperature. The results of F82H and JLF-1 with hoop stress of 400 MPa showed small creep strains (<0.25%) after irradiation (Fig. III.6.1-2). Irradiation creep rate in these steels is linearly dependent on the applied stress below 200 MPa. However, at a higher hoop stress level, their creep rates are nonlinear. The creep compliance coefficient for F82H and JLF-1 is consistent with the values obtained for the same steels irradiated in FFTF. These data contribute to a part of materials database for ITER test blanket design work.

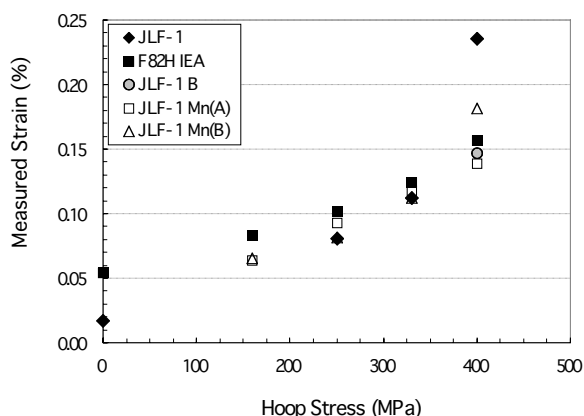


Fig. III.6.1-2 Hoop stress dependence of irradiation creep at 573 K / 5dpa.

6.1.3 Irradiation Effects on Precipitates' Stability

The stability of precipitate of RAFs under neutron irradiation at 573K has been studied [6.1-3], and reported that F82H, ORNL9Cr-2WVTa, and JLF-1 shows the size distribution change of precipitates after neutron irradiation up to 5 dpa at 573K. To investigate this phenomenon with higher accuracy, F82H was irradiated with 6.4MeV Fe^{3+} ion beam at 573K and 773K up to 10 dpa. [6.1-4] It was found that the precipitates distribution and its morphology in irradiated region are different from those in un-irradiated region in F82H, and the lath structure becomes ambiguous in irradiated regions. The dark filed images shown in Fig. III.6.1-3 revealed that the precipitates, M_{23}C_6 , in irradiated region of F82H were tuned to amorphous phase at 573K, but not at 773K. This suggested that the radiation induced amorphization of M_{23}C_6 were observed in Fe ion irradiated F82H at 573K, but not at 773K, and the glass transition temperature T_g of M_{23}C_6 in F82H could be estimated between 573K and 773K. This phase instability of precipitates could be the driving force of the size distribution change of precipitates and affects its mechanical properties, and further analyses will be performed to investigate this possibility.

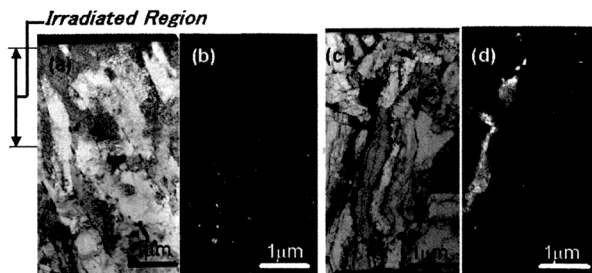


Fig. III.6.1-3 TEM images of Fe-ion irradiated F82H at 573K up to 10 dpa; (a) bright field image, (b) dark field image with diffraction pattern from amorphous M_{23}C_6 : and of Fe ion irradiated at 773K up to 10dpa; (c) bright field image, (d) dark field image.

References

- 6.1-1 Wakai, E., *et al.*, *Fusion Sci. Technol.*, **47**, 856 (2005).
- 6.1-2 Ando, M., *et al.*, "Creep Behavior of Reduced Activation Ferritic/Martensitic Steels Irradiated at 573 up to 5 dpa," *Proc. 12th Int. Conf. Fusion Reactor Materials*, ICFRM-12 (2006), to be published in *J. Nucl. Mater.*.
- 6.1-3 Tanigawa, H., *et al.*, *Mater. Trans.*, **46**, 469 (2005).
- 6.1-4 Tanigawa, H., *et al.*, "Phase Stability of Precipitates in

Ion / Neutron -Irradiated Reduced-Activation Ferritic / Martensitic Steels,” *Proc. 12th Int. Conf. Fusion Reactor Materials*, ICFRM-12 (2006), to be published in *J. Nucl. Mater.*.

6.2 Transition Phase Activities in IFMIF

IFMIF is an accelerator-based D-Li neutron source designed to produce an intense neutron field that will simulate the neutron environment of a D-T fusion reactor. IFMIF will provide a neutron flux equivalent to 2 MW/m^2 in a volume of 500 cm^3 and will be used in the development and qualification of materials for fusion systems. Prior to Engineering Validation and Engineering Design Activity (EVEDA), transition phase activities have been under way. Major achievements during 2005 are summarized as follows.

6.2.1 Accelerator

The RFQ linac of the IFMIF accelerates a 125mA deuteron beam from 0.1 to 5MeV. In order to accelerate such a large current beam, an operation frequency of 175MHz is selected. The length of RFQ linac becomes 12 m to obtain the output energy of 5MeV, with the required RF-input power of 2.3MW. For the RF-input coupler, a multi-loop antenna system using co-axial transmission line has been developed from the point view of withstand voltage. It is possible to define a better power balance by using a configuration with a four-loop antenna in comparison with the other configurations, like single-loop or two-loop antenna systems [6.2-1]. The resonant frequencies of operation mode (TE_{210}) and higher modes (TE_{110} , TE_{111} and TE_{211}) in a longitudinal RFQ length were analyzed for the configuration with four-loop antenna system, using a 3-dimensional electromagnetic code (MW-Studio). The calculated result is shown in Fig. III.6.2-1. In the case of 4m-length, the obtained frequency difference between operation mode (TE_{210}) and the most closely higher mode (TE_{111}) was 2.126 MHz, greater than a criterion of 2MHz where operation mode would not be affected by the higher mode [6.2-2]. As a result, the 12m-long RFQ can be realized by connecting three 4m-long RFQ modules with the four-loop antenna system using two coupling plates. As the total number of RF-Input couplers is twelve (3x4), the withstand voltage required for each loop antenna is around 200kW-CW, which is possible by using co-axial waveguide size of more than

4 1/16 inch. In conclusion, a feasibility of the RF-Input coupler system using four-loop antenna was revealed.

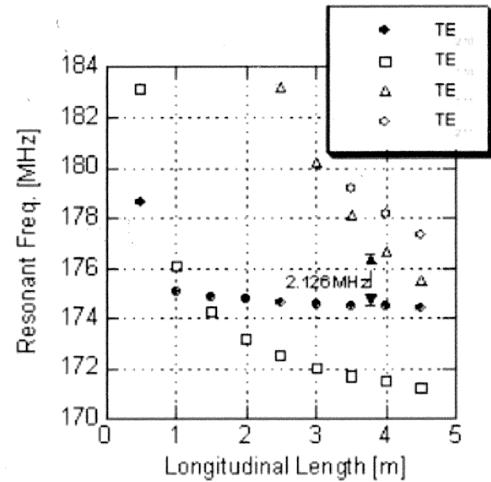


Fig. III.6.2-1 Trends of calculated resonant frequencies of an operation mode (TE_{210}) and higher modes (TE_{110} , TE_{111} and TE_{211}) for the various longitudinal lengths of IFMIF-RFQ.

6.2.2 Target Facility

The Li target system consists of two main components: the target assembly and the Li loop. A three-dimensional view of the target assembly is shown in Fig. III.6.2-2. The target assembly is a stainless steel alloy except for the back wall made of 316L stainless steel or a Reduced-Activation Ferritic/Martensitic (RAFM) steel such as F82H.

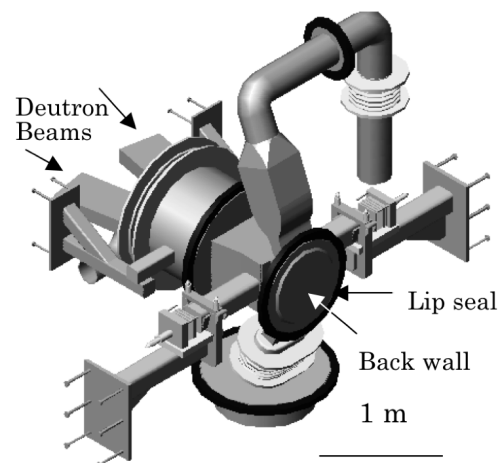


Fig. III.6.2-2 Three Dimensional View of Target Assembly and Backwall.

Since the backwall is operating under a severe neutron irradiation of 50 dpa/y and a maximum nuclear heating rate of 25 W/cm^3 , thermo-structural design is one of critical issues in a target design.

A thermal-stress analysis of a back-wall part of the IFMIF target assembly suffering nuclear heating up to 25 W/cc by the neutrons was performed using an FEM code ABAQUS. To reduce thermal-stress in a back-wall made of 316L stainless steel in the previous study, reduced-activation ferritic martensitic (RAFM) steel F82H was chosen in the present analysis. Temperature, thermal-stress and displacement distributions in the back-wall were calculated. Figure III.6.2-3 shows the von Mises stress of the back-wall made of F82H under conditions of back-wall thickness 1.8 mm and heat transfer coefficient between the backwall and the assembly 15.8 W/m²K corresponding to the minimum contact pressure of 0.1 MPa.

The maximum stress was 320 MPa enough lower than the permissible level of F82H, 450 MPa at 300 °C, while the stress in cases of 316L even with the back-wall thickness 1.8-5.0 mm and the heat transfer coefficient 15.8-158 W/m²K was larger than the permissible level, 160 MPa at 300 °C. Therefore, F82H is preferable as the back-wall material [6.2-3].

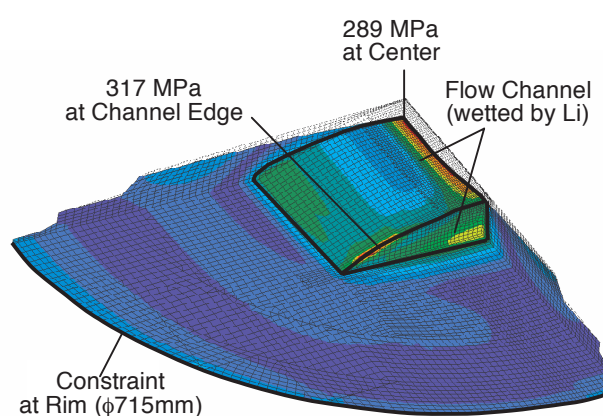


Fig. III.6.2-3 Contour of von Mises stress on quadrant model of back-wall. (3-D view from accelerator side)

Dose estimation was performed using a code QAD-CGGP2R, considering effect of a radioactive nuclide beryllium-7 (⁷Be). This nuclide is generated at a rate of 5×10^{15} Be/s through the deuteron-lithium (D-Li) reactions and emits a 0.478 MeV γ -ray with a half-life of 53 days, and thus is the most significant radioactive source in the IFMIF Li loop. Under an assumed condition of uniform deposition of ⁷Be on inner surfaces of the loop components, dose equivalent rate around the components without radiation shields was several orders higher than a guideline, 10 μ Sv/h equivalent to an ICRP

recommendation. In the loop components the maximum rate of $\sim 10^7$ μ Sv/h was obtained at the outer-surface of the main heat exchanger having the largest inner-surface area wetted by Li. The thicknesses of iron or lead necessary for radiation shielding were respectively 22.0 or 6.5 cm. By assuming that only 10 % of ⁷Be was deposited by removing the rest using a cold trap, the shielding thicknesses were reduced to be 18.4 cm (iron) and 5.3 cm (lead). The efficient removal of ⁷Be using a cold trap is highly recommended [6.2-4].

6.2.3 Test Cell Facilities

Type N thermocouples will be used for the temperature measurement of the irradiation samples in the IFMIF. It is known that their thermo-electric characteristics are varied under neutron irradiation, called as decalibration due to the composition change in the materials of the two legs of thermocouple (Type N: Ni-14.2%Cr-1.4%Si / Ni-4.4%Si-0.1%Mg). The decalibration was evaluated from the calculated result of the transmutation of elements in type N thermocouple and the electromotive force data of Ni-Fe binary alloys. The main transmutation element is iron and the composition change is 0.35/0.39 % (in +/- legs) during one year irradiation. As it is expected that the effects of Fe in the both legs compensate each other, the decalibration may be less than the case that only one side leg includes 0.1% Fe. The decalibration of indicated temperature for such case is shown in Figure III.6.2-4. Based on the result, less than 10 degrees between 250 and 650 °C, type N thermocouple may be used in the IFMIF.

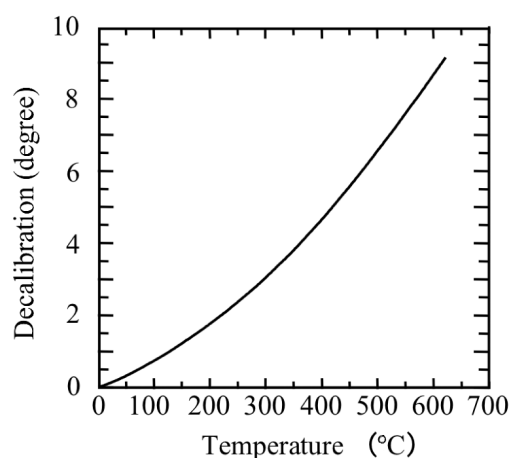


Fig. III.6.2-4 Evaluated decalibration of type N thermocouple due to neutron irradiation during one year.

6.2.4 Design Integration

An analysis of dose rate around the shielding wall of the test cell in the IFMIF was calculated by using a Monte Carlo transport code MCNPX and cross section data library LA-150. The material of shielding wall was assumed to be heavy weight concrete and normal concrete. A comparative study was carried out to investigate the effects of iron or stainless steel SS316 lining covering the shielding wall and cooling water pipes installed between the lining and the concrete. Heavy weight concrete is a good shielding material. However it is more effective to cover with the stainless steel lining. The amount of cooling water pipes installed into stainless lining is small and no prominent effect is found in the shielding performance.

6.2.5 EVEDA Consideration under Broader Approach

The technical issues of EVEDA were reconsidered for implementing under the framework of Japan-EU Broader Approach activities, and the accelerator tasks were modified to construct and test the prototype of low energy part up to 10 MeV. A preliminary design of the accelerator test facility capable of full beam power operation was conducted.

On the target facility, preparation of EVEDA task description was started to clarify contents of the EVEDA task activities. Major tasks are Li test loop, Li purification system, Erosion/Corrosion, Diagnostics, Remote handling, Li safety handling and engineering design tasks.

References

- 6.2-1 Maebara, S., *et al.*, *Fusion Eng. Des.*, **75-79**, 823 (2005).
- 6.2-2 Maebara, S., *et al.*, *J. Plasma Fusion Res.*, **82**, 21 (2005).
- 6.2-3 Nakamura, H., *et al.*, "Thermo-Structural Design of the Replaceable Backwall in IFMIF Liquid Lithium Target," *Proc. 12th Int. Conf. Fusion Reactor Materials*, ICFRM-12 (2006), to be published in *J. Nucl. Mater.*.
- 6.2-4 Ida, M., *et al.*, "Analytical Estimation of Accessibility to Activated Lithium Loop in IFMIF," *Proc. 12th Int. Conf. Fusion Reactor Materials*, ICFRM-12 (2006), to be published in *J. Nucl. Mater.*.

7. Tritium Technology

7.1 Tritium Processing Technology Development for Breeding Blanket

A series of simulation studies has been carried out to evaluate the applicability of a palladium membrane diffuser for the Blanket Tritium Recovery (BTR) system [1]. It was concluded that the palladium membrane diffuser was not practical for the primary loop of the blanket sweep gas, since the hydrogen partial pressure in the sweep gas was significantly low for the membrane.

The hydrogen transportation properties of a ceramic proton conductor, which is a candidate for advanced BTR system, have been studied. In this year, our attention was focused on the effect of the electrode on the hydrogen transportation. If the areas of the triple phase boundary (the contact point of gas, electrolyte and electrode) increase, the hydrogen transportation rate should be enhanced. To decrease the grain size of the metal electrode by sputtering may be a solution for the increase of the areas of the triple phase. However, the triple phase boundary is often covered by the metal of the electrode. The hydrogen atoms can easily permeate in a palladium (Pd) electrode, so that the Pd electrode results in high performance for the hydrogen transportation. Figure III.7.1-1 shows the comparison of overall conductivity between the conventional Pt pasted electrode and the Pd sputtering electrode. The Pd sputtering electrode increased the conductivity slightly at lower hydrogen partial pressure.

The pressure swing adsorption (PSA) method has been studied as a new water detritiation technique for

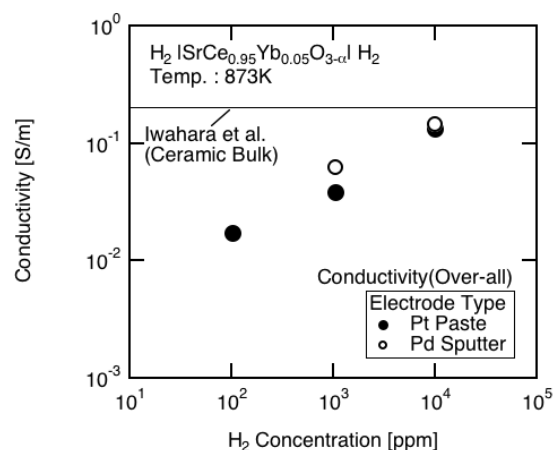


Fig. III.7.1-1 Comparison of the overall conductivity between the conventional Pt pasted electrode and the Pd sputtering electrode.

processing a large amount of tritiated water generated in a future DEMO plant. The research focused on the adsorption and desorption properties of faujasite-type zeolites of varying cations and $\text{SiO}_2/\text{Al}_2\text{O}_3$ ratio. The experimental $\text{HTO}/\text{H}_2\text{O}$ separation factor and dehydration energy of the zeolites were evaluated. As an example, the separation factor and the dehydration energy of NaY5.0 zeolite ($\text{SiO}_2/\text{Al}_2\text{O}_3$ ratio: 5.0) are 1.19 and 47.7 kJ/mol, respectively.

Reference

7.1-1 Kawamura, K., *et al.*, *Fusion Eng. Des.*, **81**, 809 (2006).

7.2 Tritium Accounting Technology Development

The micro GC having cryogenic column only can measure hydrogen isotopes within a few minutes with a reasonable cost. One of its unfavorable points is that the column must be used at cryogenic temperature. The study of hydrogen adsorption property of various kinds of zeolite has been carried out to develop a new column that is used around 200 K without liquid nitrogen (cooled by mechanical method). In this year, hydrogen adsorption property of mordenite and Y type zeolite were tested. Figure III.7.2-1 shows adsorption isotherm of hydrogen on the mordenite. The mordenite should have good separation capability at around 200 K as a column material.

7.3 Basic Study on Tritium Behavior

Deuterium retention and blistering on tungsten exposed to high fluences (up to 10^{27} D/m²) of high flux (10^{22} D⁺/m²/s) and low energy (38 eV) deuterium plasma were examined with scanning electron microscopy (SEM) and thermal desorption spectroscopy (TDS) As

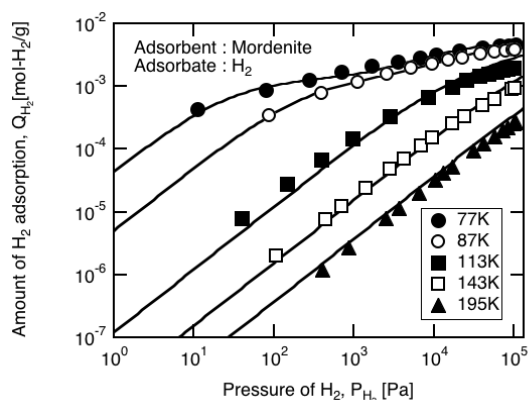


Fig. III.7.2-1 Adsorption isotherms of H_2 on mordenite at various temperature.

shown in Fig. III.7.3-1, peculiar phenomenon of blister bursting with a tail, or a small hole or a vanished cap was found on some grains after plasma exposure or TDS experiment. In addition, bursting release of deuterium with sudden peaks was also found in the TDS spectra below 700 K at the heating rate of 0.5 K/s (Fig. III.7.3-2). A new model named “step-cascade model” was proposed to explain the phenomenon of blister bursting [7.3-1].

Case studies on tritium inventory and permeation in a DEMO plant have been carried out as a part of demo fusion reactor design activity at JAERI/JAEA. The

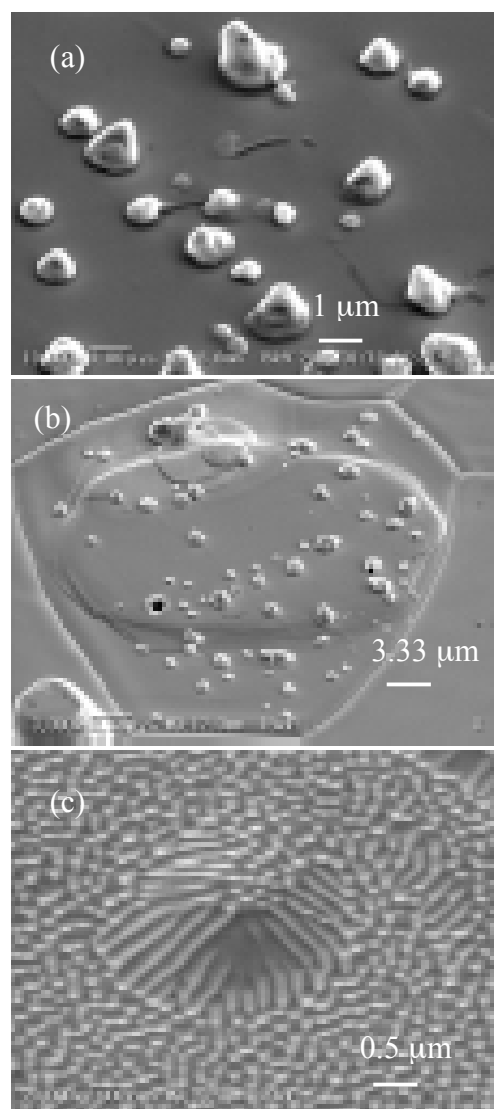


Fig. III.7.3-1 Blister bursting with a tail (a) and a small hole (b) of the recrystallized W exposed at 520 K to a fluence of 10^{26} D/m² as well as a vanished cap (c) of the recrystallized W exposed at 630 K and then 980 K to a fluence of 10^{27} D/m².

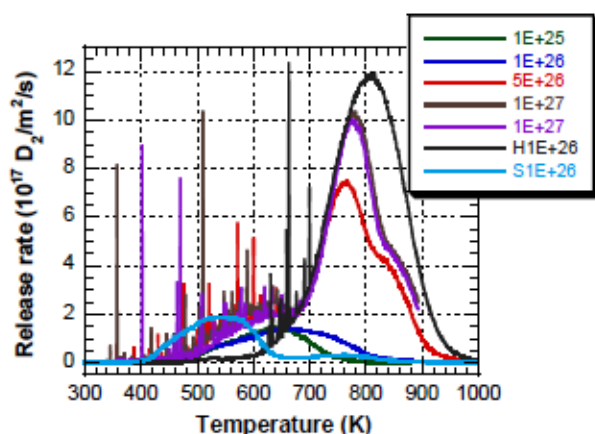


Fig. III.7.3-2 TDS spectra of the recrystallized W samples exposed to varying fluence at room temperature in comparison with the recrystallized W exposed to 10^{26} D/m² at 520 K denoted with H1E-26 and the single W exposed to 10^{26} D/m² at room temperature denoted with S1E-26.

results revealed that tritium concentration and inventory in the coolant attributed to permeation from the blanket (plasma facing first wall and breeding region) is expected to be much higher both of these guidelines unless designated permeation barriers are used. Therefore, permeation must be reduced by a factor of 100 in order to satisfy the guidelines. Tungsten coating on the first wall and glassy coating on the blanket cooling tubes may be good countermeasures for permeation reduction in the DEMO reactor [7.3-2].

A series of tritium sorption and desorption experiments for various materials used in ITER has been carried out to develop an effective decontamination method. The desorption rates of tritium from the various materials were measured with practical N₂ purge gas operation. The materials tested were epoxy paint, acrylic resin, and butyl rubber. In the case where water vapor concentration in the purge gas is less than 10 ppm, the desorption rates were much smaller in compared with the data for the N₂ gas purge with a high water vapor concentration. The desorption rate depends on the water vapor concentration largely. Figure III.7.3-3 shows a typical desorption behavior of tritium by N₂ gas purge with moisture. By the N₂ gas purge without moisture, only a little of tritium could be desorbed, and the desorption rate promptly decreased. However, the N₂ purge gas with moisture could desorb 2-3 times larger amount of tritium in comparison with N₂ purge gas without moisture. This would be due to the isotope

exchange reaction. Another important result was that the amount of tritium removed by N₂ purge gas with 700 ppm moisture was almost equal to that of 7000 ppm moisture. The effect of moisture was clearly observed, but the excessive amount of moisture was not required.

The tritium released into the facility is oxidized to water by the noble metal catalyst at high temperature, and is then removed by an adsorption bed as water. The tritium in a facility is thus controlled to prevent environmental release. On the other hand, it has been found that bacteria common in soil of forest oxidized hydrogen into water at atmosphere temperature by a team of Ibaraki University. We pay attention to this remarkable result, and started studies to develop an original tritium removal method using the bacteria under the collaboration with Ibaraki University. We fabricated bio-reactors using the above bacteria and connected to the Caisson Assembly for Tritium Safety study (12 m³) in TPL, where tritium could be released intentionally up to 37 GBq, and its detritiation factor (DF) was measured. The result showed that the bio-reactor could oxidize tritium gas in reasonable speed compared with the catalytic reactor and that the DF corresponded to the level required for ITER. Other cooperative researches have been performed with Kyushu University, Shizuoka University and Toyama University.

Characteristics of high level tritiated water up to 1 EBq/m³ has been investigated for more than 5 years. The pH & ORP level (acid and corrosive) changed with the tritium concentration [7-3-3].

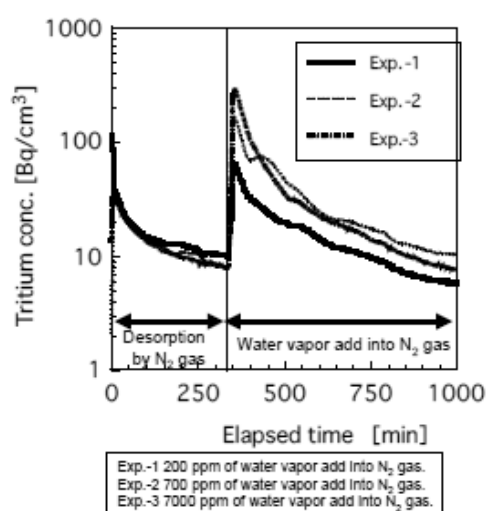


Fig. III.7.3-3 Tritium removal behavior.

References

- 7.3-1 Shu, W.M., *Proc. 3rd Int. Workshop on Tritium-Material Interactions*, 27 (2005).
 7.3-2 Nakamura, H., *et al.*, *Fusion Eng. Des.*, **81**, 1339 (2006).
 7.3-3 Hayashi, T., *et al.*, *Fusion Eng. Des.*, **81**, 1365 (2006).

7.4 Successful Operation Results of Tritium Safety Systems in TPL

The safety system of Tritium Process Laboratory (TPL) consists of Glove Box Gas Purification System (GPS), Air Cleanup System (ACS), Effluent Tritium Removal System (ERS) and Dryer Regeneration System (DRS). The GPS was operated for about 8,100 hours by controlling tritium concentration in the glove boxes. The ACS was operated for cleaning 97,900 m³ of air during the experiments of Caisson Assembly and maintenance of the glove boxes, experimental apparatus and other tritium operations. The ERS removed about 4.5 TBq of tritium mainly out of the exhaust gas from the experimental apparatus. The DRS removed 281 liters of tritiated water (160 GBq) from the GPS and ACS dryers.

The tritium safety system of TPL has been in service to support operations with use of tritium since 1988. Some maintenance work such as periodical inspection or replacement of a superannuated glove box has been carried out in this fiscal year. Figure III.7.4-1 shows monthly environmental tritium release from the stack of TPL during this fiscal year. Total amount of released tritium was 72 GB, which is sufficiently lower than the target value at TPL.

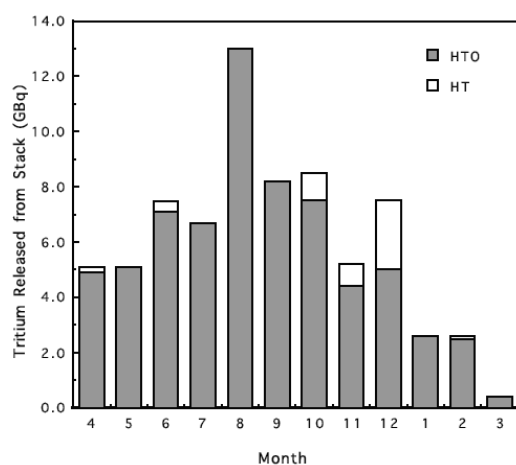


Fig. III.7.4-1 Monthly environmental tritium release.

8. Fusion Neutronics

8.1 Blanket Neutronics Experiments [8.1-5]

8.1.1 Experiment of the Assembly with Water Layers

In fusion DEMO reactors, the blanket is required to provide a tritium breeding ratio (TBR) more than unity. The water cooled pebble bed blanket being developed by JAEA consists of Li₂TiO₃ or Li₂O pebbles with enriched ⁶Li, beryllium pebbles, ferritic steel F82H and water. Prediction uncertainties are more than 10% for the TBR based on the previous study [8.1-1], and studies have been performed for enhancement of the accuracy. Neutronics experiments were conducted on simple mockup by using DT neutrons in the previous studies [8.1-1 – 8.1-4]. In the present study, neutronics experiments have been extended to introduce water so that the experimental mockup can better simulate the blanket structure and more detailed tritium production rate (TPR) can be obtained [8.1-5].

Figure III.8.1-1 shows a schematic view of the experimental assembly. The mockup is constructed by a set of layers of the first wall panel, partition panel, Li₂TiO₃ and beryllium with the dimensions of 16, 7.8, 12 and 101.6 mm in thickness, respectively. The first wall and partition panels are mainly composed of F82H and water. The first wall panel is composed of the 3 mm thick front wall, 6 mm thick water and 7 mm thick back wall. The partition panel is composed of the 1.8 mm thick front wall, 4.2 mm thick water and 1.8 mm thick back wall.

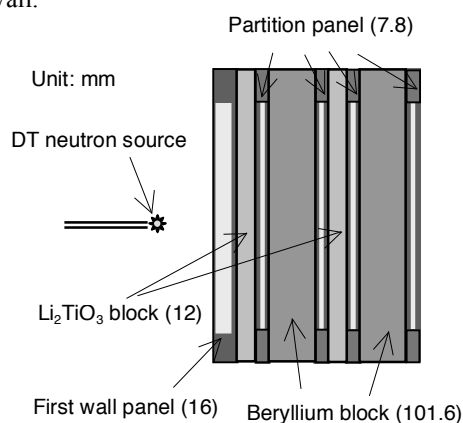


Fig. III.8.1-1 Schematic view of the experimental assembly [8.1-5].

Numerical calculations have been conducted using the Monte Carlo neutral particle transport code MCNP-4C with the Japanese Evaluated Nuclear Data Library JENDL-3.3. Figure III.8.1-2 shows distributions

of the ratio of the calculation value to experimental one (C/E) for the local TPRs. The C/Es in the first and second Li_2TiO_3 layers are 0.99 and 1.04 for the integrated tritium productions. The C/E is 1.02 for sum of the integrated tritium productions in the first and second Li_2TiO_3 layers. It can be concluded that sum of the integrated tritium productions are much accurately predicted.

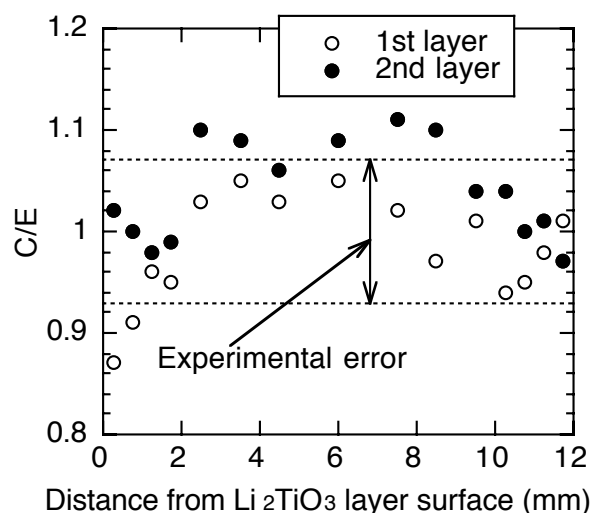


Fig. III.8.1-2 Distributions of the ratio of the calculation value to experimental one (C/E) for the local TPRs on the JENDL-3.3 [8.1-5].

8.1.2 Experiment of the Assembly with Breeder Pebble Bed Layer

No experimental studies have been reported so far about the pebble bed layer. For the first time, nuclear properties are experimentally examined on the pebble bed layer by using DT neutrons in the present study [8.1-5]. Calculation methods are discussed on the evaluation for TPR of the pebble bed layer, and the precise modeling method is proposed using the hexagonal close-packed heterogeneous geometry.

Figure III.8.1-3 shows the experimental assembly. The mockup is composed of Li_2O pebble bed layer, beryllium block and F82H. The pebble diameter is 1 mm, and the packing fraction is 57.8 %. The Li_2O pebbles were also applied as the detectors for TPR. Tritium activities produced in the pebbles were measured with a liquid scintillation counter.

The experiment was analyzed by Monte Carlo calculations for the pebble bed layer using the homogeneous and heterogeneous geometries. The homogeneous geometries have been applied in the blanket design calculation. A calculation method for the

heterogeneous geometry is proposed in this study, and the differences between TPRs for the heterogeneous and homogeneous geometries are discussed. The hexagonal close-packed model was assumed in the heterogeneous geometry, and all pebbles and void among the pebbles were simulated using the repeated-structures modeling method. The pebble packing fraction is 74 % in the hexagonal close-packed model, while it is 57.8 % in the experiment. Uniform annular gaps are assumed at the boundaries between adjacent pebbles in the calculation to adjust the packing fraction in the experiment in this study.

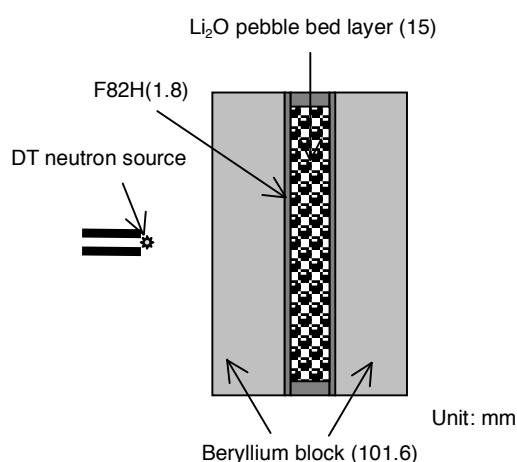


Fig. III.8.1-3 Schematic view of the experimental assembly [8.1-5].

Figures III.8.1-4 and III.8.1-5 show distributions of the TPRs and C/Es on TPRs, respectively. The average C/Es are 0.97 and 0.99 in the homogeneous and heterogeneous geometries, respectively. Total TPR obtained by the homogeneous geometry is smaller than that by the heterogeneous one. The calculation accuracy could be improved by applying the proposed method. With increasing ^6Li enrichment, the results by homogeneous geometries still much decrease. Impacts of these reductions on blanket designs are very large, and it can be concluded that evaluations are required on a TBR by the Monte Carlo calculation using heterogeneous geometries.

References

- 8.1-1 Sato, S., *et al.*, *Nucl. Fusion*, **43**, 527 (2003).
- 8.1-2 Sato, S., *et al.*, *Fusion Sci. Technol.*, **47**, 1046 (2005).
- 8.1-3 Sato, S., *et al.*, *Nucl. Fusion*, **45**, 656 (2005).
- 8.1-4 Sato, S., *et al.*, *Fusion Eng. Des.*, **81**, 1183 (2006).
- 8.1-5 Sato, S., *et al.*, *J. Plasma and Fusion Res.*, **82**, 306 (2006).

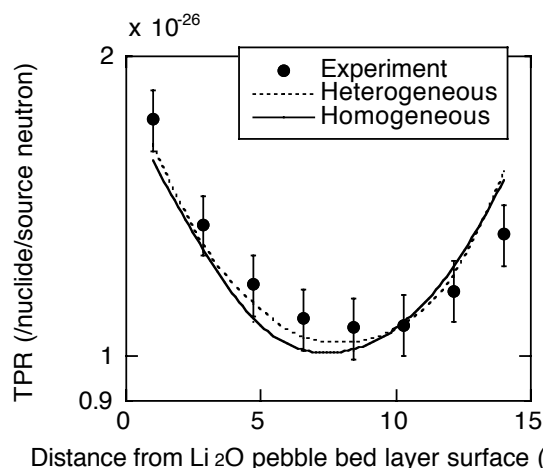


Fig. III.8.1-4 Distributions of TPRs as a function of the distance from the Li_2O pebble bed layer surface [8.1-5].

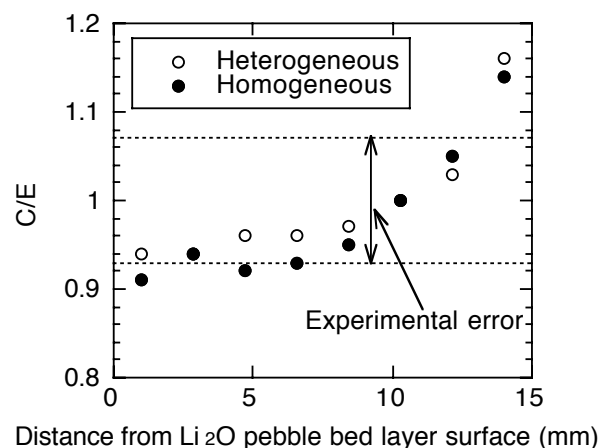


Fig. III.8.1-5 Distributions of C/E's on TPRs as a function of the distance from the Li_2O pebble bed layer surface [8.1-5].

8.2 Cross Section Measurements of Fusion Materials

8.2.1 Charged-Particle Emission DDX Measurement

It is important to measure double-differential cross sections of emitted charged-particles (DDXc) induced with DT neutron for evaluation of kinetic energy released in materials and primary knock-on atom spectra in fusion reactor materials.

The measurement of DDXc for fluorine has been carried out by using a DT neutron beam at FNS and a counter telescope with a Si surface barrier detector. Figure III.8.2.1 plots the obtained DDXc for $^{19}\text{F}(\text{n},\text{xp})$ reactions and the data in JENDL-3.3. From the comparison, a remarkable difference was pointed out between the obtained result and JENDL. A further analysis and a verification of evaluated nuclear data based on our experiment are in progress.

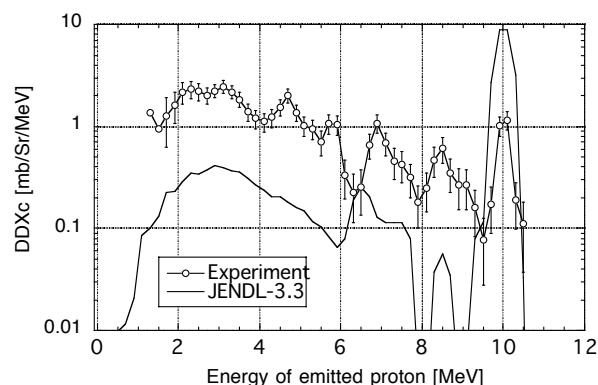


Fig. III.8.2-1 DDXc measured for $^{19}\text{F}(\text{n},\text{xp})$ reactions at 30 degrees of emission angle and the data in JENDL-3.3.

8.2.2 Activation Cross Sections of IFMIF Accelerator Structural Materials

In the design of IFMIF (International Fusion Materials Irradiation Facility), long-term operation with more than 70 % total facility availability is required. However, the deuteron-induced activation of structural materials composing the IFMIF accelerator limits the maintenance time, which makes the long-term operation difficult. Therefore, the accurate estimation of deuteron-induced radioactivity is important to select low activation structural materials. As a part of systematical study for the selection of candidate materials, we performed deuteron-induced activation cross section measurements for iron, nickel, chromium, manganese and gold by the stacked-foil technique at the TIARA (Takasaki Ion Accelerators for Advanced Radiation Application) facility. These results were compared with other experimental values and computed data using ACSELAM and TALYS. In addition, SS316 and F82H samples were irradiated with 41 MeV-deuteron beam to measure each activity.

Figure III.8.2-2 shows the cross section for the $^{52}\text{Fe}(\text{d},\text{x})^{52}\text{Mn}$ reaction. The present results agreed with the previous and computed ones within a factor of 1.5. We have also obtained the activation cross sections for the reactions $^{48}\text{V}(\text{d},\text{x})^{48}\text{V}$ or ^{52}Mn , $^{55}\text{Mn}(\text{d},\text{x})^{54}\text{Mn}$, $^{54}\text{Fe}(\text{d},\text{x})^{54}\text{Fe}$ or $^{55-57}\text{Co}$, $^{55-57}\text{Ni}(\text{d},\text{x})^{55-57}\text{Co}$ or $^{60,61}\text{Cu}$ and $^{197}\text{Au}(\text{d},\text{x})^{194}\text{Au}$ in 26-47 MeV range.

The activities for SS316 and F82H on each nuclide were compared with the calculated values which were derived from the cross section data measured in our work and the number of incident deuteron. For ^{48}V , ^{54}Mn and ^{181}Re , the calculated values were 50% larger than the measured ones. For ^{52}Mn , ^{56}Co and ^{57}Co , the calculated values were in agreement with the measured

ones within 11%.

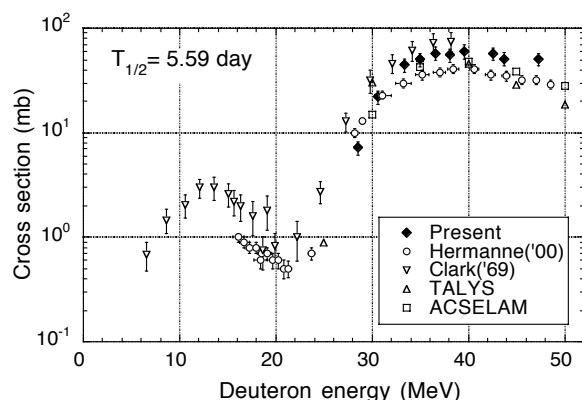


Fig. III.8.2-2 Cross section for the $^{nat}\text{Fe}(d,x)^{52}\text{Mn}$ reaction.

8.3 Beam Analyses of the Armor Tiles

Hydrogen isotopes retention on plasma facing components (PFCs) is an important issue for the fuel recycling, plasma control, etc. In the case of carbon-based materials as PFC, co-deposited layers of carbon compounds with hydrogen isotopes are formed on PFC surfaces due to plasma-wall interactions. Therefore, it is necessary to measure hydrogen isotope depth profiles in these layers with the thickness of several tens of micrometers. A powerful and unique method using a monochromatic neutron beam instead of an ion beam, namely, Neutron Elastic Recoil Detection Analysis (NERDA) has been developed.

A proof-of-principle experiment was performed with some standard polyethylene or deuterated polyethylene samples. Hydrogen and deuterium depth profiles were estimated using energy spectra of recoil particles and a response function which corrects the detection energy spread caused by the geometrical configuration of an experimental condition. All profiles indicated homogeneous distributions of the nominal density [8.3-1].

The application of NERDA was also demonstrated using two PFC samples of JT-60U. Hydrogen profiles in the inner and outer baffle plates are shown in Fig. III.8.3-1. It is found that hydrogen existed in two regions of (I) at the surface, (II) around the depth of 600 μm . Retentions of the region (I) and (II) were estimated to be 2.9×10^{22} and $4.5 \times 10^{22} / \text{m}^2$, respectively. The NERDA method is applicable to measuring absolute depth profiles in fusion reactor materials.

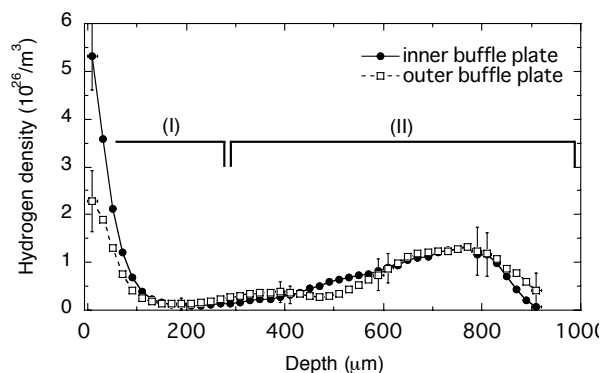


Fig. III.8.3-1 Hydrogen profiles in the inner and outer baffle plates of JT-60U.

Reference

8.3-1 Kubota, N., *et al.*, *Fusion Eng. Des.*, **81**, 227 (2006).

8.4 Gamma-Ray Measurement for Alpha Particle Diagnostics in Plasma

As a new method of the diagnosis for confined 3.5-MeV α particle in D-T plasmas, we proposed the detection of 2.186-MeV gamma-ray induced by $\text{D}(\alpha,\gamma)^6\text{Li}$ reaction and carried out the verification of the gamma-ray diagnostics technique with an ion beam.

Helium ions accelerated up to 4 MeV were bombarded into a thick deuterated polyethylene. The emitted gamma-ray was measured with a Ge-detector surrounded with lead blocks and boron carbide plates. Figure III.8.4-1 shows the emission rate of 2.186 MeV gamma-ray for the helium ion energy. The emission rate shows a tendency to enhance above 3.0 MeV. From our experiment, $\text{D}(\alpha,\gamma)^6\text{Li}$ reaction rate is estimated to be $10^{13} \text{ m}^{-3} \text{ s}^{-1}$ in the ITER typical plasma condition. So we obtained a prospect of the gamma-ray measurement as the confined α diagnostics by using a high efficiency detector.

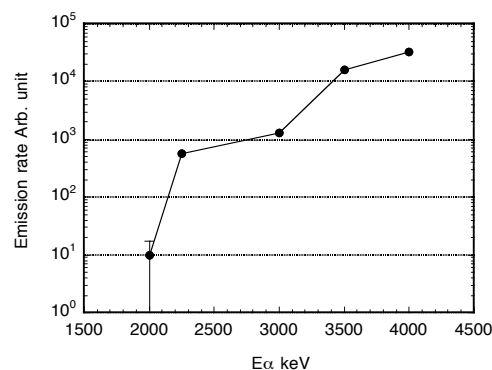


Fig. III.8.4-1 Energy dependency of 2.186-MeV gamma-ray emission rate induced by $\text{D}(\alpha,\gamma)^6\text{Li}$ reaction.

8.5 Operation of the FNS Facility

Operation of Fusion Neutronics Source (FNS) has been carried out to execute a variety of experiments under collaboration with JAEA and domestic universities, according to various requests for operation pattern. The total operation time was 707 hours in this fiscal year. In these experiments, six fixed targets with 370 GBq were used for the experiments at 80° beam line. Also one rotating target with 33 TBq was used for the experiments at 0° beam line. A total amount of 7.23 TBq tritium in vacuum exhaust gas was processed by Tritium Adsorption Processor (TAP) system.

Following maintenance activities has been performed in the year. As a periodic check-up, the oil-free vacuum pumps have been overhauled. The control circuit of the accelerator was inspected every six months.

Following renewal activities has been carried out. Ion beam collimator was replaced with improved one to enhance the neutron generation area. Isolation flange for measurement of a target electric current has been substituted because it has been damaged by radiation.

9. Vacuum Technology

For R&Ds on fuel supplying/pumping system, performance tests have started with the newly developed gas separation device (Fig.III.9-1). This new device has been developed to demonstrate a large amount of H₂/He gas separation, which will be design database of a large gas separation system for fusion reactors. The new device has 8 gas-separation columns, which are arranged radially from a main gas-supplying port. Each gas-separation column is connected to the main gas-supplying port with a connecting pipe, which has the same length to each column to minimize a passing-gas time-lag among 8 columns. In 2005, major efforts have been concentrated to perform a system check of the new device, because the device consists of more than 60 electro-magnetic valves, which are controlled by a sequence program of more than 50,000 lines. After baking at 350 °C, the device was successfully evacuated up to 1 Pa, which is the nominal operation pressure of the device.

As one of the applications of gas separation technology, results of separation/recovery tests on gas mixture of 4-fluoro carbon and 6-fluoro ethane, which was performed under collaboration between JAEA and a Japanese industry [9-1].

Reference

- 9-1 Tanzawa, S., *et al.*, *IEEE Trans. on Semiconductor Manufacturing*, **18**, 495 (2005).

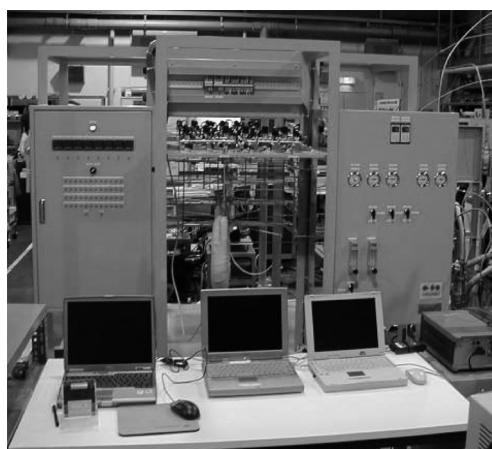


Fig. III.9-1 New gas separation device with radially arranged columns.

10. Technology Transfer

JAEA has successfully transferred a vacuum instrumentation technology to industrial entities, by which a high quality control of automotive products can be expected [10-1]. Mechanical properties of aluminum alloy casting products are deteriorated by some gas pores formed in the casting, so automotive manufactures are processing to reduce the inferior castings caused by the porosity and routinely inspecting the quality of the products by some suitable methods. However, a reliable method for evaluating the gas concentrations and species in the castings by easy operation is highly required. On the other hand, the vacuum thermo-microbalance was developed and improved to measure an absolute μg order of the outgassing from fusion related materials [10-2].

Based on the background, the outgassing measurement device applicable to the aluminum castings has been developed, and its brand name was registered to Japan Patent Office as “Gravi-Mass” (see Fig. III.10-1), which consists of a vacuum chamber, an electric furnace, a quadrupole mass spectrometer and a precise weight sensor as.

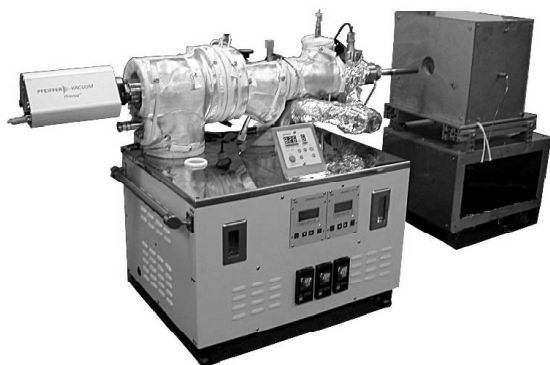


Fig. III.10-1 Photo of the Gravi-Mass.

A sample weight of the aluminum alloy casting products was in advance, measured by the weight sensor, then the sample was introduced into the furnace and heated up to 740 °C. The time integrated outgassing values of each gas species were measured by the mass spectrometer.

After the sample heating, an overall weight loss due to the outgassing was measured by the weight sensor. The weight loss value was proportionally distributed to

the outgassing values of each gas, so that the gas concentration of the aluminum casting could be evaluated by the weight loss of each gas (H_2 , H_2O , Hydro-carbons, etc). The converted weight loss of the outgassing is an absolute value with high reliability regardless of the environmental temperature and pressure.

JAEA has granted Nikkin-Flux Co., Ltd. that is involved in manufacturing, sales, test and analysis of nonferrous metals, a commercializing license on the Gravi-Mass through JAEA's holding patents. As for applying the Gravi-Mass to the manufacturing line, Enkei Corporation that is an aluminum wheel maker, examines the effect on the quality control due to introduction of the Gravi-Mass to the production process.

References

- 10-1 JAEA News Release, Nov. 10, 2005.
(<http://www.jaea.go.jp/english/02/press2005/p06012301/index.html>)
- 10-2 Abe, T., *et al.*, *J. Vac. Soc. Jpn.*, **36**, 263 (1993).

IV. INTERNATIONAL THERMONUCLEAR EXPERIMENTAL REACTOR (ITER) AND BROADER APPROACH (BA)

1. Overview of the ITER Program and Activities

1.1 ITER Transitional Arrangements (ITA)

In January 2003 the ITER Transitional Arrangements (ITA) started under the auspices of the IAEA, following the successful completion of the Coordinated Technical Activities (CTA). The purpose of the ITA is to prepare for an efficient start of the Agreement, if and when so decided, and to maintain the integrity of the ITER Project. Along the work plan approved by the ITER Preparatory Committee, the Design and R&D Tasks have been carried out among the Participant Teams (PTs). Based on the task agreement between the International Team (IT) and each PT, these shared Tasks make the implementation of preparing the procurement documents for facilities and equipments that are scheduled to be ordered at an early stage of ITER construction such as superconducting magnets and vacuum vessel sectors. In FY2005 JAERI and its successor, JAEA, were in charge of sixty-six Design Tasks that are described in section II.

1.2 Progress of Negotiations and Prospective Schedules

The process of selecting a location for ITER construction took over two years, and was finally concluded in 2005. After bilateral negotiations between Japan and the European Union (EU), the decision to site ITER in Cadarache was reached by six-Party agreement on the occasion of the Ministerial Meeting for ITER on 28 June 2005, based on a bilateral agreement between EU and Japan over the roles of the Host and the non-Host for the ITER Project.

The negotiations returned to finalizing the ITER



Fig. IV.1.2-2 Cadarache site.

Joint Implementation Agreement (JIA), which will establish the ITER International Fusion Energy Organization, and the choice of Director-General Nominee for the Organization. Three meetings of the Negotiators were held between September and December 2005. In accordance with the bilateral agreement between EU and Japan, Japan proposed Mr. Kaname Ikeda as a candidate for the Director General Nominee. On the 5th Preparatory Meeting for ITER Decision Making held in Vienna on 7 November 2005, this proposal was agreed and Mr. Ikeda was nominated as Director General for the prospective ITER Organization.

At the 12th Negotiations meeting held on 6 December 2005 in Jeju (Korea), India joined the ITER negotiation as a full Party.

The 6th Preparatory Meeting for ITER Decision Making was held at the Tokyo International Exchange Center in Tokyo on 1 April 2006 to finalize the ITER negotiations and to take key decisions on the future of the project. Following interviews with all Parties, the Delegations unanimously agreed on the EU proposal to designate Dr. Norbert Holtkamp as ITER Principal Deputy Director-General Nominee.



Fig. IV.1.2-1 The 2nd Ministerial Meeting for ITER.



Fig. IV.1.2-3 The 6th Preparatory Meeting for ITER.



Fig. IV.1.2-4 The ITER joint work site in Cadarache.

The ITER Joint Work Site in Cadarache was inaugurated on 15 December 2005. On 30 January 2006 the first ITER International Project Team staff began working at the Cadarache Joint Work Site. The current

participants to the project are the European Union, Japan, the People's Republic of China, India, the Republic of Korea, the Russian Federation and the USA.

The schedule for ITER construction is shown in Table IV.1.2-1 with recent progress as of March 2006.

Table IV.1.2-1 Schedule for ITER construction.

Year	2000	2001	2002	2003	2004	2005	2006	2007	2008
EDA		Final Design Report ↓ Engineering Design Activity (EDA) ↓ Final Report							
Meeting	Exploration	Domestic Site Evaluation	Site Evaluation Process (JASS)			Site decision ↓ Final Draft of the ITER Joint Implementation Agreement	Domestic Procedure		
Technical Activities		Canada Site proposal ↑	Japan, EU ↑				Establishment of ITER Organization ↑		
BA			CTA	ITER Transitional Arrangements (ITA)				ITER construction	
								Broader Approach	

2. ITA Design Task

2.1 Superconducting Magnet

Extensive activities are underway to optimize the design of the ITER superconducting magnet system for cost reduction and to confirm its manufacturing feasibility. As part of the activities, full scale trial fabrications of a cable for a Toroidal Field (TF) coil conductor, jacket sections for a central solenoid (CS) conductor and TF structures were performed in 2005 as follows.

2.1.1 Trial Fabrication of a TF Cable

The manufacturing method of a superconducting cable was successfully established in the CS Model Coil (CSMS) in the ITER Engineering Design Activities. To enhance the critical current of the conductor, however, a different configuration of the cable was proposed for the TF coil conductor. This includes a reduction in void fraction at cable space and cross-sectional area of a central cooling channel from those of the CSMC conductor, as shown in Table IV.2.1-1. These changes make the fabrication of the TF cable difficult because six sub-cables are subjected to a severe deformation from a circular shape to a triangle to form a cable, which will then be compacted largely to a specified diameter in steps. A trial fabrication of full scale TF cable was therefore performed to demonstrate manufacturing feasibility.

A cabling machine shown in Fig. IV.2.1-1 was prepared. In the first trial using hard copper wires, some damages were found during the reduction of a cable diameter. Through several trials, the following measures were implemented.

- 1) The shape of the forming rollers was improved so as to avoid strand crimping.
- 2) The reduction ratios of cable diameter were optimized.
- 3) Pulling force of the hauling-off device was enhanced up to 20 kN.

Owing to these measures, a full scale TF cabling using copper wires was manufactured without damage. The cross sectional view of the TF conductor consisting of the cable and jacket is shown in Fig. IV.2.1-2 together with that of the CSMC conductor for comparison. The manufacturing feasibility of the TF cable was thus demonstrated. A cable using actual Nb_3Sn strands will be performed in 2006.

Table IV.2.1-1 Major parameters.

	TF cable	CSMC cable
OD of cable	41.1 mm	38.5mm
OD of central spiral	9 mm	12 mm
Number of strands	1422 (3x3x5x5+12)x6	1152 (3x4x4x4x6)
Diameter of strand	0.82 mm	0.81 mm
Void fraction	32%	36%

OD: Outer diameter

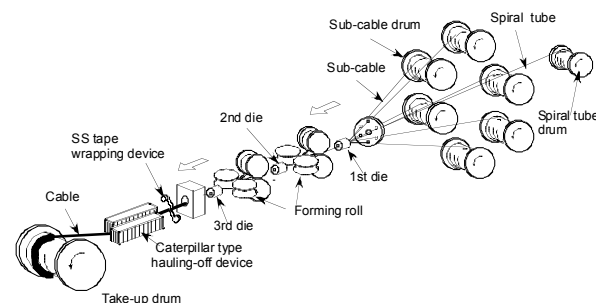


Fig. IV.2.1-1 Cabling machine of TF cable. The sub-cable is twisted around the central cooling channel and the cable is wrapped by 0.08-mm thick stainless steel (SS) tape.

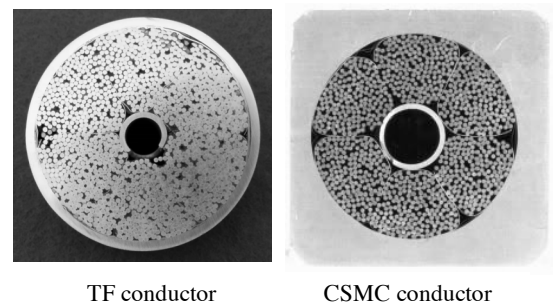


Fig. IV.2.1-2 Cross-sectional views of TF conductor and CSMC conductor.

2.1.2 Jacket Development

A jacket material for the CS conductor requires lower thermal expansion from room temperature to 4 K than that of usual stainless steel in order to obtain sufficient loading to CS winding packs by a preload structure during cool down. To satisfy this requirement, JK2LB developed by JAEA was selected as a CS jacket material.

The jacket material has also to satisfy other requirements on the mechanical properties, namely 0.2% yield strength of more than 1,000 MPa and fracture toughness $K_{IC}(J)$ of more than 130 $\text{MPa}\sqrt{\text{m}}$ [2.1-1].

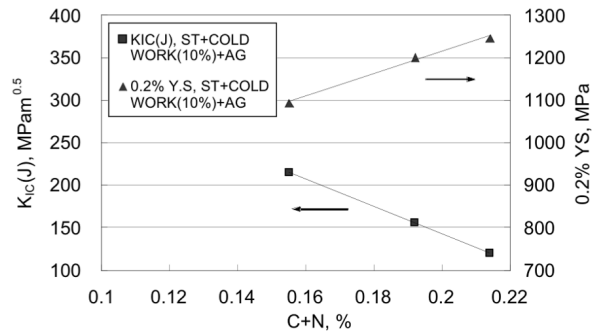


Fig. IV.2.1-3 Measured 0.2% yield strength and fracture toughness of JK2LB with cold work of 10 % and aging treatment.

A trial fabrication of full scale JK2LB jacket sections was performed to demonstrate fabrication processes [2.1-2], and CS jacket sections which satisfied dimensional requirements could successfully be fabricated. Tensile and fracture toughness tests were performed using samples cut from the jacket. Cold work was imposed to the samples to simulate a compaction during conductor fabrication and coil winding. Test results showed that the cold work of the jacket significantly degraded the fracture toughness while it enhanced yield strength. Consequently, it was figured out that chemical component of JK2LB should be optimized in order to balance between yield strength and fracture toughness to achieve ITER requirement. Figure IV.2.1-3 shows results of 0.2% yield strength and fracture toughness of JK2LB with the cold work of 10% as a function of nitrogen + carbon content. Since carbon content can be kept less than 0.025%, nitrogen content is decided to be 0.09 to 0.15% from the results.

In 2006, CS jacket sections with the optimized nitrogen content will be manufactured and their mechanical properties will be confirmed to satisfy the ITER requirements.

2.1.3 TF Structure Development

Activities to develop rational manufacturing procedure of the TF structures are in progress at industrial level in Japan. Significant progress has been obtained in the qualification of TF structural materials and in the manufacturing demonstration of radial plates.

Trail productions of four materials of JJ1 (0.03C-10Mn-12Cr-12Ni-5Mo-0.24N) and nitrogen strengthened 316LN (ST316LN, 0.03C-2Mn-18Cr-11Ni-2Mo-0.20N), which have the same sizes as actual TF structures, were successfully completed without

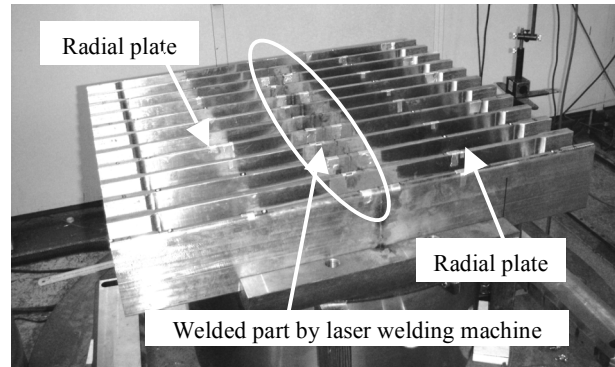


Fig. IV.2.1-4 Overview of welded radial plate (test piece) with 4 kW YAG laser welding machine.

major difficulties [2.1-3]. Characterization of these materials were then performed and their quality and mechanical properties were demonstrated to satisfy the ITER requirements such as 4K yield strength of more than 1,000 MPa for JJ1 and more than 900 MPa for ST316LN, and no inclusions and ferrite structure.

Regarding radial plate manufacture, several trials were performed to establish basic technologies on the machining and welding procedures to be used in actual radial plate manufacture [2.1-3, 2.1-4]. In order to demonstrate a connection of radial plate segments, two grooved radial plates (test pieces) clamped by restraint jigs were welded together along the shape of the U groove by using 4 kW YAG laser welding machine, as shown in Fig. IV.2.1-4. A manual TIG welding followed the laser welding to compensate the lack of laser power for full penetration. Vertical distortion (normal to the radial plate plane) due to welding was measured along the length of the radial plate, and the maximum distortion was found to be 0.3 mm which occurred only in vicinity of the welds. In addition, the shrinkage near the welds was about 0.73 mm, which is very small. Thus, by employing the laser welding, welding with small distortion has been demonstrated, which is one of the most critical technologies for radial plate manufacture.

References

- 2.1-1 Hamada, K., *et al.*, *Cryog. Eng.*, **41**, 131 (2006) (in Japanese).
- 2.1-2 Hamada, K., *et al.*, *IEEE Trans. ASC.*, **16**, 787 (2006).
- 2.1-3 Okuno, K., *et al.*, *IEEE Trans. ASC.*, **16**, 880 (2006).
- 2.1-4 Abe, K., *et al.*, *IEEE Trans. ASC.*, **16**, 807 (2006).

2.2 Vacuum Vessel

The present reference Vacuum Vessel (VV) provides a large number of interface structures, such as keys and housings to support the blanket modules. This increases the number of weld joints in the VV, so that the distance between weld joints becomes much shorter than that in the previous design, for which fabrication feasibility has already been demonstrated in the EDA R&D of VV. The weld joints of housings for blanket support are very close to the reinforced ribs connected between inner and outer walls of VV especially in the inboard cylindrical region. The critical issues in the present VV design are therefore to confirm feasibilities of welding and weld inspection even with the expected large welding distortion and the low accessibility for welding and weld inspection.

JA-PT is now fabricating a partial VV mock-up (shown in Fig. IV.2.2-1), simulating an inboard cylindrical, in order to confirm the fabrication methods and weld inspection methods and in order to examine whether distortions caused by welding are within tolerances. The basic data necessary for preparing the technical specifications of the VV procurement, such as weld distortions, minimum space required for welding and inspection, welding and inspection accessibilities to the weld joints in the present design and applicability of weld inspections, will be obtained through the fabrication of the partial mock-up.

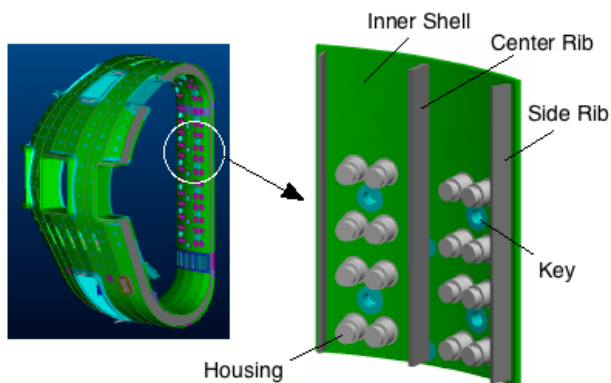


Fig. IV.2.2-1 VV partial mock-up under fabrication.

2.3 Blanket and Divertor

Preparation works of the procurement of blanket and divertor have been performed this year.

As for blanket, design and analysis works for confirmation of the structure integrity related to electro-magnetic (EM) force, detailed structure design of blanket module #10, investigation of the attachment

and detachment techniques for the first wall panel in the Hot Cell and the detailed thermo-mechanical analysis of the first wall panel for identification of the minimum acceptable defect size between the dissimilar HIP joints of Cu alloy / SUS. With respect to the 3-D EM analyses have been performed for 40 ms linear and 18 ms exponential decays and 30ms liner current decay of VDE III/F-DW, based on revised plasma disruption scenarios. Additionally, EM loads for 35ms linear and 16ms exponential decays were derived using the calculated results. EM loads of all modules for 35 ms linear and 16ms exponential decays are within the allowable range. EM loads of linear and exponential decays are generally similar and the differences between them are less than 10% except Mr under VDE (F-UP). Taking into account that the modified stub key with stub bore of 132mm can be applicable to outboard modules from #11 to #17 and #18 module, limit and plastic analyses have been performed considering gap between key and key groove, in order to estimate the allowable loads of the inter-modular and stub keys. The allowable loads of the inter-modular key for the combined load are Mr of 1160 [kNm] and Fz of 560 [kN] for VDEIII not including the dynamic amplification factor of 1.5. Those of the stub key are 612 [kNm] and 252 [kN] for VDE III. The allowables for VDEII are 20% less than those for VDEIII. It was clarified that the results of EM analysis satisfied these acceptable values. Further analysis and evaluation should be continued to clarify the structure integrity in the new cases of disruption scenarios.

With respect to the thermo-mechanical analysis of the first wall, it was identified that the as large as 1mm diameter defect may not cause crack propagation in the normal operation condition, based on the experimental data of non irradiated condition. This result suggests that the minimum size requirement of the NDE of the Cu/SUS HIP joints is about 1mm which size is enough detectable by UT. Irradiated data shows the comparable values, therefore, the effect of irradiation should be further incorporated in the evaluation.

With respect to the investigation of the FW panel replacement methods in the Hot Cell, mainly cutting and re-welding for the First Wall at the maintenance stage, have been selected and shield block structure reflecting requirements from the replacement methods has been investigated based on the concepts developed

by the IT. For the selection of the replacement methods, YAG Laser beam method has been selected for both cases out of a number of candidate methods in consideration of the usage in the Hot Cell and of the high applicability through the narrow cavity in the shield block. Then also key requirements to the design from the application point of view, namely YAG Laser and remote handling tools, are listed up.

As one of the provisional activities on the ITER divertor procurement, coolant system of Divertor Acceptance Test System (DATS), a high heat flux test facility with hydrogen ion beam system, has been modified to enable flow testing and high heat flux testing under ITER relevant divertor coolant condition. This coolant system now has a high pressure boost pump and a high pressure circulating pump. In addition, a feed-coolant heater was installed in the vacuum vessel. Major specification of this coolant system is summarized in Table IV.2.3-1. As shown in this table, DATS can perform not only high heat flux testing of ITER divertor components but also future breeding blanket testing using high temperature and pressure coolant.

Table IV.2.3-1 Major specification of DATS coolant system.

<u>Boost pump</u>	
- Coolant press.	~ 25 MPa
- Coolant temp.	room temperature
- Flow rate	Max. 60 L/min
<u>Circulating pump</u>	
- Coolant press.	~ 25 MPa
- Coolant temp.	up to 400°C
- Flow rate	Max. 250 L/min
<u>Feed-coolant heater</u>	
- Output	Max. 8.4 kW (1.4kW x 6 lines)
<u>Aux. heater system</u>	
- Output	Max. 12.6 kW

2.4 Remote Maintenance

Update of the vehicle manipulator for blanket maintenance has been studied according to the design changes such as blanket segmentation and structure, taking account of the interference between modules and remote handling equipment. The stress/structural and kinematic (CAD) analyses were performed for the compact design of the vehicle manipulator and rail in

order to avoid the interference between modules and vehicle manipulator. The results are as follows.

- (1) The guide roller mechanisms between rail and vehicle were newly designed to reduce their space by adopting supporting pads combined with the guide rollers and suitable material for satisfying the allowable Hertz's stress. This rearrangement enabled to reduce the size of the rail from 500 mm to 400 mm in height.
- (2) The double helical gear was also adopted instead of spur gear in the reference design as the sector gear for the rotation of the vehicle around the rail. This resulted that the diameter of the sector gear was reduced from 1460 mm to 996 mm.

According to the above results, the vehicle manipulator has been modified by about 30 % in weight, compared with the reference design (shown in Fig. IV.2.4-1).

In addition to the design study, the Blanket Test Platform (BTP) has been updated in order to improve the sensing technique for module installation and removal. The mock-up composed of typical inboard and outboard modules has been also updated considering the detailed interfaces such as key structure and gap between modules based on the latest IT design. Bench tests are now underway to clarify the specifications such as configuration and surface roughness of the target for sensing the relative position between target and manipulator for autonomous module replacement.

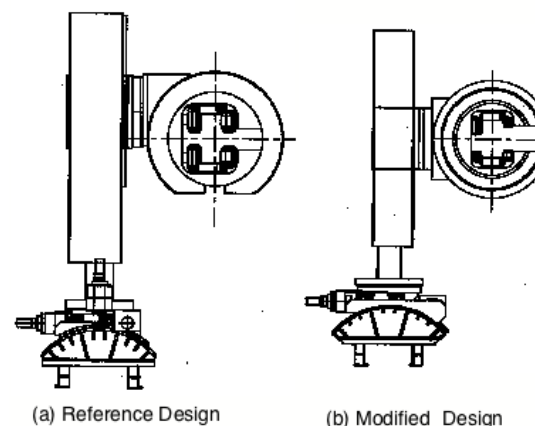


Fig. IV.2.4-1 Modification of vehicle manipulator.

2.5 EC and NBI Heating System

2.5.1 The Progress on Accelerator R&D for ITER NB

The H⁺ accelerator for the ITER NB is designed to produce 1 MeV, 40 A D⁺ ion beams for neutral beams

injection of 16.5 MW per module. However, acceleration of such high current beam with long pulse (> 1 s) has never been achieved in the past. For a demonstration of such high power negative ion beams at a current of ampere level and the energy up to 1 MeV, a five stage MeV accelerator has been developed at JAEA. One of the unique features of the MeV accelerator is the vacuum insulation. At the beginning of the R&D, the H^- ion acceleration was limited due to flashover along the inner surface of the insulator stack made of fiber reinforced plastic (FRP). The voltage holding capability of the MeV accelerator was drastically improved by a large stress ring, which reduces the electric field concentration at triple junction (interface of the FRP, metal flange and vacuum). The objective of the present R&D is a demonstration of high current density H^- ion beams up to MeV level energy to fulfill the ITER requirement (1 MeV, 200 A/m²). Figure IV.2.5-1 shows the progress of the MeV accelerator, by plotting the achieved beam current density and the beam energy. Up to now, the H^- ion beam of 146 A/m² was successfully accelerated up to 836 keV, as the highest record of the current density at MeV level energy beams. Note that the power density of the beams obtained in the present experiment is 122 MW/m² (836 keV \times 146 A/m²). This power density is more than twice higher than those of the existing negative ion sources in JT-60U and LHD NB systems. Thus the present beams generated by the JAEA MeV accelerator have achieved the ITER relevant power density.

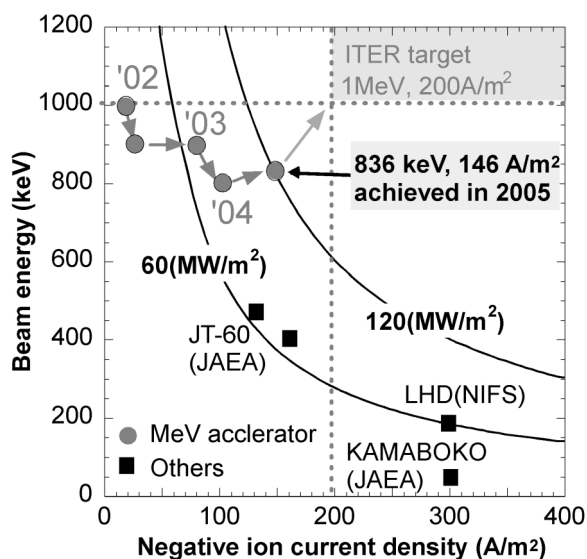


Fig. IV.2.5-1 Progress of MeV accelerator.

2.5.2 Design Modification of Equatorial EC Launcher

Under the ITA design task, the design study of an equatorial-port electron cyclotron (EC) heating launcher was carried out. Main purpose of the study is to increase the reliability and to find out the way to reduce the fabrication cost.

The conceptual sketch of the equatorial EC launcher design is shown in Fig. IV.2.5-2 (a). It consists of the front shield and the port plug, which three steering mirrors, the dog-legged transmission line, the torus window, the internal shields, several cooling pipes and small tubes and so on. Since almost all components should be cooled, the cooling lines are intricately placed in the port plug, which may decrease the reliability of the fabrication and the refurbishment and to increase the their cost. As the countermeasure, the front part of the waveguides and the miter bends circled around in Fig. IV.2.5-2 (b) were removed. Instead, an additional large mirror was placed at the location of the miter bends. This concept is called “quasi-optical transmission”. In addition, the initial result of millimeter-wave transmission analysis showed that the peak power density of heat load on the steering mirror was reduced from 3.2 MW/m² to 1.0 MW/m². This result suggests that the design of the mirror could be more relaxed and the reliability increase.

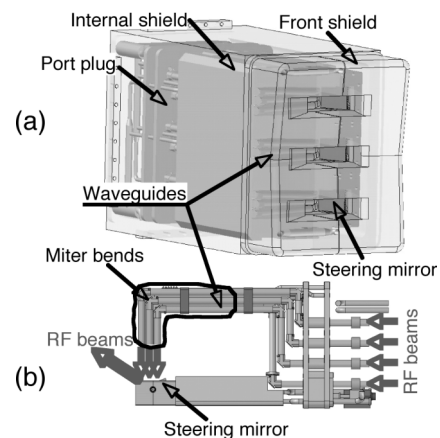


Fig. IV.2.5-2 ITER equatorial launcher, (a) entire structure and (b) transmission line.

2.6 Operation Scenario

2.6.1 Plasma Operation Scenario

The ITA task related plasma operation scenario has been studied to contribute to the detailed design of ITER through analyses of plasma equilibria for the

plasma ramp-down and plasma disruption scenarios taking account of recent development of operation scenario and disruptions.

Plasma ramp-down scenario of Design Scenarios of fusion power 400 MW with burn time 400 s has been revised. To mitigate the heat load on the limiter, the divertor configuration was kept until low plasma current of 4.5MA. In this scenario, the waveforms of the coil currents and voltages produced by this scenario are within the limitations.

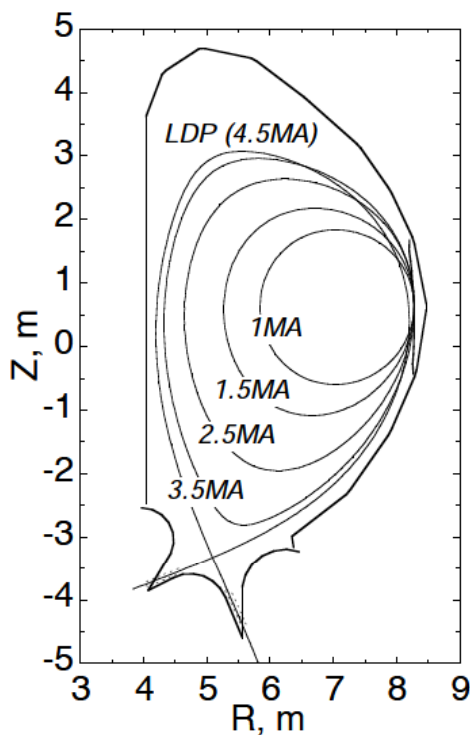


Fig. IV.2.6-1 Time evolution of the plasma boundary during the current ramp-down phase from 4.5MA to 1MA in Scenario 2.

2.6.2 Disruption Studies

For the disruption simulation studies, sensitivity study on the location of null point due to changes in the internal inductance (l_i) has been performed. The null point location moves downward and approaches to the divertor coil when l_i is reduced with keeping currents in CS3L and PF6 coils and the plasma shape in the upper region is matched. This is because the efficiency to generate the null point by the divertor coil becomes higher with flatter current profile of the plasma (decreasing l_i) for the same divertor coil current.

The efficacy of the divertor dome has been examined from the viewpoints of the electromagnetic (EM) load during disruptions. In the case of downward

VDE (toward X-point) disruptions, EM loads on the blanket module (BM) and divertor cassette (DV) has been compared by both cases. EM loads on #1 and #18 BMs are $\approx 10\%$ larger in the case of without dome than with dome. EM load on DV will also be 10-15% larger in the case of without dome than with dome.

2.7 Tritium-Material Interaction

The confinement and removal of tritium are key subjects for safety of ITER. It is essentially required to accumulate basic data on these subjects for the ITER design and operation.

The ITER buildings are final confinement barriers of tritium. Several concrete samples were exposed to the tritiated water vapor, whose concentration was from 740 to 1100 Bq/cm³ with moisture less than 10000 pm for a period. The tritiated vapor exists up to about 2 cm from the surface of the sample only for two months exposure. It is expected that the tritiated water vapor would reach the outer surface of the wall of the hot cell during the ITER operation period, so that a trace amount of tritium may be released to environment from the wall of the building not from the stack. The lining with resins is required in a controlled area, and is expected to decrease the penetration rate of tritium vapor.

The tritium released in the buildings is removed by ADS, where the tritium is oxidized by catalysts and is removed as water. Special gas of SF₆ is used in ITER, and is expected to be released in an accident such as fire. To study the effect of SF₆, the performance tests of ADS was carried out with air containing $\sim 1\%$ of hydrogen, $\sim 1\%$ of methane and $\sim 1\%$ of SF₆. The SF₆ gas was decomposed in the case of the catalyst temperature higher than 673 K. It was observed that powders were produced with the decomposition of SF₆. In addition, a part of the water was reduced to hydrogen due to the existence of the powders. Consequently, the detritiation factor of ADS was decreased to less than 50 from >1000 of its initial value. It is required to monitor continuously and to reduce the amount of the SF₆ gas released into the tritium handling area for the minimization of the poison effect by some ideas for the arrangement of components in the buildings.

Tritiated water is produced in the regeneration process of ADS, and is subsequently processed by the ITER WDS. One of the key components of WDS is an

electrolysis cell made of organic compound, Nafion. A series of irradiation tests of Nafion has been carried to examine whether the electrolysis cell satisfies 2-3 years' operation or not (ITER design), by ^{60}Co gamma-rays of 10 Gy/h at room temperature. The samples maintain an enough tensile strength and ion exchange capacity for the irradiation up to 850 kGy which is equivalent to the dose for the three years' operation of the electrolysis cell under the ITER operation condition. The tensile strength measurement of the electrolyte is unrealistic in the normal operation, however, the amount of dissolved fluorine ions from Nafion could be correlated closely with the tensile strength and the ion exchange capacity. As an alternative approach, measuring the concentration of the fluorine ions can provide us the information about the damage of the electrolyte.

2.8 Neutronics

We have developed the CAD/MCNP interface program to easily perform Monte Carlo fusion nuclear design calculation with high accuracy using the detailed calculation geometry. Usually only the solid region data exist in the CAD data. The void region data do not exist in the CAD data, while the definition of these data is required for MCNP input data. The prototype of the CAD/MCNP interface program has been newly developed for creating the void region data automatically. The void region data have been created by subtracting the solid region data using the Boolean operation. The program has also the function on dividing automatically the overall data to small cubes to simplify the void region data. It has been applied to 3D CAD data on the ITER benchmark model. It could be demonstrated that the void region data were successfully created on the ITER model using the developed program.

2.9 Plasma Diagnostics

Under the ITA Design Task on plasma diagnostics, "Support to the ITER diagnostic design," design works on Impurity Influx Monitor (divertor), Microfission Chambers, Thomson Scattering (edge) System, and Integrator for magnetic measurement have been carried out. The conceptual design of the upper port plug has been performed, which has contributed to the Diagnostic Port Engineering Taskforce.

2.9.1 Impurity Influx Monitor (Divertor)

The design work of the impurity influx monitor (divertor) has been carried in order to correspond to the change in ITER design. To simplify the optics, the design of the collection optics is changed to a simple Cassegrain telescope system. In addition, a micro-lens-array is inserted just in front of the fiber bundle in order to increase the light intensity by extending the image size in the toroidal direction on the divertor target. The ray-trace analysis has shown that the spatial resolution of ITER requirement (50 mm) will be achieved by these optical systems [2.9-1]. Moreover, optical designs of in-situ sensitivity calibration system, an adjustment system (Fig. IV.2.9-1) and a focusing system, and a conceptual design of the shutter system for the first mirror have been carried out.

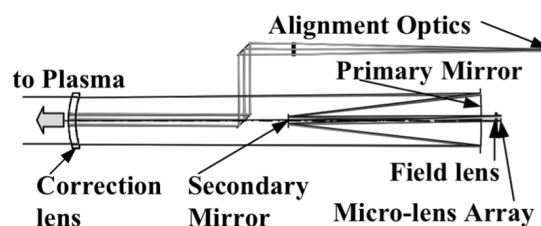


Fig. IV.2.9-1 Collection optics with optical alignment system.

2.9.2 Microfission Chamber

In ITER, neutron monitor has to measure the total neutron emission rate in the range of fusion power from 1 kW to 1 GW with a temporal resolution of 1 ms.

A single microfission chamber with 10 mg of U^{235} to be installed in a gap between a shielding blanket module and a vacuum vessel can cover the range of the fusion power from 100 kW to 1 GW. For the low fusion power operation including D-D operation, a microfission chamber bundle has been newly proposed [2.9-2]. The microfission chamber bundle consisting of 13 microfission chamber units with a diameter of 14 mm and a length of 400 mm has been designed. The estimated dynamic range of the microfission chamber bundle is 1 kW – 400 kW in fusion power.

The engineering design such as the nuclear heating and the heat transport analyses have been carried out. It has been found that the gamma heating is 5-6 times as large as that of the neutron heating and the total nuclear heating rate is $\sim 1.5 \times 10^5 \text{ W/m}^3$ for the chamber housing

of SS316L at the 500 MW operation. Heat transport analyses has indicated that the detector temperature might be kept less than 250°C by the thermal conduction to the vacuum vessel with the thermal conduction rate of 100 W/m²K or higher.

2.9.3 Thomson Scattering System (Edge)

A high output energy (5 J) and high repetition rate (100 Hz) laser system is required for the edge Thomson scattering system in ITER. A YAG laser (Nd:YAG laser) is a first candidate for the laser system satisfying the requirements. It is important to develop a high beam quality and single longitudinal mode (SLM) laser oscillator in order to realize the high power laser system. The SLM laser oscillator, which includes the laser head and the resonator, has been designed based on estimation of the output power for the SLM laser oscillator. A feedback control scheme of the resonator and an interface for the amplification system to achieve the required laser performance have also been investigated [2.9-3].

2.9.4 Integrator for Magnetic Measurement

The advanced integrator system, which covers a wide range of the input voltage from stable plasmas to MHD unstable plasmas, is being developed in JT-60 toward a long-pulse operation of tokamak [2.9-4]. In order to improve the integrator durability against the repeated excessive voltage inputs from disruptive plasmas, we have newly developed and tested three types of the signal input circuit; High voltage diode resistant up to ± 2 kV (Type I), Power Mos FET, +1 kV / -0.6 kV (Type II), and Precise attenuator insertion with an FB compensator (Type III). Through linearity, drift and integration tests using one of JT-60 magnetic sensors, we have concluded that the Type III circuit is acceptable for actual application to the magnetic measurements in long-pulse tokamak operations (see I.2.2.2).

It is expected that, during ITER operation, a small ($\leq 1\mu\text{A}$) current will be injected in common-mode (that is, between the coil winding and machine ground) into the integrator. For the common mode current, it has been shown that the current is well below the sensitivity of the integrator and the drift speed ($\sim 20\ \mu\text{V}\cdot\text{s/s}$). A proper system design for the magnetic measurements would be able to reject the common mode current of concern.

2.9.5 Port Plug

Diagnostic components installed in vacuum vessel ports are integrated in the “port plug”, which serves both as the neutron shield and diagnostic container and enables diagnostics to access to the plasma in the harsh radiation circumstances of ITER. Only basic concept of the integration in the port plug has been given so far since designs of both the port plug and diagnostic devices are under progress. As one of these integration activities, the integration design of the upper port plug No.11 (Up#11) has been performed, and the structure concept of the port plug has been investigated for electro-magnetic and neutron load analyses.

Three diagnostics will be installed in Up#11, i.e., the edge Thomson scattering system, the visible-IR TV divertor viewing system and the neutron activation system. To integrate these diagnostic systems in the port plug, the labyrinth of optical path, the driving and cooling systems for shutters and mirrors, the maintenance space and the interaction of each other were considered. Figure IV.2.9-2 shows the conceptual integrated design of Up#11. A change in the design of the diagnostic/shield module just behind the blanket shield module (BSM) was considered in order to keep a space enough for maintenance and installation of diagnostic mirrors and a shutter mechanism. The neutron shield in the module is moved in front of the vacuum flange instead. The structure and the position of BSM supports, which is a main component inducing the electro-magnetic load, have been arranged to consider optical path inside the BSM.

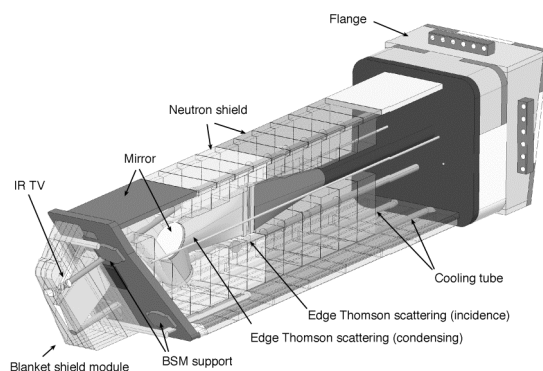


Fig. IV.2.9-2 Conceptual design for the upper port plug No.11.

References

- 2.9-1 Ogawa, H., *et al.*, “Design of Impurity Influx Monitor (Divertor) for ITER,” *JAEA-Technology* 2006-015 (2006).
- 2.9-2 Nishitani, T., *et al.*, “Design of Micro-Fission Chambers for ITER Low Power Operations,” *JAEA-Technology* 2005-047 (2005).
- 2.9-3 Hatae, T., *et al.*, “Design of Single-Longitudinal-Mode Laser Oscillator for Edge Thomson Scattering System in ITER,” *JAEA-Technology* 2006-21 (2006).
- 2.9-4 Kawamata, Y., *et al.*, “Development of an Intelligent Digital Integrator for Long-Pulse Operation in a Tokamak,” *19th Symp. on Fusion Eng.* (2005).

3. Domestic Activities

3.1 Site Preparation

A site-dependent design was studied to prepare for siting of ITER in Japan until the decision of the site to France at June.

Site layout plan of major buildings and structures of ITER in the Rokkasho-Site was constructed to apply the information of the ground near the site and the results of site dependent design in Japan. Through this study, the most appropriate site layout was constructed with satisfaction of (i) bedrock level at the tokamak complex building is relatively high and it can be reduced the cost of excavation and foundation work, (ii) total amount of excavation soil for site preparation is minimized and the flexibility of the layout is ensured with flat ground level, (iii) accessibility of human and equipments, reduction of noise and vibration to the environment can be obtained.

The layout in the tokamak complex building, which is most important building for the installation of tokamak machine, was planned. To draw up this arrangement plan, final design report (FDR) was reviewed systematically. An additional study was performed for the adaptation of a regulatory framework including technical safety requirement in Japan. We proposed the tokamak complex building with seismic isolation to combine with the hot cell building. Through the studies, a layout plan was constructed including maintenance plan for personal access and component route with in the building from assembly to operation period.

3.2 Codes and Standards

In the Japan Society of Mechanical Engineering, a special committee among the Committee of Codes for Power Generation Facilities initiated examination for the codes and standards for the ITER superconducting magnets, which Japanese Domestic Agency (DA) will procure. The structure of organization in JSME for its implementation and the roadmap for establishment have been made. The first draft of the QA codes is now being reviewed in the subcommittee of QA and materials. The first draft of the ITER superconducting magnet construction codes is now being prepared under discussion with the ASME advisory group.

4. Contributions to International Tokamak Physics Activity (ITPA)

Naka Fusion Research Establishment continued to contribute to all the aspects of International Tokamak Physics Activity (ITPA). Its emphasis is inter-machine experiments of key plasma characteristics, aiming at development of methodologies of projection and control of ITER and power reactor plasmas, based on physics understanding. The following shows main contributions to ITPA, details of which are described in section I, II and III.

4.1 Transport Physics Topical Group

Two group meetings were held and six JAEA staff participated. JFT-2M experiments showed that ambient turbulence is modulated at GAM frequency. JT-60U, JET, AUG and DIII-D contributed to the ITPA Profile Database. Limited ability to reproduce experimental profiles in hybrid discharges is recognised using transport modelling.

4.2 Confinement Database and Modeling Topical Group

Two group meetings were held and four JAEA staff participated. The shaping of the plasma cross section appears to affect the confinement performance, and this may possibly explain the variation of the β dependence [4.2-1]. AUG plasmas with low $\delta_{\text{upper}} < 0$ display strong β degradation; on the other hand, JET plasmas with ‘good’ shaping do not display β degradation.

Reference

- 4.2-1 Takizuka, T., *et al.*, *Plasma Phys. Control. Fusion*, **48**, 799 (2006).

4.3 Pedestal and Edge Physics Topical Group

Two group meetings were held and six JAEA staff participated. Several small/no ELM regimes such as EDA, grassy ELM, HRS, QH-mode, type II and V ELMs with good confinement properties have been obtained in Alcator C-Mod, ASDEX-Upgrade, DIII-D, JET, JFT-2M, JT-60U and NSTX. All these regimes show considerable reduction of instantaneous ELM heat load onto divertor target plates in contrast to conventional type I ELM, and ELM energy losses are evaluated as less than 5% of the pedestal stored energy.

These small/no ELM regimes are characterized with low collisionality and high triangularity [4.3-1]. JT-60U experiments show that counter plasma rotation is important for the access to the high frequency grassy ELM regime [4.3-2].

References

- 4.3-1 Oyama, N., *et al.*, *Plasma Phys. Control. Fusion*, **48**, A171 (2006).
4.3-2 Oyama, N., *et al.*, *Nucl. Fusion*, **45**, 871 (2005).

4.4 Steady-State Operation Topical Group

Two group meetings were held and two JAEA staff participated. In JT-60U, high $\beta_N \sim 2.3$ was sustained for 28.6 s at $q_{95} \sim 3.2$. Benchmarking of NBI/NBCD was carried out on ASTRA, ACCOME and OFMC.

4.5 MHD Topical Group

Two group meetings were held and ten JAEA staff participated. The recommendation for the lower bound of the current quench time t_{CQ} has been revised in the light of an updated database: $t_{CQ}/S > 1.67 \text{ ms/m}^2$, where S is the poloidal cross-section area of the plasma before the disruption (previously 1.8 ms/m^2). A runaway electron discharge was maintained without current quench in JT-60U [4.5-1].

Reference

- 4.5-1 Kawano, Y., *et al.*, *Proc. 32nd EPS Conf.*, P2.068 (2005).

4.6 Scrape-Off-Layer and Divertor Physics Topical Group

Two group meetings were held and three JAEA staff participated. Both carbon deposition at the tile edge and D/C ratio in JT-60U were lower than other tokamaks with carbon wall. Global particle balance under “wall saturated condition” during a series of the long pulse discharges in JT-60U was presented. C deposition rates on the target were similar in many experiments (e.g. JT-60U: 2.7×10^{20} C/s, JET: $4.3\text{--}6.5 \times 10^{20}$ C/s), while large differences in D/C were seen (JT-60U: 0.02–0.1, JET: 0.3–0.8).

4.7 Diagnostics Topical Group

One group meeting was held and five JAEA staff participated. A new example of asymmetries in the neutron emission profile in JT-60U was presented.

Development of a novel high repetition-rate CO₂ laser for the collective Thomson scattering for α -particle diagnostics was presented. JT-60U has contributed to the development of integrators for long pulses (1000 s).

5. CODAC Design Activity

The ITER Instrumentation and Control (I&C) system, which controls ITER facility, consists of four parts; Control, Data Access and Communication (CODAC), Plant System, Interlock System (SIS) and Safety related I&C System.

Although CODAC design is responsible for the international organization (IO), large contributions are expected from all of the participating teams. In order to conceptualize CODAC design, preparatory work has been started. Each plant control system design is strongly depend on the CODAC system architecture. Thus, the design study of CODAC is indispensable for the plant systems in ITER and is important for the design of the plant systems procured by Japan home team.

The Final CODAC Design Report of 1998 ITER document has been reviewed in detail. Definition of CODAC has been clarified to determine system boundaries. ITER plant operation scenarios, ITER global operation states and plant system operation states were also reviewed and summarized to identify with functional requirements. CODAC consists of centrally-positioned Supervisory Control System (SCS), pulse control system, plant monitoring system, etc. The SCS controls the transition of the entire ITER plant from one operation state to another, and provides high level commands to the plant systems, in order to achieve integrated control of the entire plant. The SCS also monitors the operation state of each plant systems to ensure it is operating within its proper operational envelope.

6. Broader Approach Activities

According to the Joint Declaration by the Representatives of the parties to the ITER negotiations adopted on the occasion of the ministerial meeting for ITER in Moscow on 28 June 2005; the project of the broad approach will be carried out in Japan. Broader approach activities will be carried out complementally in parallel with ITER project for realization of fusion energy generation by cooperation of Japan and Europe (participation of the others to the activities is also open).

Regarding the candidate projects, which were proposed at and assessed by the ITER project promotion committee and a report, "the Broad Approach project to be carried out in Japan" was summarized.

Assessment and selection of the candidate projects were done from the following viewpoints;

i) early realization of fusion energy generation, ii) further improvement of presence and ability of our country through ITER project and towards fusion DEMO reactor, by implementation of the Broader Approach activities, iii) attractiveness for researchers domestic and overseas, iv) well balanced implementation of all the project for synergistic effects brought by cooperation of coordinated projects and personnel education/training for a long period of time.

As results, the following projects will be carried out as the Broader Approach activities;

The first, International Fusion Energy Research Center (consisting of DEMO Design and Research-and-Development Coordination Center, ITER remote experiment center and a fusion computer center) at Rokkasho, Aomori

The second, Satellite Tokamak (Advanced JT-60) at Ibaragi Naka

The third, engineering design of The International Fusion Materials Irradiation Facility (IFMIF-EVEDA) at Rokkasho Village, Aomori

The joint Broader Approach activities will be implemented on the basis of the Agreement for the Joint Implementation of the Broader Approach Activities in the Field of Fusion Energy Research (hereinafter "the Broader Approach Agreement") to be concluded between the Government of Japan and the European Atomic Energy Community.

The Broader Approach Agreement is now under negotiation with proposal of items for research and

development to Europe based on the agreed flame works and financial situations. EURATOM and Japan will make contributions in cash and in-kind to the Broader Approach activities. The joint Broader Approach activities will be implemented on a time frame compatible with the ITER construction phase on the basis of technical reports adopted by joint working groups of experts from EURATOM and Japan which will be updated by the Steering Committee to be established under the Broader Approach Agreement.

V. FUSION REACTOR DESIGN STUDY

1. Conceptual Design of DEMO Reactor

Fusion DEMO plant is requested to demonstrate 1) an electric power generation of 1GW level, 2) self-sufficiency of T fuel, 3) year-long continuous operation. From the economical aspect, the reactor size should be as compact as ITER. To meet these requirements, a DEMO reactor concept named SlimCS was proposed in 2005 [1-1].

SlimCS produces a fusion output of 2.95GW with a major radius of 5.5m, aspect ratio (A) of 2.6, normalized beta (β_N) of 4.3 and maximum field of 16.4T. The conceptual view is depicted in Fig. V.1-1. It is expected that the zero output at the sending end is obtained at $\beta_N = 2$, $n/n_{GW} = 0.4$ and $f_{BS} = 0.35$ and that a step-by-step power-up eventually attains 1GWe output at $\beta_N = 4.3$, $n/n_{GW} = 1.1$ and $f_{BS} = 0.77$, where n/n_{GW} and f_{BS} are the line-averaged electron density against the Greenwald density and the bootstrap fraction, respectively. SlimCS uses technologies foreseeable in 2020's such as Nb₃Al superconductor, water-cooled solid breeder blanket, low activation ferritic steel F82H as the blanket structural material, and tungsten monoblock divertor plate. Neutron wall load is designed at 3MW/m². Divertor heat flux, which can be a critical issue for such a compact reactor, is mitigated to 10MW/m² at the peak by small inclination (15°) of divertor plates and flux expansion in the divertor region.

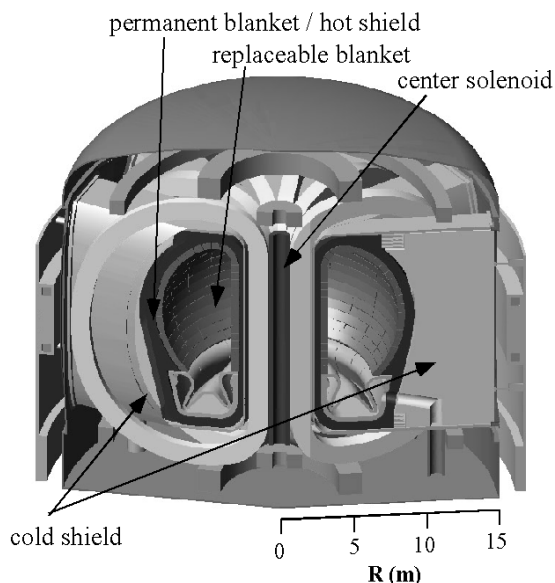


Fig. V.1-1 Conceptual view of SlimCS.

SlimCS can be as compact as advanced commercial reactor designs such as ARIES-RS and CREST (Fig.V.1-2), even with the assumption of relatively conservative plasma parameters. This is because such a low-A plasma, being stable for higher elongation (κ), can have higher n_{GW} and β_N limits. Another merit of low-A is that the first wall area on the low field side, where smaller electromagnetic (EM) force acts on disruptions, is wide compared with that of conventional-A. This means that tritium can be efficiently bred with large blanket modules on the low field side. As a result, the demand for tritium breeding on the high field side is comparatively reduced so that small blanket modules, being robust to stronger EM force but less efficient for tritium breeding, can be arranged on the side.

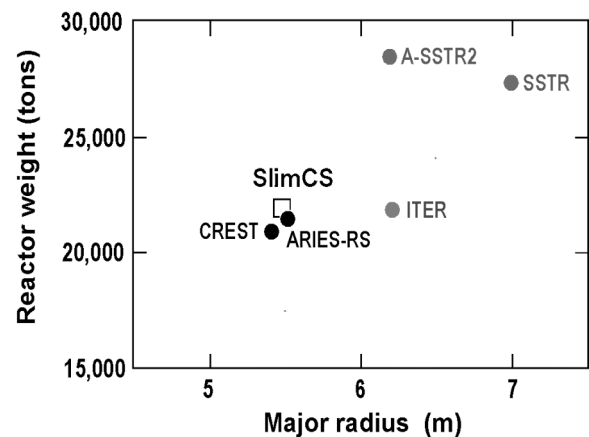


Fig. V.1-2 Comparison of major radius and reactor weight for various fusion reactors.

Reference

- 1-1 Tobita, K., *et al.*, *Fusion Eng. Des.*, **81**, 1151 (2006).

2. Non-Inductive Current Ramp Simulation

From the practical control aspect of a compact, CS-free tokamak reactor concept "VECTOR", a fully non-inductive, very slow current buildup scenario were investigated via a consistent simulation using Tokamak Simulation Code [2-1, 2-2, 2-3]. The L-mode based, improved core confinement transport model, *e.g.* current diffusive ballooning mode (CDBM), has clarified detailed dynamics of the stable formation of the internal transport barrier (ITB) by non-inductive means of off-axis current sources. First, in accordance with the strong ITB formation, the bootstrap (BS) current was confirmed to substantially increase by more than $f_{bs} > 50\%$ and to enhance the current buildup efficiency, saving a great deal of the driving power of the non-inductive current sources. Second, the integrated, non-inductive scenario was shown to meet the following control and physics requirements set by (a) plasma shaping compatible with recharging of the coil currents, (b) available NB-heating power, (c) avoidance of Current Hole formation under over driving, non-inductive current sources, (d) reasonable HH factor = $t_E/t_{E,y2} < 1.3$ and (e) allowable Greenwald density limit of $n < n_{GW}$. Third, a safe plasma takeoff from limiter to diverter configuration, as well as a safe landing to limiter structures at discharge termination, was also demonstrated. Furthermore, a new operation scenario was computationally examined to control the ITB structure by means of small, but long-duration perturbation (~ 80 sec in reactor plasmas) of negative or positive inductive current sources. Thus, the q -profile was first shown to undergo a drastic change over a wide range from positive to negative magnetic shear configuration, and vice versa.

References

- 2-1 Nakamura, Y., *et al.*, "Simulation Modeling of Fully Non-Inductive Buildup Scenario in High Bootstrap Current Tokamaks without Center Solenoids," *Proc. 32nd EPS Conf. on Plasma Phys.*, P2-051 (2005).
- 2-2 Nakamura, Y., *et al.*, "Non-Inductive Operation Scenario of Plasma Current Ramp-Down in CS-Less, Advanced Tokamak Reactor," *Proc. 15th International Toki Conf. on "Fusion & Adv. Technol."*, PS2-22 (2005).
- 2-3 Nakamura, Y., *et al.*, "Computational Study of Non-Inductive Current Buildup in Compact DEMO Plant with Slim Center Solenoid," *1st IAEA TM on First Generation of Fusion Power Plants -Design and Technology-*, PPCA1-V (2005).

3. Study of Advanced Shield Materials

In general, a hydrogen-rich material has the potential to be an effective neutron shield because the contained hydrogen nuclei work as a moderator of fast neutrons, reducing the fast neutron flux. It is notable that some hydrides have a considerably higher hydrogen content than polyethylene, water and solid hydrogen. The material that we have focused attention on is borohydrides which has been developed for a fuel cell [3-1]. The anticipated hydrogen concentration of $Mg(BH_4)_2$, which will probably be a new candidate shielding material, is as high as 1.32×10^{23} H-atoms/cm³, surpassing those of already known VH_2 (1.05×10^{23} H-atoms/cm³) and TiH_2 (9.1×10^{22} H-atoms/cm³).

In order to assess capability of such hydrides as a advanced shield material, neutronics calculation was carried out for the SlimCS design [3-2]. In the design, the shields are located on the inboard and outboard sides, and originally they were designed to be 30 and 70cm in thickness, respectively, using steel-and-water. When the steel-andwater is replaced with steel-and-hydride, it was found that $Mg(BH_4)_2$, TiH_2 and ZrH_2 could reduce the thickness of the outboard shield by 23, 20 and 19%, respectively. When $Mg(BH_4)_2$ is mixed with ferritic steel (F82H) at the ratio of 1:1, the gamma-ray flux is reduced to 1/300 compared with that for pure $Mg(BH_4)_2$. These results indicates that borohydrides in combination with steel can work as an attractive shield material for fusion.

References

- 3-1 Orimo, S., *et al.*, *Mater. Sci. Eng.*, B **108**, 51 (2006).
- 3-2 Hayashi, T., *et al.*, *Fusion Eng. Des.*, **81**, 1285 (2006).

Appendix

A.1 Publication List (April 2005 – March 2006)

A.1.1 List of JAERI/JAEA Report

- 1) Alvani, C., Casadio, S., (Tsuchiya, K.), et al., “Li Depletion Effects on Li_2TiO_3 Reaction with H_2 in Thermo-mechanical Environment Relevant to Breeding Blanket for Fusion Power Plant,” JAERI-Review 2005-024 (2005).
- 2) Department of Fusion Engineering Research and Department of Materials Science, “Achievement of Element Technology Development for Breeding Blanket,” JAERI-Review 2005-012 (in Japanese).
- 3) Department of Fusion Facilities and Department of Fusion Plasma Research, “Progress in JT-60 Innovative Technologies,” JAERI-Review 2005-037 (2005) (in Japanese).
- 4) Honda, A., Okano, F., Ohshima, K., et al., “PLC Control of NBI Cryogenic Facility for JT-60U” JAEA-Technology 2006-020 (2006) (in Japanese).
- 5) Ida, M., Nakamura, H., Yamamura, T. et al., “Thermal Analysis of IFMIF Target Assembly,” JAEA-Technology 2006-003 (2006) (in Japanese).
- 6) Ida, M., Nakamura, H., Chida, T., et al., “Review of JAEA Activities on the IFMIF Liquid Lithium Target in FY2005,” JAEA-Review 2006-009 (2006).
- 7) IFMIF International Team, “Minutes of the IFMIF Technical Meetings May 17-20, 2005 Tokyo, Japan,” JAERI-Review 2005-027 (2005).
- 8) JT-60 Team., “Review of JT-60U Experimental Results in 2003 and 2004,” JAEA-Review 2005-005 (2005).
- 9) Kikuchi, K., Akino, N., Ikeda, Y., et al., “Characteristics of Voltage Holding and Outgassing on the Accelerator of JT-60 N-NBI Ion Source,” JAEA-Technology 2006-016 (2006) (in Japanese).
- 10) Kondo, K., Ochiai, K., Kubota, N., et al., “Development of Measurement Technique for Charged-particle Emission Double-differential Cross section using Pencil-beam Neutron Source,” JAEA-Research 2006-016 (2006).
- 11) Nakamichi, M., Kawamura, H., “An Irradiation Experiment for Qualification of Insulating Coating,” JAERI-Research 2005-015 (2005).
- 12) Nishitani, T., Yamauchi, M., Izumi, M., et al., “Design of Micro Fission Chambers for ITER Low Power Operations,” JAERI-Tech 2005-047 (2005).
- 13) Obara, K., Kakudate, S., Yagi, T., et al., “Continuous Running Test of Radiation Residence Motor Driving Equipment under High Gamma Irradiation,” JAEA-Technology 2006-023 (2006) (in Japanese).
- 14) Ogawa, H., Sugie, T., Katsunuma, A., et al., “Design of Impurity Influx Monitor (Divertor) for ITER,” JAEA-Technology 2006-015 (2006).
- 15) Ohmori, J., Nakahira, M., Takeda, N., et al., “Applicability Assessment of Plug Weld to ITER Vacuum Vessel by Crack Propagation Analysis,” JAEA-Technology 2006-017 (2006).
- 16) Sato, K., Hashimoto, M., Nagamatsu, N., et al., “Study of the Layout Plan in the Tokamak Complex Building for ITER,” JAEA-Technology (2006) (in Japanese).
- 17) Sato, K., Uehara, M., Tamura, K., et al., “Study of Site Layout in the Rokkasho Site,” JAEA-Technology 2006-024 (2006) (in Japanese).
- 18) Sato, S., Yamauchi, M., Nishitani, T., et al., “Analysis of Heat Load in ITER NBI Duct and Neutron Streaming through Pressure Relief Line,” JAEA-Technology 2006-032 (2006).
- 19) Sueoka, M., Suzuki, T., Hosoyama, H., “Development of a Profile Control System for the JT-60 Plasma Equilibrium Control,” JAEA-Technology 2006-022 (2006) (in Japanese).
- 20) Takeda, N., Kakudate, S., Nakahira, M., et al., “Study on Compact Design of Remote Handling Equipment for ITER Blanket Maintenance,” JAEA-Technology 2006-025 (2006).

- 21) Tsuchiya, K., Kawamura, H., Nagao, Y., “Breeding Blanket Development -Tritium Release from Breeder-,” JAEA-Technology 2005-003 (2005).
- 22) Tsuchiya, K., Kawamura, H., Nakamichi, M., “Fabrication Test and Characterization of Lithium Zirconate Pebbles Fabricated by a Rotating Granulation Method,” JAEA-Technology 2006-002 (2006)(in Japanese).
- 23) Uehara, K., and Nagashima, T., “Current Profiles and Major Disruptions in a Lower-Hybrid Current Drive Tokamak,” JAEA-Research 2006-002 (2006).
- 24) Watanabe, K., Takayanagi, T., Okumura, Y., et al., “ H Ion Beam Acceleration in a Single Gap Multi-Aperture Accelerator,” JAEA-Technology 2005-002 (2006).
- 25) Yamada, H., Kawamura, H., “Neutron Irradiation Test of Copper Alloy/Stainless Steel Joint Materials,” JAEA-Technology 2005-001 (2005).
- 26) Yamaki, D., Nakazawa, T., Tanifuji, T., et al., “Observation of Microstructural Changes in Li_2TiO_3 Caused by Multi-ion Beam Irradiation,” JAEA-Review 2005-001, 212 (2006).
- 27) Yamamoto, M., Okano, F., Tsuzuki, K., et al., “The development of the boron coating device for the JFT-2M,” JAERI-Tech 2005-061(2005).
- 28) Yamamoto, M., Tsuzuki, K., Kimura, H., et al., “The development of the device for 3D-Measurement of the Magnetic Field Profile in the Toroidal Direction,” JAERI-Tech 2005-060(2005).
- 29) Yutani, T., Nakamura, H., Sugimoto, M., “Compatibility of Reduced Activation Ferritic/ Martensitic Steel Specimens with Liquid Na and NaK in Irradiation Rig of IFMIF,” JAERI-Tech 2005-036 (2005).

A.1.2 List of papers published in journals

- 1) Akino, N., Ebisawa, N., Honda, A., et al., "Long Pulse Operation of NBI Systems for JT-60U," *Fusion Sci. Technol.*, **47**, 758 (2005).
- 2) Amemiya, H., and Uehara, K., "Method for Detection of Separatrix Surface Using Differential Double Probe," *Jpn. J. Appl. Phys.*, **45**, 247 (2006).
- 3) Angelone, M., Pillon, M., (Ochiai, K.), et al., "Radiation Hardness of a Polycrystalline Chemical-Vapor-Deposited Diamond Detector Irradiated with 14 MeV Neutrons," *Rev. Sci. Instrum.* **77**, 23505 (2006).
- 4) Asai, K., Iguchi, T., (Nishitani, T.), et al., "Improved In-situ Calibration Technique for ITER Ex-Vessel Neutron Yield Monitor," *Fusion Eng. Des.*, **81**, 1497 (2006).
- 5) Bakhtiari, M., Kramer, G. J., (Kusama, Y.), et al., "Role of Bremsstrahlung Radiation in Limiting the Energy of Runaway Electrons in Tokamaks," *Phys. Rev. Lett.*, **94**, 215003 (2005).
- 6) Bakhtiari, M., Tamai, H., (Kawano, Y.), et al., "Study of Plasma Termination using High-Z Noble Gas Puffing in the JT-60U Tokamak," *Nucl. Fusion*, **45**, 318 (2005).
- 7) Batistoni, P., Angelone, M., (Ochiai, K.), et al., "International Comparison of Measuring Techniques of Tritium Production for Fusion Neutronics Experiments Status and Preliminary Results," *Fusion Eng. Des.*, **75-79**, 911 (2005).
- 8) Baylor, L.R., Combs, S.K., (Maruyama, S.), et al., "Pellet Fueling Technology Development Leading to Efficient Fueling of ITER Burning Plasmas," *Physics of Plasmas*, **12**, 056103 (2005).
- 9) Combs, S. K., Baylor, L. R., (Maruyama, S.), et al., "Pellet Delivery and Survivability through Curved Guide Tubes for Fusion Fueling and its Implication for ITER," *Fusion Eng. Des.*, **75-79**, 691 (2005).
- 10) Cordey, J.G., Thomsen, K., (Takizuka, T.), et al., "Scaling of the Energy Confinement Time with β and Collisionality Approaching ITER Conditions," *Nucl. Fusion*, **45**, 1078 (2005).
- 11) Costley, A.E., Sugie, T., Vayakis, G., et al., "Technological Challenges of ITER Diagnostics," *Fusion Eng. Des.*, **74**, 109 (2005).
- 12) Donne, A.J.H., Fasoli, J., (Ozeki, T.), et al., "Summary of the International Energy Agency Workshop on Burning Plasma Physics and Simulation," *Fusion Sci. Technol.*, **49**, 79 (2006).
- 13) Elio, F., Ioki, K., Utin, Y., et al., "Special Blanket Design in the NB Region of ITER," *Fusion Eng. Des.*, **75-79**, 601 (2005).
- 14) Enoda, M., Akiba, M., Tanaka, S., et al., "Overview of Design and R&D of Test Blankets in Japan," *Fusion Eng. Des.*, **81**, 415 (2006).
- 15) Enoda, M., Akiba, M., Tanaka, S., et al., "Plan and Strategy for ITER Blanket Testing in Japan," *Fusion Sci. Technol.*, **47**, 1023 (2005).
- 16) Enoda, M., Hatano, T., Tsuchiya, K., et al., "Development of Solid Breeder Blanket at JAERI," *Fusion Sci. Technol.*, **47**, 1060 (2005).
- 17) Ezato, K., Suzuki, S., Dairaku, M., et al., "Critical Heat Flux Testing on Screw Cooling Tube made of RAFM-Steel F82H for Divertor Application," *Fusion Eng. Des.*, **75-79**, 313 (2005).
- 18) Ezato, K., Suzuki, S., Dairaku, M., et al., "Experimental Examination of Heat Removal Limitation of Screw Cooling Tube at High Pressure and Temperature Conditions," *Fusion Eng. Des.*, **81**, 347 (2006).
- 19) Fujii, T. and JT-60 Team, "Operational Progress of the 110GHz-4MW ECRF Heating System in JT-60U," *J. Physics*, **25**, 45 (2005).
- 20) Fujita, T., Suzuki, T., Oikawa, T., et al., "Current Clamp at Zero Level in JT-60U Current Hole Plasmas," *Phys. Rev. Lett.*, **95**, 075001 (2005).
- 21) Fujita, T. and the JT-60 team, "Steady State Operation Research in JT-60U with Extended Pulse Length," *Nucl. Fusion*, **46**, S3 (2006).
- 22) Furukawa, M. and Tokuda, S., "Mechanism of Stabilization of Ballooning Modes by Toroidal Rotation Shear in Tokamaks," *Phys. Rev. Lett.*, **94**, 175001 (2005).

- 23) Furukawa, M., Yoshida, Z. and Tokuda, S., "Regularization of Singular Eigenfunctions of an Operator with Continuous Spectra: with Applications for Ballooning Modes in Toroidally Rotating Tokamaks," *Phys. Plasmas*, **12**, 072517 (2005).
- 24) Giancarli, L., Chuyanov, V., (Akiba, M.), et al., "Breeding Blanket Modules Testing in ITER: An International Program on the Way to DEMO," *Fusion Eng. Des.*, **81**, 393 (2006).
- 25) Hagiwara, M., Itoga, T., (Sugimoto, M.), et al., "Measurement of Neutron Emission in Li(d,xn) Reaction with Thick and Thin Targets for 40-MeV Deuterons," *Fusion Sci. Eng.*, **48**, 1320 (2005).
- 26) Hamada, K., Nakajima, H., Takano, K., et al., "Fatigue Assessments of the ITER TF Coil Case based on; JJ1 Fatigue Tests," *Fusion Eng. Des.*, **75**, 87(2005)
- 27) Hanada, M., Seki, T., Takado, N., et al., "Experimental Study on Spatial Uniformity of H- Ion Beam in a Large Negative Ion Source," *Fusion Eng. Des.*, **74**, 311 (2005).
- 28) Hayashi, N., Takizuka, T., Ozeki, T., "Profile Formation and Sustainment of Autonomous Tokamak Plasma with Current Hole Configuration," *Nucl. Fusion*, **45**, 933 (2005).
- 29) Hayashi, T., Ochiai, K., Masaki, K., et al., "Deuterium depth profiling in JT-60U W-shaped divertor tiles by nuclear reaction analysis," *J. Nucl. Mater.*, **349**, 6 (2006).
- 30) Hayashi, T., Tobita, K., Nishio, S., et al., "Neutronics Assessment of Advanced Shield Materials Using Metal Hydride and Boron hydride for Fusion Reactors," *Fusion Eng. Des.*, **81**, 1285 (2006).
- 31) Hayashi, T., Itoh, T., Kobayashi, K., et al., "Safety Handling Characteristics of High-Level Tritiated Water," *Fusion Eng. Des.*, **81**, 1365 (2006).
- 32) Hayashi, T., Suzuki, T., Yamada, M., et al., "Tritium Accounting Stability of a ZrCo Bed with "in-bed" Gas Flowing Calorimetry," *Fusion Sci. Technol.*, **48**, 317 (2005).
- 33) Hegeman, J. B. J., van der Laan, J. G., Kawamura, H., et al., "The HFR Petten High Dose Irradiation Programme of Beryllium for Blanket Application," *Fusion Eng. Des.*, **75-79**, 769 (2005).
- 34) Hino, T., Yoshida, H., Akiba, M., et al., "Deutrium Retention in Carbon flakes and Tungsten-Carbon mixed flakes produced by Deuterium Arc Discharge," *Nucl. Fusion*, **45**, 893 (2005).
- 35) Hirai, T., Ezato, K., Majerus, P., "ITER Relevant High Heat Flux Testing on Plasma Facing Surfaces," *Mater. Trans.*, **46-3**, 412 (2005).
- 36) Hirohata, Y., Shibahara T., (Arai, T.), et al., "Retention of hydrogen isotopes in divertor tiles used in JT-60U," *Fusion Sci. Technol.*, **48**, , 557(2005).
- 37) Hirohata, Y., Shibahara, T., (Arai, T.), et al., "Hydrogen Retention in Divertor Tiles in JT-60 for Hydrogen Discharge Period," *J. Nucl. Mater.*, **337-339**, 609 (2005).
- 38) Hirose, T., Shiba, K., Ando, M., et al., "Joining Technologies of Reduced Activation Ferritic/Martensitic Steel for Blanket Fabrication," *Fusion Eng. Des.*, **81**, 645 (2006).
- 39) Hoshino, K., Yamamoto, T., Tamai, H., et al., "Heating, Current Drive, and Advanced Plasma Control in JFT-2M," *Fusion Sci. Technol.*, **49**, 139 (2006).
- 40) Hoshino, T., Tsuchiya, K., Hayashi, K., et al, "Non-stoichiometry of Li₂TiO₃ under Hydrogen Atmosphere Condition," *Fusion Eng. Des.*, **75-79**, 939 (2005).
- 41) Hoshino, T., Yasumoto, M., Tsuchiya, K., et al., "Vapor Species Evolved from Li₂TiO₃ Heated at High Temperature under Various Conditions," *Fusion Eng. Des.*, **81**, 555 (2005).
- 42) Ichimasa, M., Awagakubo, S., Takahashi, M., et al., "Tritium Elimination Syatem Using Tritium Gas Oxidizing Bacteria," *Fusion Sci. Technol.*, **48**, 759 (2005).
- 43) Ida, M., Nakamura, H., Shimizu, K., et al., "Thermal and Thermal-Stress Analyses of IFMIF Liquid Lithium Target Assembly," *Fusion Eng. Des.*, **75-79**, 847 (2005).
- 44) Ide, S., and the JT-60 team, "Long Pulse Operation of High Performance Plasmas in JT-60U," *Plasma Sci. Technol.*, **8**, 1 (2006).
- 45) Ide, S., and the JT-60 team, "Overview of JT-60U Progress towards Steady-State Advanced Tokamak," *Nucl. Fusion*, **45**, S48 (2005).

- 46) Ido, T., Miura, Y., Hoshino, K., et al., "Observation of the Interaction between the Geodesic Acoustic Mode and Ambient Fluctuation in the JFT-2M Tokamak," Nucl. Fusion, **46**, 512 (2006).
- 47) Ido, T., Miura, Y., Kamiya, K., et al., "Geodesic-Acoustic-Mode in JFT-2M Tokamak Plasmas," Plasma Phys. Control. Fusion, **48**, S41 (2006).
- 48) Idomura, Y., Tokuda, S. and Kishimoto, Y., "Global Profile Effects and Structure Formations in Toroidal Electron Temperature Gradient Driven Turbulence," Nucl. Fusion, **45**, 1571 (2005).
- 49) Iida, H., Petrizzi, L., Khripunov, V., et al., "Nuclear Analyses of Some Key Aspects of the ITER Design with Monte Carlo Codes," Fusion Eng. Des., **74**, 133 (2005).
- 50) Imbeaux, F., Artaud, J. F., (Fujita, T.), et al., "Multi-machine transport analysis of hybrid discharges from the ITPA profile database," Plasma Phys. Control. Fusion, **47**, B179 (2005).
- 51) Inagaki, S., Takenaga, H., Ida, K., et al., "Comparison of Transient Electron Heat Transport in LHD Helical and JT-60U Tokamak Plasmas," Nucl. Fusion, **46**, 133 (2006).
- 52) Inoue, T., Hanada, M., Kashiwagi, M., "Design Study of a Neutral Beam Injector for Fusion DEMO Plant at JAERI," Fusion Eng. Des., **81**, 1291 (2006).
- 53) Inoue, T., Taniguchi, M., Morishita, T., et al., "R&D on a High Energy Accelerator and a Large Negative Ion Source for ITER," Nucl. Fusion **45**, 790 (2005).
- 54) Ioki, K., Elio, F., Maruyama, S., et al., "Selection of Design Solutions and Fabrication Methods and Supporting R&D for Procurement of ITER Vessel and FW/Blanket," Fusion Eng. Des., **74**, 185 (2005).
- 55) Ioki, K., Elio, F., Nakahira, M., et al., "Recent Progress of ITER FW/Blanket Design and Preparations for Fabrication," Fusion Eng. Des., **81**, 443 (2006).
- 56) Isayama, A. and the JT-60 Team, "Steady-State Sustainment of High- β Plasmas through Stability Control in Japan Atomic Energy Research Institute Tokamak-60 Upgrade," Phys. Plasmas, **12**, 056117 (2005).
- 57) Isayama, A. and the JT-60 Team, "Suppression of Neoclassical Tearing Modes towards Stationary High-Beta Plasmas in JT-60U," Plasma Sci. Technol., **8**, 36 (2006).
- 58) Isayama, A., Inagaki, S., Watanabe, K.Y., "Observation of Localized Oscillations at $m/n=2/1$ Rational Surface during Counter Neutral Beam Injection in the Large Helical Device," Plasma Phys. Control. Fusion, **48**, L45 (2006).
- 59) Ishikawa, M., Takechi, M., Shinohara, K., et al., "Energetic Ion Transport by Abrupt Large-Amplitude Event Induced by Negative-Ion-Based Neutral Beam Injection in the JT-60U," Nucl. Fusion, **45**, 1474 (2005).
- 60) Isobe, K., Nakamura, H., Kaminaga, A., et al., "Characterization of JT-60U Exhaust Gas during Experimental Operation," Fusion Eng. Des., **81**, 827 (2006).
- 61) Isono, T., Koizumi, N., Okuno, K., et al., "Design Study of Superconducting coils for the Fusion DEMO Plant at JAERI," Fusion Eng. Des., **81**, 1257 (2006).
- 62) Iwai, Y., Hayashi, T., Kobayashi, K., et al., "Case Study on Unexpected Tritium Release Happened in a Ventilated Room of Fusion Reactor," Fusion Sci. Technol., **48**, 460 (2005).
- 63) Iwai, Y., Yamanishi, T., Hayashi, T., et al., "Study on Tritium Removal Performance by Gas Separation Membrane with Reflux Flow for Tritium Removal System of Fusion Reactor," Fusion Sci. Technol., **48**, 456 (2005).
- 64) Iwai, Y., Yamanishi, T., Isobe, K., et al., "Distinctive radiation durability of ion exchange membrane in SPE water electrolyzer for ITER water detritiation system," Fusion Eng. Des., **81**, 815 (2006).
- 65) Iwai, Y., Yamanishi, T., Nishi, M., et al., "Application of Pressure Swing Adsorption to Water Detritiation Process," J. Nucl. Sci. Technol., **42**, 566 (2005).
- 66) Iwai, Y., Yamanishi, T., Nishi, M., et al., "Durability of Irradiated Polymers in Solid-Polymer-Electrolyte Water Electrolyzer," J. Nucl. Sci. Technol., **42**, 636 (2005).
- 67) Joffrin, E., Sips, A.C.C. (Isayama, A.), et al., "The 'Hybrid' Scenario in JET: towards Its Validation for ITER," Nucl. Fusion, **45**, 626 (2005).

- 68) Jones, L., Bianchi, A., (Ioki, K.), et al., "ITER Vacuum Vessel Sector Manufacturing Development in Europe," *Fusion Eng. Des.*, **75-79**, 607 (2005).
- 69) Kajijita, S., Ohno, N., Takamura, S., et al., "Comparison of He I Line Intensity Ratio Method and Electrostatic Probe for Electron Density and Temperature Measurements in NAGDIS-II," *Phys. Plasmas*, **13**, 013301 (2006).
- 70) Kajiwaru, K. and JT-60 Team, "Electron Cyclotron Heating Assisted Startup in JT-60U," *Nucl. Fusion*, **45**, 694 (2005).
- 71) Kamada, Y., Oyama, N., Ide, S., et al., "Impact of the Edge Pedestal Characteristics on the Integrated Performance in Advanced Tokamak Operation Modes on JT-60U," *Plasma Phys. Control. Fusion*, **48**, A419 (2006).
- 72) Kamiya, K., Kawashima, H., Ido, T., et al., "Reduced Divertor Heat Loads, Plasma Shape Effects, and Radial Electric Field Structures in JFT-2M HRS H-mode Plasmas," *Nucl. Fusion*, **46**, 272 (2006).
- 73) Kamiya, K., Oyama, N., Ido, T., et al., "Characterization of Coherent Magnetic Fluctuations in JFT-2M High Recycling Steady High-Confinement Mode Plasmas," *Phys. Plasmas*, **13**, 032507 (2006).
- 74) Kaneko, J., Tanaka, T., (Ochiai, K.), et al., "Radiation Detector Made of a High-Quality Polycrystalline Diamond," *Diamond & Related Materials*, **14**, 2027 (2005).
- 75) Kasai, S., Kamiya, K., Shinohara, K., et al., "Plasma Diagnostics in JFT-2M," *Fusion Sci. Technol.*, **49**, 225 (2006).
- 76) Kawamura, Y., Enoeda, M., Yamanishi, T., et al., "Feasibility Study on The Blanket Tritium Recovery System Using The Palladium Membrane Diffuser," *Fusion Eng. Des.*, **81**, 809 (2006).
- 77) Kawamura, Y., Iwai, Y., Nakamura, H., et al., "Tritium Recovery from Solid Breeder Blanket by Water Vapor Addition to Helium Sweep Gas," *Fusion Sci. Technol.*, **48**, 654 (2005).
- 78) Kawano, Y., Nakano, T., Asakura, N., et al., "Electron Density Behavior during Fast Termination Phase of Post-Disruption Runaway Plasma," *J. Plasma Fusion Res.*, **81**, 743 (2005).
- 79) Kawano, Y., Nakano, T., Isayama, A., et al., "Characteristics of Post-disruption Runaway Electrons with Impurity Pellet Injection," *J. Plasma Fusion Res.*, **81**, 593 (2005).
- 80) Kawashima, H., Sakurai, S., Shimizu, K., et al., "Divertor Modeling for the Design of the National Centralized Tokamak with High Beta Steady-State Plasmas," *Fusion Eng. Des.*, **81**, 1613 (2006).
- 81) Kawashima, H., Shimizu, K., Takizuka, T., et al., "Development of Integrated SOL/Divertor code and Simulation Study in JAEA," *Plasma and Fusion Res.*, **1**, 031 (2006).
- 82) Kawashima, H., Sengoku, S., Uehara, K., et al., "Study of SOL/Divertor Plasmas in JFT-2M," *Fusion Sci. Technol.*, **49**, 168 (2006).
- 83) Khomyakov, S., Elio, F., Ioki, K., et al., "Dynamic Amplification of Reaction Forces in the Blanket Module Attachment during Plasma Disruption of ITER," *Fusion Eng. Des.*, **81**, 485 (2006).
- 84) Kikuchi, M., Nishio, S., Kurita, G., et al., "Blanket-Plasma Interaction in Tokamaks: Implication from JT-60U, JFT-2M and Reactor Studies," *Fusion Eng. Des.*, **81**, 1589 (2006).
- 85) Kimura, A., Kasada, R., (Jitsukawa, S.), et al., "Ferritic steel-blanket systems integration R&D - Compatibility Assessment," *Fusion Eng. and Des.*, **81**, 909 (2006).
- 86) Kinjo, T., Nishikawa, M., (Enoeda, M.), et al., "Introduction of Tritium Transfer Step at Surface Layer of Breeder Grain for Modeling of Tritium Release Behavior from Solid Breeder Materials," *Fusion Eng. Des.*, **81**, 573 (2006).
- 87) Kishimoto, H., Ishida, S., Kikuchi, M., et al., "Special Topic: Advanced Tokamak Research on JT-60," *Nucl. Fusion*, **45**, 986 (2005).
- 88) Klix, A., Verzilov, Y., Nishitani, T., et al., "Tritium Breeding Experiments with Blanket Mock-ups Containing ^6Li -Enriched Lithium Titanate and Beryllium Irradiated with DT Neutrons," *Fusion Eng. Des.*, **75-79**, 881 (2005).
- 89) Kobayashi, K., Hayashi, T., Nishi, M., et al., "Sorption and Desorption of Tritiated Water on Four Kind of Materials for ITER," *Fusion Eng. Des.*, **81**, 1379 (2006).

- 90) Kobayashi, K., Terada, O., Miura, H., et al., "The Oxidation Performance Test of Detritiation System under Existence of CO and CO₂," *Fusion Sci. Technol.*, **48**, 476 (2005).
- 91) Kohyama, A., Abe, K., (Jitsukawa, S.), et al., "Recent Accomplishments and Future Prospects of Materials R & D in Japan," *Fusion Sci. and Technol.*, **47**, 836 (2005).
- 92) Koizumi, N., Matsui, K., Kume, K., et al., "Rapid Normal Zone Propagation Observed in a 13T-46kA Nb₃Al Cable-in-Conduit Conductor," *IEEE Trans. ASC*, **15**, 1363 (2005).
- 93) Koizumi, N., Takeuchi, T., Okuno, K., "Development of Advanced Nb₃Al Superconductors for a Fusion DEMO Plant," *Nucl. Fusion*, **45**, 431 (2005).
- 94) Kondo, H., Fujisato, A. (Nakamura, H.), et al., "Surface Wave on High Speed Liquid Lithium Flow for IFMIF," *Fusion Eng. Des.*, **75-79**, 865 (2005).
- 95) Kondo, H., Fujisato, A., (Nakamura, H.), et al., "Experimental Study of Lithium Free-Surface Flow for IFMIF Target Design," *Fusion Eng. Des.*, **81**, 687 (2006).
- 96) Kondo, K., Takagi, S., Murata, I., et al., "New Approach to Measure Double-Differential Charged-Particle Emission Cross Sections of Several Materials for A Fusion Reactor," *Fusion Eng. Des.*, **81**, 1527 (2006).
- 97) Kononov1, S.V., Mikhailovskii1, A.B., Ozeki, T., et al., "Role of Anomalous Transport in Onset and Evolution of Neoclassical Tearing Modes," *Plasma Phys. Control. Fusion*, **47**, B223 (2005).
- 98) Krasilnikov, A., Sasao, M., (Nishitani, T.), et al., "Status of ITER Neutron Diagnostic Development," *Nucl. Fusion*, **45**, 1503 (2005).
- 99) Kubo, H. and the JT-60 Team, "Study of Particle Behavior for Steady-State Operation in JT-60U," *Plasma Sci. Technol.*, **8**, 50 (2005).
- 100) Kubota, N., Ochiai, K., Kutsukake, C., et al., "Beam Analyses of Hydrogen Isotopes for the TFTR Tiles used in the D-T Experiment," *Fusion Eng. Des.*, **81**, 227 (2006).
- 101) Kulsartov, T. V., Hayashi, K., Nakamichi, M., et al., "Investigation of Hydrogen Isotope Permeation through F82H Steel with and without a Ceramic Coating of Cr₂O₃-SiO₂ Including CrPO₄ (Out-of-Pile Tests)," *Fusion Eng. Des.*, **81**, 701 (2005).
- 102) Kurihara, K., Kawamata, Y., Sueoka, M., et al., "The Basic Methods for Understanding of Plasma Equilibrium toward Advanced Control," *Fusion Eng. Des.*, **74**, 527 (2005).
- 103) Kurita, G., Bialek, J., Tuda, T., et al., "Critical β Analyses with Ferromagnetic and Plasma Rotation Effects and Wall Geometry for a High β Steady State Tokamak," *Nucl. Fusion*, **46**, 383 (2006).
- 104) Kusama, Y. and JFT-2M group, "JFT-2M Program," *Fusion Sci. Technol.*, **49**, 89 (2006).
- 105) La Haye, R.J., Prater, R., (Isayama, A.), et al., "Cross-Machine Benchmarking for ITER of Neoclassical Tearing Mode Stabilization by Electron Cyclotron Current Drive," *Nucl. Fusion*, **46**, 451 (2006).
- 106) Li, J. Q., Kishimoto, Y., Dong, J. Q., et al., "Dynamics of Secondary Large-scale Structure in ETG Turbulence Simulations," *Plasma Sci. and Technol.*, **8**, 1 (2006).
- 107) Lorenzetto, P., Boireau, B., (Ioki, K.), et al., "Manufacture of Blanket Shield Modules for ITER," *Fusion Eng. Des.*, **75-79**, 291 (2005).
- 108) Lorenzetto, P., Peacock, A., (Ioki, K.), et al., "EU R&D on the ITER First Wall," *Fusion Eng. Des.*, **81**, 355 (2006).
- 109) Lukash, V., Sugihara, M., Gribov, Y., et al., "Analysis of the Direction of Plasma Vertical Movement during Major Disruptions in ITER," *Plasma Phys. Control. Fusion*, **47**, 2077 (2005).
- 110) Luo, G.-N., Shu, W.M. and Nishi, M.F., "Incident Energy Dependence of Blistering at Tungsten Irradiated by Low Energy High Flux Deuterium Plasma Beams," *J. Nucl. Mater.*, **347**, 111 (2005).
- 111) Luo, G.-N., Shu, W.M. and Nishi, M.F., "Influence of Blistering on Retention in W Irradiated by High Flux Deuterium Plasmas of Tens of eV," *Fusion Eng. Des.*, **81**, 957 (2006).
- 112) Maebara, S., Moriyama, S., Saigusa, M., et al., "Power-Balance Control by Slug Tuner for the 175MHz Radio-Frequency Quadrupole (RFQ) Linac in IFMIF Project," *Fusion Sci. Technol.*, **47**, 941 (2005).

- 113) Maebara, S., Moriyama, S., Saigusa, M., et al., "Development of an RF-Input Coupler with a Multi-Loop Antenna for the RFQ Linac in IFMIF Project," *Fusion Eng. Des.*, **75-79**, 823 (2005).
- 114) Makochekanwa, C., Kato, H., Hoshino, M., et al., "Experimental and Theoretical Clastic Cross Sections for Electron Collisions with the C₃H₆ Isomers," *J. Phys. Chem.*, **124**, 024323 (2006).
- 115) Masaki, K., Sugiyama, K., Hayashi, T., et al., "Retention Characteristics of Hydrogen Isotopes in JT-60U," *J. Nucl. Mater.*, **337-339**, 553 (2005).
- 116) Matsuhiro, K., Nakamura, H., Hayashi, T., et al., "Evaluation of Tritium Permeation from Lithium Loop of IFMIF Target System," *Fusion Sci. Technol.*, **48**, 625 (2005).
- 117) Matsumoto, T., Naitou, H., Tokuda, S., et al., "Nonlinear Acceleration of the Electron Inertia-Dominated MHD Modes due to Electron Parallel Compressibility," *Phys. Plasmas*, **12**, 092505-1-7(2005).
- 118) Matsumoto, T., Naitou, H., Tokuda, S., et al., "Nonlinear Behaviors of Collisionless Double Tearing Mode induced by Electron Inertia," *Nucl. Fusion*, **45**, 1264 (2005).
- 119) Miyato, N., Li, J. Q. and Kishimoto, Y., "Study of a Drift Wave-Zonal Mode System Based on Global Electromagnetic Landau-fluid ITG Simulation in Toroidal Plasmas," *Nucl. Fusion*, **45**, 425 (2005).
- 120) Moeslang, A., Heinzl, V. (Sugimoto, M.), et al., "The IFMIF Test Facilities Design," *Fusion Eng. Des.*, **81**, 863 (2006).
- 121) Mori, M., "Japanese activities in ITER Transitional Arrangements," *Fusion Eng. Des.*, **81**, 69 (2006).
- 122) Morioka, A., Nishimura, S., Muroga, T., et al., "Nuclear Technology and Potential Ripple Effect of Superconducting Magnets for Fusion Power Plant," *Fusion Eng. Des.*, **81**, 1675 (2006).
- 123) Morioka, A., Sakurai, S., Okuno, K., et al., "Development of a Heat-Resistant Neutron Shielding Resin for the National Centralized Tokamak," *J. Plasma Fusion Res.*, **81**, 645 (2005).
- 124) Moriyama, S. and JT-60 Team, "Compact Antenna for Two-Dimensional Beam Scan in the JT-60U Electron Cyclotron Heating /Current Drive System," *Rev. Sci. Instrum.*, **76**, 113504-1 (2005).
- 125) Moriyama, S. and JT-60 Team, "Development and Contribution of RF Heating and Current Drive System to Long Pulse, High Performance Experiments in JT-60U," *Fusion Eng. Des.*, **74**, 343 (2005).
- 126) Moriyama, S. and Shinozaki, S., "Concept and Results of New Operation Scheme with Improved Control System for Radio Frequency Heating in JT-60U," *Jpn. J. Appl. Phys.*, **44**, 6224 (2005).
- 127) Munakata, K., Kawamura, H., Uchida, M., "Reaction of Titanium Beryllide with Water Vapor," *Fusion Eng. Des.*, **75-79**, 997 (2005).
- 128) Murata, I., Yamamoto, Y., (Kondo, K.), et al., "Fusion-Driven Hybrid System with ITER Model," *Fusion Eng. Des.*, **75-79**, 871 (2005).
- 129) Nagao, Y., Tsuchiya, K., Ishida, T., et al., "Development of Tritium Production M for In-Pile Tests of Fusion Blanket in the JMTR," *Fusion Eng. Des.*, **81**, 619 (2006).
- 130) Nagasaki, K., Isayama, A., Hayashi, N., et al., "Stabilization of Neoclassical Tearing Mode by ECCD and Its Evolution Simulation on JT-60U Tokamak," *Nucl. Fusion*, **45**, 1608 (2005).
- 131) Nagashima, Y., Hoshino, K., Ejiri, A., et al., "Observation of Nonlinear Coupling between Small-Poloidal Wave-Number Potential Fluctuations and Turbulent Potential Fluctuations in Ohmically Heated Plasmas in the JFT-2M Tokamak," *Phys. Rev. Lett.*, **95**, 095002-1(2005).
- 132) Nagashima, Y., Itoh, K., Itoh, S-I., et al., "Bispectral Analysis Applied to Coherent Floating Potential Fluctuations Obtained in the Edge Plasmas on JFT-2M," *Plasma Phys. Control. Fusion*, **48**, S1 (2006).
- 133) Nagata, M., Ogawa, H., Yatsu, S., et al., "Experimental Studies of the Dynamics of Compact Toroid Injected into the JFT-2M Tokamak," *Nucl. Fusion*, **45**, 1056 (2005).
- 134) Nakamura, H., Hayashi, T., Kobayashi K., et al., "Evaluation of Tritium Behavior in the Epoxy Painted Concrete wall of ITER Hot Cell," *Fusion Sci. Technol.*, **48**, 452 (2005).
- 135) Nakamura, H., Sakurai, S., Suzuki, S., et al., "Case Study on Tritium Inventory in the Fusion DEMO Plant at JAERI," *Fusion Eng. Des.*, **81**, 1339 (2006).

- 136) Nakamura, H., Takemura, M., Yamauchi, M., et al., "Accessibility Evaluation of the IFMIF Liquid Lithium Loop Considering Activated Erosion/Corrosion Materials Deposition," *Fusion Eng. Des.*, **75-79**, 1169 (2005).
- 137) Nakano, T., Koide, Y., Honda, A., et al., "Relation Between the Oxygen Contents in the Neutral Beam and in the Core Plasma in JT-60U," *J. Plasma Fusion Res.*, **81**, 708 (2005).
- 138) Nishi, H., "Notch Toughness Evaluation of Diffusion-Bonded Joint of Alumina Dispersion- strengthened Copper to Stainless Steel," *Fusion Eng. Des.*, **81**, 269 (2006).
- 139) Ninomiya, H., "Conference Summary: Progress in Experiments on Confinement, Plasma-Material Interactions and Innovative Confinement Concepts," *Nucl. Fusion*, **45**, 513 (2005).
- 140) Nishi, M., Yamanishi, T., Hayashi, T., et al., "Study on Tritium Accountanct in Fusion DEMO Plant at JAERI," *Fusion Eng. Des.*, **81**, 745 (2006).
- 141) Nishimura, A., Hishinuma, Y., (Okuno, K.), et al., "14 MeV Neutron Irradiation Effect on Superconducting Magnet Materials for Fusion Device," *Adv. Cryog. Eng. (Material)*, **52**, 208 (2006).
- 142) Nishimura, A., Hishinuma, Y., Tanaka, T., et al., "Design, Fabrication and Installation of Cryogenic Target System for 14 MeV Neutron Irradiation on Superconducting Magnet Materials," *Fusion Eng. Des.*, **75-79**, 173 (2005).
- 143) Nishimura, A., Muroga, T., (Nishitani, T.), et al., "Nuclear Technology of Superconducting Magnet for Fusion Power Plant and Potential Ripple Effect," *Fusion Eng. Des.*, **81**, 1675 (2006).
- 144) Nishio, S., Ohmori, J., Kuroda, T., et al., "Consideration on Blanket Structure for Fusion DEMO Plant at JAERI," *Fusion Eng. Des.*, **81**, 1271 (2006).
- 145) Nishitani, T., Sugie, T., Morishita, N., et al., "Temperature Dependence of the Transmission Loss in KU-1 and KS-4V Quartz Glasses for the ITER Diagnostic Window," *Fusion Eng. Des.*, **74**, 871 (2005).
- 146) Nishitani, T., Yamauchi, M., Nishio, S., et al., "Neutronics Design of the Low Aspect Ratio Tokamak Reactor, VECTOR," *Fusion Eng. Des.*, **81**, 1245 (2006).
- 147) Nomoto, Y., Suzuki, S., Ezato, K., et al., "Structural Design of Japanese Solid Breeder Test Blanket Modules for ITER," *Fusion Eng. Des.*, **81**, 719 (2006).
- 148) O'hira, S., Luo, G. -N., Nakamura, H., et al., "New Conceptual Design of a Test Module Assembly for Tritium Permeation Experiment," *Fusion Sci. Technol.*, **48**, 621 (2005).
- 149) O'hira, S., Yamanishi, S., Hayashi, T., "Operation Scenarios and Design Requirements for Fuel Processing in Future Fusion Reactor Facilities," *J. Nucl. Sci. Technol.*, **43**, 354 (2005).
- 150) Ochiai, K., Nakao, M., Hori, J., et al., "Measurements of Deuteron-Induced Activation Cross Sections for IFMIF Accelerator Structural Materials in the Energy Range of 22-40 MeV," *Fusion Eng. Des.*, **81**, 1459 (2006).
- 151) Ochiai, K., Velzilov, Y., Nishitani, T., et al., "International Benchmark Activity of Tritium Production Measurement for Blanket Neutronics," *Fusion Sci. Technol.*, **48**, 378 (2005).
- 152) Ochiai, K., Kondo, K., Murata, I., et al., "Measurement of Energetic Charged Particles Produced in Fusion Materials with 14 MeV Neutron Irradiation," *Fusion Eng. Des.*, **75-79**, 859 (2005).
- 153) Ogawa, H., Ogawa, T., Tsuzuki, K., "CT Injection Experiments in JFT-2M," *Fusion Sci. Technol.*, **49**, 209 (2006).
- 154) Ogiwara, H., Kohyama, A., Tanigawa, H., et al., "Irradiation-induced hardening mechanism of ion irradiated JLF-1 to High Fluences", *Fusion Eng. and Des.*, **81**, 1091(2006)
- 155) Ohwaki, H., Sugihara, M., Hatayama, A., "Modeling of Plasma Current Decay during Disruptions Caused by Massive Impurity Injection," *Plasma Fusion Res.*, **1**, 16 (2006).
- 156) Oikawa, T., Isayama, A., Fujita, T., et al., "Evolution of the Current-density Profile Associated with Magnetic-Island Formation in JT-60U," *Phys. Rev. Lett.*, **94**, 125003-1 (2005).
- 157) Oikawa, T., Suzuki, T., Isayama, A., et al., "Observation of the Bootstrap Current Reduction at Magnetic Island in a Neoclassical Tearing Mode Plasma," *Nucl. Fusion*, **45**, 1101 (2005).

- 158) Okano, K., Suzuki, T., Umeda, N., et al., "Experimental Validation of Beam Particle Self Interaction in JT-60U by Use of N-NB," J. Plasma Fusion Res., **81**, 579 (2005).
- 159) Okubo, N., Wakai, E., Matsukawa, S., et al., "Heat Treatment effects on microstructures and DBTT of F82H steel doped with boron and nitrogen," Mater. Trans., **46**, 193(2005)
- 160) Okubo, N., Wakai, E., Matsukawa, S., et al., "Tempering treatment effect on mechanical properties of F82H steel doped with boron and nitrogen," Mater. Trans., **46**, 1779 (2005)
- 161) Olivares, R. U., Oda, T., (Tsuchiya, K.), et al., "Behavior of Li_2TiO_3 under Varied Surface Condition," Fusion Eng. Des., **75-79**, 765 (2005).
- 162) Onozuka, M., Shimizu, K., (Shibanuma, K.), et al., "Investigation of the Dynamic Behavior of the ITER Tokamak Assembly using a 1/5.8-scale Model," Fusion Eng. and Des., **81**, 155(2006).
- 163) Oyama, N., Sakamoto, Y., Isayama A., et al., "Energy Loss for Grassy ELMs and Effects of Plasma Rotation on the ELM Characteristics in JT-60U," Nucl. Fusion, **45**, 871 (2005).
- 164) Polevoi, A. R., Shimada, M., Sugihara, M., et al., "Requirements for Pellet Injection in ITER Scenarios with Enhanced Particle Confinement," Nucl. Fusion, **45**, 1451 (2005).
- 165) Sakamoto, K., Kasugai, A., Minami, R., et al., "Development of Long Pulse and High Power 170GHz Gyrotron," J. Phys. Conf. Series. **25**, 8 (2005).
- 166) Sakamoto, K., Takahashi, K., Kasugai, A., et al., "Conceptual Study of ECH/ECCD System for Fusion DEMO Plant," Fusion Eng. and Des., **81**, 1263(2006).
- 167) Sakamoto, Y., and the JT-60 Team, "Enhanced performance and control issues in JT-60U long pulse discharges," Plasma Phys. Control. Fusion, **47**, B337 (2005).
- 168) Sakamoto, Y., Fujita, T., Ide, S., et al., "Stationary High Confinement Plasmas with Large Bootstrap Current Fraction in JT-60U," Nucl. Fusion, **45**, 574 (2005).
- 169) Sakasegawa, H., Ohtsuka, (Tanigawa, H.), et al., "Microstructural evolution during creep of 9Cr-ODS steels," Fusion Eng. and Des., **81**, 1013(2006).
- 170) Sato, K., Ezato, K., Taniguchi, M., et al., "Proposal of Hot-pressed, Rod-shaped Tungsten Armor Concept for ITER Divertor and its High-Heat-flux Performance," J. Nucl. Sci. Technol., **42-7**, 643 (2005).
- 171) Sato, K., Yoshiie, T., (Kutsukake, C.), et al., "Point Defect Formation in V-4Cr-4Ti and F82H Irradiated with Fission and Fusion Neutrons," Mater. Trans., **46**, 445 (2005).
- 172) Sato, M., Sakurai, S., Nishio, S., et al., "Concept of Core and Divertor Plasma for Fusion DEMO Plant at JAERI," Fusion Eng. Des., **81**, 1277 (2006).
- 173) Sato, S., Iida, H., Yamauchi, M., et al., "Shielding Design of the ITER NBI Duct for Nuclear and Bremsstrahlung Radiation," Radiat. Prot. Dosimetry, **116**, 28 (2005).
- 174) Sato, S., Nakao, M., Verzilov, Y., et al., "Experimental Studies on Tungsten-Armor Impact on Nuclear Responses of Solid Breeding Blanket," Nucl. Fusion, **45**, 656 (2005).
- 175) Sato, S., Verzilov, Y., Nakao, M., et al., "Neutronics Experiments using Small Partial Mockup of the ITER Test Blanket Module with Solid Breeder," Fusion Sci. Technol., **47**, 1046 (2005).
- 176) Sato, S., Verzilov, Y., Ochiai, K., et al., "Progress in the Blanket Neutronics Experiments at JAERI/FNS," Fusion Eng. Des., **81**, 1183 (2006).
- 177) Seki, M., Moriyama, S., Shinozaki, S., et al., "Performance of the LH Antenna with Carbon Grill in JT-60U," Fusion Eng. Des., **74**, 273 (2005).
- 178) Shiba, K., Hirose, T., "Deformation Behavior of Reduced Activation Martensitic Steel during Tensile Test," Fusion Eng. Des., **81**, 1051 (2006).
- 179) Shikama, T., Toh, K., (Yamauchi, M.), et al., "Radiation Sensitive Scintillator/Optical Fibre System for Radiation Dosimetry in Burning Plasma Machine," Nucl. Fusion, **46**, 46 (2006).
- 180) Shimizu, T., Miyazaki, I., (Nishitani, T.), et al., "Measurements of (n,n') Reaction Cross-Sections of ^{79}Br , ^{90}Zr , ^{197}Au and ^{207}Pb with Pulsed d-D Neutrons," Annals of Nucl. Energy, **32**, 949 (2005).

- 181) Shimomura, Y., et al., "Preparation of ITER Construction and Operation," *Fusion Eng. Des.*, **81**, 3 (2006).
- 182) Shinohara, K., Sato, M., Kawashima, H., et al., "Ripple Reduction with Ferritic Insert in JFT-2M," *Fusion Sci. Technol.*, **49**, 187 (2006).
- 183) Shinohara, K., Suzuki, Y., Sakurai, S., et al., "Orbit Following Calculation of Energetic Ions in the Design of Ferritic Insertion in the JT-60U," *Plasma Fusion Res.*, **1**, 007 (2006).
- 184) Shinohara, K., Takechi, M., Ishikawa, M., et al., "Instability in the Frequency Range of Alfvén Eigenmode Induced by Negative-Ion-Based Neutral Beam in JT-60U," *J. Plasma Fusion Res.*, **81**, 547 (2005).
- 185) Shu, W.M., Matsuyama, M., Suzuki, T., et al., "Monitoring of Tritium in Diluted Gases by Detecting Bremsstrahlung X-rays," *Fusion Eng. Des.*, **81**, 803 (2006).
- 186) Shu, W.M., Ohira, S., Suzuki, T., et al., "Radiochemical Reactions between Tritium Molecule and Carbon Dioxide," *Fusion Sci. Technol.*, **48**, 684 (2005).
- 187) Stober, J., Lomas, P. J., Saibene, G., et al., "Small ELM Regimes with Good Confinement on JET and Comparison to Those on ASDEX Upgrade, Alcator C-mod and JT-60U," *Nucl. Fusion*, **45**, 1213 (2005).
- 188) Suzuki, S., Enoda, M., Hatano, T., et al., "Key Achievements in Elementary R&D on Water-Cooled Solid Breeder Blanket for ITER Test Blanket Module in JAERI," *Nucl. Fusion*, **46**, 285 (2005).
- 189) Suzuki, S., Ezato, K., Hirose, T., et al., "First Wall and Divertor Engineering Research for Power Plant in JAERI," *Fusion Eng. Des.*, **81**, 93 (2006).
- 190) Takahashi, K., Illy, S., Heidinger, R., et al., "Development of Reliable Diamond Window for EC Launcher on Fusion Reactors," *Fusion Eng. Des.*, **74**, 305 (2005).
- 191) Takahashi, K., Kobayashi, N., Kasugai, A., et al., "Design and Development of EC H&CD Antenna Mirrors for ITER," *Fusion Eng. Des.*, **81**, 281 (2006).
- 192) Takahashi, K., Kobayashi, N., Kasugai, A., et al., "Development of EC Launcher Components for ITER," *J. Phys. Conf. Series*, **25**, 75 (2005).
- 193) Takahashi, H., Kudo, Y., Tsuchiya, K., et al., "Fracture Mechanics Analysis Including the Butt Joint Geometry for the Superconducting Conductor Conduit of the National Centralized Tokamak," *Fusion Eng. Des.*, **81**, 1005 (2006).
- 194) Takahashi, Y., Yoshida, K., Mitchell, N., "Quench Detection Using Pick-up Coils for the ITER Central Solenoid," *IEEE Trans. Appl. Supercond.*, **15**, 1395 (2005).
- 195) Takechi, M., Fujita, T., Ishii, Y., et al., "MHD Instabilities Leading to Disruptions in Low Beta JT-60U Reversed Shear Plasmas," *Nucl. Fusion*, **45**, 1694 (2005).
- 196) Takechi, M., Fukuyama, A., Ishikawa, M., "Alfvén Eigenmodes in Reversed Shear Plasmas in JT-60U Negative-Ion-Based Neutral Beam Injection Discharges," *Phys. Plasmas*, **12**, 082509 (2005).
- 197) Takenaga, H., Asakura, N., Higashijima, S., et al., "Study of Plasma Wall Interactions in the Long-Pulse NB-Heated Discharges of JT-60U towards Steady-State Operation," *J. Nucl. Mater.*, **337**, 802 (2005).
- 198) Takenaga, H., Asakura, N., Kubo, H., et al., "Compatibility of Advanced Tokamak Plasma with High Density and High Radiation Loss Operation in JT-60U," *Nucl. Fusion*, **45**, 1618 (2005).
- 199) Takenaga, H., Nakano, T., Asakura, N., et al., "Study of Global Wall Saturation Mechanisms in Long-Pulse ELMy H-Mode Discharges on JT-60U," *Nucl. Fusion*, **46**, S39 (2006).
- 200) Tamai, H., Akiba, M., Azechi, H., et al., "Design Study of National Centralized Tokamak Facility for the Demonstration of Steady State High- β Plasma Operation," *Nucl. Fusion*, **45**, 1676 (2005).
- 201) Tani, K., Tobita, K., Tsuji-Iio, S., et al., "Confinement of Alpha Particles in a Low Aspect Ratio Tokamak Reactor," *IEEE Trans., FM*, **125**, 938 (2005).
- 202) Tanifuji, T., Yamaki, D., Jitsukawa, S., "Tritium Release from Neutron-irradiated Li₂O: Transport in Porous Sintered Pellets," *Fusion Eng. Des.*, **81**, 595 (2005).
- 203) Tanigawa, H., Sakasegawa, H., Klueh, R.L., "Irradiation Effects on Precipitation in Reduced-Activation Ferritic/Martensitic Steels," *Materials Transactions*, **46**, 469 (2005).

- 204) Tobita, K., Nishio, S., Enoda, M., et al., "Design Study of Fusion DEMO Plant at JAERI," *Fusion Eng. Des.*, **81**, 1151 (2006).
- 205) Tsuchiya, B., Nagata, S., (Yamauchi, M.), et al., "Radiation Damage of Proton Conductive Ceramics under 14 MeV Fast Neutron Irradiation," *Fusion Sci. Technol.*, **47**, 891 (2005).
- 206) Tsuchiya, K., Akiba, M., Azechi, H., et al., "Engineering Design and Control Scenario for Steady-State High-Beta Operation in National Centralized Tokamak," *Fusion Eng. Des.*, **81**, 1599 (2006).
- 207) Tsuchiya, K., Kawamura, H., Casadio, S., et al., "Effect of Gelation and Sintering Conditions on Granulation of Li_2TiO_3 Pebbles from Li-Ti Complex Solution," *Fusion Eng. Des.*, **75-79**, 877 (2005).
- 208) Tsuchiya, K., Kawamura, H., Tanaka, S., "Evaluation of Contact Strength of Li_2TiO_3 Pebbles with Different Diameters," *Fusion Eng. Des.*, **81**, 1065 (2005).
- 209) Tsuchiya, K., Uchida, M., Kawamura, H., "General Properties on Compatibility between Be-Ti Alloy and SS 316LN," *Fusion Eng. Des.*, **81**, 1057 (2005).
- 210) Tsuzuki, K., Hirai, T., Kusama, Y., et al., "Exposure of Reduced Activation Ferritic Steel F82H to TEXTOR Plasma," *Fusion Eng. Des.*, **81**, 925 (2005).
- 211) Umeda, N., Yamamoto, T., Hanada, M., "Recent Progress of Negative Ion Based Neutral Beam Injector for JT-60U," *Fusion Eng. Des.*, **74**, 385(2005).
- 212) Umeda, N., Ikeda, Y., Hanada, M., "Beam Deflection by PG Filter in the Negative Ion Source for JT-60U NBI System," *Rev. Sci. Instrum.* **77**, 03A529 (2006).
- 213) Urano, H., Kamada, Y., Takizuka, T., et al., "Pedestal Characteristics of H-Mode Plasmas in JT-60U and ASDEX Upgrade," *J. Plasma Fusion Res.*, **81**, 280 (2005).
- 214) Urano, H., Kamiya, K., Koide, Y., et al., "Roles of Plasma Rotation and Toroidal Field Ripple on H-mode Pedestal Structure in JT-60U," *Plasma Phys. Control. Fusion*, **48**, A193 (2006).
- 215) Urano, H., Takizuka, T., Kamada, Y., et al., "Reduced Heat Transport between Edge-Localized-Mode Bursts at Low Collisionality and Small Poloidal Larmor Radius," *Phys. Rev. Lett.*, **95**, 035003-1 (2005).
- 216) Usigome, M., Ide, S., Itoh, S., et al., "Development of Completely Solenoidless Tokamak Operation in JT-60U," *Nucl. Fusion*, **46**, 207 (2006).
- 217) Utin, Y., Chuyanov, V., (Ioki, K.), et al., "Design Progress of the ITER Vacuum Vessel and Ports," *Fusion Eng. Des.*, **75-79**, 571 (2005).
- 218) Verzilov, Y., Nishitani, T., Ochiai, K., et al., "Development of a New Fusion Power Monitor based on Activation of Flowing Water," *Fusion Eng. Des.*, **81**, 1477 (2006).
- 219) Verzilov, Y., Ochiai, K., Nishitani, T., "Methods for the Tritium Production Rate Measurement in Design-Oriented Blanket Experiments," *Fusion Sci. Technol.*, **48**, 650 (2005).
- 220) Wakai, E., Ando, M., Matsukawa, S., et al., "Effect of Initial Heat Treatment on DBTT of F82H Steel Irradiated by Neutrons," *Fusion Sci. and Technol.*, **47**, 856 (2005).
- 221) Wakai, E., Jitsukawa, S., Tomita, et al., "Radiation Hardening and -Embrittlement due to He Production in F82H Steel Irradiated at 250 °C in JMTR," *J. Nucl. Mater.*, **343**, 285 (2005).
- 222) Wakai, E., Ohtsuka, H., Matsukawa, et al., "Mechanical Properties of Small Size Specimens of F82H Steel," *Fusion Eng. and Des.*, **81**, 1077 (2006).
- 223) Wakai, E., Sato, M., Okubo, N., et al., "Effect of Heat Treatments on Mechanical Properties and Microstructures of $^8\text{Cr-}^2\text{W}$ (F82H) Steel Doped with Boron or Boron and Nitrogen," *J. Jpn. Inst. of Met.*, **69**, 460 (2005).
- 224) Wakai, E., Taguchi, T., Yamamoto, S., et al., "Effects of Helium Production and Heat Treatment on Neutron Irradiation Hardening of F82H Steels Irradiated with Neutrons," *Mater. Trans.*, **46**, 481 (2005).
- 225) Wakisaka, M., Kaneko, J., (Ochiai, K.), et al., "Analysis of Neutron Propagation from the Skyshine Port of a Fusion Neutron Source Facility," *Nucl. Instrum. Methods*, **A 554**, 347 (2005).
- 226) Walker, C.I, Barnsley, R., (Itami, K.), et al., "ITER Diagnostics: Maintenance and Commissioning in the Hot Cell Test Bed," *Fusion Eng. Des.*, **74**, 685 (2005).

- 227) Yamada, H., Kawamura, H., Tsuchiya, K., et al., "The Effect of Neutron Irradiation on Mechanical Properties of YAG Laser Weldments Using Previously Irradiated Material," J. Nucl. Mater., **340**, 57 (2005).
- 228) Yamada, H., Sato, S., Mohri, K., et al., "Neutron Irradiation Effect on Mechanical Properties of SS/SS Hip Joint Materials for ITER Shielding Blankets," Fusion Eng. Des., **81**, 631 (2005).
- 229) Yamaki, D., Jitsukawa, S., "Model Calculation of Tritium Release Behavior from Lithium Titanate," Fusion Eng. Des., **81**, 589 (2005).
- 230) Yamanishi, T., Hayashi, T., Kawamura, Y., et al., "Interlinked Test Results for Fusion Fuel Processing and Blanket Tritium Recovery Systems Using Cryogenic Molecular Sieve Bed," Fusion Sci. Technol., **48**, 63 (2005).
- 231) Yamanishi, T., Iwai, Y., Kawamura, Y., et al., "A Design Study for Tritium Recovery System from Cooling Water of a Fusion Power Plant," Fusion Eng. Des., **81**, 797 (2006).
- 232) Yamauchi, M., Hori, J., Ochiai, K., et al., "Analysis of Sequential Charged Particle Reaction Experiments for Fusion Reactors," Fusion Eng. Des., **81**, 1577 (2006).
- 233) Yamauchi, M., Nishitani, T., Nishio, S., "Neutron Shielding and Blanket Neutronics Study on Low Aspect Ratio Tokamak Reactor," IEEE Trans. FM., **125**, 943 (2005).
- 234) Yamauchi, M., Ochiai, K., Morimoto, Y., et al., "Experiment and Analyses for 14 MeV Neutron Streaming through Dogleg Duct," Radiat. Prot. Dosimetry, **116**, 542 (2005).
- 235) Yamauchi, M., Takemura, M., Nakamura, H., et al., "Activity Estimation for the IFMIF Liquid Lithium Loop due to the Erosion and Corrosion of Target Back-wall," Fusion Sci. Technol., **47**, 1008 (2005).
- 236) Yoshida, H., Yokoyama, K., Taniguchi, M., et al., "High Flux Ion Beam Acceleration at the 100-eV Level for Fusion Plasma Facing Material Studies," Fusion Eng. Des., **81**, 361 (2006).
- 237) Yoshida, K., Takahashi, Y., Isono, T., et al., "Updating the Design of the Feeder Components for the ITER Magnet System," Fusion Eng. Des., **75-79**, 241 (2005).
- 238) Yoshida, H., Yamauchi, Y., (Arai, T.), et al., "Hydrogen Retention in Divertor Tiles in JT-60 for Hydrogen Discharge Period," J. Nucl. Mater., **337-339**, 604 (2005).
- 239) Yoshikawa, A., Shibahara T., (Arai, T.), et al., "Depth Profile Of Hydrogen And Its Retention In Divertor Target Tile of JT-60 Exposed to Hydrogen Discharges," Fusion Eng. Des., **81**, 289 (2006).
- 240) Yoshino, R., "Neural-Net Predictor for Beta Limit Disruption in JT-60U," Nucl. Fusion, **45**, 1232 (2005).
- 241) Zanino, R., Egorov, S., (Takahashi, Y.), et al., "Preparation of the ITER Poloidal Field Conductor Insert (PFCI) Test," IEEE Trans. Appl. Supercond., **15**, 1346 (2005).

A.1.3 List of papers published in conference proceedings

- 1) Abe, K., Nakajima, H., Hamada, K., et al., "Manufacturing Study and Trial Fabrication of Radial Plate for ITER Toroidal Field Coil," Proc. 19th Inter. Conf. on Magnet Technology (2005), to be published in IEEE Trans. ASC..
- 2) Aiba, N., Tokuda, S., Ishizawa, T., "Analysis of an Aspect Ratio Effect on the Stability of External MHD Modes in Tokamaks with Newcomb Equation," 19th Inter. Conf. on Numerical Simulation of Plasmas and 7th Asia Pacific Plasma Theory Conf. (2005).
- 3) Aiba, N., Tokuda, S., Ishizawa, T., et. al., "Ideal MHD Stability Code MARG2D for the Analysis of External MHD Modes in JT-60U Plasma," Proc. 47th Annual Meeting of DPP-APS (2005).
- 4) Asakura, N., Takechi, M., Matshunaga, G., et al., "ELM Propagation and Fluctuations in SOL and Divertor on JT-60U Tokamak," Proc. 32nd EPS Conf. on Plasma Phys., P5-006(CD-ROM) (2005).
- 5) Barabash, V., the ITER International Team, (Akiba, M.), et al., "Materials Challenges for ITER -Current Status and Future Activities," 12th Int. Conf. on Fusion Reactor Materials (2005), to be published in J. Nucl. Mater..
- 6) Baylor, L.R., Combs, S.K., Maruyama, S., et al., "Pellet Fueling of ITER Burning Plasmas," Proc. 21st Symp. on Fusion Eng. (2005) (CD-ROM).
- 7) Combs, S. K., Baylor, L. R., Maruyama, S., et al., "Experimental Study of Pellet Delivery to the ITER Inner Wall through a Curved Guide Tube at Steady-State Pressure," Proc. 21st Symp. on Fusion Eng. (2005) (CD-ROM).
- 8) Ebisawa, N., Akino, N., Grisham, L., et al "Recent Activities of Negative Ion Based NBI System on JT-60U," Proc. 21st Symp. on Fusion Eng. (2005) (CD-ROM).
- 9) Fukumoto, N. and JFT-2M group, "Compact Toroid Injection System for JFT-2M," Proc. 15th Int. Toki Conf., PS2-15 (2005).
- 10) Giancarli, L., Chuyanov, V., (Akiba, M.), et al., "Test Blanket Modules in ITER; An Overview on Proposed Designs and Required DEMO-Relevant Materials," 12th Int. Conf. on Fusion Reactor Materials (2005), to be published in J. Nucl. Mater..
- 11) Hamada, K., Nakajima, H., Takano, K., et al., "Demonstration of JK2LB Jacket Fabrication for ITER Central Solenoid," Proc. 19th Inter. Conf. on Magnet Technology (2005), to be published in IEEE Trans. ASC..
- 12) Hamamatsu, K., Takizuka, T., Hayashi, N., et. al., "Monte-Carlo Simulation of Electron Cyclotron Current Drive in NTM Magnetic Islands," Proc. 32nd EPS Conf. on Plasma Phys., P5-098(CD-ROM) (2005).
- 13) Hatae, T., Kondoh, T., Naito, O., et al., "Recent R&D of Thomson Scattering Diagnostics for JT-60U and ITER," Proc. 12th Int. Symp. on Laser-Aided Plasma Diagnostics (CD-ROM), 309 (2006).
- 14) Hatae, T., Nakatsuka, M., Yoshida, H., et al., "Application of Phase Conjugate Mirrors to Thomson Scattering Diagnostics in JT-60U and ITER," Proc. 5th Conf. of Asia Plasma & Fusion Association (2005), to be published in J. Korean Phys. Soc..
- 15) Hayashi, N., Takizuka, T., Sakamoto, Y., et. al., "Structural Mechanism of Strong Internal Transport Barrier in JT-60U Reversed-Shear Plasma," 10th IAEA Technical Meeting on H-mode Physics and Transport Barriers (2005).
- 16) Hayashi, T., Tobita, K., Nishio, S., et al., "Possibility of Tritium Self-Sufficiency in Low Aspect Ratio Tokamak Reactor with the Outboard Blanket Only," 15th Int. Toki Conf., (2005), to be published in Fusion Eng. Des..
- 17) Hirohashi, M., Ishiyama, A., (Koizumi, N.), et al., "Numerical Simulation of the Critical Current and n-Value in Nb₃Sn Strand Subjected to Bending Strain," Proc. 19th Inter. Conf. on Magnet Technology (2005), to be published in IEEE Trans. ASC..
- 18) Hirohata, Y., Oya, Y., Yoshida, H., et al., "Depth Profile and Retention of Hydrogen Isotopes in Graphite Tiles Used in the W-Shaped Divertor of JT-60U," Proc. 12th Int. Conf. on Fusion Reactor Materials (2005), to be published in J. Nucl. Mater..
- 19) Hirohata, Y., Tanabe, T., (Arai, T.), et al., "Deuterium and Hydrogen Retention Properties of the JT-60 and JT-60U Divertor Tiles," Satellite meeting of the 7th Int. Symp. of Fusion Nuclear Technology (2005), to be published in Fusion Eng. Des..

- 20) Hirose, T., Shiba, K., Enoeda, M., et al., "Stress Corrosion Cracking Susceptibility of Ferritic/Martensitic Steel in Super Critical Pressurized Water," 12th Int. Conf. on Fusion Reactor Materials (2005), to be published in J. Nucl. Mater..
- 21) Ida, M., Nakamura, H. and Sugimoto, M., "Analytical Estimation of Accessibility to Activated Lithium Loop in IFMIF," 12th Int. Conf. on Fusion Reactor Materials (2005), to be published in J. Nucl. Mater..
- 22) Idomura, Y., "Gyrokinetic Simulations of ETG Turbulence and Zonal Flows in Positive/Reversed Shear Tokamaks," Proc. Festival de Theorie 2005 (2005).
- 23) Ikeda Y., the NBI group, the NCT Design Team, "Progress of Neutral Beam Injection System on JT-60U for Long Pulse Operation," Proc. 5th General Scientific Assembly of Asia Plasma and Fusion Association (2005), to be published in J. Korea Phy. Soc..
- 24) Ikeda, Y., Umeda, N., Akino, N., et al., "Present Status of Negative Ion Based NBI System for Long Pulse Operation on JT-60U," Proc. 4th IAEA Technical meeting on Negative Ion Based Neutral Beam Injectors (2005), to be published in Nucl. Fusion.
- 25) Isayama, A., Oyama, N., Urano, H., et al., "Measurement of Toroidal Structure of Electron Temperature with Electron Cyclotron Emission Diagnostic in JT-60U," Proc. 21st Symp. on Fusion Eng. (2005) (CD-ROM).
- 26) Ishii, Y., Azumi, M. and Smolyakov, A., "Magnetic Island Evolution in Rotating Plasmas," Proc. Joint Conf. of 19th Inter. Conf. on Numerical Simulation of Plasma and 7th Asia Pacific Plasma Theory Conf., 300 (2005).
- 27) Ishii, Y., Azumi, M., Smolyakov, A., "Rapid Evolution of the Magnetic Island in the Rotating Plasma," Proc. 47th Annual Meeting of DPP-APS, 237 (2005).
- 28) Ishimoto, Y., Gotoh, Y., Arai, T., et al., "Transport of Carbon Impurity Using $^{13}\text{CH}_4$ Gas Puffing in JT-60U," Proc. 12th Int. Conf. on Fusion Reactor Materials (2005), to be published in J. Nucl. Mater..
- 29) Isobe, K., Nakamura, H., Kaminaga, A., et al., "Characterization of JT-60U Exhaust Gas during Experimental Operatin," Proc. 7th Int. Symp. on Fusion Nuclear Technology (2005), to be published in Fusion Eng. Des..
- 30) Itami, K., Sugie, T., Vayakis, G., et al., "Study of an Erosion Monitor for the ITER Diverter Target Plates," Proc. 32nd EPS Conf. on Plasma Phys., P4-091(CD-ROM) (2005).
- 31) Kagei, Y., Kishimoto, Y., Miyoshi, T., "A Finite Volume Approach to the Fully Compressible MHD Simulation of High Beta Tokamak Plasmas," Proc. 47th Annual Meeting of DPP-APS, 240 (2005).
- 32) Kasugai, A., Minami R., Takahashi K., et al., "Development of a 170GHz High-Power and CW Gyrotron for Fusion Application," Digest of Int. Conf. of Infrared and Millimeter Waves, TB4-1 (2005).
- 33) Kawamura, H., Mishima, Y., Yoshida, N., et al., "Status of Beryllium R&D in Japan," Proc. 7th Int. Workshop on Beryllium Technology (2005), to be published in Nucl. Technol..
- 34) Kawano, Y., Nakano, T., Isayama, A., et al., "Characteristics of Runaway Plasmas in JT-60U," Proc. 32nd EPS Conf. on Plasma Phys., P2-068(CD-ROM) (2005).
- 35) Kikuchi, M., Suzuki, T., Sakamoto, Y., et al., "Measurement of Local Electrical Conductivity and Thermodynamical Coefficients in JT-60U," Proc. 32nd EPS Conf. on Plasma Phys., P1-043(CD-ROM) (2005).
- 36) Kimura, A., Kasada, R., (Tanigawa, H.), et al., "Recent Progress in US-Japan Collaborative Research on Ferritic Steels R&D," 12th Int. Conf. on Fusion Reactor Materials (2005), to be published in J. Nucl. Mater..
- 37) Kinjyo, T., Nihikawa, M., Enoeda, M., "Estimation of Tritium Release Behavior from Solid Breeder Materials under the Condition of ITER Test Blanket Module," 12th Int. Conf. on Fusion Reactor Materials (2005), to be published in J. Nucl. Mater..
- 38) Kobayashi, Y., Isobe, K., Kaminaga, A., et al., "Analysis of Exhaust Gas In JT-60U Tokamak Operation," Proc. 21th Symp. on Fusion Eng. (2005) (CD-ROM).
- 39) Koizumi, N., Nunoya, Y., Okuno, K., "A New Model to Simulate Critical Current Degradation of a Large CICC by Taking into Account Strand Bending," Proc. 19th Inter. Conf. on Magnet Technology (2005), to be published in IEEE Trans. ASC..
- 40) Kondoh, T., Hayashi, T., Kawano, Y., et al., "CO₂ laser Collective Thomson Scattering for Alpha-Particle Diagnostics," Proc. 9th IAEA Technical Meeting on Energetic Particles in Magnetic Confinement Systems, NIFS-PROC-63, 189 (2006).

- 41) Konoshima, S. and the JT-60 team, "Radiated Power Profile Observed by a Tangentially Viewing IR Imaging Bolometer in JT-60U Tokamak," Proc. 32nd EPS Conf. on Plasma Phys. P4-092(CD-ROM) (2005).
- 42) Kononov, S.V., Mikhailovskii, A.B., Ozeki, T., et al., "Role of Anomalous Transport in Onset and Evolution of Neoclassical Tearing Modes," Proc. 32nd EPS Conf. on Plasma Phys. I4-004(CD-ROM)(2005).
- 43) Kudo, Y., Sawai, T., Sakurai, S., et al., "Fabrication of $^8\text{Cr}-^2\text{W}$ Ferritic Steel Tile for Reduction in Toroidal Magnetic Field Ripple on JT-60U," Proc. 5th Asia Plasma & Fusion Association (2005), to be published in Supplementary Issue of J. of Korean Physical Society.
- 44) Kurihara, K. and the JT-60 team, "Current Status of Experimental Study and Device Modifications in JT-60U," Proc. of the 21st Symp. on Fusion Eng. (2005) (CD-ROM)
- 45) Maebara, S., Moriyama, S., Sugimoto, M., et al., "A 175MHz RFQ design for IFMIF project," Proc. the 2005 Particle Accelerator Conference (2005), TPPT004 (CD-ROM).
- 46) Matsumoto, T., Kishimoto, Y., Li, J. Q., "Statistical Characteristics of Turbulent Plasmas Dominated by Zonal Flows," Proc. Joint Conf. of 19th Inter. Conf. on Numerical Simulation of Plasma and 7th Asia Pacific Plasma Theory Conf., 258 (2005).
- 47) McDonald, D.C., ITPA H-mode Threshold Database WG, (Takizuka, T.), et al., "The Impact of Statistical Models on Scalings Derived from Multi-Machine H-mode Threshold Experiments," 10th IAEA Technical Meeting on H-mode Physics and Transport Barriers (2005).
- 48) Mishima, Y., Yoshida, N., Kawamura, H., et al., "Recent Results on Beryllium and Beryllides in Japan," 12th Int. Conf. on Fusion Reactor Materials (2005), to be published in J. Nucl. Mater..
- 49) Miura, Y., Takenaga, H., Kubo, H., et al., "Burn Control Study Using Burning Plasma Simulation Experiments in JT-60U," Proc. 32nd EPS Conf. on Plasma Phys., P2-069 (CD-ROM) (2005).
- 50) Miyato, N., Kishimoto, Y. and Li, J. Q., "Zonal Flow and GAM Dynamics and Associated Transport Characteristics in Reversed Shear Tokamaks," Proc. Joint Conf. of 19th Inter. Conf. on Numerical Simulation of Plasma and 7th Asia Pacific Plasma Theory Conf., 32 (2005).
- 51) Miyoshi, H., Ohno, N., (Asakura, N.), et al., "Intermittent Fluctuation Property of JT-60U Edge Plasmas," Proc. 32nd EPS Conf. on Plasma Phys., P1-045(CD-ROM) (2005).
- 52) Nagashima, Y., Itoh, K., Itoh, S-I., et al., "Observation of Coherent Bicoherence and Biphasic in Potential Fluctuations around Geodesic Acoustic Mode Frequency on JFT-2M," 10th IAEA Technical Meeting on H-mode Physics and Transport Barriers (2005).
- 53) Nakahata, T., Yoshikawa A., (Ishimoto, Y.), et al., "Dynamics of Deuterium Implanted in Boron Coating Film for Wall Conditioning," Proc. 12th Int. Conf. on Fusion Reactor Materials (2005), to be published in J. Nucl. Mater..
- 54) Nakamura, H., Ida, M., Chida, T., et al., "Thermo-Structural Design of the Replaceable Backwall in IFMIF Liquid Lithium Target," 12th Int. Conf. on Fusion Reactor Materials (2005), to be published in J. Nucl. Mater..
- 55) Nakamura, H., Kobayashi, K., Yokoyama S., et al., "Measurement of Tritium Trapped in the Irradiation Defects Produced by High Energy Proton and Spallation Neutron in SS316," 12th Int. Conf. on Fusion Reactor Materials (2005), to be published in J. Nucl. Mater..
- 56) Nakamura, Y., Tobita, K., Tsutsui, H., et al., "Computational Study of Non-Inductive Current Buildup in Compact DEMO Plant with Slim Center Solenoid," PPCA1-V, 1st IAEA Technical Meeting on First Generation of Fusion Power Plants -Design and Technology (2005)
- 57) Nakamura, Y., Tsutsui, H., Tobita, K., et al., "Simulation Modeling of Fully Non-Inductive Buildup Scenario in High Bootstrap Current Tokamaks without Center Solenoids," Proc. 32nd EPS Conf. on Plasma Phys., P2-051(CD-ROM) (2005).
- 58) Nakamura, Y., Tobita, K., Takei, N., et al., "Non-inductive Operation Scenario of Plasma Current Ramp-down in CS-less, Advanced Tokamak Reactor," 15th International Toki Conference, "Fusion & Advanced Technology", PS2-22, (2005).
- 59) Nakano, T., Tsuzuki, K., Higashijima, S., et al., "Emission Rates of CH/CD and C₂ Spectral Bands for Hydrocarbon-Loss-Events Measured in JT-60U Divertor Plasmas," Proc. 32nd EPS Conf. on Plasma Phys., P5-007(CD-ROM) (2005).

- 60) Neudatchin, S.V., Inagaki, S., Takizuka, T., et al., "Common Features of Heat Pulse Propagation across Internal Transport Barriers in JT-60U, LHD and T-10," 10th IAEA Technical Meeting on H-mode Physics and Transport Barriers (2005).
- 61) Neudatchin, S.V., Inagaki, S., Takizuka, T., et al., "Comparison of Heat Pulse Propagation across Internal Transport Barriers in JT-60U, LHD and T-10 Plasmas in a Presence of ECRH," 6th Int. Workshop on Strong Microwaves in Plasmas (2005).
- 62) O'hira, S., Shu, W., Hayashi, T., et al., "Radiochemical Characteristics of Tritium to be Considered in Fusion Reactor Facility Design," 5th Asia-Pacific Symp. on Radiochemistry (2005), to be published in J. Radioanal. & Nucl. Chem..
- 63) Oda, Y., Kawamura, K., (Takahashi, K.), et al., "An Experimental Study on a Thrust Generation Model for Microwave Beamed Energy Propulsion," Proc. 44th AIAA Aerospace Sciences Meeting and Exhibition, AIAA2006-0765 (2006).
- 64) Oda, Y., Komurasaki, K., Takahashi, K., et al., "Application of High Power Millimeter-Wave to Space Propulsion," Digest of Int. Conf. of Infrared and Millimeter Waves, MA3-4 (2005).
- 65) Oda, Y., Komurasaki, K., Takahashi, K., et al., "Experimental Study on Microwave Beaming Propulsion Using a 1MW-Class Gyrotron," 56th Int. Astronautical Conf., IAC-05-C4.6.01 (2005).
- 66) Oda, Y., Ushio, M., (Takahashi, K.), et al., "Pressure History Measurement in a Microwave Beaming Thruster," Proc. of 4th Int. Symp. on Beaming Energy Propulsion, (2005).
- 67) Ogiwara, H., Kohyama, A., Tanogawa, H. et al., "Helium effect of Microstructural Evolution in Ion-Irradiated Reduced Activation Ferritic/Martensitic Steel to High Fluences," 12th Int. Conf. on Fusion Reactor Materials (2005), to be published in J. Nucl. Mater..
- 68) Ohwaki, H., Sugihara, M., Kawano, Y., et al., "Modeling of Plasma Current Decay during the Disruption," Proc. 32nd EPS Conf. on Plasma Phys., P5-099(CD-ROM) (2005).
- 69) Okuno, K., Nakajima, H., Koizumi, N., "From CS and TF Model Coil to ITER : Lessons Learnt and Further Progress," Proc. 19th Inter. Conf. on Magnet Technology (2005), to be published in IEEE Trans. ASC..
- 70) Okuno, K., Nakajima, H., Sugimoto, H., et al. "Japanese Contributions to the Procurement of the ITER Superconducting Magnet," 15th Int. Toki Conf., (2005), to be published in Fusion Eng. Des..
- 71) Oya, Y., T. Tanabe, M., (Ishimoto, Y.), et al, "Hydrogen Isotope Behavior in the First Wall of JT-60U after DD Discharge," Proc. 12th Int. Conf. on Fusion Reactor Materials (2005), to be published in J. Nucl. Mater..
- 72) Ozeki, T., Aiba, N., Hayashi, N., et al., "Modeling of MHD Stability Consistent to the Transport," Proc. 32nd EPS Conf. on Plasma Phys. (2005).
- 73) Ozeki, T., Aiba, N., Hayashi, N., et al., "Integrated Simulation Code for Burning Plasma Analysis," IEA Large Tokamak Workshop on Burning Plasma Physics and Simulation (2005).
- 74) Peterson, B. J., Alekseyev, A. G., Konoshima, S., et al., "Imaging Bolometer Development for Application to Fusion Reactor Diagnostics," Proc. 47th Annual Meeting of DPP-APS, QP1. 00055 (2005).
- 75) Sakata, S., Totsuka, T., Kiyono, K., et al., "Progress of Data Processing System in JT-60 – Development of Remote Experiment System," 5th IAEA Technical Meeting on Control, Data Acquisition, and Remote Participation for Fusion Research (2005).
- 76) Sato, M., Isayama, A., Inagaki, S., et al., "Relativistic Downshift Frequency on ECE Measurements of Electron Temperature and Density in Torus Plasma," Proc. 32nd EPS Conf. on Plasma Phys., P4-090(CD-ROM) (2005).
- 77) Seki, M., "The Role of ITER and Associated Facilities on the Pathway towards Fusion Energy" 12th Int. Conf. on Fusion Reactor Materials (2005), to be published in J. Nucl. Mater..
- 78) Shiba, K., Nakata, T., Ando, M., et al., "Thermal creep Behavior of Japanese Reduced Activation Martensitic Steels," 12th Int. Conf. on Fusion Reactor Materials (2005), to be published in J. Nucl. Mater..
- 79) Shu, W.M., "Blistering and Retention in the Near-Surface Region of Tungsten Exposed to High Flux Deuterium Plasmas of Tens of eV," Proc. 3rd Int. Workshop on Tritium-Material Interactions, 27 (2005).
- 80) Shu, W.M., Luo, G.-N. and Yamanishi, T., "Mechanisms of Retention and Blistering in Near-Surface Region of Tungsten Exposed to High Flux Deuterium Plasmas of Tens of eV," 12th Int. Conf. on Fusion Reactor Materials (2005), to be published in J. Nucl. Mater..

- 81) Sokolov, M.A., Tanigawa, H., Odette, G.R., et al., "Fracture Toughness and Charpy Impact Properties of Several RAJS Before and After Irradiation in HFIR," 12th Int. Conf. on Fusion Reactor Materials (2005), to be published in J. Nucl. Mater..
- 82) Sugihara, M., Ohwaki, H., Kawano, Y., et al., "Extrapolation of Plasma Current Quench Time during Disruptions from Existing Machines to ITER," Proc. 32nd EPS Conf. on Plasma Phys., P2-067(CD-ROM) (2005).
- 83) Sugiyama, K., Tanabe, T., Masaki, K., et al., "Tritium Distribution Measurement of the Tile Gap of JT-60U," Proc. 12th Int. Conf. on Fusion Reactor Materials (2005), to be published in J. Nucl. Mater..
- 84) Suzuki, S., Akiba, M., "Materials and Design Interface of In-Vessel Components for Fusion Reactors," 12th Int. Conf. on Fusion Reactor Materials (2005), to be published in J. Nucl. Mater..
- 85) Suzuki, T., Isayama, A., Ide, S., et al., "Recent RF Experiments and Application of RF Waves to Real-Time Control of Safety Factor Profile in JT-60U," Radio Frequency Power in Plasmas (Proc. 16th Topical Conf. on Radio Frequency Power in Plasmas), 279 (2005).
- 86) Takatsu, H., Sugimoto, M., Jitsukawa, S., et al., "The Role of IFMIF in the Roadmap Toward Fusion Power Systems," 12th Int. Conf. on Fusion Reactor Materials (2005), to be published in J. Nucl. Mater..
- 87) Takechi, M., Fujita, T., Ishii, Y., et al., "MHD Instabilities Observed in Extremely Reversed Shear Discharges on JT-60U," Proc. 32nd EPS Conf. on Plasma Phys. P2-049(CD-ROM) (2005).
- 88) Takenaga, H., Oyama, N., Isayama, A., "Transient Electron Heat Transport and Reduced Density Fluctuation after Pellet Injection in JT-60U Reversed Shear Plasmas," Proc. 32nd EPS Conf. on Plasma Phys. P1-042(CD-ROM) (2005).
- 89) Takeuchi, T., Tagawa, K., (Koizumi, N.), et al., "Internally Cu-stabilized RHQT Nb3Al Superconductors with Ta Matrix," Proc. 19th Inter. Conf. on Magnet Technology (2005), to be published in IEEE Trans. ASC..
- 90) Takizuka, T., Urano, H., Takenaga, H., et al., "Origin of the Various Beta Dependence of ELMy H-Mode Confinement Properties," 10th IAEA Technical Meeting on H-mode Physics and Transport Barriers (2005).
- 91) Tani, K., Nishio, S., Tobita, K., et al., "Ripple Loss of Alpha Particles in a Low-Aspect -Ratio Tokamak Reactor," Proc. 19th IAEA Technical Meeting on Energetic Particles in Magnetic Confinement Systems (2005).
- 92) Tanigawa, H., Sokolov, M.A., Klueh, R.L., "Microstructural Inhomogeneity of Reduced-Activation Ferritic/Martensitic Steel," 12th Int. Conf. on Fusion Reactor Materials (2005), to be published in J. Nucl. Mater..
- 93) Tanigawa, H., Sakasegawa, H., Hashimoto, N., et al., "Irradiation Effects on Precipitation and its Impact on the Mechanical Properties of Reduced-Activation Ferritic/Martensitic Steels," 12th Int. Conf. on Fusion Reactor Materials (2005), to be published in J. Nucl. Mater..
- 94) Taniguchi, M., Inoue, T., Kashiwagi, M., et al., "Acceleration of 100A/m2 Negative Hydrogen Ion Beams in a 1 MeV Vacuum Insulated Beam Source," Proc. 10th Int. Symp. on Production and Neutralization of Negative Ions and Beams, AIP Conf. Proc., 763, 168 (2005).
- 95) Tomita, Y., Smirnov, R., Takizuka, T., et al., "Charging of Spherical Dust Particle on Plasma-Facing Wall," 19th Int. Conf. on Numerical Simulation of Plasmas and 7th Asia Pacific Plasma Theory Conf. (2005).
- 96) Tsuchiya, K., Ishitsuka, E., Kawamura, H., et al., "Contact Strength of Irradiated Beryllium Pebbles," Proc. 7th Int. Workshop on Beryllium Technology (2005), to be published in Nucl. Technol..
- 97) Tsuchiya, K., Kawamura, H., Ishida, T., "Compatibility between Be-Ti Alloys and F82H Steel," 12th Int. Conf. on Fusion Reactor Materials (2005), to be published in J. Nucl. Mater..
- 98) Tsuchiya, K., Kawamura, H., Ishida, T., "Effect of α Be on Compatibility between Be-Ti and SS316LN," Proc. 7th Int. Workshop on Beryllium Technology (2005), to be published in Nucl. Technol..
- 99) Tuda, T., Kurita G. and Fujita T., "Roles of Double Tearing Mode on the Formation of Current Hole," Proc. 19th Int. Conf. on Numerical Simulation of Plasmas and 7th Asia Pacific Plasma Theory Conf., 236 (2005).
- 100) Tuda, T., Kurita, G. and Fujita, T., "Stability of Double Tearing Mode in Current Hole Configuration," Proc. 5th Asia Plasma Fusion Association, 88 (2005).
- 101) Urano, H., Kamiya, K., Koide, Y., et al., "Roles of Plasma Rotation and Toroidal Field Ripple on H-Mode Pedestal Structure in JT-60U," 10th IAEA Technical Meeting on H-mode Physics and Transport Barriers

(2005).

- 102) Wakai, E., Ando, M., Sawai, T., et al., “Effect of Heat Treatments on Tensile Properties and Microstructures of F82H Steel Irradiated by Neutrons,” 12th Int. Conf. on Fusion Reactor Materials (2005), to be published in J. Nucl. Mater..
- 103) Yamauchi, M., Sato, S., Nishitani, T., et al., “Shielding Design of ITER Pressure Suppression System,” Proc. 21st Symp. on Fusion Eng. (2005), (CD-ROM).
- 104) Ying, A., Akiba, M., Boccaccini, L.V., et al., “Status and Perspectives of the R&D on Solid Breeder Materials for testing in ITER TBMs,” 12th Int. Conf. on Fusion Reactor Materials (2005), to be published in J. Nucl. Mater..
- 105) Yoshida, M., Kobayashi, S., Urano, et al., “Observations of the Collapse and Recovery of the Temperature Pedestal by Using Diagnostics with the Fast Temporal Resolution in JT-60U,” 10th IAEA Technical Meeting on H-mode Physics and Transport Barriers (2005).
- 106) Yoshikawa, A., Shibahara, T., (Arai, T.), et al., “Depth Profile Of Hydrogen And Its Retention In Divertor Target Tile Of Jt-60 Exposed To Hydrogen Discharges,” Proc. 7th Int. Symp. on Fusion Nuclear Technology (2005), to be published in Fusion Eng. Des..

A.1.4 List of other papers

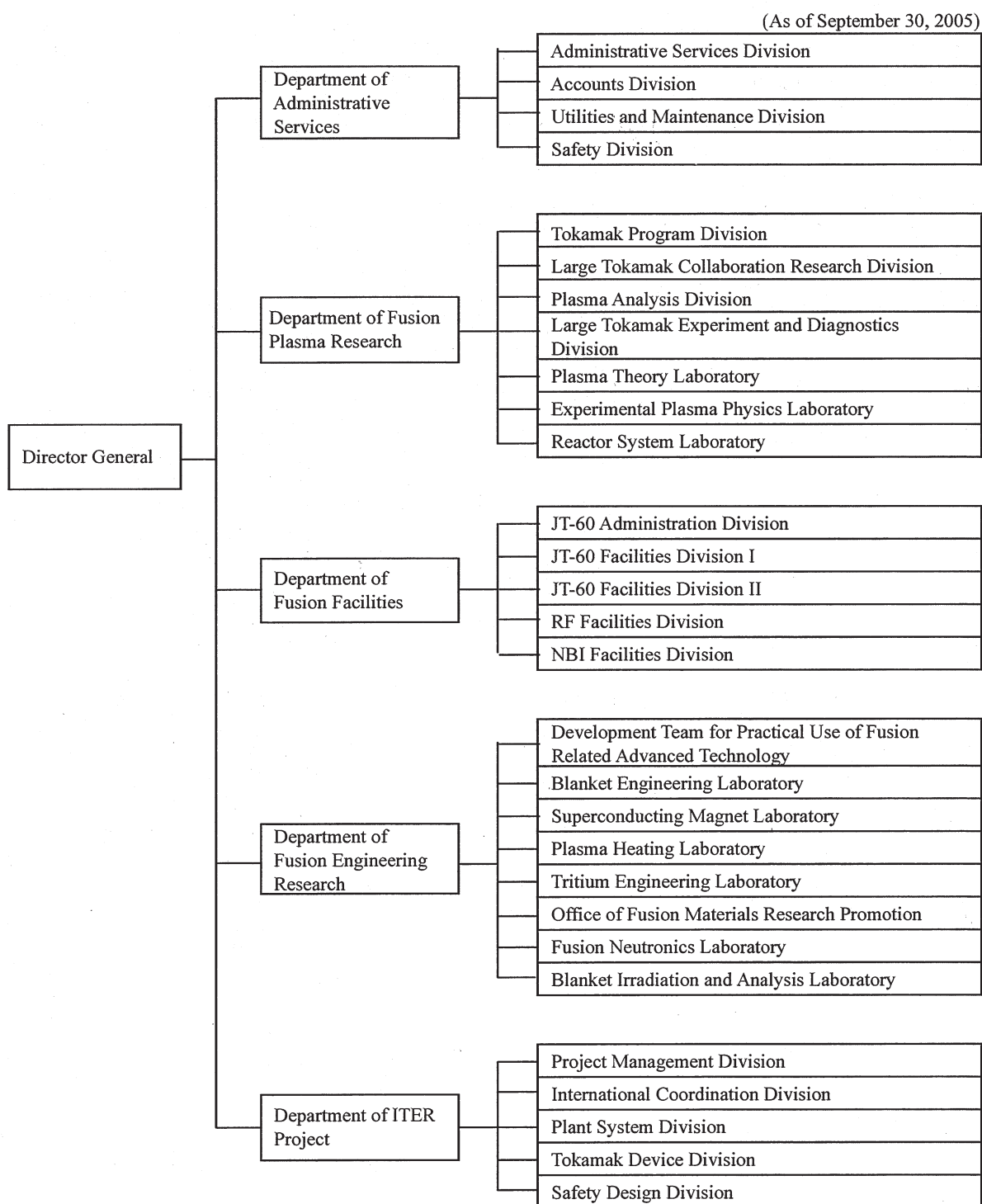
- 1) Akasaka, H., Takano, S., Kawamata, Y., "Reconfiguration Study of the JT-60 Timing System Using FPGA," Proc. 17th Topical Meeting on Eng. and Technol. (CD-ROM), (2006) (in Japanese).
- 2) Akiba, M., Matsui, H., Takatsu, H., et al., "Technology and Material Research in Fusion Power Plant Development," J. Plasma Fusion Res., **81**, 863 (2005) (in Japanese).
- 3) El-Guebaly, L.A., Forrest, R.A., (Tobita, K.), et al., "Current Challenges Facing Recycling and Clearance of Fusion Radioactive Materials," Fusion Technology Institute Report at University of Wisconsin, UWFD-1285 (2005).
- 4) Hamada, K., Nakajima, H., Kawano, K., et al., "Optimization of JK2LB Chemical Component for ITER Central Solenoid Jacket Material," J. Cryog. Eng. Soc. Japan, **41**, 131 (2006) (in Japanese).
- 5) Ido, T., Hamada, Y., Miura, Y., et al., "Zonal Flow Study with Heavy Ion Beam Probes II," J. Plasma Fusion Res., **81**, 987 (2005) (in Japanese).
- 6) Idomura, Y., "df Simulations of Microturbulence," J. Plasma Fusion Res. **81**, 581 (2005) (in Japanese).
- 7) Ikeda, Y., Kubo, S., "Plasma Profile Control by Using Local Heating and Current Drive with EC Waves," J. Plasma Fusion Res. **81**, 160 (2006) (in Japanese).
- 8) Ikeda, Y., Oikawa, T., Ide, S., "NBI Heating and Current Drive in JT-60U towards Steady-State Tokamak," J. Plasma Fusion Res., **81**, 773 (2005) (in Japanese).
- 9) Inoue, N., Yoshino, R., "Tokoton Yasashii Kakuyugou Enerugii no Hon (Book of Fusion Energy Thoroughly Understandable)," Nikkan Kogyo Shimbun, Ltd., Tokyo (2005) (in Japanese).
- 10) Inoue, T., "Background and Latest R&D Achievements," J. Plasma Fusion Res., **81**, 764 (2005) (in Japanese).
- 11) Inoue, T., Hanada, M., "R&D Progress of a Negative Ion Source and an Accelerator for Fusion Reactors," J. Plasma Fusion Res., **81**, 785 (2005) (in Japanese).
- 12) Ishimoto, Y., Gotoh, Y., Arai, T., et al., "Thermal Properties and Structure of Redeposition Layers in JT-60U," 2005 Japan-US Workshop on Heat Removal and Plasma Materials Interactions for Fusion, Fusion High Power Density Components and System, and IEA workshop on Solid Surface Plasma Facing Components (2005).
- 13) Ishio, K., Hamada, K., Nakajima, H., "Effects of Nitrogen, Niobium, Phosphorous and Carbon on the Mechanical Properties of Aged 316LN Stainless Steels at Cryogenic Temperature, 4 K," Tetsu-to-Hagane, **92**, 30 (2006) (in Japanese).
- 14) Ishio, K., Nakajima, H., "Effects of Nitrogen on the Material Properties of 316LN Stainless Steels," Tetsu-to-Hagane, **92**, 38 (2006) (in Japanese).
- 15) Kamada, Y., "Plasma Properties for the Design of the Thermonuclear Reactor," J. Atomic Energy Soc. Jpn., **47**, 45 (2005) (in Japanese).
- 16) Kamada, Y., Shimada, M., Ogawa, Y., et al., "Fusion Plasma Research toward Fusion Power Plants," J. Plasma Fusion Res., **81**, 849 (2005) (in Japanese).
- 17) Kawamata, Y., Kurihara, K., "Development of an Innovative Integrator Being Resistant to an Excessive High Voltage Input at Plasma Instabilities toward ITER," Proc. 22nd Annual Meeting on Plasma Fusion Research, 173 (2005) (in Japanese).
- 18) Koizumi, N., Nishimura, A., "Intelligible Seminar on Fusion Reactors – (9) Superconducting Coil to Generate Magnetic Field for Plasma Confinement," J. Energy Soc. Jpn., **47**, 703 (2005) (in Japanese).
- 19) Konishi, S., Enoda, M., "Intelligible Seminar on Fusion Reactors – (6) Blanket that converts Energy, and Produces Fuels," J. At. Energy Soc. Jpn., **47**, 488 (2005) (in Japanese).
- 20) Krylov, A., Inoue, T., "ITER NB System: Compact Beamline and Design Against Radiation," J. Plasma Fusion Res., **81**, No.10, 779 (2005).
- 21) Kubota, N., Ochiai, K., Kutsukake, C., et al., "Measurement of Light Element Distribution near the Surface of TFTR Plasma Facing Component using Nuclear Reaction Analysis," J. Plasma and Fusion Res., **81**, 296 (2005) (in Japanese).
- 22) Kurihara, K., "Conference Report on the 21st IEEE/NPSS Symp. on Fusion Eng. (21st SOFE, Sept. 26-29,

- 2005, Knoxville, Tennessee),” J. Plasma Fusion Res., **82**, 111 (2006) (in Japanese).
- 23) Kurihara, K., Kawamata, Y., Sueoka, M., et al., “A New Method of Current Profile Reconstruction based on the Exact Solution of Fredholm Integral Equation of the First Kind,” Proc. 22nd Annual Meeting on Plasma Fusion Research, 109 (2005) (in Japanese).
 - 24) Kusama, Y., Ishikawa, M., “Application of Diamond to Plasma Diagnostic,” New Diamond, **21**, 24 (2005) (in Japanese).
 - 25) Maebara, S. and Watanabe, K., “Development of Accelerator for IFMIF,” J. Plasma Fusion Res, **82**, 21 (2005) (in Japanese).
 - 26) Masaki, K., “Analyses of Dust in JT-60U,” 2005 Japan-US Workshop on Heat Removal and Plasma Materials Interactions for Fusion, Fusion High Power Density Components and System, and IEA workshop on Solid Surface Plasma Facing Components (2005).
 - 27) Minami, R., Kasugai, A., Takahashi, K., et al., “Development of High Power Gyrotron for CW Operation,” Inst. Elec. Info. Comm. Engineers Technical Report, **105**, 498, 39 (2005).
 - 28) Miura, Y., “Measurement and Control of Tokamak Plasma by Light,” Hikarikagaku-no-Saizensen (in Japanese).
 - 29) Morioka, A., Okuno, K., “Development of High Heat-Resistance Resin for Neutron Shielding,” Plastics, **57**, 148 (2006) (in Japanese).
 - 30) Nakahira, M., Takeda, N., “An Approach for Development of Technical Structural Standard in ITER,” Maintenology **4**, 47 (2006) (in Japanese).
 - 31) Nakamura, H., and Higashijima, S., “Hydrogen Isotopes Removal from the Vacuum Vessel Using Discharges,” J. Vacuum Soc. Japan. **49**, 62 (2006) (in Japanese).
 - 32) Nakamura, H., Horike, H., Kondo, H., et al., “Development of Liquid Lithium Target System in the IFMIF,” J. Plasma and Fusion Res., **82**, 16 (2005) (in Japanese).
 - 33) Nishitani, T., “Burning Plasma Diagnostics by Radiation Measurement,” Housyasen, **31**, 97 (2005) (in Japanese).
 - 34) O’hira, S., “Intelligible Seminar on Fusion Reactors- (11) Safety of Fusion Reactor - Safety Characteristics and Requirements -,” J. At. Energy Soc. Japan, **47**, 839 (2005) (in Japanese).
 - 35) Ohmori, Y., Kurihara, K., Matsukawa, M., et al., “Trouble of a Transformer with the No-Voltage Tap Changer,” Proc. 17th Topical Meeting on Eng. and Technol. (CD-ROM), (2006) (in Japanese).
 - 36) Okano, F., Honda, A., Ohshima, K., et al., “Application of PLC to Dynamic Feedback Control of a Large Liquid-He Refrigerator System on Nuclear Fusion Facility,” Keiso **49**, 22 (2006) (in Japanese).
 - 37) Okano, K., Kikuchi, M., Tobita, K., et al., “Path toward Commercial Fusion Power Plants,” J. Plasma Fusion Res. **81**, 839 (2005) (in Japanese).
 - 38) Okano, K., Kurihara, K., Tobita, K., “Intelligible Seminar on Fusion Reactors, 12; Next Step toward the Realization of Fusion Reactors -Future Vision of Fusion Energy Research and Development-,” J. Nucl. Sci. Technol., **48**, 48 (2006) (in Japanese).
 - 39) Oya, Y., Hirohata, Y., (Masaki, K.,) et al., “Hydrogen and Deuterium Distributions and Erosion/Deposition Profile in JT-60U,” 2005 Japan-US Workshop on Heat Removal and Plasma Materials Interactions for Fusion, Fusion High Power Density Components and System, and IEA Workshop on Solid Surface Plasma Facing Components (2005).
 - 40) Shibamura, K., “Intelligible Seminar on Fusion Reactors – (10) Remote Maintenance Robot for In-Vessel Components – Advanced Robot Technology for Handling of Large-Heavy Components with High Positioning Accuracy,” J. At. Energy Soc. Japan **47**, 761 (2005) (in Japanese).
 - 41) Sueoka, M., Kawamata, Y., Kurihara, K., “Web-Based Information Distribution Plan in JT-60 (Plasma Shape Real-Time Display and Broadcasting by Using Web Service),” Proc. 22nd Annual Meeting on Plasma Fusion Research, 116 (2005) (in Japanese).
 - 42) Sugie, T., “Radiation from High Temperature Plasmas and Spectroscopy,” in Basis and Application of Plasma Diagnostic, Corona Publishing Co. Ltd. (in Japanese).

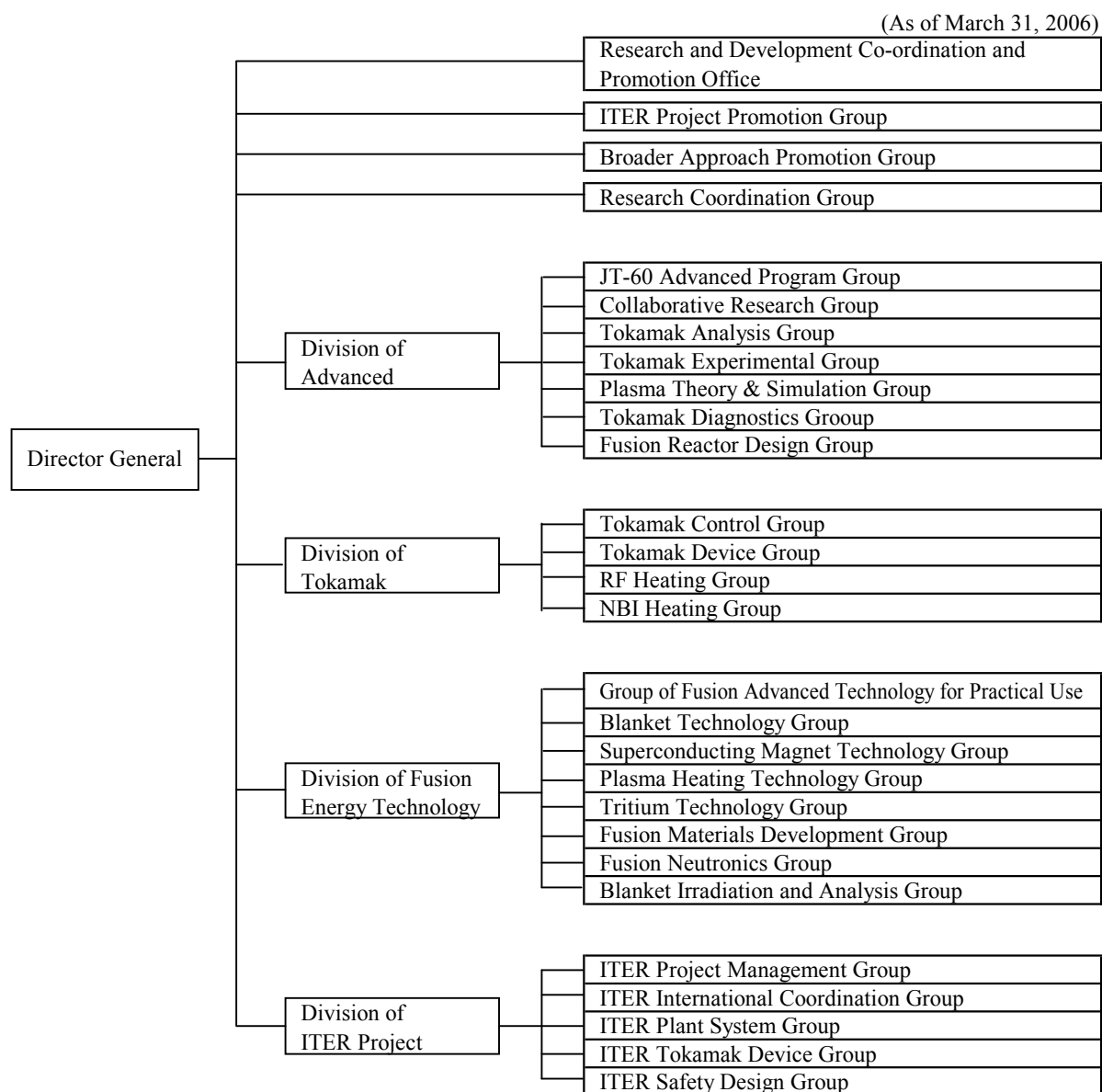
- 43) Sugimoto, M., “Status of Design and Development of International Fusion Materials Irradiation Facility (IFMIF) – Central Control/Common Instrumentation and Conventional Facilities,” J. Plasma and Fusion Res., **82**, 26 (2005) (in Japanese).
- 44) Sugimoto, M., “Status of Design and Development of International Fusion Materials Irradiation Facility (IFMIF) – Summary,” J. Plasma and Fusion Res., **82**, 28 (2005) (in Japanese).
- 45) Tanaka, S., Akiba, M., Enomoto, M., et al., “Present Status of ITER Test Blanket Development,” J. Plasma Fusion Res., **81**, 434 (2005) (in Japanese).
- 46) Tobita, K., Konishi, S., Tokimatsu, K., et al., “Challenge to Innovative Technologies and the Expected Market Appeal,” J. Plasma Fusion Res., **81**, 875 (2005) (in Japanese).
- 47) Totsuka, T., Sakata, S., Iba, K., “Status and Development of JT-60 Remote Experiment (Discharge Parameter Set-Up and Pulse Scheduling from Remote-Site),” Proc. 22nd Annual Meeting on Plasma Fusion Research, 116 (2005) (in Japanese).
- 48) Wang, F., Nakamura, (Kurihara, K.), et al., “Magnetic Sensor Dependence of CCS Method to Reproduce ST Plasma Shape,” Proc. Kyushu-Okinawa-Yamaguchi Local Meeting on Plasma Fusion Res., (2005).
- 49) Watanabe, K., Andoh, Y., “Application of NBI Technologies,” J. Plasma Fusion Res., **81**, 792 (2005) (in Japanese).
- 50) Watanabe, T., Sugama, H., Idomura, Y., “Prospects of Microturbulence Simulation,” J. Plasma Fusion Res., **81**, 698 (2005) (in Japanese).

A.2 Organization

A.2.1 Organization of Naka Fusion Research Establishment



A.2.2 Organization of Fusion Research and Development Directorate



For more information on JAEA organization, please see the following URL:

http://www.jaea.go.jp/english/01/1_5.shtml

A.3 Personnel Data

A.3.1 Scientific Staff in the Naka Fusion Research Establishment of JAERI (April 2005 - September 2005)

Naka Fusion Research Establishment

SEKI Masahiro	(Director General)
SHIMOMURA Yasuo	(Scientific Consultant)
MATSUI Hideki	(Invited Researcher)
KOHYAMA Akira	(Invited Researcher)
IDA Katsumi	(Invited Researcher)
KISHIMOTO Yasuaki	(Invited Researcher)
USHIGUSA Kenkichi	(Staff for Director General)
ISEI Nobuaki	(Staff for Director General)
OOHARA Hiroshi	(Staff for Director General)

Department of Fusion Plasma Research

NINOMIYA Hiromasa	(Director)
KIKUCHI Mitsuru	(Deputy Director)
NAGAMI Masayuki	(Prime Scientist)
TANI Keiji	
TERAKADO Yuichi	(Administrative Manager)

Tokamak Program Division

MIURA Yukitoshi	(General Manager)	
ANDO Toshinari (*18)	FUJITA Takaaki	HATAE Takaki
KURIHARA Ryoichi	KURITA Gen-ichi	MATSUMURA Hiroshi (*2)
MORI Katsuharu (*7)	MORIOKA Atsuhiko	OGURI Shigeru (*7)
OIKAWA Akira	SAKURAI Shinji	SATO Fujio (*7)
SHIINA Tomio	TAMAI Hiroshi	TSUCHIYA Katsuhiko
YAMAZAKI Takeshi (*7)		

Large Tokamak Collaboration Research Division

MIURA Yukitoshi	(General Manager)
KONOSHIMA Shigeru	SHINOHARA Kouji

Plasma Analysis Division

OZEKI Takahisa	(General Manager)	
AIBA Nobuyuki (*21)	HAMAMATSU Kiyotaka	HAYASHI Nobuhiko
KIYONO Kimihiro	KOBAYASHI Masayuki (*23)	KONOVVALOV Sergei (*6)
NAITO Osamu	OHASHI Kazumi	OHSHIMA Takayuki
SAKATA Shinya	SATO Minoru	SUZUKI Mitsuhiro (*30)
TAKIZUKA Tomonori		

Large Tokamak Experiment and Diagnostics Division

KAMADA Yutaka (General Manager)

ASAKURA Nobuyuki	CHIBA Shinichi	FUJIMOTO Kayoko (*21)
HAMANO Takashi (*19)	HAYASHI Toshimitsu (*17)	HOSHINO Katsumichi
IDE Shunsuke	INOUE Akira (*19)	ISAYAMA Akihiko
ISHIKAWA Masao (*21)	KAMIYA Kensaku	KASHIWA Yoshitoshi
KAWASHIMA Hisato	KITAMURA Shigeru	KOIDE Yoshihiko
KOKUSEN Shigeharu (*18)	KUBO Hirotaka	MATSUNAGA Go (*21)
MIYAMOTO Atsushi (*18)	NAGAYA Susumu	NAKANO Tomohide
OYAMA Naoyuki	SAKAMOTO Yoshiteru	SAKUMA Takeshi (*19)
SUNAOSHI Hidenori	SUZUKI Takahiro	TAKECHI Manabu
TAKENAGA Hidenobu	TSUBOTA Naoaki (*18)	TSUKAHARA Yoshimitsu
TSUZUKI Kazuhiro	UEHARA Kazuya	URANO Hajime
YOSHIDA Maiko (*21)		

Plasma Theory Laboratory

KISHIMOTO Yasuaki (Head)

IDOMURA Yasuhiro	ISHII Yasutomo	KAGEI Yasuhiro (*21)
MATSUMOTO Taro	MIYATO Naoaki	SUGAHARA Akihiro (*23)
TOKUDA Shinji	TUDA Takashi	

Experimental Plasma Physics Laboratory

KUSAMA Yoshinori (Head)

KASAI Satoshi	KAWANO Yasunori	KONDOH Takashi
OGAWA Hiroaki		

Reactor System Laboratory

TOBITA Kenji (Head)

NAKAMURA Yukiharu	NISHIO Satoshi	SATO Masayasu
SONG Yuntao (*4)		

Department of Fusion Facilities

KURIYAMA Masaaki (Director)

HOSOGANE Nobuyuki (Deputy Director)

YAMAMOTO Takumi

JT-60 Administration Division

TERAKADO Yuichi (General Manager)

JT-60 Facilities Division I

KURIHARA Kenichi (Head)

AKASAKA Hiromi	FURUKAWA Hiroshi (*19)	HOSOYAMA Hiromi (*8)
KAWAMATA Youichi	MATSUKAWA Makoto	OHMORI Shunzo
OHMORI Yoshikazu	OKANO Jun	SEIMIYA Munetaka
SHIBATA Kazuyuki (*19)	SHIBATA Takatoshi	SHIMADA Katsuhiro
SUEOKA Michiharu	TAKANO Shoji (*30)	TERAKADO Hiroyuki (*7)
TERAKADO Tsunehisa	TOTSUKA Toshiyuki	YAMASHITA Yoshiki (*7)
YONEKAWA Izuru		

JT-60 Facilities Division II

MIYA Naoyuki (Head)

ARAI Takashi	HAGA Saburo (*18)	HAYASHI Takao
HIRATSUKA Hajime	HONDA Masao	ICHIGE Hisashi
ISAKA Masayoshi	ISHIMOTO Yuki (*21)	KAMINAGA Atsushi
KIZU Kaname	MASAKI Kei	MATSUZAWA Yukihiro (*18)
MIYO Yasuhiko	NISHIYAMA Tomokazu	SASAJIMA Tadayuki
SHIBAMA Yusuke	SUZUKI Yutaka (*16)	TAKAHASHI Ryukichi (*2)
UEHARA Toshiaki (*19)	YAGISAWA Hiroshi (*2)	
YAGYU Jun-ichi	YAMAMOTO Masahiro	

RF Facilities Division

FUJII Tsuneyuki (Head)

ANNO Katsuto	HIRANAI Shinichi	HASEGAWA Koichi
IGARASHI Koichi (*18)	ISHII Kazuhiro (*19)	KIKUCHI Kazuo
MORIYAMA Shinichi	SATO Fumiaki (*18)	SAWAHATA Masayuki
SEKI Masami	SHIMONO Mitsugu	SHINOZAKI Shin-ichi
SUZUKI Sadaaki	TAKAHASHI Masami (*25)	TANI Takashi
TERAKADO Masayuki	YOKOKURA Kenji	

NBI Facilities Division

IKEDA Yoshitaka (Head)

AKINO Noboru	EBISAWA Noboru	GRISHAM Larry (*22)
HONDA Atsushi	KAWAI Mikito	KAZAWA Minoru
KIKUCHI Katsumi (*19)	KOMATA Masao	MOGAKI Kazuhiko
NOTO Katsuya (*18)	OHGA Tokumichi	OKANO Fuminori
OSHIMA Katsumi (*18)	TAKENOUCHI Tadashi (*28)	TANAI Yutaka (*19)
UMEDA Naotaka	USUI Katsutomi	YAMAZAKI Haruyuki (*2)

Department of Fusion Engineering Research

SEKI Shogo	(Director)
TAKATSU Hideyuki	(Prime Scientist and Deputy Director)
KATOOGI Takeshi	(Administrative Manager)

SHIHO Makoto

Development Team for Practical Use of Fusion Related Advanced Technology

ABE Tetsuya (Team Leader)

Blanket Engineering Laboratory

AKIBA Masato (Head)

ENOEDA Mikio

HOMMA Takashi

SUZUKI Satoshi

YOKOYAMA Kenji

EZATO Koichiro

NISHI Hiroshi

TANIGAWA Hisashi

HIROSE Takanori

NOMOTO Yasunobu (*12)

TANZAWA Sadamitsu

Superconducting Magnet Laboratory

OKUNO Kiyoshi (Head)

ABE Kanako (*5)

KAWANO Katsumi

NAKAJIMA Hideo

SUGIMOTO Makoto

HAMADA Kazuya

KOIZUMI Norikiyo

NUNOYA Yoshihiko

TAKANO Katsutoshi (*19)

ISONO Takaaki

NABARA Yoshihiro

OSHIKIRI Masayuki (*19)

TSUTSUMI Fumiaki (*30)

Plasma Heating Laboratory

SAKAMOTO Keishi (Head)

DAIRAKU Masayuki

INOUE Takashi

KOBAYASHI Noriyuki (*29)

ODA Yasuhisa (*31)

TANIGUCHI Masaki

HANADA Masaya

KASHIWAGI Mieko

KOMORI Shinji (*19)

SEKI Takayoshi (*2)

TOBARI Naoyuki (*21)

IKEDA Yukiharu

KASUGAI Atsushi

MINAMI Ryutaroh (*21)

TAKAHASHI Koji

WATANABE Kazuhiro

Tritium Engineering Laboratory

YAMANISHI Toshihiko (Head)

HAYASHI Takumi

KOBAYASHI Kazuhiro

NAKAMURA Hirofumi

UZAWA Masayuki (*16)

ISOBE Kanetsugu

LUO Guang-Nan (*6)

SHU Wataru

YAMADA Masayuki

KAWAMURA Yoshinori

MIURA Hidenori (*12)

SUZUKI Takumi

Office of Fusion Materials Research Promotion

SUGIMOTO Masayoshi (Head)

ANDO Masami

MATSUHIRO Kenjiro (*21)

TANIGAWA Hiroyasu

CHIDA Teruo (*3)

NAKAMURA Hiroo

UMETSU Tomotake (*14)

IDA Mizuho (*5)

NAKAMURA Kazuyuki

YUTANI Toshiaki (*29)

Fusion Neutron Laboratory

NISHITANI Takeo (Head)

ABE Yuichi

KUBOTA Naoyoshi (*21)

KAWABE Masaru (*19)

KUTSUKAKE Chuzo

KONDO Keitaro (*20)

NAKAO Makoto (*12)

OCHIAI Kentaro
SEKI Masakazu

OKADA Kouichi (*27)
TANAKA Shigeru

SATO Satoshi
YAMAUCHI Michinori (*29)

Blanket Irradiation and Analysis Laboratory

HAYASHI Kimio (Head)
HOSHINO Tsuyoshi (*21)
YAMADA Hirokazu (*12)

ISHIDA Takuya (*19)

TSUCHIYA Kunihiro

Department of ITER Project

TSUNEMATSU Toshihide (Director)
YOSHINO Ryuji (Deputy Director)
TADA Eisuke
MATSUMOTO Hiroyuki (Administrative Manager)
KOIZUMI Koichi ODAJIMA Kazuo

SHOJI Teruaki

Project Management Division

MORI Masahiro (General Manager)
ITAMI Kiyoshi
SUGIE Tatsuo

SENGOKU Seio
YOSHIDA Hidetoshi

SHIMIZU Katsuhiko

International Coordination Division

ANDO Toshiro (Head)
HONDA Tsutomu (*29)
KATAOKA Yoshiyuki (*2)
NAGAHAMA Tetsushi (*24)
SAKASAI Akira
SUGIHARA Masayoshi
YOSHIDA Kiyoshi

IIDA Hiromasa
MARUYAMA So
OIKAWA Toshihiro
SATO Kouichi (*30)
TAKAHASHI Yoshikazu

IOKI Kimihiro (*16)
MORIMOTO Masaaki (*16)
OKADA Hidetoshi (*2)
SHIMADA Michiya
TERASAWA Atsumi (*15)

Plant System Division

NEYATANI Yuzuru (Head)
KATAOKA Takahiro (*15)
OOHASHI Hironori (*10)
TAKAHASHI Hideo (*26)
YAMAMOTO Shin

NAGAMATSU Nobuhide (*9)
SATO Kazuyoshi
TAMURA Kousaku (*13)

OHMORI Junji (*29)
SEKIYA Shigeki (*14)
YAGENJI Akira (*1)

Tokamak Device Division

SHIBANUMA Kiyoshi (Head)
KAKUDATE Satoshi
NAKAHIRA Masataka

KITAMURA Kazunori (*29)
OBARA Kenjiro

MOHRI Kensuke (*11)
TAKEDA Nobukazu

Safety Design Division

O'HIRA Shigeru (Head)

HIGUCHI Masahisa,

TAKEI Nahoko

MARUO Takeshi

TAKEMURA Morio (*11)

TADO Shigeru (*15)

TSURU Daigo

Collaborating Laboratories

Tokai Research Establishment

Department of Material Science

Research Group for Radiation Effects and Analysis

JITSUKAWA Shiro (Leader)

FUJII Kimio

OKUBO Nariaki

TANIFUJI Takaaki

YAMAKI Daiju

NAITO Akira

SAWAI Tomotsugu

WAKAI Eiichi

NAKAZAWA Tetsutya

SHIBA Kiyoyuki

YAMADA Reiji

Department of Nuclear Energy System

Research Group for Reactor Structural Materials

MIWA Yukio

Neutron Science Research Center

Research Group for Neutron Scattering from Functional Materials

IGAWA Naoki

Research Group for Nanostructure

TAGUCHI Tomitsugu

Center for Proton Accelerator Facilities

Accelerator Group

HIROKI Seiji

Office of Planning

Division of Collaborative Activities

NEMOTO Masahiro

*1 Hazama Corporation

*2 Hitachi, Ltd.

*3 Hitachi Engineering & Services Co., Ltd.

- *4 Institute of Plasma Physics, Academia Science (China)
- *5 Ishikawajima-Harima Heavy Industries Co., Ltd.

- *6 JAERI Fellowship
- *7 JP HYTEC Co., Ltd.
- *8 Japan EXpert Clone Corp.
- *9 Kajima Corporation
- *10 Kandenko Co., Ltd.

- *11 Kawasaki Heavy Industries, Ltd.
- *12 Kawasaki Plant Systems, Ltd.
- *13 Konoike Construction Co., Ltd.
- *14 Kumagai Gumi Co., Ltd.
- *15 Mitsubishi Electric Corporation

- *16 Mitsubishi Heavy Industries, Ltd.
- *17 NEC Corporation
- *18 Nippon Advanced Technology Co., Ltd.
- *19 Nuclear Engineering Co., Ltd.
- *20 Osaka University

- *21 Post-Doctoral Fellow
- *22 Princeton Plasma Physics Laboratory (USA)
- *23 Research Organization for Information Science & Technology
- *24 Shimizu Corporation
- *25 Sumitomo Heavy Industries, Ltd.

- *26 Taisei Corporation
- *27 Tohoku University
- *28 Tomoe Shokai Co., Ltd.
- *29 Toshiba Corporation
- *30 Total Support Systems

- *31 University of Tokyo

A.3.2 Scientific Staff in Fusion Research and Development Directorate of JAEA (October 2005 - March 2006)

Fusion Research and Development Directorate

SEKI Masahiro	(Director General)
SHIMOMURA Yasuo	(Scientific Consultant)
MATSUI Hideki	(Invited Researcher)
KOHYAMA Akira	(Invited Researcher)
IDA Katsumi	(Invited Researcher)
KISHIMOTO Yasuaki	(Invited Researcher)

Research and Development Co-ordination and Promotion Office

SEKI Shogo	(General Manager)	
GUNJI Masato	HAGA Junji	KATOJI Takeshi
KAWASAKI Minoru	KIZAKI Eiko	KUROSAWA Hiroshi
MATSUMOTO Hiroyuki	OHNAWA Tetsuya	SUGIKAWA Yukari
TERAKADO Yuichi	TSUDA Kazuko	YOSHINARI Shuji

ITER Project Promotion Group

OKUMURA Yoshikazu	(Leader)	
DOI Kenshin	EJIRI Shintaro	IWAI Yasunori
MATSUMOTO Hiroshi	OGAWA Toshihide	

Fusion Research Coordination Group

USHIGUSA Kenkichi	(Leader)
ISEI Nobuaki	OOHARA Hirochi

Broader Approach Promotion Group

USHIGUSA Kenkichi	(Acting Leader)
-------------------	-----------------

Division of Advanced Plasma Research

NINOMIYA Hiromasa	(Unit Manager)
KIKUCHI Mitsuru	(Senior Principal Researcher)
NAGAMI Masayuki	(Supreme Researcher)
TANI Keiji	(Senior Principal Researcher)

JT-60 Advanced Program Group

MIURA Yukitoshi	(Leader)	
ANDO Toshinari (*14)	FUJITA Takaaki	HATAE Takaki
KURIHARA Ryoichi	KURITA Gen-ichi	MATSUMURA Hiroshi (*2)
MORI Katsuharu (*5)	MORIOKA Atsuhiko	OGURI Shigeru (*5)

OIKAWA Akira
SHIINA Tomio
YAMAZAKI Takeshi (*5)

SAKURAI Shinji
TAMAI Hiroshi

SATO Fujio (*5)
TSUCHIYA Katsuhiko

Collaborative Research Group

KIMURA Haruyuki (Leader)
KONOSHIMA Shigeru

SHINOHARA Kouji

Tokamak Analysis Group

OZEKI Takahisa (Leader)
AIBA Nobuyuki (*17)
KIYONO Kimihiro
OHASA Kazumi
SATO Minoru

HAMAMATSU Kiyotaka
KOBAYASHI Masayuki (*19)
OHSHIMA Takayuki
SUZUKI Mitsuhiro (*26)

HAYASHI Nobuhiko
NAITO Osamu
SAKATA Shinya
TAKIZUKA Tomonori

Tokamak Experimental Group

KAMADA Yutaka (Leader)
ASAKURA Nobuyuki
HAMANO Takashi (*15)
IDE Shunsuke
ISHIKAWA Masao (*17)
KAWASHIMA Hisato
KOKUSEN Shigeharu (*14)
MIYAMOTO Atsushi (*14)
OYAMA Naoyuki
SUNAOSHI Hidenori
TAKENAGA Hidenobu
TSUTSUMI Kazuyoshi (*14)
URANO Hajime

CHIBA Shinichi
HAYASHI Toshimitsu (*13)
INOUE Akira (*15)
KAMIYA Kensaku
KITAMURA Shigeru
KUBO Hirotaka
NAKANO Tomohide
SAKAMOTO Yoshiteru
SUZUKI Takahiro
TSUBOTA Naoaki (*14)
TSUZUKI Kazuhiro
YOSHIDA Maiko (*17)

FUJIMOTO Kayoko (*17)
HOSHINO Katsumichi
ISAYAMA Akihiko
KASHIWA Yoshitoshi
KOIDE Yoshihiko
MATSUNAGA Go(*17)
NAGAYA Susumu
SAKUMA Takeshi (*15)
TAKECHI Manabu
TSUKAHARA Yoshimitsu
UEHARA Kazuya

Plasma Theory & Simulation Group

KISHIMOTO Yasuaki (Leader)
IDOMURA Yasuhiro
MATSUMOTO Taro
TOKUDA Shinji

ISHII Yasutomo
MIYATO Naoaki
TUDA Takashi

KAGEI Yasuhiro
SUGAHARA Akihiro (*19)

Tokamak Diagnostics Group

KUSAMA Yoshinori (Leader)
KASAI Satoshi
OGAWA Hiroaki

KAWANO Yasunori

KONDOH Takashi

Fusion Reactor Design Group

TOBITA Kenji (Leader)
NAKAMURA Yukiharu

NISHIO Satoshi

SATO Masayasu

Division of Tokamak System Technology

KURIYAMA Masaaki	(Unit Manager)
HOSOGANE Nobuyuki	(Senior Principal Researcher)
YAMAMOTO Takumi	(Senior Principal Researcher)

Tokamak Control Group

KURIHARA Kenichi	(Leader)	
AKASAKA Hiromi	FURUKAWA Hiroshi (*15)	HOSOYAMA Hiromi (*6)
KAWAMATA Youichi	MATSUKAWA Makoto	OHMORI Yoshikazu
OKANO Jun	SEIMIYA Munetaka	SHIBATA Kazuyuki (*15)
SHIBATA Takatoshi	SHIMADA Katsuhiro	SUEOKA Michiharu
TAKANO Shoji (*26)	TERAKADO Hiroyuki (*5)	TERAKADO Tsunehisa
TOTSUKA Toshiyuki		

Tokamak Device Group

MIYA Naoyuki	(Leader)	
ARAI Takashi	HAGA Saburo (*14)	HAYASHI Takao
HIRATSUKA Hajime	HONDA Masao	ICHIGE Hisashi
ISAKA Masayoshi	KAMINAGA Atsushi	KIZU Kaname
MASAKI Kei	MATSUZAWA Yukihiro (*14)	MIYO Yasuhiko
NISHIYAMA Tomokazu	SASAJIMA Tadayuki	SHIBAMA Yusuke
SUZUKI Yutaka (*12)	TAKAHASHI Ryukichi (*2)	UEHARA Toshiaki (*15)
YAGISAWA Hiroshi (*2)	YAGYU Jun-ichi	YAMAMOTO Masahiro

RF Heating Group

FUJII Tsuneyuki	(Leader)	
HIRANAI Shinichi	HASEGAWA Koichi	IGARASHI Koichi (*14)
ISHII Kazuhiro (*15)	KIKUCHI Kazuo	MORIYAMA Shinichi
SATO Fumiaki (*14)	SAWAHATA Masayuki	SEKI Masami
SHIMONO Mitsugu	SHINOZAKI Shinichi	SUZUKI Sadaaki
TAKAHASHI Masami (*21)	TANI Takashi	TERAKADO Masayuki
YOKOKURA Kenji		

NBI Heating Group

IKEDA Yoshitaka	(Leader)	
AKINO Noboru	EBISAWA Noboru	GRISHAM Larry (*18)
HONDA Atsushi	KAWAI Mikito	KAZAWA Minoru
KIKUCHI Katsumi (*15)	KOMATA Masao	MOGAKI Kazuhiko
NOTO Katsuya (*14)	OHGA Tokumichi	OKANO Fuminori
OSHIMA Katsumi (*14)	TAKENOUCHI Tadashi (*24)	TANAI Yutaka (*15)
UMEDA Naotaka	USUI Katsutomi	YAMAZAKI Haruyuki (*2)

Division of Fusion Energy Technology

TAKATSU Hideyuki	(Unit Manager)
SHIHO Makoto	(Senior Principal Researcher)

Group of Fusion Advanced Technology for Practical Use

ABE Tetsuya	(Leader)
-------------	----------

Blanket Technology Group

AKIBA Masato	(Leader)	
ENOEDA Mikio	EZATO Koichiro	HIROSE Takanori
HOMMA Takashi	NISHI Hiroshi	NOMOTO Yasunobu (*8)
SUZUKI Satoshi	TANIGAWA Hisashi	TANZAWA Sadamitsu
YOKOYAMA Kenji		

Superconducting Magnet Technology Group

OKUNO Kiyoshi	(Leader)	
ABE Kanako (*4)	HAMADA Kazuya	ISONO Takaaki
KAWANO Katsumi	KOIZUMI Norikiyo	NABARA Yoshihiro
NAKAJIMA Hideo	NUNOYA Yoshihiko	OSHIKIRI Masayuki (*15)
SUGIMOTO Makoto	TAKANO Katsutoshi (*15)	TSUTSUMI Fumiaki (*26)

Plasma Heating Group

SAKAMOTO Keishi	(Leader)	
DAIRAKU Masayuki	HANADA Masaya	IKEDA Yukiharu
INOUE Takashi	KASHIWAGI Mieko	KASUGAI Atsushi
KOBAYASHI Noriyuki (*25)	KOMORI Shinji (*15)	MINAMI Ryutaroh (*17)
ODA Yasuhisa (*27)	SEKI Takayoshi (*2)	TAKAHASHI Koji
TANIGUCHI Masaki	TOBARI Naoyuki (*17)	WATANABE Kazuhiro

Tritium Technology Group

YAMANISHI Toshihiko	(Leader)	
HAYASHI Takumi	ISOBE Kanetsugu	KAWAMURA Yoshinori
KOBAYASHI Kazuhiro	MIURA Hidenori (*8)	NAKAMURA Hirofumi
SHU Wataru	SUZUKI Takumi	UZAWA Masayuki (*12)
YAMADA Masayuki		

Fusion Materials Development Group

SUGIMOTO Masayoshi	(Leader)	
ANDO Masami	CHIDA Teruo (*3)	IDA Mizuho (*4)
MATSUHIRO Kenjiro (*17)	NAKAMURA Hiroo	NAKAMURA Kazuyuki
TANIGAWA Hiroyasu	UMETSU Tomotake (*10)	YUTANI Toshiaki (*25)

Fusion Neutronics Group

NISHITANI Takeo (Leader)

ABE Yuichi

KUBOTA Naoyoshi (*17)

OCHIAI Kentaro

TANAKA Shigeru

KAWABE Masaru (*15)

KUTSUKAKE Chuzo

OKADA Kouichi (*23)

YAMAUCHI Michinori (*25)

KONDO Keitaro (*16)

NAKAO Makoto (*8)

SATO Satoshi

Blanket Irradiation and Analysis Group

HAYASHI Kimio (Leader)

HOSHINO Tsuyoshi (*17)

TSUCHIYA Kunihiko

ISHIDA Takuya (*15)

YAMADA Hirokazu (*8)

NAKAMICHI Masaru

Division of ITER Project

TSUNEMATSU Toshihide

YOSHINO Ryuji

TADA Eisuke

SUGIHARA Masayoshi

KOIZUMI Koichi

(Unit Manager)

(Supreme Researcher)

(Senior Principal Researcher)

(Senior Principal Researcher)

ODAJIMA Kazuo

ITER Project Management Group

MORI Masahiro (Leader)

ITAMI Kiyoshi

SHOJI Teruaki

SENGOKU Seio

SUGIE Tatsuo

SHIMIZU Katsuhiro

YOSHIDA Hidetoshi

ITER International Coordination Group

ANDO Toshiro (Leader)

HONDA Tsutomu (*25)

KATAOKA Yoshiyuki (*2)

NAGAHAMA Tetsushi (*20)

SAKASAI Akira

TAKAHASHI Yoshikazu

IIDA Hiromasa

MARUYAMA So

OIKAWA Toshihiro

SATO Kouichi (*26)

TERASAWA Atsumi (*11)

IOKI Kimihiro (*12)

MORIMOTO Masaaki (*12)

OKADA Hidetoshi (*2)

SHIMADA Michiya

YOSHIDA Kiyoshi

ITER Plant System Group

NEYATANI Yuzuru (Leader)

OHMORI Junji (*25)

TAKAHASHI Hideo (*22)

YAMAMOTO Shin

SATO Kazuyoshi

TAMURA Kousaku (*9)

SEKIYA Shigeki (*10)

YAGENJI Akira (*1)

ITER Tokamak Device Group

SHIBANUMA Kiyoshi (Leader)

KAKUDATE Satoshi

NAKAHIRA Masataka

KITAMURA Kazunori (*25)

OBARA Kenjiro

MOHRI Kensuke (*7)

TAKEDA Nobukazu

ITER Safety Design Groupe

O'HIRA Shigeru (Leader)

HIGUCHI Masahisa

TAKEI Nahoko

TAKEMURA Morio (*7)

TSURU Daigo

Collaborating Laboratories

Tokai Research and Development Center

Nuclear Science and Engineering Directorate

Irradiation Field Materials Research Group

JITSUKAWA Shiro (Leader)

FUJII Kimio

OKUBO Nariaki

TANIFUJI Takaaki

WAKAI Eiichi

YAMAKI Daiju

Research Group for Corrosion Damage Mechanism

MIWA Yukio

Quantum Beam Science Directorate

Nanomaterials Synthesis Group

TAGUCHI Tomitsugu

Accelerator Group

HIROKI Seiji

Industrial Collaboration Promotion Department

Administration Section

NEMOTO Masahiro

Oarai Research and Development Center

Advanced Nuclear System Research and Development Directorate

Innovative Technology Group,

ARA Kuniaki

Technology Development Department

Advanced Liquid Metal Technology Experiment Section

YOSHIDA Eiichi

- *1 Hazama Corporation
- *2 Hitachi, Ltd.
- *3 Hitachi Engineering & Services Co., Ltd.
- *4 Ishikawajima-Harima Heavy Industries Co., Ltd.
- *5 JP HYTEC Co., Ltd.

- *6 Japan EXpert Clone Corp.
- *7 Kawasaki Heavy Industries, Ltd.
- *8 Kawasaki Plant Systems, Ltd.
- *9 Konoike Construction Co., Ltd.
- *10 Kumagai Gumi Co., Ltd.

- *11 Mitsubishi Electric Corporation
- *12 Mitsubishi Heavy Industries, Ltd.
- *13 NEC Corporation
- *14 Nippon Advanced Technology Co., Ltd.
- *15 Nuclear Engineering Co., Ltd.

- *16 Osaka University
- *17 Post-Doctoral Fellow
- *18 Princeton Plasma Physics Laboratory (USA)
- *19 Research Organization for Information Science & Technology
- *20 Shimizu Corporation

- *21 Sumitomo Heavy Industries, Ltd.
- *22 Taisei Corporation
- *23 Tohoku University
- *24 Tomoe Shokai Co., Ltd.
- *25 Toshiba Corporation

- *26 Total Support Systems
- *27 University of Tokyo

国際単位系（SI）

表 1. SI 基本単位

基本量	SI 基本単位	
	名称	記号
長さ	メートル	m
質量	キログラム	kg
時間	秒	s
電流	アンペア	A
熱力学温度	ケルビン	K
物質の量	モル	mol
光の度	カンデラ	cd

表 2. 基本単位を用いて表されるSI組立単位の例

組立量	SI 基本単位	
	名称	記号
面積	平方メートル	m ²
体積	立方メートル	m ³
速度	メートル毎秒	m/s
加速度	メートル毎秒毎秒	m/s ²
波数	毎メートル	m ⁻¹
密度（質量密度）	キログラム毎立方メートル	kg/m ³
質量体積（比体積）	立法メートル毎キログラム	m ³ /kg
電流密度	アンペア毎平方メートル	A/m ²
磁界の強さ	アンペア毎メートル	A/m
（物質量の）濃度	モル毎立方メートル	mol/m ³
輝度	カンデラ毎平方メートル	cd/m ²
屈折率	（数の）1	1

表 5. SI 接頭語

乗数	接頭語	記号	乗数	接頭語	記号
10 ²⁴	ヨタ	Y	10 ⁻¹	デシ	d
10 ²¹	ゼタ	Z	10 ⁻²	センチ	c
10 ¹⁸	エクタ	E	10 ⁻³	ミリ	m
10 ¹⁵	ペタ	P	10 ⁻⁶	マイクロ	μ
10 ¹²	テラ	T	10 ⁻⁹	ナノ	n
10 ⁹	ギガ	G	10 ⁻¹²	ピコ	p
10 ⁶	メガ	M	10 ⁻¹⁵	フェムト	f
10 ³	キロ	k	10 ⁻¹⁸	アト	a
10 ²	ヘクト	h	10 ⁻²¹	ゼプト	z
10 ¹	デカ	da	10 ⁻²⁴	ヨクト	y

表 3. 固有の名称とその独自の記号で表されるSI組立単位

組立量	SI 組立単位			
	名称	記号	他のSI単位による表し方	SI基本単位による表し方
平面角	ラジアン ^(a)	rad		m・m ⁻¹ =1 ^(b)
立体角	ステラジアン ^(a)	sr ^(c)		m ² ・m ⁻² =1 ^(b)
周波数	ヘルツ	Hz		s ⁻¹
力	ニュートン	N		m・kg・s ⁻²
圧力，応力	パスカル	Pa	N/m ²	m ⁻¹ ・kg・s ⁻²
エネルギー，仕事，熱量	ジュール	J	N・m	m ² ・kg・s ⁻²
工率，放射束	ワット	W	J/s	m ² ・kg・s ⁻³
電荷，電気量	クーロン	C		s・A
電位差（電圧），起電力	ボルト	V	W/A	m ² ・kg・s ⁻³ ・A ⁻¹
静電容量	ファラド	F	C/V	m ⁻² ・kg ⁻¹ ・s ⁴ ・A ²
電気抵抗	オーム	Ω	V/A	m ² ・kg・s ⁻³ ・A ⁻²
コンダクタンス	ジーメン	S	A/V	m ⁻² ・kg ⁻¹ ・s ³ ・A ²
磁束	ウェーバ	Wb	V・s	m ² ・kg・s ⁻² ・A ⁻¹
磁束密度	テスラ	T	Wb/m ²	kg・s ⁻² ・A ⁻¹
インダクタンス	ヘンリー	H	Wb/A	m ² ・kg・s ⁻² ・A ⁻²
セルシウス温度 ^(d)	セルシウス度	°C		K
光の照度	ルーメン毎平方メートル	lx	cd・sr ^(c)	m ² ・m ⁻² ・cd=cd
（放射性核種の）放射能	ベクレル	Bq	lm/m ²	m ² ・m ⁻¹ ・cd=m ⁻² ・cd
吸収線量，質量エネルギー分与，カーマ線量当量，周辺線量当量，方向性線量当量，個人線量当量，組織線量当量	グレイ	Gy	J/kg	m ² ・s ⁻²
	シーベルト	Sv	J/kg	m ² ・s ⁻²

- (a) ラジアン及びステラジアンの使用は、同じ次元であっても異なった性質をもった量を区別するときの組立単位の表し方として利点がある。組立単位を形作るときいくつかの用例は表 4 に示されている。
- (b) 実際には、使用する時には記号rad及びsrが用いられるが、習慣として組立単位としての記号“1”は明示されない。
- (c) 測光学では、ステラジアンの名称と記号srを単位の表し方の中にそのまま維持している。
- (d) この単位は、例としてミリセルシウス度m°CのようにSI接頭語を伴って用いても良い。

表 4. 単位の中に固有の名称とその独自の記号を含むSI組立単位の例

組立量	SI 組立単位		
	名称	記号	SI 基本単位による表し方
粘力のモーメント	パスカル秒	Pa・s	m ⁻¹ ・kg・s ⁻¹
表面張力	ニュートン毎メートル	N・m	m ² ・kg・s ⁻²
角速度	ニュートン毎メートル	N/m	kg・s ⁻²
角加速度	ラジアン毎秒	rad/s	m・m ⁻¹ ・s ⁻¹ =s ⁻¹
熱流密度，放射照度	ラジアン毎平方秒	rad/s ²	m・m ⁻¹ ・s ⁻² =s ⁻²
熱容量，エン트로ピー	ワット毎平方メートル	W/m ²	kg・s ⁻³
質量熱容量（比熱容量），質量エン트로ピー	ジュール毎ケルビン	J/K	m ² ・kg・s ⁻² ・K ⁻¹
質量エネルギー（比エネルギー）	ジュール毎キログラム	J/(kg・K)	m ² ・s ⁻² ・K ⁻¹
熱伝導率	ジュール毎メートル毎ケルビン	J/kg	m ² ・s ⁻² ・K ⁻¹
体積エネルギー	ワット毎メートル毎ケルビン	W/(m・K)	m・kg・s ⁻³ ・K ⁻¹
電界の強さ	ジュール毎立方メートル	J/m ³	m ⁻¹ ・kg・s ⁻²
体積電荷	ボルト毎メートル	V/m	m・kg・s ⁻³ ・A ⁻¹
電気変位	クーロン毎立方メートル	C/m ³	m ⁻³ ・s・A
誘電率	クーロン毎平方メートル	C/m ²	m ⁻² ・s・A
透磁率	ファラド毎メートル	F/m	m ⁻³ ・kg ⁻¹ ・s ⁴ ・A ²
モルエネルギー	ヘンリー毎メートル	H/m	m ⁻³ ・kg・s ⁻² ・A ²
モルエン트로ピー	ジュール毎モル	J/mol	m ² ・kg・s ⁻² ・mol ⁻¹
モル熱容量	ジュール毎モル毎ケルビン	J/(mol・K)	m ² ・kg・s ⁻² ・K ⁻¹ ・mol ⁻¹
照射線量（X線及びγ線）	クーロン毎キログラム	C/kg	kg ⁻¹ ・s・A
吸収線量率	グレイ毎秒	Gy/s	m ² ・s ⁻³
放射強度	ワット毎ステラジアン	W/sr	m ⁴ ・m ⁻² ・kg・s ⁻³ =m ² ・kg・s ⁻³
放射輝度	ワット毎平方メートル毎ステラジアン	W/(m ² ・sr)	m ² ・m ⁻² ・kg・s ⁻³ =kg・s ⁻³

表 6. 国際単位系と併用されるが国際単位系に属さない単位

名称	記号	SI 単位による値
分	min	1 min=60s
時	h	1 h =60 min=3600 s
日	d	1 d=24 h=86400 s
度	°	1° =(π/180) rad
分	′	1′ =(1/60)° =(π/10800) rad
秒	″	1″ =(1/60)′ =(π/648000) rad
リットル	l, L	1 l=1 dm ³ =10 ⁻³ m ³
トン	t	1 t=10 ³ kg
ネーパ	Np	1 Np=1
ベル	B	1 B=(1/2) ln10 (Np)

表 7. 国際単位系と併用されこれに属さない単位で SI単位で表される数値が実験的に得られるもの

名称	記号	SI 単位であらわされる数値
電子ボルト	eV	1 eV=1.60217733 (49) ×10 ⁻¹⁹ J
統一原子質量単位	u	1 u=1.6605402 (10) ×10 ⁻²⁷ kg
天文単位	ua	1 ua=1.49597870691 (30) ×10 ¹¹ m

表 8. 国際単位系に属さないが国際単位系と併用されるその他の単位

名称	記号	SI 単位であらわされる数値
海里		1 海里=1852m
ノット		1 ノット=1 海里毎時=(1852/3600) m/s
アール	a	1 a=1 dam ² =10 ² m ²
ヘクタール	ha	1 ha=1 hm ² =10 ⁴ m ²
バール	bar	1 bar=0.1 MPa=100kPa=1000hPa=10 ⁵ Pa
オングストローム	Å	1 Å=0.1 nm=10 ⁻¹⁰ m
バール	b	1 b=100fm ² =10 ⁻²⁸ m ²

表 9. 固有の名称を含むCGS組立単位

名称	記号	SI 単位であらわされる数値
エルグ	erg	1 erg=10 ⁻⁷ J
ダイン	dyn	1 dyn=10 ⁻⁵ N
ポアズ	P	1 P=1 dyn・s/cm ² =0.1 Pa・s
ストークス	St	1 St =1cm ² /s=10 ⁻⁴ m ² /s
ガウス	G	1 G =10 ⁻⁴ T
エルステッド	Oe	1 Oe =1000(4π) A/m
マクスウェル	Mx	1 Mx =10 ⁻⁸ Wb
スチル	sb	1 sb =1cd/cm ² =10 ⁴ cd/m ²
ホト	ph	1 ph=10 ⁴ lx
ガリ	Gal	1 Gal =1cm/s ² =10 ⁻² m/s ²

表10. 国際単位に属さないその他の単位の例

名称	記号	SI 単位であらわされる数値
キュリー	Ci	1 Ci=3.7×10 ¹⁰ Bq
レントゲン	R	1 R = 2.58×10 ⁻⁴ C/kg
ラド	rad	1 rad=1cGy=10 ⁻² Gy
レム	rem	1 rem=1 cSv=10 ⁻² Sv
X線単位		1 X unit=1.002×10 ⁻⁴ nm
ジャンスキー	γ	1 γ=1 nT=10 ⁻⁹ T
ジャンスキー	Jy	1 Jy=10 ⁻²⁶ W・m ⁻² ・Hz ⁻¹
フェルミ		1 fermi=1 fm=10 ⁻¹⁵ m
メートル系カラット		1 metric carat = 200 mg = 2×10 ⁻⁴ kg
トル	Torr	1 Torr = (101 325/760) Pa
標準大気圧	atm	1 atm = 101 325 Pa
カロリ	cal	
マイクロン	μ	1 μ =1μm=10 ⁻⁶ m

